9-9-2009

Alternative Methods to Standby Gain Scheduling Following Air Data System Failure

Matthew W. Coldsnow

ALTERNATIVE METHODS TO STANDBY GAIN SCHEDULING FOLLOWING

AIR DATA SYSTEM FAILURE

THESIS

Matthew W. Coldsnow, Major, USAF

AFIT/GAE/ENY/09-S02

DEPARTMENT OF THE AIR FORCE
AIR UNIVERSITY

AIR FORCE INSTITUTE OF TECHNOLOGY

Wright-Patterson Air Force Base, Ohio

APPROVED FOR PUBLIC RELEASE; DISTRIBUTION UNLIMITED

AFIT/GAE/ENY/09-S02

ALTERNATIVE METHODS TO STANDBY GAIN SCHEDULING FOLLOWING

AIR DATA SYSTEM FAILURE

THESIS

Presented to the Faculty

Department of Aeronautics and Astronautics

Graduate School of Engineering and Management

Air Force Institute of Technology

Air University

Air Education and Training Command

In Partial Fulfillment of the Requirements for the

Degree of Master of Science in Aeronautical Engineering

Matthew W. Coldsnow, BS

Major, USAF

September 2009

APPROVED FOR PUBLIC RELEASE; DISTRIBUTION UNLIMITED

AFIT/GAE/ENY/09-S02

ALTERNATIVE METHODS TO STANDBY GAIN SCHEDULING FOLLOWING AIR

DATA SYSTEM FAILURE

Matthew W. Coldsnow, BS
Major, USAF

Approved:

_____   _____
Paul A. Blue, Lt Col, USAF (Chairman)   1 Sep 09
                                                Date

_____   _____
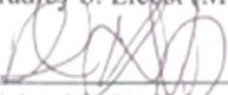Bradley S. Liebst (Member)   1 Sep 09
                                     Date

_____   _____
Richard E. Huffman, Lt Col, USAF (Member)   1 Sep 09
                                                     Date

_____   _____
Timothy R. Jorris, Lt Col, USAF (Member)   1 Sep 09
                                                   Date

AFIT/GAE/ENY/09-S02

Abstract

The United States Air Force has advanced fighter aircraft that lose the ability to operate in a large portion of their operating flight envelope when an air data system failure is experienced. These aircraft are reverted to a fixed set of standby-gains that limit their maneuverability, degrade handling qualities, and increase susceptibility to departure. The purpose of this research was to determine if three alternative methods of standby-gain-scheduling could provide robust control with minimal performance degradation despite the lack of air data.

To accomplish this, three methods of standby-gain-scheduling were developed, integrated, and tested in the Infinity Cube simulator at the Air Force Research Laboratory/RBCD building. The first method improved upon an algorithm which used inertial data to estimate an aircraft's true velocity used to drive the gains in an F-16 controller. This algorithm was validated by post-processing high-fidelity simulator data and actual flight data. The second method simply used inertial velocities to drive the gains in an F-16 controller. The final method used a disturbance observer controller which controlled aircraft dynamics without the use of gain-scheduling.

The results showed the potential for effective aircraft control with minimal performance degradation following an air data system failure. Potential benefits to this research include eliminating the need to make switch actuations to correctly schedule the standby-gains; improving aircraft performance when flying with standby-gains; allowing the pilot to continue with a combat mission instead of returning to base with an air data system failure; and helping contribute to the removal of Pitot tubes in an attempt to eliminate a failure mode and to reduce the radar cross section of an aerial vehicle.

To my wife and children

for their endless love and tremendous support!

Acknowledgments

I would like to thank my thesis advisor, Lt Col Paul Blue, for his guidance and support during school and throughout the thesis process. His dedication to his students and to the USAF is unmatched by any professional I have ever been associated with. It has been an honor working with Lt Col Blue and I am truly thankful for all his efforts.

I would also like to thank the Air Force Research Laboratory/RBCD for their tremendous support. There were many people from this organization that volunteered their time to support this thesis but the following people deserve special mention for all their time and effort: Amy Burns, Jeff Slutz, and Michael Coy. These individuals were critical to the success of the simulator testing accomplished in the Infinity Cube simulator. I sincerely appreciate all their efforts.

Matthew W. Coldsnow

Table of Contents

List of Figures

Appendix A. Tracking Task Wind Estimator Plots

Appendix B. Tracking Task Wind Estimator Plots with Tuning

Appendix C. Longshot Task Wind Estimator Plots with Tuning

Appendix D. Landing Task Wind Estimator Plots

Appendix E. Landing Task Wind Estimator Plots with Tuning

Appendix F. Aircraft Flight Data Post-Processing Plots

Appendix G. Aircraft Wind Truth Data Comparison

Appendix H. Aerodynamic Modeling Sortie Maneuver Plots

Appendix I. Turn Performance Sortie Maneuver Plots

Appendix J. Level Acceleration Sortie Maneuver Plots

List of Tables

ALTERNATIVE METHODS TO STANDBY GAIN SCHEDULING FOLLOWING AIR DATA SYSTEM FAILURE

1.0 Introduction

1.1 Motivation

Currently, the Air Force has advanced fighter aircraft that require a pilot to make switch actuations to correctly schedule flight control system standby-gains in the event of air data system failures. There are two problems with this current method. First, the pilot must take time away from other pertinent tasks to manually position the standby-gains via the landing gear handle, air-to-air refueling door switch or some other means. Second, the standby-gain settings are suboptimal for an advanced fighter flight envelope and are primarily designed to allow for the safe recovery and landing of an aircraft. This suboptimal setting can lead to decreased aircraft handling qualities and increased pilot work load throughout a majority of the normal flight envelope.

The modern high-performance aircraft flight envelope covers a wide range of dynamic pressures, resulting in a wide range of aircraft dynamics. Because of these large changes in aircraft dynamics, a dynamic mode that is stable and adequately damped in one flight condition may become unstable, or at least inadequately damped, in another flight condition [Stevens and Lewis, 2003]. Therefore, a controller must have the ability to change with its flight condition in order to provide the proper aircraft response. A way to accomplish this is to design multiple controllers at various equilibrium points

1

throughout the flight envelope and combine these individual controllers into a single controller that is scheduled according a prescribed flight condition (i.e. airspeed and altitude) [Blue et al, 2002]. This process is known as gain-scheduling. Designing gain-scheduled controllers is a very complex process, especially when implemented in a modern high-performance aircraft.

Modern high-performance flight control systems are heavily dependent on valid air data measurements (true airspeed, alpha, beta, pressure differentials, temperature etc.) to properly schedule the flight control response. Air data measurement systems have three inherent limitations. First, most air data systems currently in use are un-stealthy by nature. They contain Pitot tubes which extend away from the structure to measure undisturbed airflow. While the radar signature of a Pitot tube can be reduced, it cannot be completely eliminated. Second, the systems can be quite complex. Even the most rudimentary system has numerous probes, ports, lines, computers, and interfaces. They all add weight, volume, and maintenance workload to the aircraft. Finally, the dependency on air data measurements could lead to a loss of aircraft if those measurements should cease or become inaccurate. An ability to derive air data parameters without direct air data measurements would be useful either as a backup to the air data system, or as an entirely self contained system that eliminates the need for external and internal air data components.

1.2 Problem Statement

The purpose of this work is to compare alternative methods of standby-gain-scheduling. The first alternative method builds upon an algorithm which uses inertial

navigation system (INS) data to estimate the aircraft's true velocity [McLaren, 2008]. This estimated true velocity will then be used to drive the gain-schedule in an F-16 controller (VEST 2 controller). The second method simply uses inertial velocities to drive the gains in an F-16 controller (INS or inertial controller). The final method uses a disturbance observer which attempts to control aircraft dynamics without the use of gain-scheduling (DO controller). The goal of this research is to compare these three alternative methods of standby-gain-scheduling and draw some conclusions about their utility.

1.3 Research Objectives

If an aircraft's air data system fails, true airspeed cannot be measured with the systems on board. Inertial and global positioning system sensors can provide accurate ground velocity but without some measurement of true airspeed, automatic gain-scheduling using true airspeed becomes impossible. The objective of this research was to determine if alternative methods of standby-gain-scheduling could provide robust control despite the absence of an air data system. Accomplishment of this objective meant the design, development, and implementation of three standby-gain-scheduled controllers; a velocity estimator gain-scheduled controller (VEST 2 controller); an inertial velocity gain-scheduled controller (inertial or INS controller); and a large flight envelope disturbance observer controller (DO controller) that did not require gain-scheduling. Testing and comparing the results of each controller will allow for an overall characterization of each method of standby-gain-scheduling. Validation of the velocity

estimator algorithm itself will provide an actual measure of the estimator's performance. Using the information gathered from the comparison, implementation, testing, and validation of the controllers will provide a reasonable assessment of the potential for using each of the alternative methods of standby-gain-scheduling.

1.3.1 Compare Alternative Methods of Standby-Gain-Scheduling.

The methodology behind this analysis is to establish a baseline measure of performance by flying a nominal block 40 F-16C using Air Force Research Laboratory/RBCD's high-fidelity, pilot-in-the-loop Infinity Cube simulator. Then, assuming there is an air data system failure, a comparison of the three different standby-gain-scheduling controllers (VEST 2 controller, DO controller, and inertial or INS controller) will be performed. The VEST 2 controller will use an estimated velocity to drive the block 40 F-16C gain-scheduling. The DO controller will use a disturbance observer (DO), as a standby controller that does not require gain-scheduling. Finally, the inertial controller will use aircraft inertial velocities to drive the block 40 F-16C gain-scheduling.

1.3.2 Validate Estimated Airspeed Algorithm with Simulation and Flight Data.

The airspeed estimate from the VEST 2 controller will be compared to airspeeds from a block 40 F-16C simulator and actual aircraft flight data from a block 30 F-16D. The simulator validation will be accomplished with the controller implemented in the flight controls of the block 40 F-16C simulator. The flight data validation will be

accomplished by post-processing actual flight data from a block 30 F-16D using the same airspeed estimator algorithm used with the VEST 2 controller.

1.3.3 Assess the Potential for Using Alternative Methods of Standby-Gain-Scheduling.

The three different standby-gain-scheduling controllers will be compared to a baseline F-16 controller in a block 40 F-16C simulator. Both pilot opinion and statistical data will be recorded in an attempt to compare the performance of each controller. The end result is to validate the utility of each of the standby-gain-scheduling methods.

1.4 Approach

This thesis was a follow on to previous research which looked at estimating aircraft true airspeed following an air data system failure. Specifically, this work set out to investigate whether an estimated airspeed could be used to schedule flight control gains as an alternative to standby-gain-scheduling. Along the way, the original airspeed estimator was improved and two other alternatives to standby-gain-scheduling were investigated.

Knowing what information was available after an air data system failure provided a starting point from which to continue analysis. The available information included a last known state prior to failure, aircraft INS outputs, and global positioning system velocities. This research also assumed that measurements of alpha and beta still existed. With this information available, it was possible to test all three standby-gain-scheduling controllers. The VEST 2 controller used a geometric relationship between inertial

velocities, wind, and true airspeed combined in an algorithm to provide estimates of current wind and true airspeed components [McLaren, 2008]. The inertial controller simply used the inertial velocity information still available from an INS to schedule gains. Finally, a disturbance observer (DO) controller was designed to control a large flight envelope that was independent of gain-scheduling. After incorporating all standby-gain-scheduling controllers into an F-16C flight simulator, the three controllers were compared with the nominal block 40 F-16C controller to determine the utility of each method of standby-gain-scheduling. Finally, VEST 2 was selected for further analysis using actual aircraft data from a block 30 F-16D. The flight data was post processed using the airspeed estimator algorithm in order to validate the algorithm. The validation process was intended to demonstrate that the error of the estimator was small and minimally variable which would make it safe to assume that the original flight controller could be used in conjunction with the velocity estimator to provide aircraft control that is equivalent to the nominal block 40 F-16C controller.

1.5 Preview of Results and Implications

Three alternatives to the traditional standby-gain-scheduling were developed and compared in an F-16C simulator. The results of this research clearly show the potential for effective aircraft control with minimal performance degradation following an air data system failure. The VEST 2 controller and the inertial controller showed almost no performance degradation or increased pilot workload when compared to the nominal block 40 F-16C controller. Even though the DO controller resulted in decreased aircraft

performance and increased pilot workload, it still managed to obtain at least adequate performance with a tolerable workload throughout the designed flight envelope (0.4 – 0.8 Mach and 5,000 – 25,000 ft). This result demonstrated the potential for using a DO controller for large flight envelope control without the need for gain-scheduling.

The majority of this research was conducted under the assumption that measurements of alpha and beta were still available following an air data system failure. With an air data system failure it is highly unlikely that alpha and beta will be available. Therefore a way to obtain an accurate estimate of alpha and beta would be required for the DO to function properly in the lateral and directional axis. On the contrary, the inertial controller worked independent of alpha and beta and required no additional development to provide adequate control. For the VEST 2 algorithm to function it also needed alpha and beta. Inertial velocities were used to estimate alpha, and beta was set to zero in order to simulate an actual air data system failure. Post-processing actual aircraft data using the VEST 2 algorithm resulted in a low average estimated wind speed error (6.6 ± 3.8 knots) that was non-divergent and minimally variable in heading. Therefore, the estimated wind speed from the VEST 2 algorithm could make a viable substitute for determining true airspeed used in traditional gain-scheduling.

Alternative methods to standby-gain-scheduling could be possible as a result of this research. In the event of an air data system failure, any of the alternative methods to standby-gain-scheduling researched would eliminate the pilot's requirement to make switch actuations to correctly schedule the standby-gains in a large flight envelope. Secondly, the aircraft performance may prove to be more effective than the traditional

standby-gain settings allowing the pilot to continue with a combat mission as opposed to selecting the standby-gain, flying a particular airspeed and returning to base. Finally, this research may someday contribute to the removal of Pitot tubes in an attempt to eliminate a failure mode and to reduce the radar cross section of an aerial vehicle.

1.6 Thesis Overview

This thesis is designed to give an in-depth look at the theory and concepts used during the development of the standby-gain-scheduling controllers. Chapter 2 provides the background information necessary to understand the development behind each method of control. Then, the specific theory, concepts applied to each controller and desktop simulation results will be covered in Chapter 3. Chapter 4 contains the block 40 F-16 high-fidelity simulator results and the validation of the VEST 2 estimator. Finally, Chapter 5 draws research conclusions, discusses future applications, and recommends follow-on research.

2.0 Background

2.1 Chapter Overview

The purpose of this chapter is to provide a review of basic theory applicable to the various methods of standby-gain-scheduling control. The chapter explains pertinent aircraft systems, key terms, disturbance observer control theory, the mathematical theory behind Kalman filtering, and pilot opinion performance scales. The background presented here forms the basis for the development of the standby-gain-scheduling controllers.

2.2 Air Data Aircraft Systems

The performance of an aircraft depends on the combined effort of all its subsystems. The outputs of these subsystems are combined into several complex flight control computers which transform pilot inputs into acceptable control surface deflections leading to desired aircraft performance [McLaren, 2008]. Air data systems make up a small portion of the total aircraft, but are essential in obtaining desired aircraft responses.

2.2.1 Pitot Static Systems.

Pitot static systems are essential to modern high-performance aircraft. They produce a differential pressure reading by measuring the difference between total and static pressure. This differential pressure is read off of a gage which is calibrated to convert differential pressure measurements into indicated airspeed. Indicated airspeed

measurements provided by the Pitot static system are then converted into true airspeed which is typically used for gain-scheduling. Gain-scheduling associated with modern, large-envelope, fighter-type aircraft depend heavily on the Pitot static system.

This essential system consists of at least one Pitot tube, one or more static ports and a device for measuring differential pressure [Brandt, 2004]. Pitot tubes usually extend away from the surface of the aircraft, measuring free-stream (undisturbed) total and static pressures.
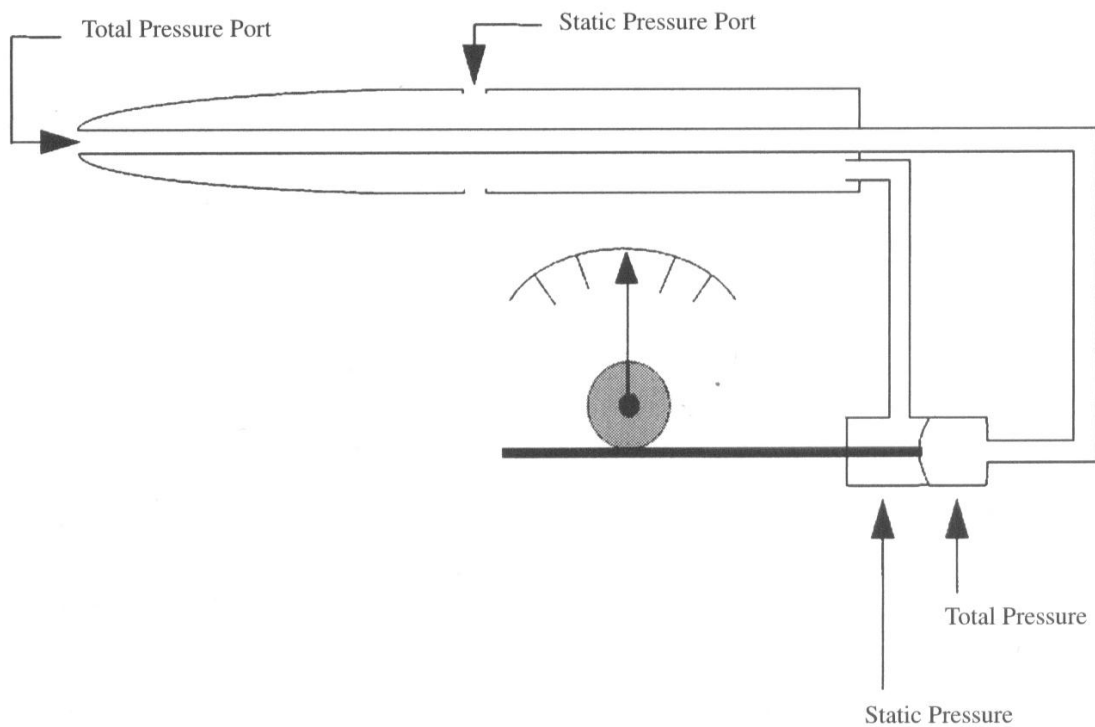
Figure 1. Pitot Tube

In the incompressible case, the total pressure port measures a combination of static

pressure and dynamic pressure. Whereas the static pressure ports, oriented parallel to the

flow field, prevent a stagnation point from developing and allow the measurement to be

as close to free-stream static pressure as possible [Brandt, 2004]. The basic concept of

using a pressure differential to measure airspeed stems from Daniel Bernoulli's discovery

that total pressure is constant along a streamline. Ignoring the effects of elevation, body

forces, and assuming steady flow, Bernoulli's equation

$$\int_1^2 V\,dV = -\int_1^2 \frac{dP}{\rho} \tag{1}$$

establishes the relationship between pressure (P), velocity (V) and density (ρ) along a

streamline [Nelson, 1998]. If the integration is performed along a streamline with the

steady flow of an inviscid, incompressible fluid for which body forces are negligible, the

result is shown below [Brandt, 2004]:

$$P_1 + \frac{1}{2}\rho V_1^2 = P_2 + \frac{1}{2}\rho V_2^2 = P_{total} \tag{2}$$

Each side of Bernoulli's equation contains a combination of static pressure (P_∞) and

dynamic pressure ($\bar{q}$) and can be re-written as:

$$P_\infty + \frac{1}{2}\rho V_\infty^2 = P_{static} + P_{dynamic} = P_\infty + \bar{q} = P_{total} \tag{3}$$

Together, both static and dynamic pressures make up the total pressure (P_{total}) along a

streamline. With total pressure and static pressure measured from the pitot static system,

one can see how rearranging equation 3 yields an equation for the free-stream velocity

(V_∞):

$$V_\infty = \sqrt{\frac{2(P_{total} - P_\infty)}{\rho}} \qquad (4)$$

This freestream velocity describes exactly how fast the aircraft is moving through the air mass and is known as true airspeed (TAS).

2.2.2 Indicated, Calibrated, Equivalent, True Airspeeds and Mach Number.

TAS is normally not attainable directly from the Pitot static system. A conversation process is necessary in order to obtain TAS. Typically, the process begins with indicated airspeed (V_i) which is measured by the pitot static system. Then, the indicated airspeed must be corrected for position and installation error (ΔV_p). This new airspeed is known as calibrated airspeed (V_c).

$$V_c = V_i + \Delta V_p \qquad (5)$$

The calibrated airspeed must then be corrected for the actual existing pressure. Making the pressure correction produces an equivalent airspeed (V_e)

$$V_e = V_c \cdot f \qquad (6)$$

where f is a compressibility correction factor. Finally, equivalent airspeed is corrected for the actual existing density. When the density correction is completed, the result is the aircraft's TAS (V_∞)

$$V_\infty = V_e \sqrt{\frac{\rho_{SL}}{\rho_\infty}} \qquad (7)$$

where ρ_{SL} is sea level density, and ρ_∞ is the density at the associated flight condition.

Recall that the free-stream velocity defined section 2.2.1 did not take compressibility effects into account. A compressible form of Bernoulli's equation can be determined by accomplishing the integration of Euler's momentum equation with density varying as well [Brandt, 2004]. The end result is a compressible form of the Bernoulli equation similar to the incompressible solution shown below:

$$V_\infty = \sqrt{\left(\frac{1}{\rho_\infty}\right) 7 P_\infty \left\{ \left[\frac{P_{total} - P_\infty}{P_\infty} + 1\right]^{\frac{2}{7}} - 1 \right\}} \qquad (8)$$

The TAS above now accounts for compressibility effects but due to several factors, this equation is difficult to implement directly into a mechanical system. For instance, obtaining an accurate measurement of free-stream density is difficult to do.

Therefore, in order to overcome this problem, airspeed indicators are manufactured with gears calibrated to use sea-level standard atmospheric values of pressure and density [Brandt, 2004]. This calibration process produces the following calibrated airspeed:

$$V_c = \sqrt{\left(\frac{1}{\rho_{SL}}\right) 7 P_{SL} \left\{ \left[\frac{P_{total} - P_\infty}{P_{SL}} + 1\right]^{\frac{2}{7}} - 1 \right\}} \qquad (9)$$

As stated earlier, an adjustment must be made to the calibrated airspeed in order to correct for position and installation error. The position and installation errors are determined through flight test and are quantified as a velocity change (ΔV_p).

As evident by equation 5, if there were no installation or position errors, indicated airspeed would be equal to calibrated airspeed.

Calibrated airspeed must now be corrected for the actual existing pressure. Making the pressure correction produces an equivalent airspeed with the following definition:

$$V_e = \sqrt{\left(\frac{1}{\rho_{SL}}\right) 7 P_\infty \left\{\left[\frac{P_{total} - P_\infty}{P_\infty} + 1\right]^{\frac{2}{7}} - 1\right\}}$$ (10)

Finally, equivalent airspeed is adjusted for actual density conditions,

$$V_\infty = V_e \sqrt{\frac{\rho_{SL}}{\rho_\infty}}$$ (11)

and the end result is TAS. The purpose of TAS is to describe how fast an aircraft is moving through an air mass. It is rarely used by pilots, but is essential for scheduling gains in a flight control system, and is necessary in calculating groundspeed [McLaren, 2008].

An extension to TAS is the free-stream Mach number (M). The free-stream Mach number is defined as the ratio of TAS to the speed of sound (a).

$$M_\infty = \frac{V_\infty}{a}$$ (12)

The speed of sound depends almost entirely on temperature. Thus, the temperature change associated with an aircraft's altitude change affects the Mach number. In other words, an aircraft that is flying 500 knots TAS at 5,000 ft would have a different Mach

number than if that same aircraft was traveling 500 knots TAS at 10,000 ft.   When

defining the Mach number in terms of pressure measurements from the Pitot static

system, there are two versions; one for Mach < 1 [Kayton and Fried, 1997]

$$M_{<1} = \sqrt{5\left(\frac{P_{total} - P_\infty}{P_\infty} + 1\right)^{\frac{2}{7}} - 1}$$ (13)

and one for Mach > 1 [Erb, 2005]

$$M_{>1} = 0.881284\sqrt{\left(\frac{P_{total} - P_\infty}{P_\infty} + 1\right)\left(1 - \frac{1}{7M^2}\right)^{\frac{5}{2}}}$$ (14)

The difference between the two conditions is due to a bow wave that forms at the mouth

of a supersonic Pitot static system [Nelson, 1998]. Using a normal shock analysis to

approximate the bow wave leads to equation 14.

2.2.3 Air-Data Computers.

Typical air-data computers are composed of pressure transducers, excitation

circuitry, signal-conditioning circuitry, a processor, and output drivers capable of

interfacing with aircraft subsystems. Their primary purpose is to take total and static

pressures along with static air temperature and compute Mach number, temperature,

speed of sound, calibrated airspeed, true airspeed, pressure altitude, baro-corrected

altitude, density, and density altitude [Kayton and Fried, 1997].

2.2.4 Alpha and Beta Sensors.

The measurement for aircraft angle of attack (AOA) is important for many

reasons. From aircraft safety in the form of stall warnings; to approaches and landings; to

basic fighter maneuvering (BFM); the AOA sensor provides critical information to a pilot. There are a few different types of sensors used to measure AOA. The first type of sensor is a body mounted sensor in the form of a probe or vane shown in figure 2.
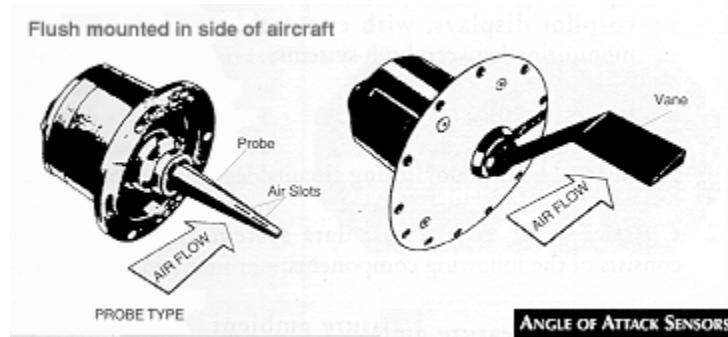
Figure 2. Angle of Attack Sensors

Body mounted sensors attempt to minimize position error by locating the probe or vane along the fuselage, close to the aircraft center of mass [Nelson, 1998]. The pivot vane sensor is mass-balanced and seeks to align itself with the undisturbed free-stream airflow. The probe sensor has two slots spaced at equal angles to measure pressure. A transducer computes the pressure differential between the two slots and the probe rotates to zero out the pressure differential. The rotation is measured and converted into an AOA measurement.

Another type of AOA sensor illustrated in Figure 3 is a nose-mounted air-data boom, with pressure probes and flow-direction vanes.

Figure 3. Nose-mounted Air-data Boom

This type of sensor is used almost extensively in flight test programs [Nelson, 1998] and contains both AOA and sideslip angle vanes.

The AOA and sideslip sensors measure the aerodynamic angles alpha (α) and beta (β). They are referred to as the aerodynamic angles since they are the only two angles that specifically relate the aerodynamic forces and moments in the body-fixed coordinate system (BFCS) to the wind axis system [Stevens and Lewis, 2003]. The BFCS is defined from the center of mass with the x-axis parallel to the fuselage reference line, the y-axis out the right wing and the z-axis down. To get from the BFCS to the wind axis, the forces and moments must first be rotated about the body y-axis by α to the stability axis. Then, a rotation from the stability axis by β about the body z-axis yields the forces and moments in the wind axis. Both the wind and stability axis have advantages but in this research, the desire to roll about the stability axis will become important later when discussing changes in AOA.

Finally, α and β can be defined in terms of the body axis using velocities $u, v,$ and $w.$

17
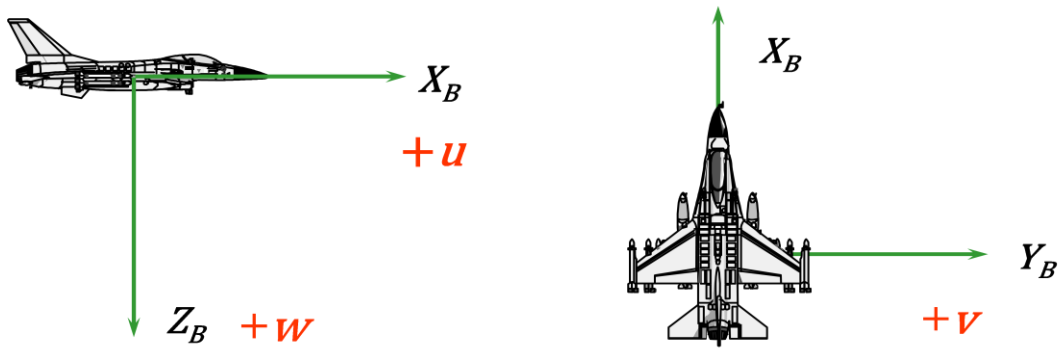
Figure 4. Aircraft Body Axis Designation

Where, u is the velocity along the x-body (X_B) axis, v is the velocity along the y-body (Y_B) axis, and w is the velocity along z-body (Z_B) axis. Applying these relations defines both α and β in the following form:

$$\alpha = \tan^{-1}\left(\frac{w}{u}\right) \tag{15}$$

$$\beta = \sin^{-1}\left(\frac{v}{\sqrt{u^2 + v^2 + w^2}}\right) \tag{16}$$

2.2.5 Velocity Triangle.

When an aircraft is flying, its velocity vector can be entirely described by three separate velocities: ground velocity $(\boldsymbol{V}_G)$, true velocity $(\boldsymbol{V}_T)$, and wind velocity $(\boldsymbol{V}_W)$. Under zero sideslip conditions, an aircraft points and flies along the true velocity vector. The wind vector alters the aircraft's track over the ground by its magnitude and direction. Ground velocity is the sum of these two velocity vectors shown in the relationship below:

$$\boldsymbol{V}_G = \boldsymbol{V}_T + \boldsymbol{V}_W \tag{17}$$

Typically, V_G is determined from inertial or global positioning system measurements, while V_T, as described in the Pitot static section, is obtained from the Pitot static system [Kayton and Fried, 1997]. This leaves V_W as the only remaining unknown in the velocity triangle depicted below.
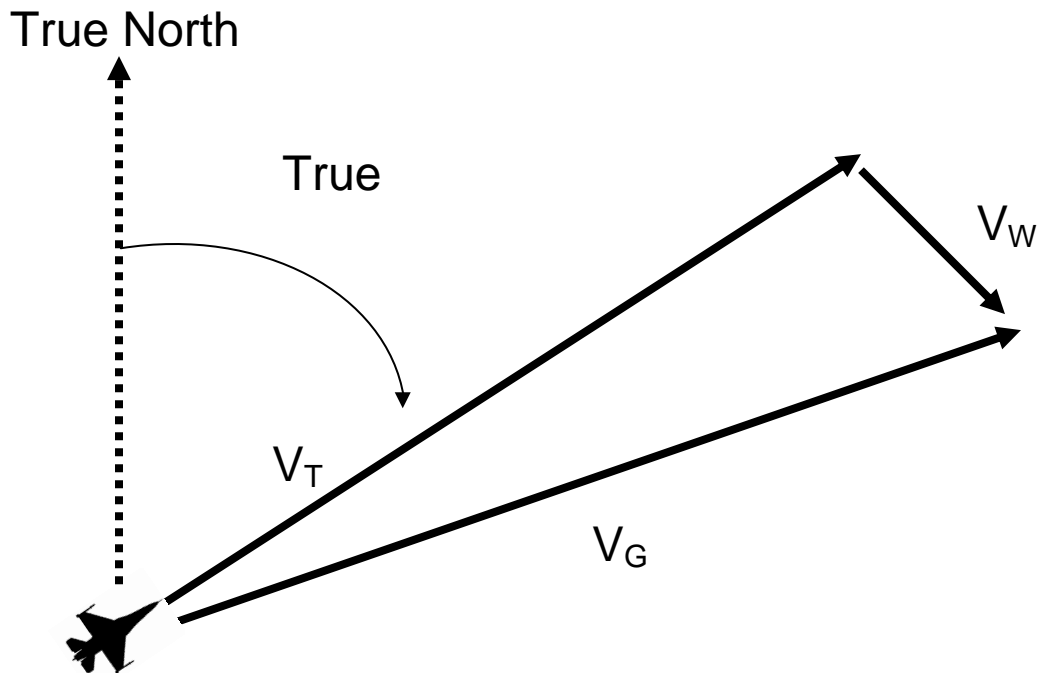
Figure 5. Velocity Triangle

This relationship is used almost exclusively for the calculation of winds experienced by an aircraft.

Additionally, an aircraft's true heading with no sideslip is determined by the angle from true north to V_T. The ground track heading is the angle from true north to V_G. As shown in Figure 5, the difference between the two headings is a result of wind conditions [McLaren, 2008].

2.2.6 Inertial Navigation System Aided Global Positioning System.

An inertial navigation system (INS) is used on aircraft to keep track of position, velocity, and attitude over time. There are two fundamental error sources which affect the performance of an INS [Kayton and Fried, 1997]. These errors appear in the measurements of forces made by accelerometers and in the measurements of angular rates made by gyroscopes. Through the use of a Kalman filter (discussed in 2.4.4), these errors can be minimized [Kayton and Fried, 1997]. Even so, the errors associated with accelerometers and gyroscopes cause an INS to "drift" away from the actual position. This can be corrected with the use of a global positioning system (GPS) update. A GPS update provides an updated position to the INS, effectively bounding the error in position, velocity and attitude [Kayton and Fried, 1997].

2.2.7 Flight Control Gain-Scheduling.

The difference in the aircraft flight performance envelopes of the 1930's and today is enormous. The modern aircraft flight envelopes cover a wide range of dynamic pressures. Assuming a standard lapse rate of temperature exists, the dynamic pressure envelope can be calculated. Figure 6 depicts the change in dynamic pressure over a large portion of the subsonic flight envelope (sea level to 36,000 feet and 0.1 to 0.9 Mach).
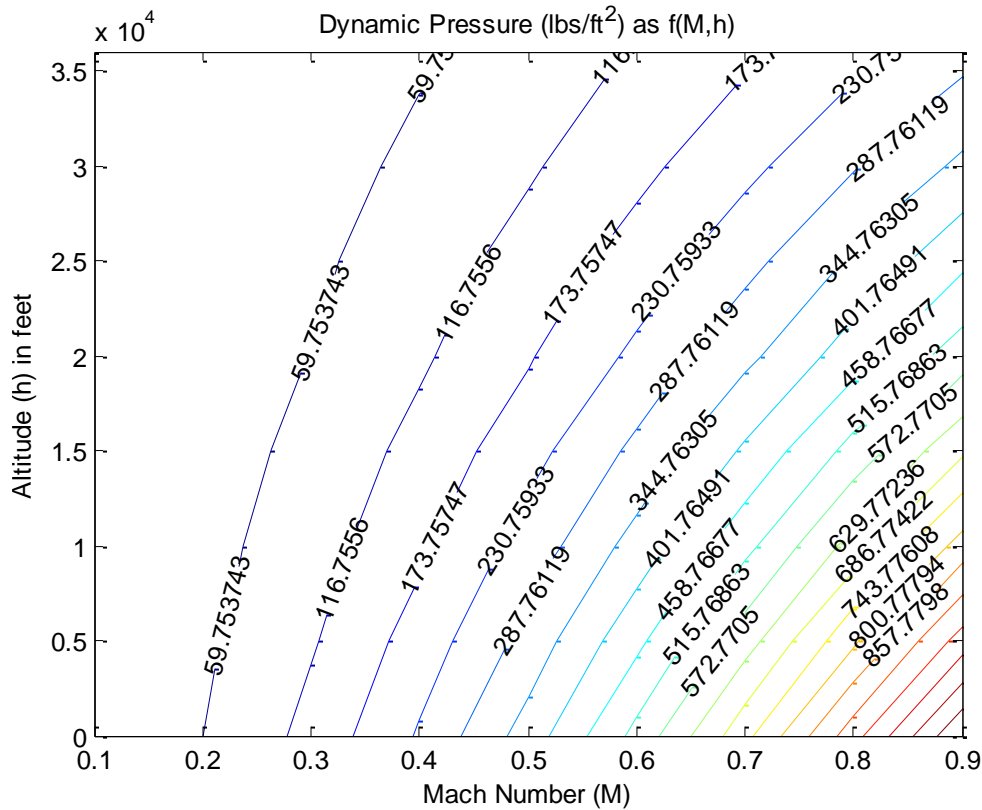
Figure 6. Dynamic Pressure Envelope

The differences in dynamic pressure throughout the flight envelope lead to large variations in aircraft dynamics. Because of these large changes in aircraft dynamics, a dynamic mode that is stable and adequately damped in one flight condition may become unstable, or at least inadequately damped, in another flight condition [Stevens and Lewis, 2003]. In order to remedy this problem, multiple feedback controllers are designed at various equilibrium points throughout the flight envelope and scheduled as a function of dynamic pressure. Gain-scheduling combines these feedback controllers into one controller that correlates with a prescribed flight condition (i.e. true airspeed and altitude) [Blue et al, 2002].

Designing a gain-scheduled controller is a very complex process, especially when implemented in a modern high-performance aircraft. However, through the use of gain-scheduling, modern aircraft can provide desired performance and maintain desired stability criteria throughout the entire modern high-performance flight envelope [McLaren, 2008].

2.2.8 Aircraft Failure Modes.

Aircraft redundancy deals with having multiple same-type independent systems or channels that allow an aircraft to continue to fly in the event of a single component failure. Redundant systems, such as flight controls systems or static ports, are essential for safe flight. However, on limited occasions, entire aircraft systems do fail. These failures drive the need for standby systems which, at the very least, allow for the safe recovery and landing of an aircraft. Following an air data system failure, a standby controller is used for just this purpose.

Typically, a flight Control System (FLCS) transitions to a fixed set of standby-gains which are optimized for a specific altitude and airspeed with the landing gear handle up, and a different altitude and airspeed with the landing gear handle down. If the aircraft has leading edge flaps, they are typically set to a fixed position that is associated with a specific configuration or switch position. There may also be another set of standby-gains associated with an air refueling switch, or some other switch to define an additional set of standby-gains. Handling qualities during standby-gain operations are usually degraded with certain limits placed on the minimum and maximum airspeeds. An aircraft may also be more susceptible to departure when standby-gains are used.

Knowing this, limits may be placed on angles of attack to minimize the chance of aircraft departures when standby-gains are used.

As evident by the limitations above, aircraft performance following an air data system failure can be limited. An example of this limited aircraft performance is shown in Figure 7 where aircraft responses are shown in both the normal and the standby-gain mode of a block 40 F-16C simulator.
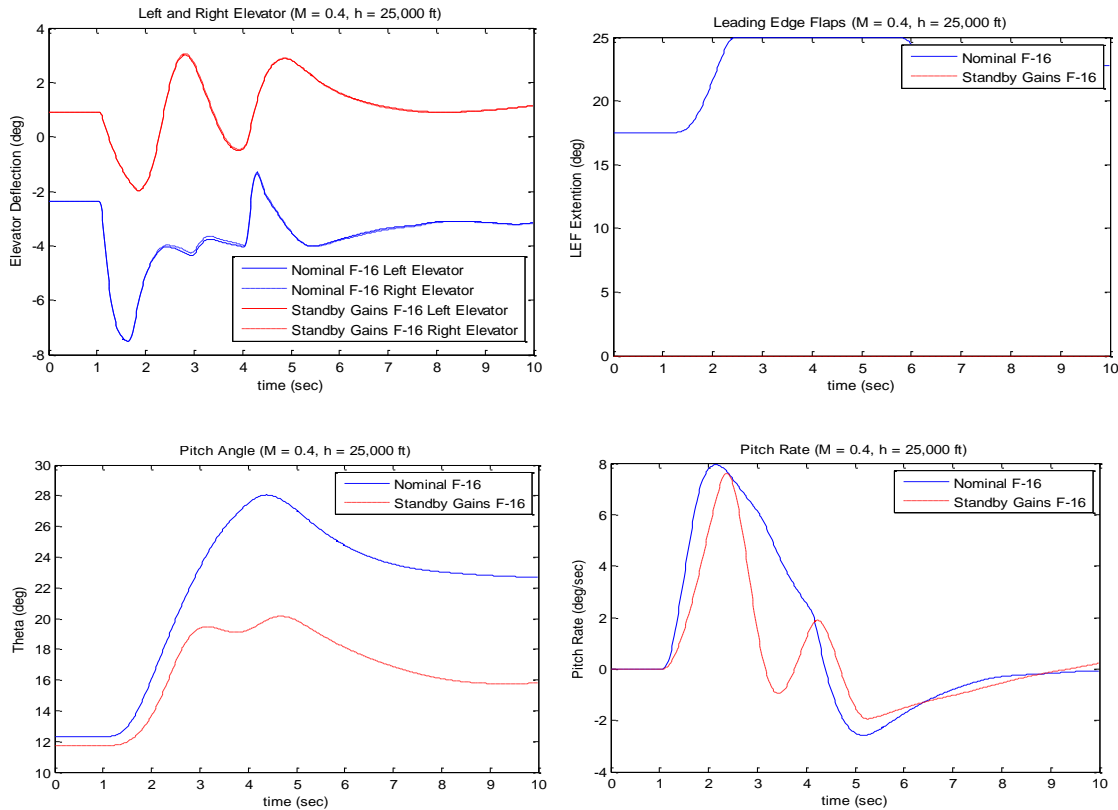
Figure 7. Block 40 F-16C Aircraft Responses at 0.4 Mach and 25,000 feet

It is obvious from the aircraft commands and responses that there can be significant degradation in aircraft performance when an aircraft must operate in the standby-gain mode.

With this degradation, modern high-performance aircraft can no longer take advantage of the entire flight envelope as aircraft performance now depends on a select set of gains typically driven by aircraft configuration. In this case, pilots must exercise great care as they transition from one phase of flight to another.

2.3 Disturbance Observer

Classical aircraft control includes feedback systems designed to provide improved aircraft handling qualities over the bare airframe. Improvements to the bare airframe include a stability augmentation system (SAS), capable of providing suitable damping and natural frequencies, and a control augmentation system (CAS), providing the pilot with a particular type of response to control inputs [Stevens and Lewis, 2003]. These augmented control systems must satisfy stringent performance specifications throughout a large flight envelope, despite changes in aircraft dynamics that vary significantly across the entire flight envelope [Blue et al, 2002]. In order to provide the level of performance necessary throughout the entire flight envelope, a gain-scheduling system is used. The development of an aircraft gain-scheduled controller is a challenging task that requires significant amount of time and effort. The disturbance observer (DO) controller combines all the above systems into one simple controller, capable of producing the desired performance over a wide range of flight conditions.

The disturbance observer is a type of control system that contains both disturbance rejection capabilities and insensitivity to modeling errors [Ackermann, 2002]. Combining these two capabilities with a feedback system which specifies the desired dynamics can produce a "controller that „forces' the closed-loop dynamics to behave like the specified „desired dynamics' despite disturbances, modeling uncertainties, and variations in aircraft dynamics due to changing flight conditions" [Blue et al, 2002]. An example of a pitch axis DO controller designed by Blue et al is shown below.
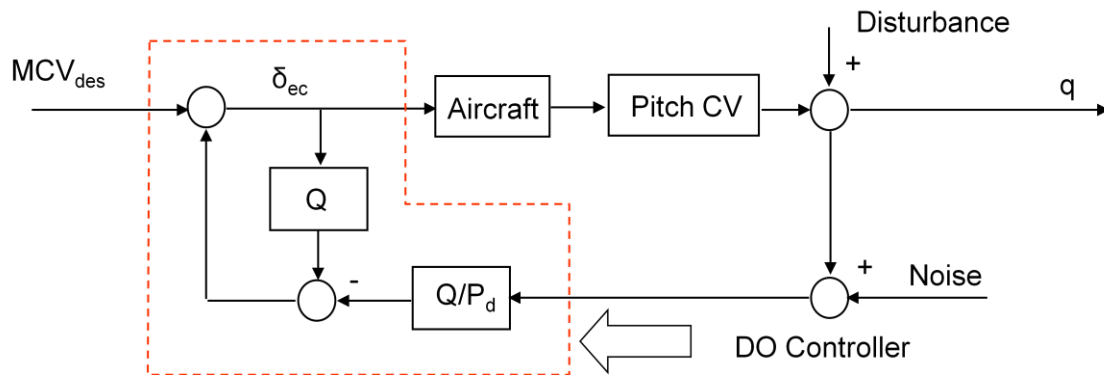
Figure 8. Pitch Axis Disturbance Observer Controller

Typically, the architecture of a DO includes a nominal plant model in the controller, to estimate disturbances; however, as implemented above, this DO architecture is used specifically to define the desired dynamics [Blue et al, 2002]. In this case, choosing pitch-rate (q) as the command variable (CV) allows the desired dynamics (P_d) to be chosen from the pitch-rate flying qualities specifications in MIL-STD-1797B. With the desired dynamics chosen, the design goal is to produce the following input-output relationship:

$$q = P_d MCV_{des} \tag{18}$$

Where the commanded pitch-rate input (MCV_{des}) and P_d combine to produce the desired

pitch-rate flying qualities in q.   In this case, δ_{ec} is defined as the desired elevator

command sent to the elevator actuator in order to obtain the desired pitch-rate. The filter,

Q, is the only remaining variable that is unknown and thus, it becomes the design

variable. The objective in designing the filter Q to ensure the pitch-rate command

provides the desired response despite changing flight conditions, disturbances, sensor

noise, and model uncertainty [Blue et al, 2002].

2.3.1 The Model and Desired Dynamics.

Before discussing the design of Q, the desired longitudinal dynamics and the

model development require some attention. As stated above, the desired dynamics were

chosen from MIL-STD-1797B in order to provide Level 1 pitch-rate command tracking

throughout the design flight envelope $h \in [5000; 25000]$ feet and $M \in [0.4; 0.8]$ [Blue

et al, 2002]. The pitch-rate flying qualities specifications taken from MIL-STD-1797B

are shown in Figure 9.
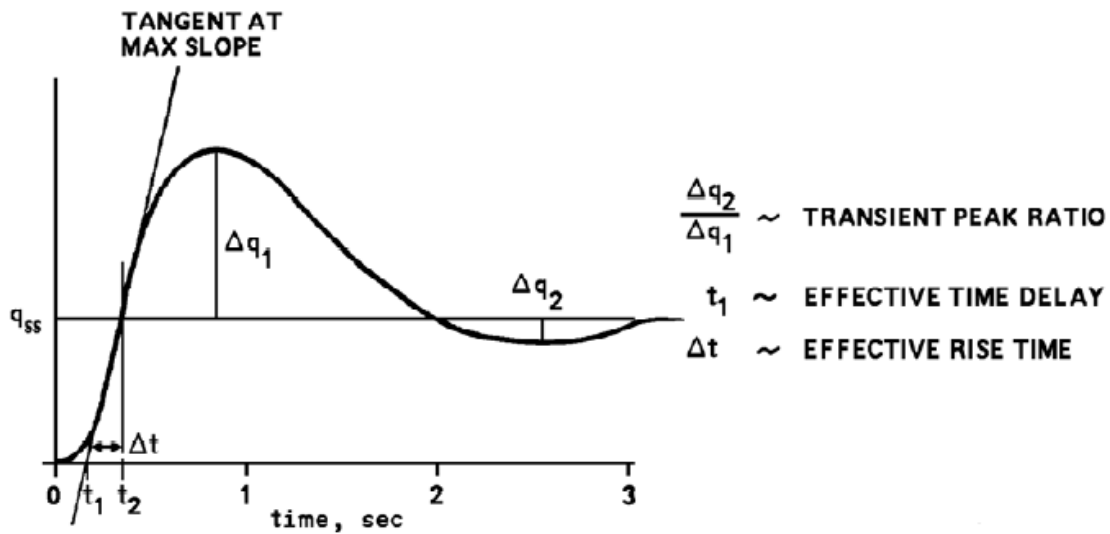
Figure 9. Pitch-Rate Response to Step Input of Pitch Controller

The characteristics of the pitch response specify an effective rise time, Δ_t, an effective time delay, t_1, and a transient peak ratio, $\frac{\Delta q_2}{\Delta q_1}$. The values of these specifications, shown in Table 1, are given ranges in which they must fall to guarantee Level 1 flying qualities.

Table 1. Pitch-Rate Response Characteristics to a Step Input

			Effective Rise Time*	
Level	Effective Time Delay	Transient Peak Ratio	Flight Phase Categories A and B	Flight Phase Category C
1	$t_1 \leq .12$ sec	TPR $\leq .3$	$9/V_T \leq \Delta t \leq 500/V_T$	$9/V_T \leq \Delta t \leq 200/V_T$
2	$t_1 \leq .17$ sec	TPR $\leq .6$	$3.2/V_T \leq \Delta t \leq 1600/V_T$	$3.2/V_T \leq \Delta t \leq 645/V_T$
3	$t_1 \leq .21$ sec	TPR $\leq .85$		

*V_T is true airspeed in ft/sec

27

With these ranges, a transfer function meeting the minimum requirements for Level 1

pitch-rate flying qualities can be chosen and implemented into the pitch axis DO design.

In the pitch-axis DO design, the aircraft model used contains the standard short

period equations of motion coupled with a first order approximation of the actuator

dynamics [Blue et al, 2002]. In the following short period equation, α is the angle-of-

attack, and δ_{ed} is the elevator deflection

$$\begin{bmatrix} \dot{\alpha} \\ \dot{q} \end{bmatrix} = \begin{bmatrix} Z_\alpha & 1 \\ M_\alpha & M_q \end{bmatrix} \begin{bmatrix} \alpha \\ q \end{bmatrix} + \begin{bmatrix} Z_{\delta e} \\ M_{\delta e} \end{bmatrix} \delta_{ed} \tag{19}$$

$$\delta_{ed} = G_a \delta_{ec} \tag{20}$$

$$G_a = \frac{20.2}{s + 20.2} \tag{21}$$

and G_a is the first order approximation of actuator dynamics. These equations form the

basis for the longitudinal aircraft model. The dimensional coefficients, Z_α, M_α, M_q, $Z_{\delta e}$,

and $M_{\delta e}$ depend mainly on altitude (h) and Mach number (M) at trimmed level flight

[Blue et al, 2002]. Therefore, with the proper data from the following flight conditions,

$$M = [0.35\ 0.45\ 0.55\ 0.65\ 0.75\ 0.85] \tag{22}$$

$$h = [1000\ 5000\ 15000\ 25000][ft] \tag{23}$$

these dimensional coefficients can be written as polynomial functions of h and M [Blue et

al, 2002].

$$G(h, M) = \begin{bmatrix} \dot{\alpha} \\ \dot{q} \end{bmatrix} = \begin{bmatrix} Z_\alpha(h, M) & 1 \\ M_\alpha(h, M) & M_q(h, M) \end{bmatrix} \begin{bmatrix} \alpha \\ q \end{bmatrix} + \begin{bmatrix} Z_{\delta e}(h, M) \\ M_{\delta e}(h, M) \end{bmatrix} \delta_{ed} \tag{24}$$

Combining this version of the short period dynamics with the actuator dynamics yields

the following model:

$$Aircraft = G(h, M) \cdot G_a \tag{25}$$

28

Even though this aircraft model accurately represents an aircraft's short period dynamics throughout the flight envelope $h \in [5000; 25000]$ feet and $M \in [0.4; 0.8]$, there are obvious modeling errors that exist when modeling longitudinal dynamics [Blue et al, 2002].

In an attempt to account for these modeling errors, Blue et al combine the aircraft model with a multiplicative uncertainty, $(1 + \Delta_m)$ to account for some of the existing uncertainties in the aircraft model.

$$Aircraft = G(h, M) \cdot G_a \cdot (1 + \Delta_m) \tag{26}$$

The multiplicative uncertainty can be broken down even further where $\Delta_m = W_u \cdot \Delta$, $\|\Delta\|_\infty < 1$ and W_u defines the frequency content of the uncertainty. Typically, W_u is small at low frequencies where the model represents the actual system fairly well (short period dynamics), and larger at high frequencies where model uncertainties increase [Ackermann, 2002]. In block diagram form, the multiplicative uncertainty is illustrated in figure 10 below.
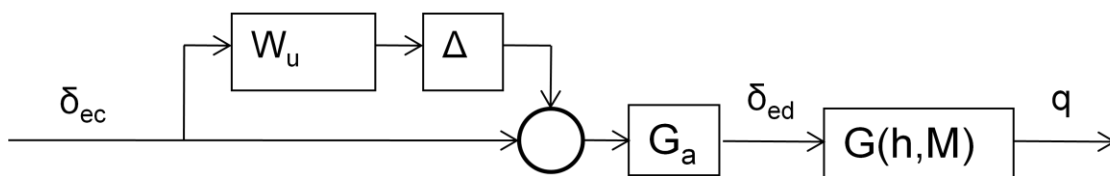
Figure 10. Multiplicative Uncertainty Block Diagram

The final adjustments to the model include adding a performance weight, W_p, and a command weight, W_{cmd} to the system. The performance weight and command weight come from guidance given in MIL-STD-1797B and are typical frequency ranges of a

pilot's command and the frequency range of desired model matching [Blue et al, 2002].
Figure 11 shows the finalized architecture that accounts for a range of modeling
uncertainties.
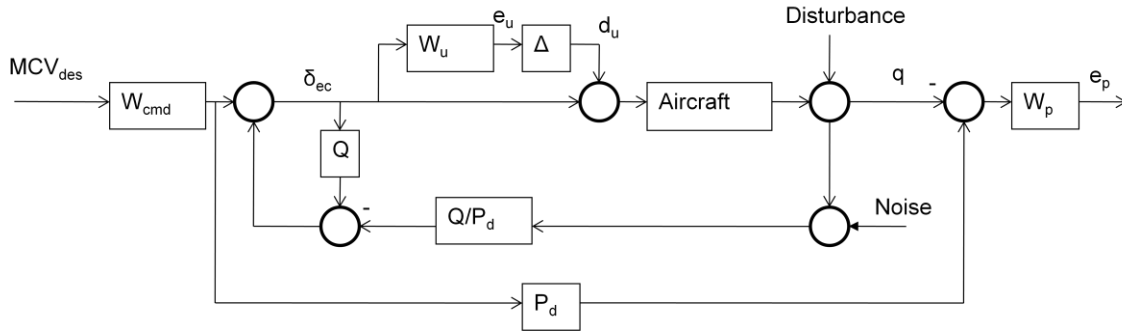
Figure 11. Pitch Axis Disturbance Observer Model and Controller

Now that the architecture is finalized and a certain range of modeling uncertainties are
accounted for, the design of the filter Q can be discussed.

2.3.2 The Filter Q.

Using the methods of H_∞ parameter space control design, the filter Q can be
designed to provide Robust Stability and Nominal Performance. But first, taking a look
at the input-output transfer functions associated with the proposed architecture provides
insight about Q and the expected characteristics of the closed-loop system [Blue et al,
2002]. In order to simplify the analysis, the initial architecture proposed in figure 8, prior
to the addition of the multiplicative uncertainty, command weight and performance
weight will be used.

With this architecture, the transfer function containing the loop gain L

$$L(h, M) = \frac{Q}{1-Q} \frac{G(h, M) \cdot G_a}{P_d} \tag{27}$$

is useful when checking the stability of the closed loop system and will be addressed

momentarily. As far as the input-output relations go, the first transfer function of interest

is the tracking transfer function H.

$$H(h, M) = \frac{q}{MCV_{des}} = \frac{P_d \cdot G(h, M) \cdot G_a}{P_d \cdot (1-Q) + G(h, M) \cdot G_a \cdot Q} \tag{28}$$

Looking specifically at Q with a unity gain in the low frequency range, yields the desired

input-output design objective as $\frac{q}{MCV_{des}} \longrightarrow P_d$. The second transfer function is the

disturbance rejection transfer function S with the following form:

$$S(h, M) = \frac{q}{d} = \frac{P_d \cdot (1-Q)}{P_d \cdot (1-Q) + G(h, M) \cdot G_a \cdot Q} \tag{29}$$

with d as the disturbance. Again, looking at Q with a unity gain in the low frequency

region indicates that good disturbance rejection is achieved as $\frac{q}{d} \longrightarrow 0$. The third transfer

function is the sensor noise rejection transfer function T and has the following form:

$$T(h, M) = \frac{q}{n} = \frac{-G(h, M) \cdot G_a \cdot Q}{P_d \cdot (1-Q) + G(h, M) \cdot G_a \cdot Q} \tag{30}$$

with n as the noise. This time it is evident that Q, in the high frequency region ($Q \rightarrow 0$),

provides the desired noise rejection as $\frac{q}{n} \longrightarrow 0$. The final input output relationship is

simply the performance error transfer function of the following form:

$$E(h, M) = P_d - H(h, M) \tag{31}$$

Looking at the error transfer function in conjunction with the tracking transfer function indicates that Q needs to be a low pass filter with a unity gain which will drive the error to zero at low frequencies.

Now, knowing the form of Q to be a low pass filter of unity gain, we can proceed with the H$_\infty$ parameter space control design. It is imperative that for $\frac{Q}{P_d}$ to be realizable, Q must have at least the same degree as P_d [Ackermann, 2002]. Assuming that P_d is a second order transfer function Q would have the following form

$$Q = \frac{\omega_Q^2}{s^2 + 2\zeta_Q \omega_Q s + \omega_Q^2} \tag{32}$$

with the design parameters ω_Q and ζ_Q. Using the H$_\infty$ parameter space methods, the variables ω_Q and ζ_Q are mapped into a plane of feasible solutions which are bounded by stability and performance conditions [Blue et al, 2002]. Using the finalized architecture, which contains the added uncertainties and weights, the following mapping conditions are used to guarantee Hurwitz and Robust Stability as well as Nominal Performance.

$$Roots\left(p_{ce}(h, M, \omega_Q, \zeta_Q)\right) \subset \mathbb{C}^- \qquad (Hurwitz\ Stability) \tag{33}$$

$$\left\|W_u \cdot T(h, M, \omega_Q, \zeta_Q)\right\|_\infty \leq 1 \qquad (Robust\ Stability) \tag{34}$$

$$\left\|W_p \cdot E(h, M, \omega_Q, \zeta_Q) \cdot W_{cmd}\right\|_\infty \leq 1 \qquad (Nominal\ Performance) \tag{35}$$

Hurwitz Stability simply implies that the poles of the characteristic equation are all in the left half plane. The roots of the characteristic equation contain the loop gain and can be found using $P_{ce}(h, M, \omega_Q, \zeta_Q) = numerator\left(1 + L(h, M, \omega_Q, \zeta_Q)\right)$. Robust Stability bounds the solution space by including the multiplicative uncertainties that account for

modeling inaccuracies. Finally, Nominal Performance bounds the plane of feasible solutions by ensuring that both the command and performance characteristics fall within the desired frequency range. The areas where all three parameter space conditions are met indicate the feasible region for variables ω_Q and ζ_Q, resulting in a filter Q with Robust Stability and Nominal Performance.

2.4 Simultaneous Linear Equations

Solving a set of simultaneous linear algebraic equations is often used in conjunction with matrix operations to simplify both the annotation and computer computation. The matrix form of a linear system of equations is $\boldsymbol{Ax} = \boldsymbol{b}$, where $\mathbf{A}$ is a matrix of known coefficients corresponding to the vector of unknowns in $\mathbf{x}$ and $\mathbf{b}$ is a vector of known constants. When it comes to the solution of $\boldsymbol{Ax} = \boldsymbol{b}$, there can be one unique solution, an infinite number of solutions, or no solution [Brogan, 1991]. In order to determine what type of solution exists, an analysis on an augmented matrix defined by $\boldsymbol{W} = [\boldsymbol{A}|\boldsymbol{b}]$ can be conducted. Comparing the rank of $\mathbf{A}$ (r_A) with the rank of $\mathbf{W}$ (r_W) indicates whether or not solutions exist [Brogan, 1991]. If $r_W \neq r_A$, then no solution exists. Likewise if $r_W = r_A$, then at least one solution exists. In an underdetermined case, the $\mathbf{A}$ matrix has more rows (m) than columns (n) and $r_W = r_A < n$ indicating an infinite number of solutions. On the contrary, when $r_W = r_A = n$, one unique solution exists. Or put another way, when the matrix $\mathbf{A}$ is square and nonsingular, the set of linear equations has one unique solution [Wylie, 1960]. The most common solution method involves the use of matrix inversion and takes the form $\boldsymbol{x} = \boldsymbol{A}^{-1}\boldsymbol{b}$.

2.4.1 Least Squares Solution to the Over-determined Case.

The over-determined case exists when there are more equations than unknowns. No solution will exist if the equations are inconsistent. Inconsistent equations arise due to inaccuracies in the measurements of **b,** or inaccurate assumed relationships between **x** and **b** expressed through **A** [Brogan, 1991]. In this case, an approximate solution to the vector **x** is the desired method. The least squares approach provides an estimate of **x** by placing an equal weighting on all equations and assumes that the errors will average out. In the over-determined case, no one **x** can satisfy all simultaneous equations. Therefore, the error vector **e**, now joins the linear system of equations in the form $e = Ax - b$. The goal of the least squares estimate is to minimize the sum of the squares of the e_i components [Brogan, 1991]. In other words, **x** is estimated in order to minimize

$$\|e\|^2 = e^T e = (b - Ax)^T (b - Ax) \tag{36}$$

The solution to the least squares estimate can be found by formulating the following optimization problem written in standard form:

$$\min_x \|x\|^2 \rightarrow \min_x \frac{1}{2} x^T x \tag{37}$$

Subject to:

$$h(x) = Ax - b = 0 \tag{38}$$

With a slight change of variables ($\|x\|^2 \ for \ \|e\|^2$), the problem can be formulated to find the **x** that makes the constraint $Ax - b = 0$ true. If no **x** exists to satisfy the constraint, the minimization problem will find the **x** that makes $Ax - b$ as close to zero as possible.

If a minimum does exist, the following gradient conditions must be satisfied from the

Lagrangian, $L(x, v) = \frac{1}{2}x^T x + v^T(Ax - b)$:

$$L_x(x^*, v^*) = x^T + v^T A = 0 \quad \rightarrow \quad x = -A^T v \tag{39}$$

$$L_v(x^*, v^*) = Ax - b = 0 \tag{40}$$

where L_x and L_v are partial derivatives of $L(x, v)$ and v is a Lagrange multiplier.

Combining equations 39 and 40 yields:

$$v = -(AA^T)^{-1}b \tag{41}$$

Then, inserting equation 41 into 39 provides the solution to the minimization problem

$\min_x \|x\|^2$ which really describes how $\|e\|^2$ can be minimized by **x**.

$$x = A^T(AA^T)^{-1}b = (A^T A)^{-1}A^T b \tag{42}$$

2.4.2 Weighted Least Squares.

A weighted least squares approximation starts with equation 36 and continues to

use all equations, but instead of equal weighting to all equations, a covariance matrix **R** is

used to place weights on more reliable ones. The covariance matrix represents the noise

on the vector **b** [Brogan, 1991], and **x** minimizes the relationship

$$e^T R^{-1} e = (b - Ax)^T R^{-1}(b - Ax) \tag{43}$$

Applying the method of orthogonal projections yields the weighted least squares solution

shown below [Brogan, 1991]:

$$x = (A^T R^{-1} A)^{-1} A^T R^{-1} b \tag{44}$$

2.4.3 Recursive Weighted Least Squares.

The least squares and weighted least squares process use batch processing to process all data equations in one batch. The recursive weighted least squares process uses each new set of data as it is received [Brogan, 1991]. For example, assume a set of m measurements

$$z_k = Ax + e \tag{45}$$

were used to solve for a weighted least squares estimate of **x**. The solution **x** to the weighted least squares estimate is the same solution described above. However, with the addition of a new set of data, the previous solution becomes

$$x_k = (A^T R^{-1} A)^{-1} A^T R^{-1} z_k \tag{46}$$

and the new set of data becomes

$$z_{k+1} = H_{k+1} x + e_{k+1} \tag{47}$$

Where H_{k+1} is synonymous with the **A** matrix but corresponds to z_{k+1}. Combining the old and new data together, a new estimate of **x**, labeled x_{k+1}, can be obtained which minimizes

$$J = \begin{bmatrix} e^T & e_{k+1}^T \end{bmatrix} \begin{bmatrix} R^{-1} & 0 \\ 0 & R_{k+1}^{-1} \end{bmatrix} \begin{bmatrix} e \\ e_{k+1} \end{bmatrix} \tag{48}$$

Where R_{k+1}^{-1} is equivalent to R^{-1} but applied to the new data z_{k+1}. The solution incorporating the new data is of the form

$$x_{k+1} = x_k + K_{k+1} [z_{k+1} - H_{k+1} x_k] \tag{49}$$

36

Where $K_{k+1} = P_k H_{k+1}^T [H_{k+1} P_k H_{k+1}^T + R_{k+1}]^{-1}$ and $P_k \triangleq (A^T R^{-1} A)^{-1}$ which is

available from x_k. If another set of data is used, the process can be continued on a

recursive basis with the addition of

$$P_{k+1} = P_k - K_{k+1} H_{k+1} P_k \tag{50}$$

to finish the process [Brogan, 1991].

2.4.4 Discrete Kalman Filter.

A simple discrete Kalman filter is an extension to the recursive weighted least

squares. When data is received over a long period of time, one of the problems with a

recursive weighted least squares estimation is that P_{k+1} gets very small. This in turn

causes the new Kalman gain, K_k, to become small as well. When this happens,

corrections made to x_k in order to determine x_{k+1} become small and the filter fails to

respond to new data [Brogan, 1991]. In order to fix this problem, data de-weighting is

used. Additive data de-weighting prevents the **P** matrix from getting too small and is of

the form

$$M_k = P_k + Q \cdot \Delta t \tag{51}$$

where **Q** is a positive definite matrix and Δt is the time step between samples. The time

step between samples accounts for the discritization of the Kalman filter which enables

the filtering of digital signals. The presence of additive de-weighting is felt in the

Kalman gain shown below:

$$K_{k+1} = M_k H_{k+1}^T [H_{k+1} M_k H_{k+1}^T + R_{k+1}]^{-1} \tag{52}$$

Combining this with equation 50 and substituting M_k for P_k yields

$$P_{k+1} = M_k - M_k H_{k+1}^T [H_{k+1} M_k H_{k+1}^T + R_{k+1}]^{-1} H_{k+1} M_k \qquad (53)$$

and completes the last step in a discrete Kalman filter process.

The bare essentials for creating a Kalman filter include knowledge (model) of system dynamics, initial conditions (estimated or actual), measurement characteristics, and statistical descriptions of uncertainties, noises, and measurement errors [Maybeck, 1982]. The recursive steps above are an example of a discrete Kalman filter when **P**, **Q**, and **R**, are given the appropriate statistical interpretation [Brogan, 1991]. Kalman filters are used extensively in modern control theory to estimate variables of a linear system with noisy measurements [Brogan, 1991]. The noise is assumed to be white (not time dependent) and Gaussian (probability density at any point in time is bell-shaped). The types of models used to estimate system dynamics are error and perturbation models [Maybeck, 1982].

When system dynamics are represented more appropriately by a nonlinear model, an extended Kalman filter may be used [Maybeck, 1982]. By substituting the nonlinear **h** for the linear **H** in equation 47,

$$z_{k+1} = h_{k+1}(x) + e_{k+1} \qquad (54)$$

and taking the Jacobian of z_{K+1} with respect to **x**, yields

$$\frac{\partial z_{k+1}}{\partial x} = [\widetilde{H}_{k+1}](x) + e_{k+1} \qquad (55)$$

which can be used to provide a perturbation measurement model [Maybeck, 1982]. In this case, $\widetilde{H}_{k+1} = \frac{\partial h_{k+1}(x)}{\partial x}$, and provides a linear relationship between the measurements, **z**, and the state to be estimated, **x** [Kayton and Fired, 1997]. With this, the extended

38

Kalman filter also requires an update to x_{k+1} (equation 49) as shown below [Maybeck, 1982]:

$$x_{k+1} = x_k + K_k \left[z_{k+1} - h_{k+1} - \tilde{H}_{k+1} x_k \right] \tag{56}$$

2.4.5 Statistical Analysis of Kalman Filters.

The estimates produced from Kalman filters can vary based on many uncertainties. Therefore, to truly determine the overall performance of a Kalman filter, it is recommended that an ensemble average of many runs (15-25 are typical for aerospace applications) be accomplished [Maybeck, 1982]. An ensemble average is the average of each data point correlating to a specific time over all runs. With an ensemble average calculated, a temporal average (single average over entire runtime) can be used to obtain a single value that attempts to describe the performance of a filter. Standard deviations can also be used to help determine how well the filter is tuned. The "ability to provide a realistic performance evaluation of a proposed filter design is an integral part of the iterative design process" and is essential when tuning a Kalman filter [Maybeck, 1982]. Ultimately, the primary objective of analyzing Kalman filter data is to tune the filter such that it yields the best estimation performance possible.

2.5 Cooper-Harper Ratings and Pilot-Induced Oscillation Ratings

Pilot opinion of aircraft performance is an essential part of aircraft design and testing. Together, the pilot and aircraft form a system which must perform at an adequate level in order to complete the mission. Since the pilot is ultimately responsible for

mission accomplishment, his/her opinion matters [Liebst, Summer Quarter 2007]. A pilot's opinion on how an airplane flies is still the best source of information [Hodgkinson, 1999]. This information is best categorized using the Cooper-Harper Handling Qualities Rating Scale.

The Cooper-Harper (CH) scale is universally used to enable the pilot to award a number corresponding to how an aircraft handles. The goal of this number is to make comparisons between aircraft and/or to show compliance with a specific handling task. Handling tasks are flown under various conditions in order to determine the Handling Qualities of an aircraft. Handling Qualities are those qualities or characteristics that govern the ease and precision with which a pilot is able to perform the tasks required in support of the aircraft mission [Cooper-Harper, 1989]. An example of the Cooper-Harper Handling Qualities Rating Scale is illustrated in Figure 12.
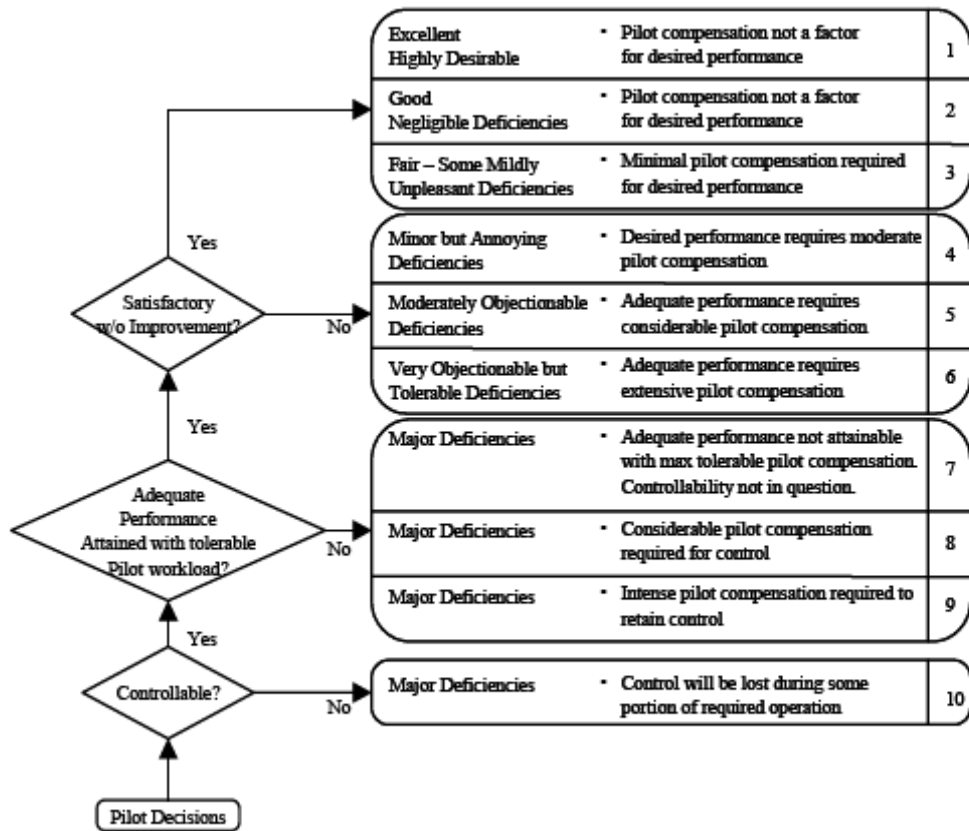
Figure 12. Cooper-Harper Handling Qualities Rating Scale

The CH scale has ten points ranging from 1 (best) to 10 (worst). Evaluation Pilots arrive at one of these points by answering a series of questions regarding task performance and pilot workload. Even though the CH scale improves repeatability by leading the pilot through a series of decisions, it is still not perfect.

This imperfection is brought about by the nature of humanity. Human opinions can vary based on subtle changes in pilot behavior, pilot distractions, fatigue, and a host of other poorly-understood, interacting factors [Hodgkinson, 1999]. In an attempt to mitigate these factors, Bailey recommends the following format for evaluation:

1. Perform the task
2. Comment extemporaneously during the task
3. Assign an initial rating using the Cooper-Harper decision tree
4. Give detailed comments using the provided comment card
5. Give the formal rating: then the quantitative performance is revealed to the pilot.

Using this method does not guarantee reliable and repeatable results but it does take steps towards mitigating the risk of scattered CH ratings. Even so, the most important information gathered during a handling qualities task evaluation is not the CH rating itself, but the pilot comments associated with the CH rating.

Another scale used to assess the flying qualities problems that arise is the Pilot-in-the-Loop Oscillation (PIO) scale.
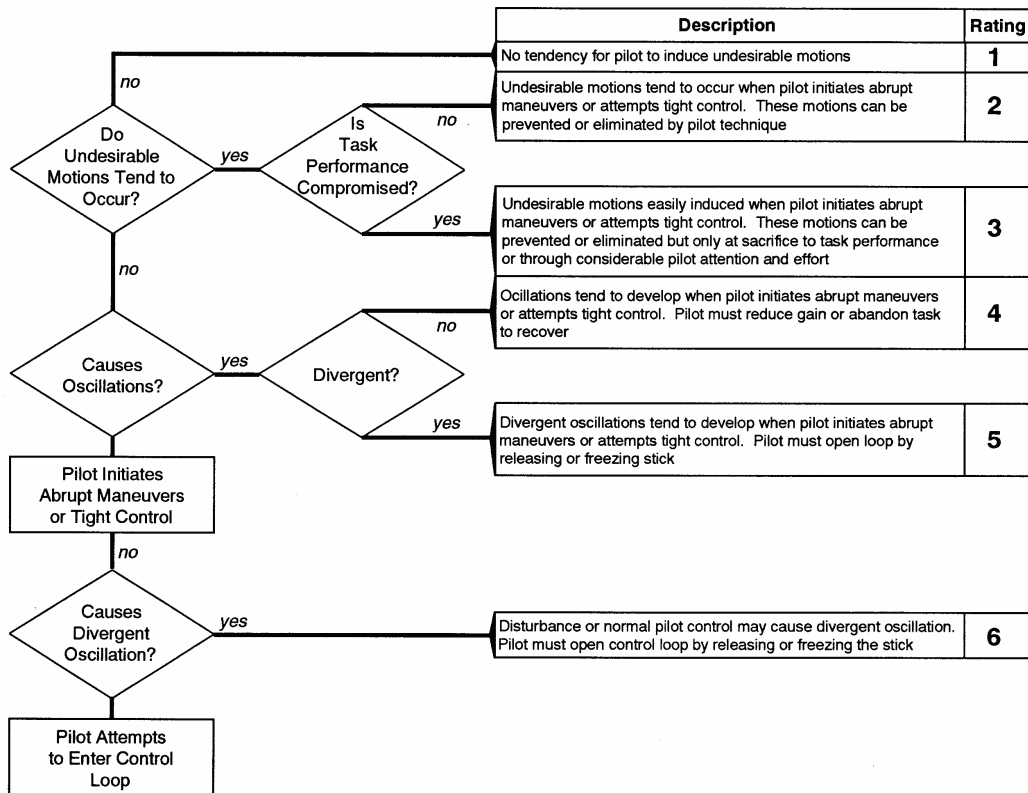
Figure 13. Pilot-in-the-Loop Oscillation Scale

This scale, similar in design to the CH scale, helps identify the flying qualities problems that cause PIOs [Hodgkinson, 1999]. PIOs are unintentional sustained oscillations that result from the efforts of a pilot to control the aircraft. PIOs are most often associated with "high-gain tasks" (challenging tasks) or events that cause a pilot to suddenly and dramatically increase his/her gain [Leggett, 2007]. A combination of increased pilot gain and phase lags associated with modern fly-by-wire control systems or actuator rate limits are some of the key ingredients making aircraft prone to PIOs.

Because the pilot opinion matters, the Pilot-in-the-Loop Oscillation scale and the Cooper-Harper Handling Qualities Rating Scale will be around as long as pilots are controlling aircraft. Combining the PIO scale and the CH Handling Qualities Rating scale gives valuable pilot feedback on aircraft performance and handling qualities that cannot be ignored.

2.6 Summary

This chapter presented the technical and mathematical background material necessary for understanding the development of each standby-gain-scheduling method presented in Chapter 3. The development of the alternative methods to standby-gain-scheduling will build upon the basic concepts, terminologies and aircraft systems presented in this chapter.

3.0. Methodology

3.1 Chapter Overview

The purpose of this chapter is to describe the test methodology, explain the controller development process and present initial desktop simulation results for each standby-gain-scheduled controller. The test methodology for the entire thesis used a build-up approach that progressed through desktop simulation, transitioned to high-fidelity simulation in the Infinity Cube, and ended with the post-processing of actual aircraft data (for VEST 2 only). The controller development built upon the basic fundamentals described in Chapter 2 to develop each of the alternative methods of standby-gain-scheduling control (velocity estimation control, inertial velocity control and disturbance observer control). Initial desktop testing was accomplished to prepare the standby-gain controllers for the Infinity Cube simulator testing. The preliminary results from computer desktop simulations along with a detailed explanation of each standby-gain-scheduled controller are presented in the individual controller sections of this chapter.

3.2 Test Methodology

In general, the test methodology utilized a build-up approach that began with desktop simulation; transitioned to pilot-in-the-loop desktop simulation; and culminated with a high-fidelity, pilot-in-the-loop simulation in the Infinity Cube simulator at Air Force Research Laboratory/RBCD facility. Initial desktop computer simulations were

run to verify the DO and VEST 2 method of control. The velocity estimation algorithms were tested using a point mass model to down select methods of estimation. Then the velocity estimator algorithms were tested using a six-degree-of-freedom, Stevens and Lewis, non-linear F-16 model in conjunction with the Aviation Visual Design Simulator (AVDS) to provide a pilot-in-the-loop desktop simulator [Rasmussen Simulation Technologies, 2006]. The disturbance observer controller also used AVDS in conjunction with the Stevens and Lewis model to obtain a first-look at the DO controllers handling qualities. These test prepared the velocity estimator algorithm controller and the DO controller for implementation and follow-on simulator testing conducted in the Infinity Cube simulator at the Air Force Research Laboratory/RBCD building. In the Infinity Cube simulator, the inertial controller was also implemented so that each of the alternatives to standby-gain-scheduling (velocity estimation control, inertial velocity control, and disturbance observer control) could be compared with a baseline block 40 F-16C controller. In addition to simulator testing, actual aircraft data were post-processed with the VEST 2 algorithm to validate the simulator results for the velocity estimator algorithm. The development of each method of standby-gain-scheduling control and the results of the initial desktop simulation are presented in this chapter. The results of the Infinity Cube simulator testing and the VEST 2 validation are presented in Chapter 4.

3.3 Gain-Scheduling with Estimated Airspeed

The first method of standby-gain-scheduling uses estimated velocity to calculate the dynamic pressure used to schedule gains. Following an air data system failure, the velocity estimating algorithm (VEST 2), which is a modified version of the McLaren's

velocity estimator (VEST) [McLaren, 2008], uses the remaining available data to estimate velocity. The estimated airspeed controller uses a geometric relationship between inertial velocities, wind and true airspeed combined in an algorithm that provides estimates of current wind and true airspeed. Various geometric relationships were explored in order to determine the best method for estimating velocity.

3.3.1 Three Vector Approach.

The three vector method combines the velocity triangles associated with three separate measured groundspeed velocity vectors into the figure below [Gray, 1998].
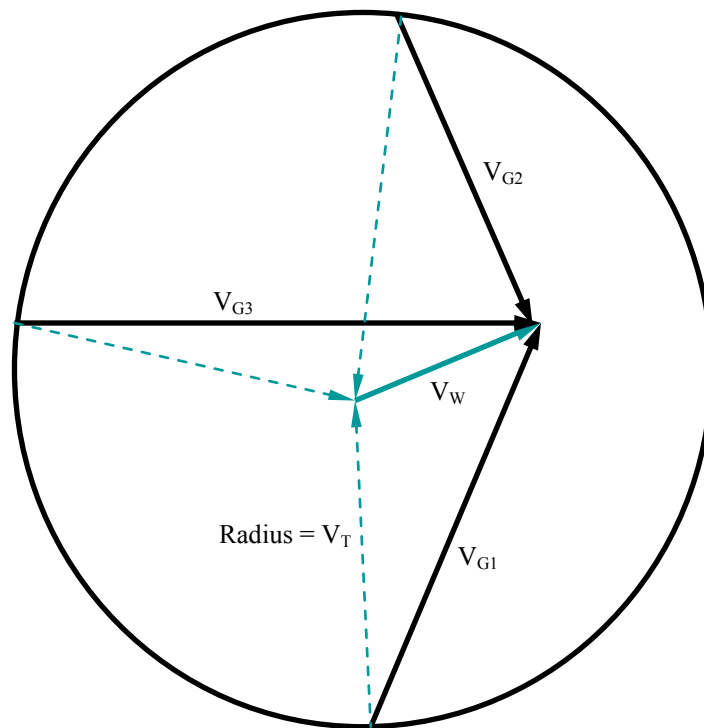
Figure 14. Three Vector Velocity Triangle

With the head of each groundspeed vector superimposed at a single point, the tails all lie on a circle with a radius equivalent to the TAS. The wind vector completes the three

velocity triangles by connecting the TAS vector at the center of the circle with the tips of

the ground speed vector [Gray, 1998]. This relationship holds when all three recorded

ground speed vectors meet the following constraints: heading stabilized; same true

airspeed and altitude; same throttle setting; and no sideslip. The final assumption, critical

to this geometric analysis, is that the wind vector is constant. This allows the wind vector

to be shared by all three velocity triangles.

With this relationship and at least three measured ground velocity vectors, the

equation for a circle can be used in a least squares process to estimate the north and east

components of true and wind speed [McLaren 2008]. Together, these components make

up the horizontal component of the true velocity vector and wind vector. Extending this

process to the third dimension allows for the calculation of the complete true and wind

velocity vectors. In this case, the equation of a sphere

$$(x_i - x_c)^2 + (y_i - y_c)^2 + (z_i - z_c)^2 = R^2 \qquad (57)$$

combined with the batch processing power of a least squares estimator can be used to

estimate the north, east, and down components of TAS and wind speed. If the origin of

the coordinate system associated with the sphere is located at the tip of the ground

velocity vectors and the tail is described by (x_i, y_i, z_i) where $i = [1 \dots n]$ defines the

number of ground velocity vector samples, and the center of the sphere is defined by

(x_c, y_c, z_c), then R can be estimated to find the sphere of best fit to the ground velocity

vectors. When the sphere equation is expanded out and grouped to isolate knowns and

unknowns you get

$$
\underbrace{[(-2x_i)\ (-2y_i)\ (-2z_i)\ (1)]}_{A}
\underbrace{\begin{bmatrix} x_c \\ y_c \\ z_c \\ x_c^2 + y_c^2 + z_c^2 - R^2 \end{bmatrix}}_{x}
= \underbrace{[-(x_i^2 + y_i^2 + z_i^2)]}_{b} \quad (58)
$$

.

When implemented in a least squares batch process, **A** becomes known coefficient

matrix, **b** is a vector of measurements, and **x** is the vector of unknowns. The solution to

this problem as described in section 2.4.1 has the following form

$$
x = (A^T A)^{-1} A^T b \tag{59}
$$

which yields estimated values of **x** that minimize the error in fitting a sphere to ground

velocity vectors. Finally, from **x**, all components of wind speed and TAS can be

calculated using the velocity triangle relationship.

3.3.2 Two Vector Approach.

Another method used to estimate velocity is a subset of the three vector method

that uses two ground vectors and two aircraft heading measurements [McLaren, 2008].

This method was designed to eliminate the constant true airspeed constraint [McLaren,

2008], a necessary step when talking about a modern-day advanced fighter flight

envelope. This method uses aircraft headings from true north and inertial velocities

available from the onboard INS. When combined together, as in the three vector case,

the following geometry results.
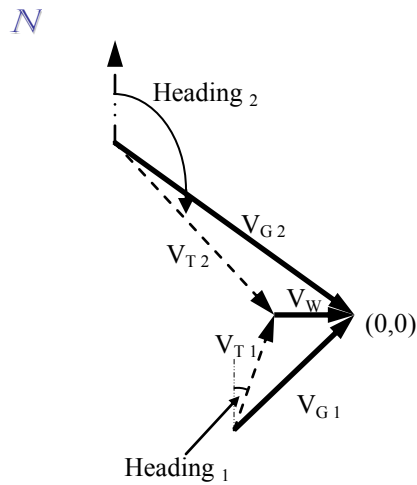
Figure 15. Two Vector Velocity Triangle

Input headings define the direction from the tails of the ground velocity vector to the true velocity vectors, and the heads of the true velocity vectors intersect at the tail of the wind vector. As aforementioned, the largest constraint was removed by eliminating the need to have TAS be constant. However, this methodology does have a limitation in that it assumes there is no vertical component of wind. This assumption yields a two dimensional solution by equating the down component of true airspeed to the down component of inertial airspeed. Realistically, this is not a bad assumption as the majority of winds run parallel to the surface of the earth.

The solution to the two vector approach is developed from the figure 16.
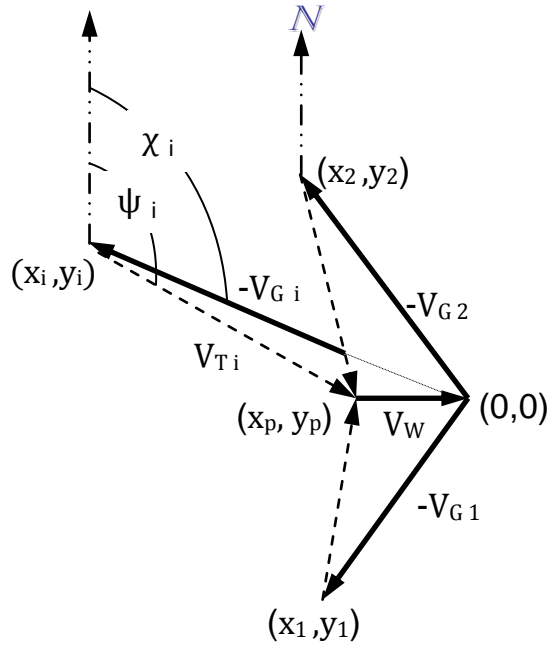
Figure 16. Sampled Two Vector Approach

The point (x_p, y_p) is located at the intersection of the true airspeed vectors. The tails of

the ground velocity vector define the points (x_1, y_1) and (x_2, y_2) respectively. If more

ground velocity vectors were available, the process would continue with additional input

angles and ground velocity vectors.

A least squares approach similar to the three vector approach was developed by

McLaren and is formed from the following equations:

$$\tan(\psi_i) = \frac{(x_p - x_i)}{(y_p - y_i)} \tag{60}$$

$$x_i = V_{G_i} \sin(\chi_i + \pi) \tag{61}$$

$$y_i = V_{G_i} \cos(\chi_i + \pi) \tag{62}$$

51

where ψ_i is the heading from true north to the true velocity vector, and χ_i is the heading from true north to each ground velocity vector. Using a few substitutions and equation manipulations, the final relationship can be put in terms of knowns and unknowns.

$$\tan(\psi_i)y_p - x_p = \tan(\psi_i)V_{G_i}\cos(\chi_i + \pi) - V_{G_i}\sin(\chi_i + \pi) \qquad (63)$$

Written in the form $\boldsymbol{Ax} = \boldsymbol{b}$ yields

$$[\tan(\psi_i) - 1]\begin{bmatrix} y_p \\ x_p \end{bmatrix} = \boldsymbol{b}_i \qquad (64)$$

where $\boldsymbol{b} = \tan(\psi_i)V_{G_i}\cos(\chi_i + \pi) - V_{G_i}\sin(\chi_i + \pi)$. Using the solution to the least squares approximation, $\boldsymbol{x} = (\boldsymbol{A}^T\boldsymbol{A})^{-1}\boldsymbol{A}^T\boldsymbol{b}$, provides an estimate of the horizontal wind speed components. Using this estimate with the known ground velocity vectors and assuming no wind speed in the vertical, the velocity triangles provide the relationship from which to estimate the components of true airspeed.

3.3.3 Kalman Filter Approach.

A recursive weighted least squares Kalman filter, as described in section 2.4.3, was integrated in both the two vector [McLaren, 2008] and three vector methods so a comparison could be drawn between their velocity estimation capabilities. The process by which both methods were integrated into a Kalman filter will be shown below and then some preliminary results obtained from a desktop simulation will be discussed.

As stated in the two vector method, the estimated values are the north and east components of wind speed. Defining these states in terms of the Kalman filter process, leads to the following estimated state vector, $\boldsymbol{x}_k = \begin{bmatrix} V_{W_n} \\ V_{W_e} \end{bmatrix}$. Recall from the development of the two vector method that the heading from true north to the velocity vector, and the

north (V_{G_n}) and east (V_{G_e}) ground speed components were known or derived from measured quantities. In terms of the Kalman filter, these are the known inputs. The heading of the true airspeed vector, considered the measurement, is derived from measured and estimated quantities as follows:

$$h_k = \tan^{-1}\left(\frac{V_{ture_e}}{V_{ture_n}}\right) = \tan^{-1}\left(\frac{V_{G_e} - V_{w_e}}{V_{G_n} - V_{w_n}}\right) \tag{65}$$

The measured inertial heading from the INS measures heading from true north to the body fixed frame x-axis. During turns, this measurement is slightly different from the heading of the true velocity vector. The quantity $\cos(\theta)\left[\sin(\phi)\alpha - \beta\right]$ accounts for this difference by accounting for the sideslip, roll, and bank encountered during turns [McLaren, 2008]. When this term is included, the measurement now becomes

$$h_k = \tan^{-1}\left(\frac{V_{G_e} - V_{w_e}}{V_{G_n} - V_{w_n}}\right) + \cos(\theta)\left[\sin(\phi)\alpha - \beta\right] \tag{66}$$

which represents the measured heading from true north to the true velocity vector. Incorporating this measurement into the Kalman filter yields

$$z_{k+1} = h_{k+1}(x_1, x_2) + e_{k+1}$$

$$= \tan^{-1}\left(\frac{V_{G_e} - V_{w_e}}{V_{G_n} - V_{w_n}}\right) + \cos(\theta)\left[\sin(\phi)\alpha - \beta\right] + e_{k+1} \tag{67}$$

where $h(x)$ is a nonlinear perturbation measurement model. In order to account for the non-linearities in the measurement model, the recursive weighted least squares Kalman filter now becomes an extended (discrete) Kalman filter. Recalling from section 2.4.4, H is used to define the linear relationship between the measurements, z, and the state to be estimated, x [Kayton and Fired, 1997]. This relationship defines H as

$$H_k = \frac{\partial h}{\partial x} = \left[\frac{\partial h}{\partial V_{W_n}}, \frac{\partial h}{\partial V_{W_e}}\right] \tag{68}$$

and is the last relationship needed to complete the extended Kalman filter process.

Finally, because $h(x)$ is a perturbation model, the states' initial conditions must also be in the form of perturbations. Assuming a linear lapse rate of winds ($a = \frac{3.3}{1000} \frac{knots}{feet}$) with respect to an aircraft's change in altitude [McLaren, 2008], provides a simple model of the form

$$x_k = \begin{bmatrix} \Delta V_{W_n} \\ \Delta V_{W_e} \end{bmatrix} = \left[\frac{a}{\sqrt{V_{W_n}^2 + V_{W_e}^2}}\right]\begin{bmatrix} V_{W_n} \\ V_{W_e} \end{bmatrix} \tag{69}$$

and gives estimated initial conditions in the form of deltas. The remainder of the process is the same as defined in section 2.4.4 and is listed below:

$$M_k = P_k + Q \cdot \Delta t \tag{70}$$

$$x_{k+1} = x_k + K_k[z_{K+1} - h_{k+1} - H_{k+1}x_k] \tag{71}$$

$$P_{k+1} = M_k - M_k H_{k+1}^T [H_{k+1} M_k H_{k+1}^T + R_{k+1}]^{-1} H_{k+1} M_k \tag{72}$$

For this problem, **P** is the error covariance matrix, **Q** is the growth in the wind estimate uncertainty, and **R** is the noise on the input heading measurement. This extended Kalman filter continuously estimates V_{W_n} and V_{W_e} with each new measurement taken. Then, using the velocity triangle relationship, the true velocity vector is computed in the same manner as the two vector least squares estimate. With the exception of an adjustment to the wind lapse rate, the Kalman filter above is the velocity estimator, VEST, developed by McLaren.

One of the weaknesses of the VEST algorithm is its dependence on aircraft heading. First, VEST must have an accurate method for obtaining heading measurements. This is not a problem with a GPS aided INS described in section 2.2.6. The second limitation is that VEST must have heading changes in order to accurately estimate the wind velocity vector. VEST is also dependent upon alpha and beta, which is typically obtained through the Pitot static system. Finally, in order to keep VEST from failing to respond to changing wind conditions, it becomes extremely sensitive to high-g rapid onset maneuvers.

In an attempt to improve upon the limitations of VEST, a Kalman filter version of the three vector method is presented below. The advantages of the three vector method include no heading measurements required, vertical component of wind is not assumed zero, INS measurements required for estimation are readily available, and there are no Pitot static system dependent variables required for estimation.

Starting with the three vector relationship, the estimated state

$$
\boldsymbol{x}_k = \begin{bmatrix} V_{W_n} \\ V_{W_e} \\ V_{W_d} \\ V_{W_n}^2 + V_{W_e}^2 + V_{W_d}^2 - V_{true}^2 \end{bmatrix} \tag{73}
$$

is comprised of interrelated components of wind speed and true airspeed magnitude. The states are then estimated from the following relationship previously developed in section 2.4.4:

$$
\boldsymbol{h}_k = \begin{bmatrix} \left(-2V_{G_n}\right) & \left(-2V_{G_e}\right) & \left(-2V_{G_d}\right) & (1) \end{bmatrix} \begin{bmatrix} V_{W_n} \\ V_{W_e} \\ V_{W_d} \\ V_{W_n}^2 + V_{W_e}^2 + V_{W_d}^2 - V_{true}^2 \end{bmatrix} \tag{74}
$$

55

where h_k is the negative groundspeed measurement, $\left[-\left(V_{G_n}^2 + V_{G_e}^2 + V_{G_d}^2\right)\right]$. In terms of

the Kalman filter, this measurement yields

$$z_{K+1} = \left[(-2V_{G_n})\ (-2V_{G_e})\ (-2V_{G_d})\ (1)\right] \begin{bmatrix} V_{W_n} \\ V_{W_e} \\ V_{W_d} \\ V_{W_n}^2 + V_{W_e}^2 + V_{W_d}^2 - V_{true}^2 \end{bmatrix} + e_{k+1} \quad (75)$$

Where $h_{k+1}(x_1, x_2)$ is a nonlinear perturbation measurement model. Knowing this, H is

used to describe a linear relationship between the measurements described by z, and the

estimated state.

$$H_k = \frac{\partial h}{\partial x} = \left[\frac{\partial h}{\partial V_{W_n}}, \frac{\partial h}{\partial V_{W_e}}, \frac{\partial h}{\partial V_{W_d}}, \frac{\partial h}{\partial V_{ture}}\right] \quad (76)$$

Finally, because $h(x)$ is a perturbation model, the states' initial conditions must also be

in the form of perturbations. Various methods of calculating perturbation initial

conditions were tried. However, the best results were obtained when all perturbation

initial conditions were set to zero. With the initial conditions set to zero, the following

equations below complete the Kalman filter process:

$$M_k = P_k + Q \cdot \Delta t \quad (77)$$

$$x_{k+1} = K_k[z_{K+1} - h_{k+1}] \quad (78)$$

$$P_{k+1} = M_k - M_k H_{k+1}^T [H_{k+1} M_k H_{k+1}^T + R_{k+1}]^{-1} H_{k+1} M_k \quad (79)$$

Using a point mass model, a comparison was drawn between the least squares

three vector estimate, the VEST two vector method Kalman filter and the three vector

Kalman Filter. The inputs to the point mass model were designed to test the assumptions

associated with each filter. In particular, the largest assumption tested was how the

performance of the three vector method would be affected by varying true airspeed. The

plot below shows the error between the actual and estimated values of wind heading.
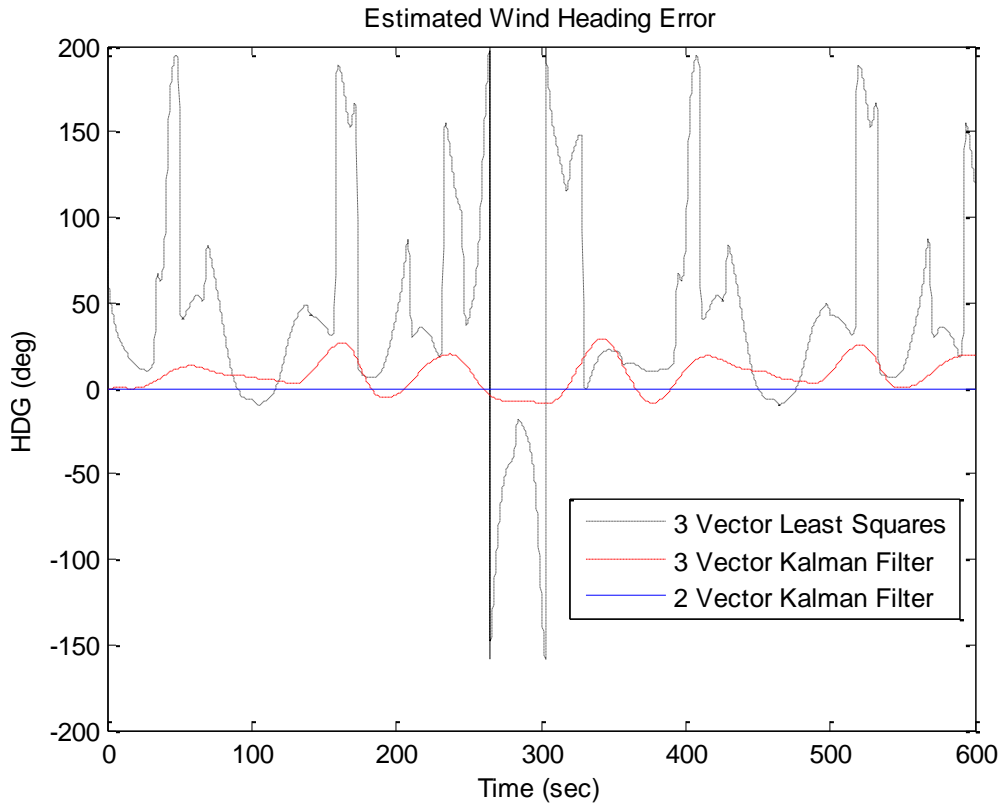

Figure 17. Estimated Wind HDG Error (Desktop Simulation)

Even though significant improvement was made between the least squares three

vector estimation and the three vector Kalman filter version, it still did not perform as

well as VEST. Looking at the wind speed error between the three estimators showed

similar results.
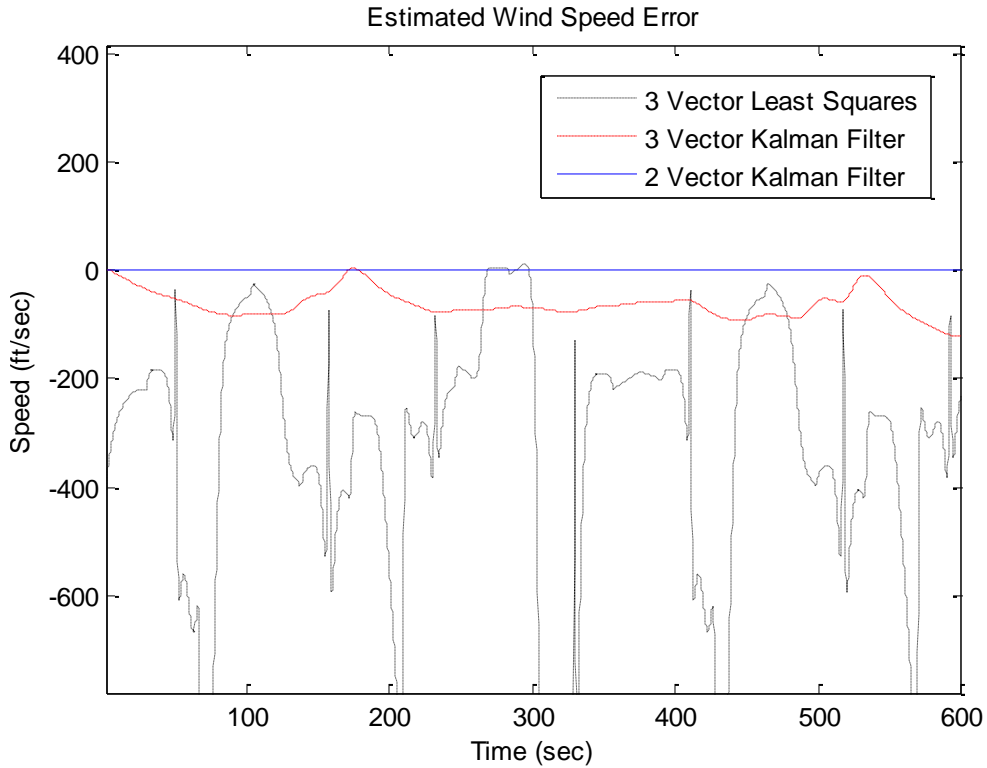
Figure 18. Estimated Wind Speed Error (Desktop Simulation)

There are a couple explanations as to why this occurred. First, violating the assumption that all three ground speed vectors were recorded at the same true airspeed creates problems with the estimation. Second, the addition of the unknown variable V_{W_d} increases the design space allowing for a wider variation in estimated answers. The vertical wind heading, defined by $\gamma_{wind} = \tan^{-1}\left(\frac{V_{W_d}}{V_{W_{horizontal}}}\right)$, is a function of V_{W_d}. A plot below of the estimated vertical wind heading has large variations, contributing to the error in estimated wind speed and heading.

58

Figure 19. Estimated Gamma Wind Error (Desktop Simulation)

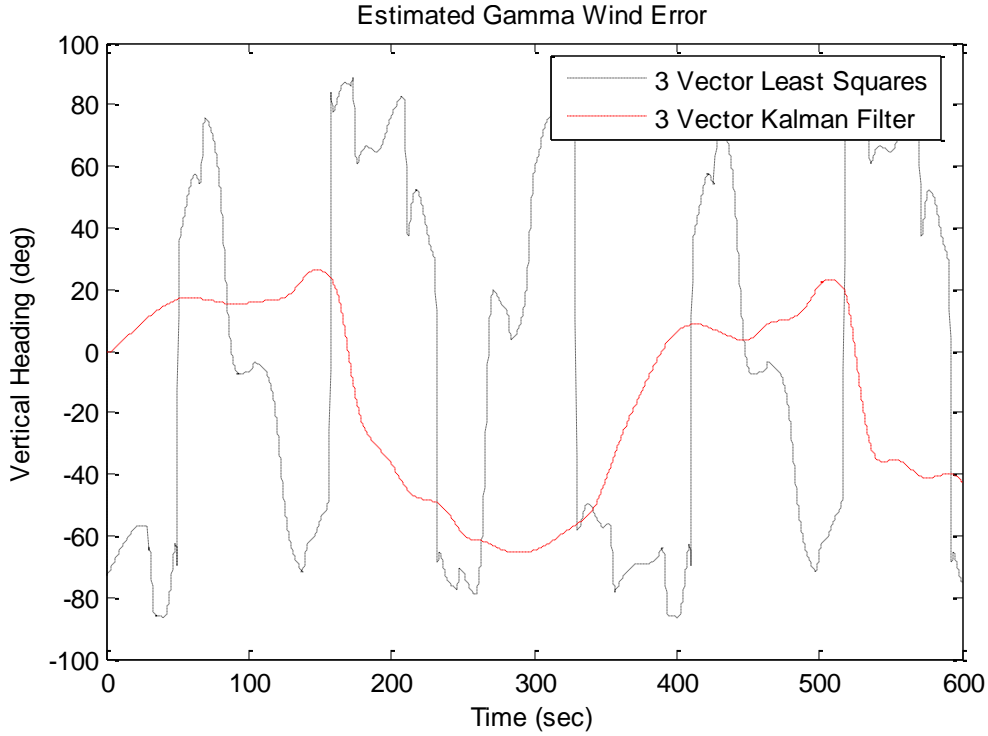As a result of this preliminary study, the VEST algorithm was chosen for implementation and further refinement.

Using the VEST algorithm as a starting point, and posing the problem in a way that directly estimated V_{true_n} and V_{true_e}, allowed for a slightly different implementation of the two vector method. First, estimating the components of true airspeed instead of wind speed required some adjustment to the VEST algorithm. The basic principle behind the two vector method remained the same, but instead of using equation 66 as the starting point, the following form was used:

$$\boldsymbol{h_k} = \tan^{-1}\left(\frac{V_{true_e}}{V_{true_n}}\right) + \cos(\theta)\left[\sin(\phi)\alpha - \beta\right] \tag{80}$$

59

Then, instead of using a linear lapse rate of winds with respect to an aircraft's change in altitude as the perturbation initial conditions [McLaren, 2008], perturbation initial conditions using the change in ground speed components was used to estimate the change in TAS components.

$$x_k = \begin{bmatrix} \Delta V_{true_n} \\ \Delta V_{ture_e} \end{bmatrix} = \begin{bmatrix} \left(V_{G_{n_k}} - V_{G_{n_{k-1}}}\right) \\ \left(V_{G_{e_k}} - V_{G_{e_{k-1}}}\right) \end{bmatrix} \tag{81}$$

Finally, the linear relationship between the measurements and the states, H_k was calculated as follows.

$$H_k = \frac{\partial h}{\partial x} = \left[\frac{\partial h}{\partial V_{ture_n}}, \frac{\partial h}{\partial V_{ture_e}} \right] \tag{82}$$

The rest of the Kalman filtering process remains the same as described in VEST but instead of using the velocity triangle to calculate the true airspeed components, the velocity triangle is used to calculate the wind speed components.

This subtle difference in solving the two vector problem has a distinct advantage when it comes to modern high-performance aircraft. High-performance aircraft can lose 50 knots per second or more in level high-g turns. So, instead of using a perturbation model that supplies initial conditions based on the changes in aircraft altitude, this model represents changes in true airspeed and may provide a more accurate estimate of TAS during high-g aircraft maneuvering.

Finally, a combination of both VEST, which estimates wind speed based on a change in altitude, and the VEST TAS Kalman filter just described, yields VEST 2 shown in figure 20.
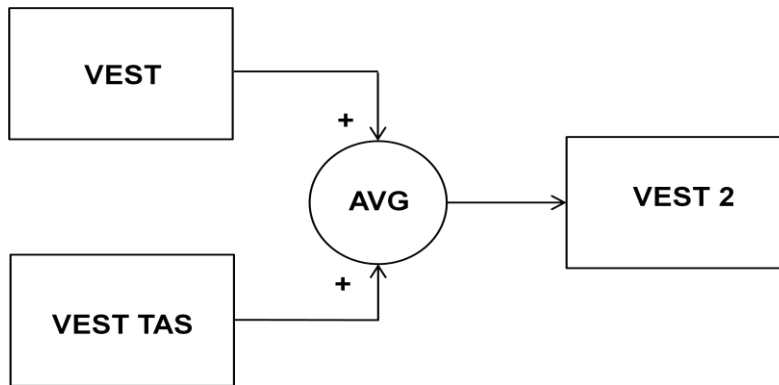
Figure 20. VEST 2

By taking the average of the two outputs, VEST 2 attempts to take into account not only
the wind speed changes associated with an altitude change but also the true airspeed
changes associated with high-g maneuvering. A computer simulation and comparison
between all three methods (VEST, VEST 2, and VEST TAS) will be described in the
following section.

3.3.4 Desktop Simulation Wind Estimation Results.

A desktop computer simulation using Simulink© and the Stevens and Lewis
nonlinear F-16 model was used to conduct preliminary testing on VEST, VEST TAS, and
VEST 2. Recall from section 3.3.3 that VEST estimates wind speed based on a change in
altitude, VEST TAS estimates wind speed based on a change in inertial velocities and
VEST 2 simply averages the outputs of VEST and VEST TAS. For simulation purposes,
a nonlinear wind model illustrated in Figure 21 was added to the Steven and Lewis
nonlinear simulation so that the effectiveness of each estimator could be tested.
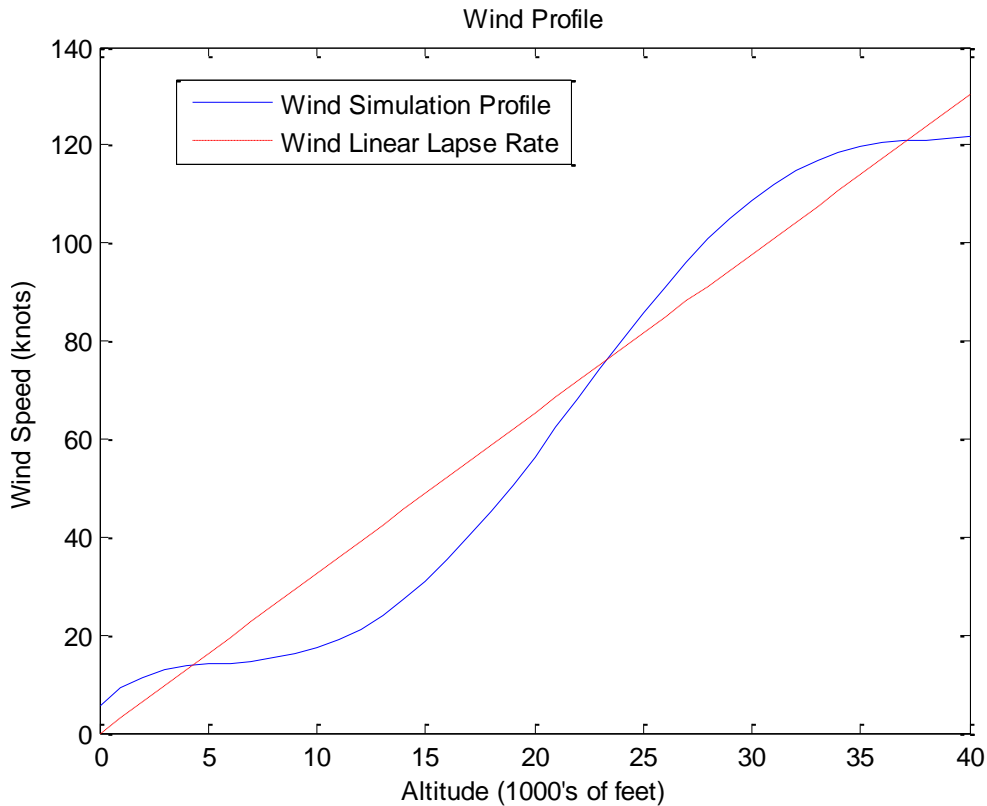
Figure 21. Wind Model Profile

Figure 21 also shows the linear lapse rate model used in the VEST algorithm. The wind

speed, as depicted above, varied as a function of altitude and the wind heading varied as a

function of time (sine wave with heading ± 10 deg). Additionally, a proportional auto-

throttle based on velocity feedback was used. When maneuvering, the auto-throttle

would attempt to keep the aircraft at the equilibrium airspeed. However, during the

profile, the maneuvers flown would exceed the capabilities of the auto-throttle and

airspeed would increase or decrease. Because of the maneuvers flown, a wide range of

airspeeds were covered on each profile. This was essential in testing the effectiveness of

the estimators during aggressive flight in a large flight envelope.

The outputs to the nonlinear F-16 model were tied into the Aviation Visual Design

Simulator (AVDS) which allowed a simulated F-16 to be flown around with a

Sidewinder Precision 2 Joystick. Using this joystick provided the first real feedback with

a pilot in the control loop. A series of four different flight profiles with different initial

conditions were flown and pilot control inputs were recorded. Each profile lasted 10

minutes and included maneuvers flown at varying g's, airspeeds and altitudes. Over all

four flight profiles, the maneuvers flown included level turns, loops, split S's, pitchbacks,

slicebacks, barrel rolls, turn reversals, wings level climbs, turning climbs, and straight

and level flight. Each flight profile contained most of the maneuvers but not every

profile contained all the maneuvers.

Additionally, all profiles flown were started with a different wind direction. The

initial wind directions were 023, 157, 203 and 337. Flying each profile at each start

heading produced 16 total runs. Using the calculated wind error, an ensemble average

(average of each data point associated with a specific time) of the 16 runs was taken and

then the temporal average and standard deviations were calculated from the ensemble

average. The results for the VEST wind speed estimate are shown in Figures 22 and 23
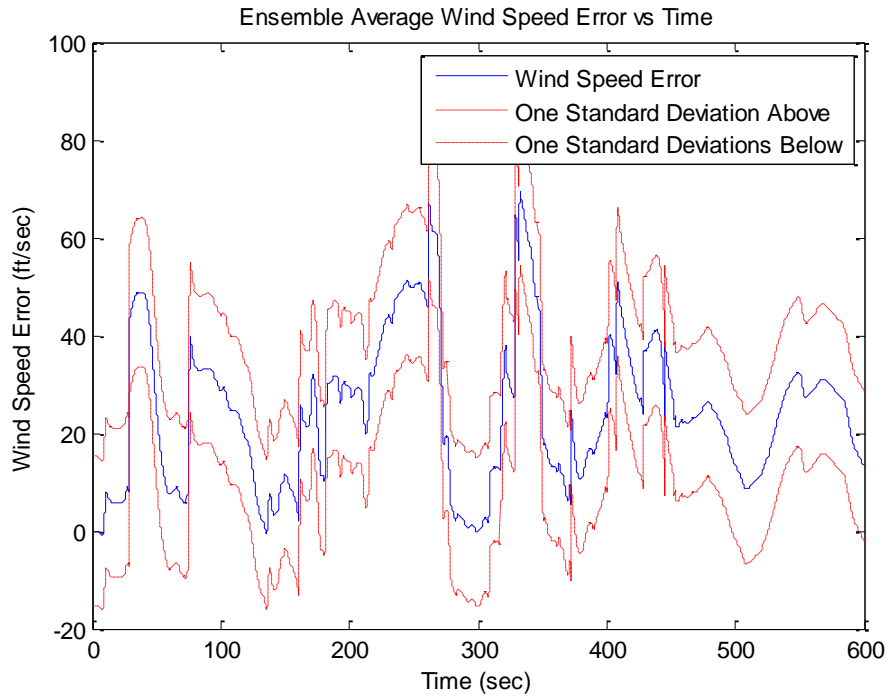
respectively.

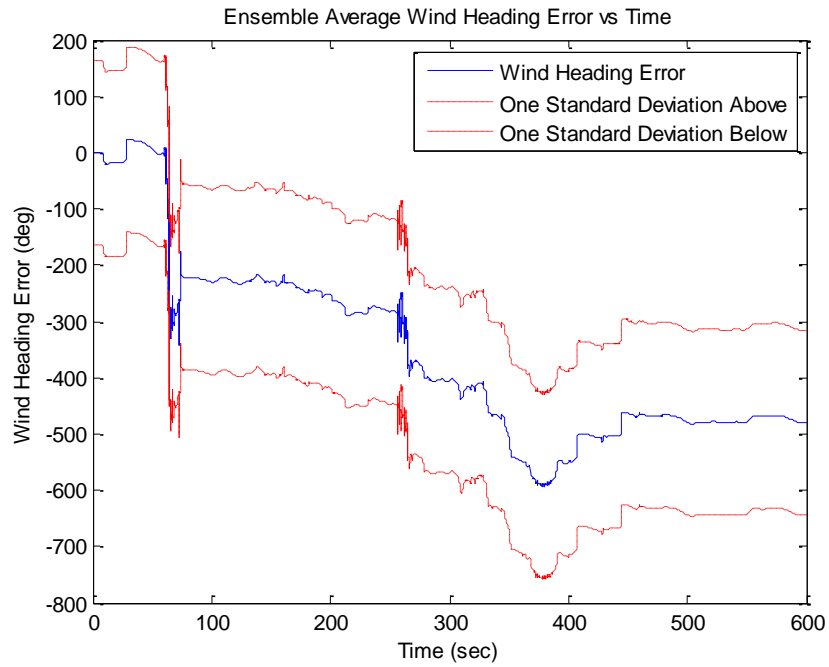**Figure 22. VEST Wind Speed Error**

Figure 23. VEST Wind HDG Error

It is obvious that the results obtained from the preliminary three-degree-of-freedom point mass simulation were not as accurate when implemented into a six-degree of-freedom simulation. However, as mentioned in section 3.3.3, the VEST, VEST TAS, and VEST 2 algorithms are extremely sensitive to high-g rapid onset maneuvers at high flight path angles. To fix this problem, limits were placed on the residual, of the VEST, VEST TAS, and VEST 2 Kalman filters. The residual is the difference between the measurements and the estimates of those measurements

$$residule = [\boldsymbol{z}_{K+1} - (\boldsymbol{h}_{k+1} + \boldsymbol{H}_{k+1}\boldsymbol{x}_k)] \tag{99}$$

and provides a measure of correction used to update the propagated states. The limits placed on the residual were associated with flight path angle which enabled the filter to maintain responsiveness while simultaneously preventing large fluctuations caused by rapid onset, high-g maneuvers at high flight path angles. Figures 24-29 show the results for VEST, VEST TAS, and VEST 2 with the new residual logic.

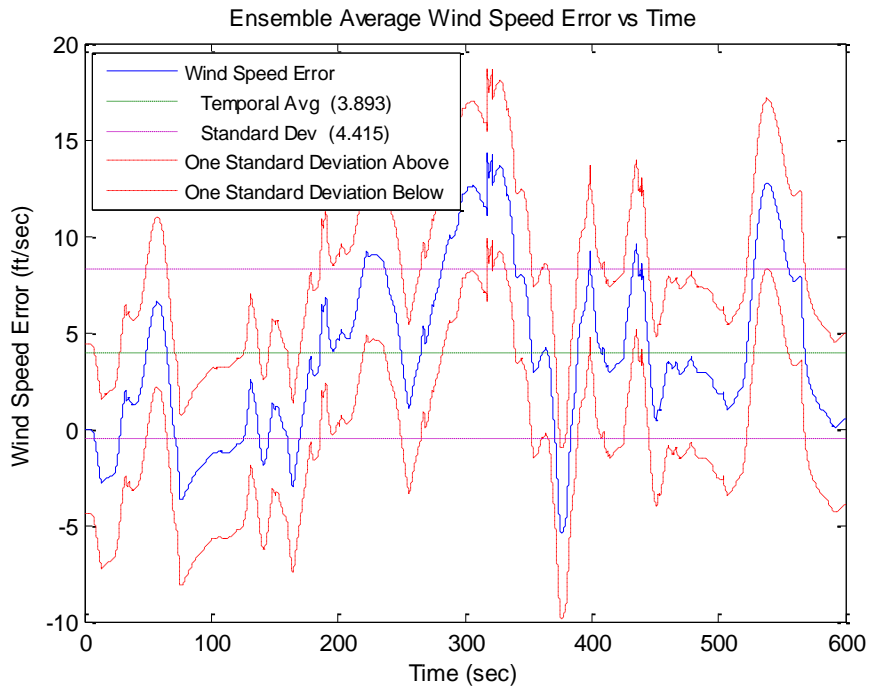**Figure 24. VEST Wind Speed Error with Residual Logic**
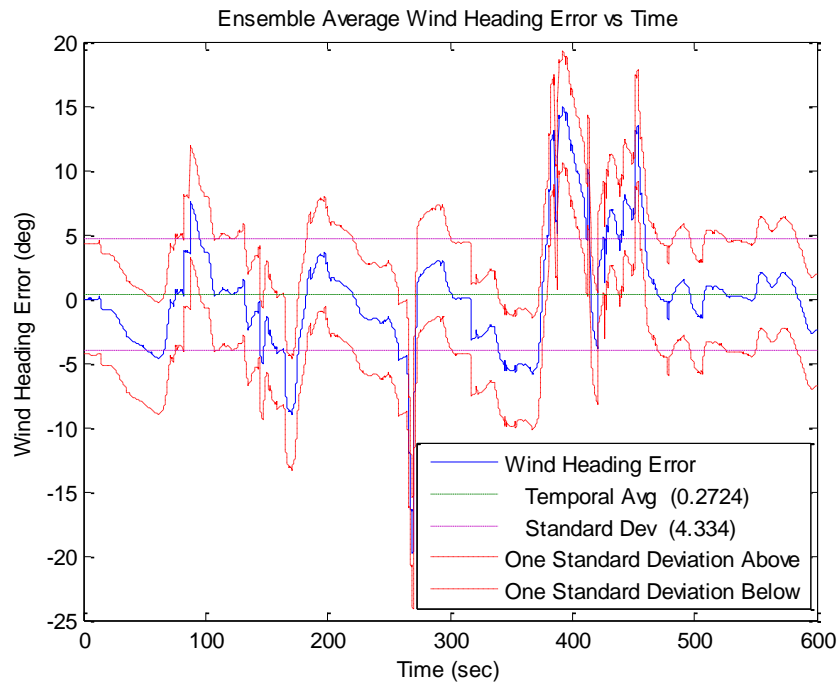

Figure 25.   VEST Wind HDG Error with Residual Logic
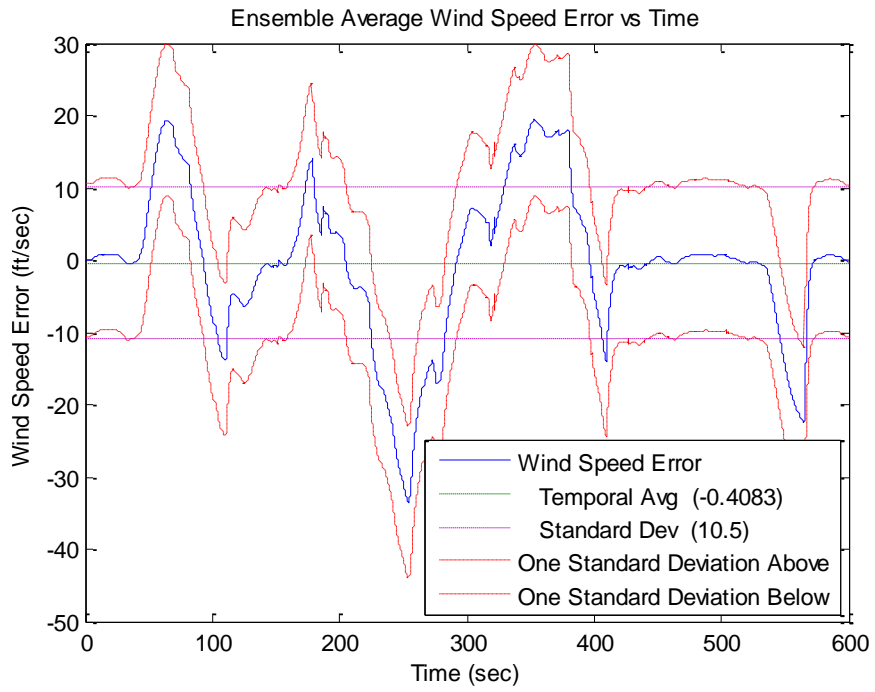
66

Figure 26. VEST TAS Wind Speed Error with Residual Logic
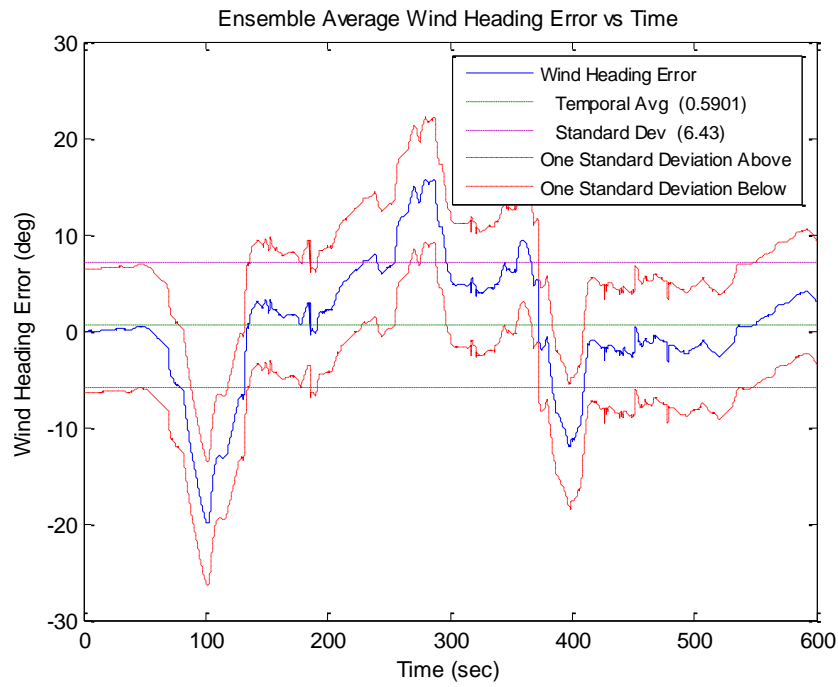

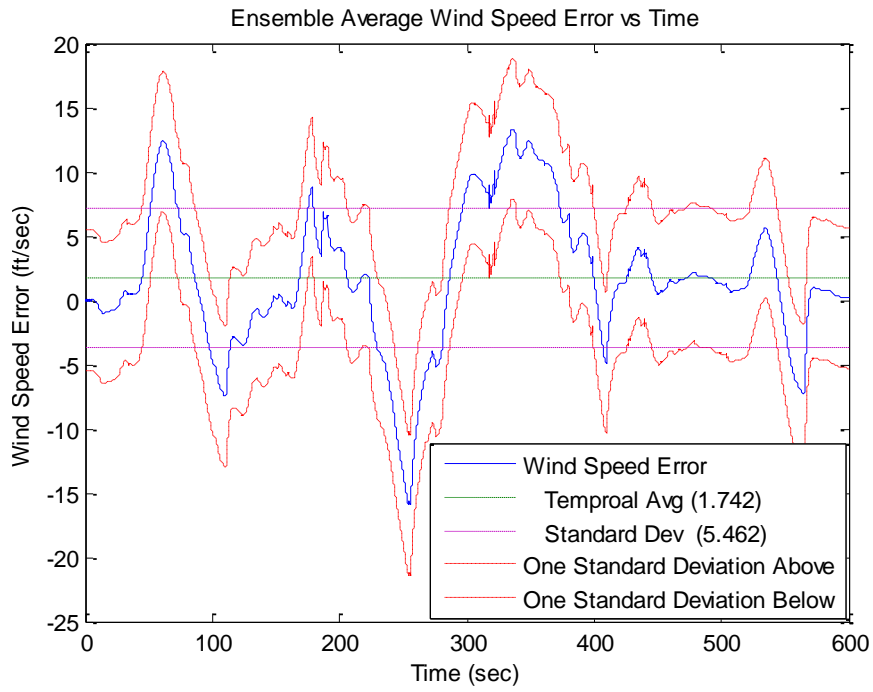**Figure 27. VEST TAS Wind HDG Error with Residual Logic**

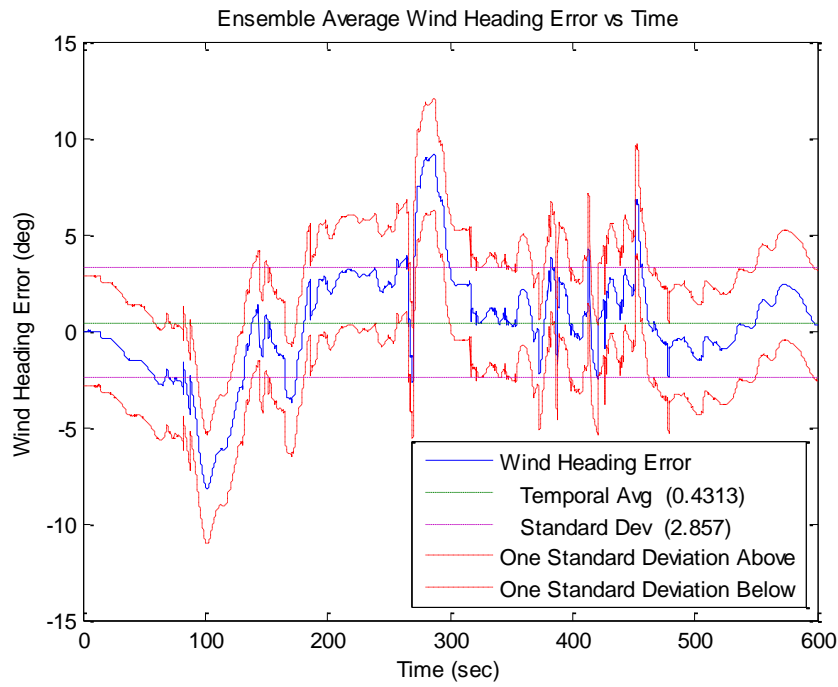**Figure 28. VEST 2 Wind Speed Error with Residual Logic**

Figure 29. VEST 2 Wind HDG Error with Residual Logic

68

The results of the three estimators are compiled into a table below.

Table 2. Wind Estimator Results (Measured Alpha and Beta)

Measured Alpha and Beta	**VEST**	**VEST TAS**	**VEST 2**
Wind Speed Error Temporal Average (ft/sec)	3.893	-0.4083	1.742
Wind Speed Error Standard Deviation (ft/sec)	±4.415	±10.5	±5.462
Wind Heading Error Temporal Average (deg)	0.2724	0.5901	0.4313
Wind Heading Error Standard Deviation (deg)	±4.334	±6.43	±2.857

Now that the results looked reasonable in VEST, VEST TAS, and VEST 2, an attempt was made to remove the alpha and beta dependency in each estimator. Recall from equation 66, the quantity $\cos(\theta)\,[\sin(\phi)\alpha - \beta]$ adjusts the measured heading from true north in order to account for the sideslip, roll, and bank encountered during turns [McLaren, 2008]. Since, alpha and beta are usually part of the Pitot static system, removing their inputs to the velocity estimators attempts to simulate an actual air data system failure. Table 3 shows the results from the same 16 runs accomplished earlier with no alpha and beta measurements available.

Table 3. Wind Estimator Results (No Alpha and Beta)

No Alpha and Beta	VEST	VEST TAS	VEST 2
Wind Speed Error Temporal Average (ft/sec)	31.9156	24.0380	27.9768
Wind Speed Error Standard Deviation (ft/sec)	±16.5286	±13.0558	±13.1726
Wind Heading Error Temporal Average (deg)	*77.7446*	*82.9833*	*80.3639*
Wind Heading Error Standard Deviation (deg)	*±53.9652*	*±64.7452*	*±59.0462*

Quantities indicated in **bold italics** appeared to be divergent when plotted. The results from this run indicate that alpha and/or beta were critical to the success of all three estimators.

Since alpha and beta are essential, a simple estimator was developed using equations 15 and 16 and substituting the TAS velocity components (u, v, w) with inertial velocity components $(V_{G_n}, V_{G_e}, V_{G_d})$ [McLaren, 2008]. Recall that both alpha and beta are functions of the body-fixed frame velocities. The inertial velocity components are part of the navigation frame. A conversion from the navigation frame to the body frame [Stevens and Lewis, 2003] of the form

$$C_{b/n} = \begin{bmatrix} c\theta c\psi & c\theta s\psi & -s\theta \\ (-c\phi s\psi + s\phi s\theta c\psi) & (c\phi c\psi + s\phi s\theta s\psi) & s\phi c\theta \\ (s\phi s\psi + c\phi s\theta c\psi) & (-s\phi c\psi + c\phi s\theta s\psi) & c\phi c\theta \end{bmatrix} \quad (100)$$

can be used with the yaw angle (ψ), pitch angle (θ), and roll angle (ϕ) to correct from the navigation frame to the body frame. With this conversion, the estimated body components become

$$u_g = \begin{bmatrix} 1 & 0 & 0 \end{bmatrix} \cdot C_{b/n} \cdot \begin{bmatrix} V_{G_n} \\ V_{G_e} \\ V_{G_d} \end{bmatrix} \tag{101}$$

$$v_g = \begin{bmatrix} 0 & 1 & 0 \end{bmatrix} \cdot C_{b/n} \cdot \begin{bmatrix} V_{G_n} \\ V_{G_e} \\ V_{G_d} \end{bmatrix} \tag{102}$$

$$w_g = \begin{bmatrix} 0 & 0 & 1 \end{bmatrix} \cdot C_{b/n} \cdot \begin{bmatrix} V_{G_n} \\ V_{G_e} \\ V_{G_d} \end{bmatrix} \tag{103}$$

and when combined with the alpha and beta equations produce the estimates listed below.

$$\alpha_{est} = \tan^{-1}\left(\frac{w_g}{u_g}\right) \tag{104}$$

$$\beta_{est} = \sin^{-1}\left(\frac{v_g}{\sqrt{u_g^2 + v_g^2 + w_g^2}}\right) \tag{105}$$

These estimates were used in the VEST, VEST TAS, and VEST 2 algorithms. Table 4 is the result of the 16 runs described above with estimated values of alpha and beta.

Table 4. Wind Estimator Results (Estimated Alpha and Beta)

Estimated Alpha and Beta	VEST	VEST TAS	VEST 2
Wind Speed Error Temporal Average (ft/sec)	22.6815	14.4442	18.5629
Wind Speed Error Standard Deviation (ft/sec)	±28.2473	±24.487	±25.4451
Wind Heading Error Temporal Average (deg)	71.9580	-25.414	23.2720
Wind Heading Error Standard Deviation (deg)	±65.6092	±56.858	±57.8454

The estimated values in Table 4 are not great, but there was some improvement over the previous case. In fact, all the headings estimated by the VEST algorithms went from being divergent to non-divergent. In order to determine if one estimate was more important than the other, α_{est} was used with $\beta_{est} = 0$. The results of these 16 runs are displayed in Table 5.

Table 5. Wind Estimator Results (Estimated Alpha, Beta = 0)

Estimated Alpha (Beta = 0)	VEST	VEST TAS	VEST 2
Wind Speed Error Temporal Average (ft/sec)	22.8876	13.4124	18.15
Wind Speed Error Standard Deviation (ft/sec)	±15.0974	±16.304	±14.2162
Wind Heading Error Temporal Average (deg)	56.906	-9.7440	23.581
Wind Heading Error Standard Deviation (deg)	±41.0665	±59.7321	±48.2201

This showed some promise as all three estimators were definitely non-divergent with improved accuracy over an alpha and beta estimate. However, the variability of the estimated wind heading still needs improvement. Finally, holding alpha at zero and estimating beta produces the results listed in the Table 6.

Table 6. Wind Estimator Results (Estimated Beta, Alpha = 0)

Estimated Beta (Alpha = 0)	VEST	VEST TAS	VEST 2
Wind Speed Error Temporal Average (ft/sec)	62.4971	49.4777	55.9874
Wind Speed Error Standard Deviation (ft/sec)	±33.0942	±26.837	±29.0576
Wind Heading Error Temporal Average (deg)	*-62.1054*	*-14.5156*	*-38.3105*
Wind Heading Error Standard Deviation (deg)	*±114.0008*	*±84.6579*	*±98.5504*

Again, quantities indicated in **bold italics** appeared to be divergent when plotted. These results are unsatisfactory as all three estimators diverged in heading.

Based on this comparison, the best approach appeared to include the use of a measured alpha and beta. In any other method, the wind heading variability was rather large and undesirable. Thus, the actual alpha and beta measurements were used in further testing under the assumption that there is a method of accurately measuring alpha and beta.

All three Kalman filters had similar results. Therefore, under the premise that a robust Kalman filter capable of estimating velocities both as a function of changes in altitude and as a function of changes in true airspeed, VEST 2 will be used for further testing.

The desktop simulator was setup such that the last know wind and true airspeed components were sent to the VEST 2 wind estimator after a simulated air data system failure (simulated failure occurred one second into the run). To check the robustness of VEST 2, false initial conditions were sent to VEST 2 using the same 16 runs discussed

earlier. The intent was to see how long it would take VEST 2 to converge on the actual wind velocity vector. Figures 30 and 31 are plots of both the ensemble wind speed and ensemble wind heading errors for false initial conditions.
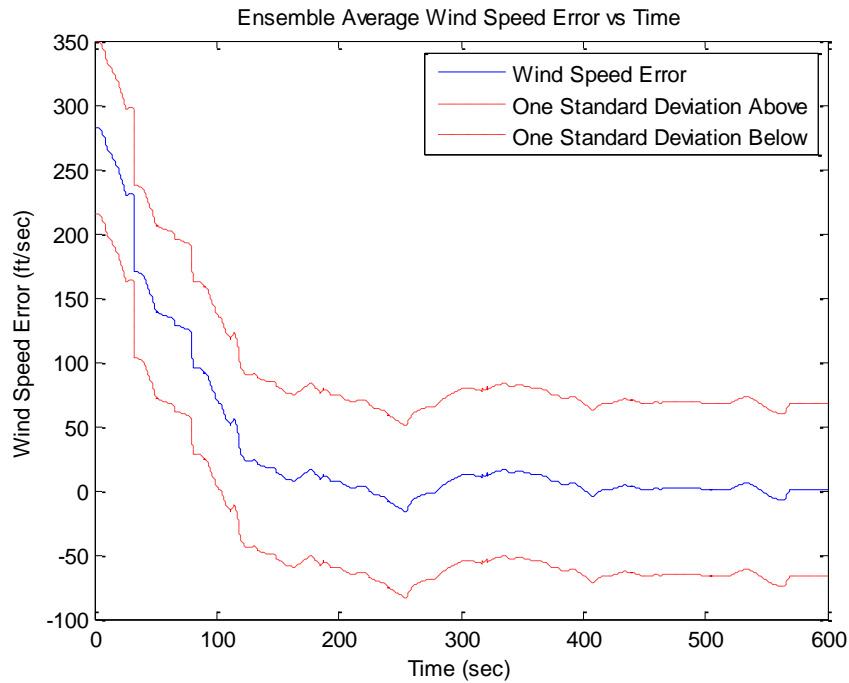

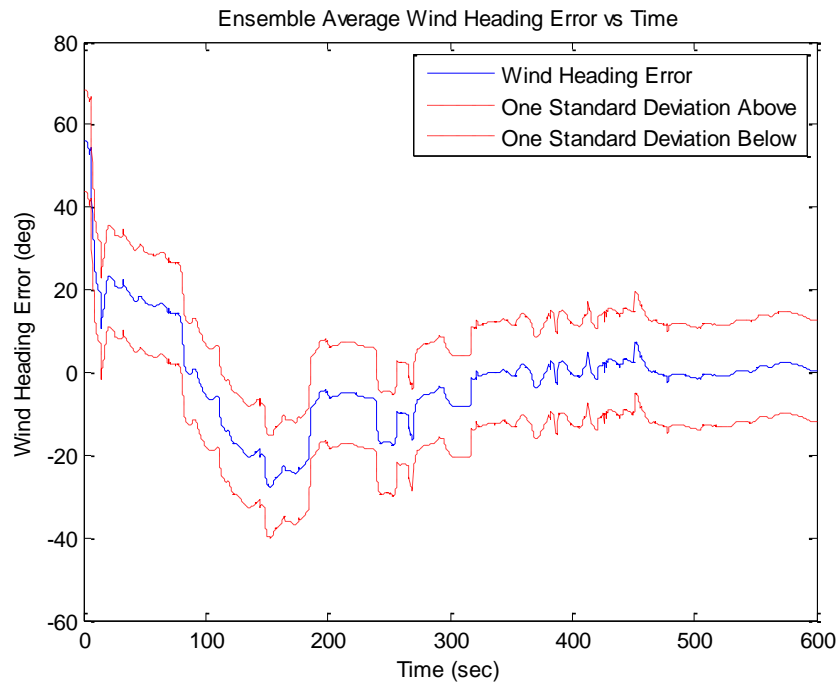**Figure 30. VEST 2 Wind Speed Error (False Initial Conditions)**

Figure 31. VEST 2 Wind HDG Error (False Initial Conditions)

It was apparent that VEST 2 started to produce good estimates around 200 seconds and converged by 400 seconds. This showed that VEST 2 was capable of functioning even if passed incorrect initial conditions. Knowing this opens the possibility for VEST 2 to function as a back-up system that continuously runs from take-off to landing without the need for last know conditions. In just a little over three minutes of flight, VEST 2 was capable of producing valid estimates necessary to correctly schedule gains.

3.4 Gain-Scheduling with Inertial Velocities

The second method of standby-gain-scheduling is extremely simple. After an air data system failure, assume a standard atmosphere to estimate density and simply use inertial velocities or GPS velocities to calculate an inertial dynamic pressure ($\bar{q}_{inertial}$).

$$\bar{q}_{inertial} = \frac{1}{2}\rho_{std}V^2_{inertial} \tag{83}$$

Then use this inertial dynamic pressure to schedule aircraft gains. The underlying assumption is that even though winds are present in inertial velocities, they are usually much smaller than the aircraft's true airspeed velocity vector. Thus, if we drive the gains with something close to actual dynamic pressure, the aircraft performance should be similar to the performance of an aircraft scheduled with actual dynamic pressure.

3.5 Flight Control without Gain-Scheduling (Disturbance Observer)

The third method of standby-gain-scheduling following an air data system failure is through the use of a disturbance observer (DO). The object of this controller is to produce the desired response throughout a large flight envelope regardless of the aircraft's airspeed or altitude. As described in section 2.3.1, the DO controller to be tested in this thesis was designed for the flight envelope $h \in [5000; 25000]$ feet and $M \in [0.4; 0.8]$. Below is a plot of the specific dynamic pressure changes associated with this envelope.
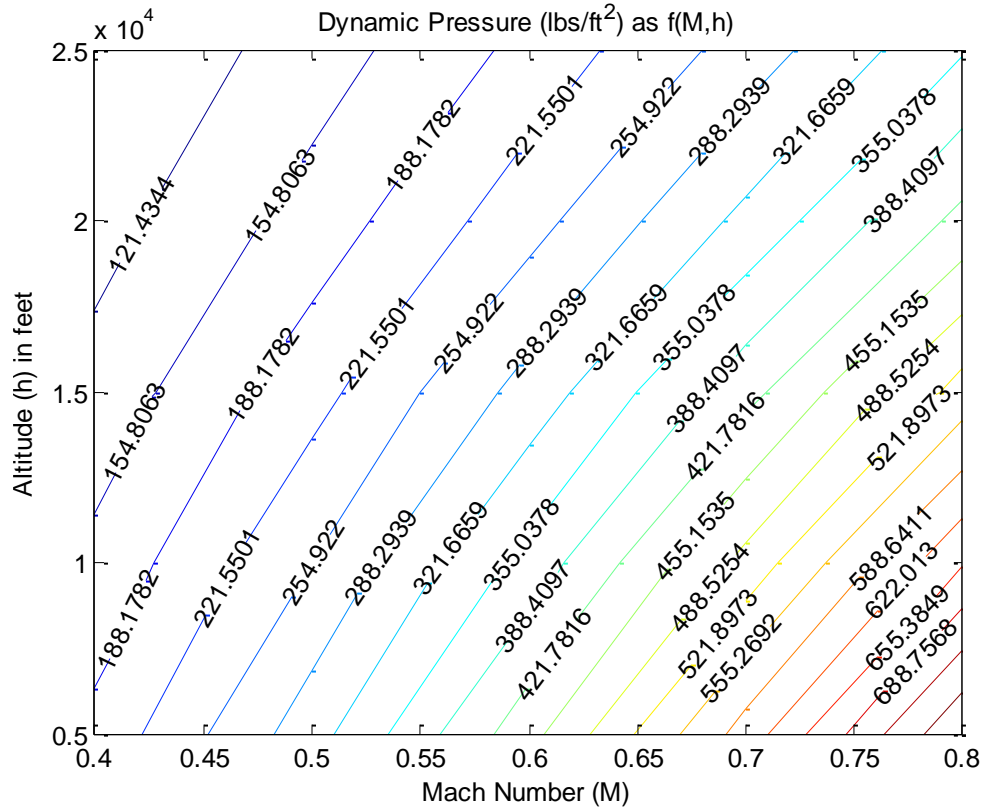
Figure 32. Tested Dynamic Pressure Envelope

The wide variance in dynamic pressure would normally require gain-scheduling to provide the desired aircraft response throughout the design flight envelope. But with proper implementation of the DO, a modern high-performance aircraft can achieve the desired performance without the need to gain-schedule.

3.5.1 Pitch Axis Design.

The process described in section 2.3 describes the methodology used by Blue et al to design a large envelope DO controller for the pitch axis. Recalling that the pitch-rate (q) was chosen as the feedback variable meant that the desired dynamics needed to be

chosen in terms of pitch-rate. The desired dynamics (P_d) for the pitch axis were chosen

to meet the Level 1 pitch-rate command tracking criteria described in Table 1. A second

order transfer function of the form

$$P_{d\_pitch} = \frac{\omega_p^2}{s^2 + 2\zeta_p\omega_p s + \omega_p^2} \tag{84}$$

with $\omega_p = 4$ and $\zeta_p = 0.5$ was selected [Blue et al, 2002]. A step input to this transfer

function (Figure 33) was accomplished to determine if the response met the MIL-STD-

1797B minimum requirements for Level 1 pitch-rate command tracking.
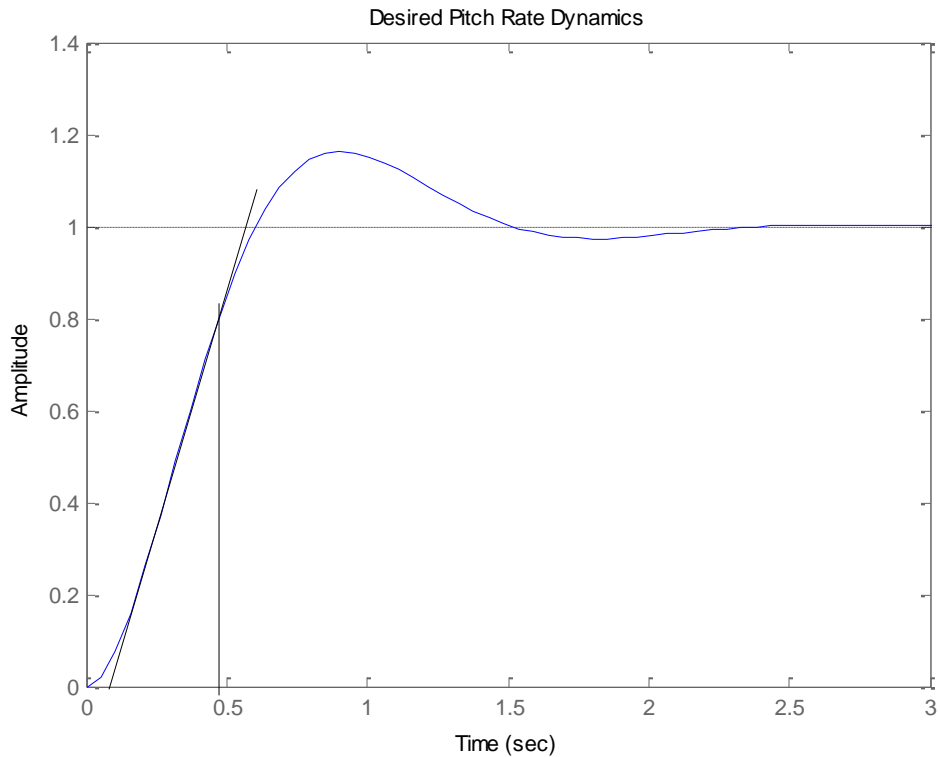
Figure 33. Step Response to Desired Pitch-Rate Dynamics

The results to this step input show that $t_1 = 0.095 \le t_{1\,max}$ and $\frac{\Delta_{q\,2}}{\Delta_{q\,1}} = 0.1688 \le 0.3$.

For $\Delta_{t\,max} = \frac{500}{V_T}$, the largest velocity associated with the design flight envelope will give

the smallest $\Delta_{t\,max}$. This occurs at M = 0.8 and h = 5,000 feet where $\Delta_{t\,max} = 0.569$.

For $\Delta_{t\,min} = \frac{9}{V_T}$, the lowest velocity associated with the design envelope will give the

largest $\Delta_{t\,min}$. This occurs at M = 0.4 and h = 25,000 feet where $\Delta_{t\,min} = 0.022$.

Ensuring that $\Delta_t = 0.335$ is between these two bounds along with the other criteria

above specifies Level 1 pitch-rate flying qualities.

Now that the desired dynamics are set, the model development described in

section 2.3.1 is the same. Recall, figure 11 represented the finalized architecture and

included modeling uncertainties ($W_u = 2 \cdot \frac{s+0.2 \cdot 1256}{s+2 \cdot 1256}$), command weights ($W_{cmd} = \frac{10}{s+10}$)

and performance weights ($W_p = 18 \cdot \frac{s}{(s+1)^2}$) [Blue et al, 2002]. Using this model, the

filter Q_{pitch} can be determined using the methods of H_∞ parameter space control design.

Recalling that Q_{pitch} must be at least the same order as P_{d_pitch}, a second order transfer

function of similar form was chosen.

$$Q_{pitch} = \frac{\omega_{Q\_pitch}^2}{s^2 + 2\zeta_{Q\_pitch}\omega_{Q\_pitch}s + \omega_{Q\_pitch}^2} \tag{85}$$

The sensitivity analysis described in section 2.3.2 was used to select the values

$\omega_{Q\_pitch} = 26.5$ and $\zeta_{Q\_pitch} = 0.5$ [Blue et al, 2002].

Now that all the values of the pitch axis DO are known, a comparison was made

at the four corners of the flight envelope between the open loop dynamics and the closed

loop DO controlled dynamics. To do this, a unit step input was commanded to the

elevator command input of a Stevens and Lewis non-linear F-16 model. The open loop
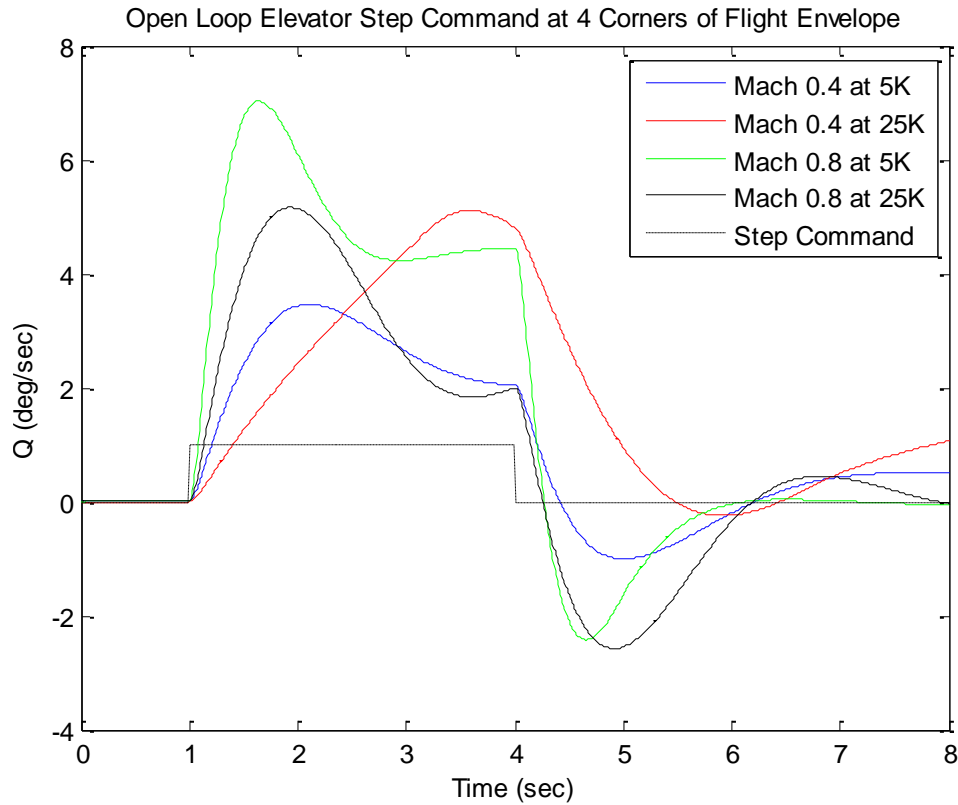
results are illustrated in figure 34.

Figure 34. Open Loop Elevator Step Response

It is evident from the open loop step command that the dynamics vary significantly over

the design flight envelope. When wrapping the DO control system around the non-linear
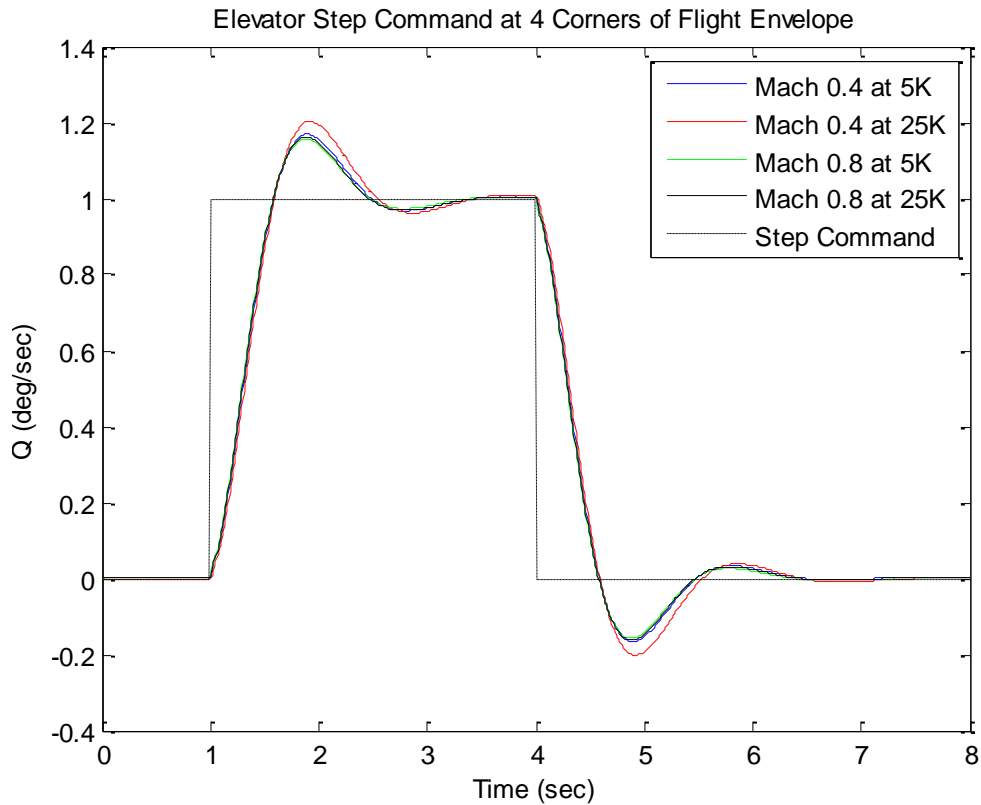
simulation, the following results were obtained.

Figure 35. Disturbance Observer Elevator Step Response

Now the dynamics are very similar and provide the desired pitch-rate responses at each of the four corners of the flight envelope.

3.5.2 Roll Axis Design.

For high performance fighters, it is desired to roll about the stability axis in an attempt to minimize changes in AOA [Liebst, Spring Quarter 2007]. A large roll about the body axis would drastically change the angle of attack (AOA), making gross acquisition and tracking tasks difficult. Knowing this, the stability axis roll rate (p_s) was chosen as the feedback control variable used to control roll rate. Recalling form section

2.2.4, a simple transformation from the body axis to the stability axis involves the

measured angle, alpha, and the body axis roll (p) and yaw (r) rates. Defining p_s as

$$LCV = p_s = p\cos(\alpha) + r\sin(\alpha) \tag{86}$$

provides the roll rate command necessary to roll about the stability axis [Honeywell,

1996], which helps minimize changes in AOA during rolling maneuvers. Below is a
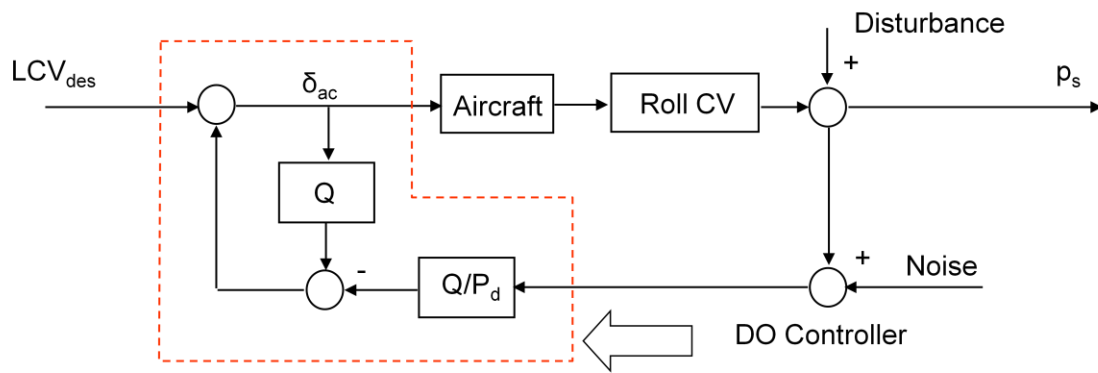
figure showing the roll DO controller

Figure 36. Roll Axis Disturbance Observer Controller

where δ_{ac} is defined as the desired aileron command sent to the aileron actuator in order

to obtain the desired roll rate. Even though lateral and directional characteristics are

interrelated, roll will be assumed independent of yaw and designed separately.

Therefore, looking only at roll and knowing that the approximation of the aileron-to-roll-

rate transfer function is first order [Stevens and Lewis, 2003], the desired dynamics for

roll will be of the form

$$P_{d\_roll} = k_{roll} \cdot \frac{1/T_{roll}}{s + 1/T_{roll}} \tag{87}$$

where k_{roll} is a gain placed on the desired dynamics and T_{roll} represents the roll mode time constant. There is considerable data relating the roll time constant associated with roll damping and pilot rating. From MIL-STD-1797B, the roll mode time constant associated with fighter aircraft in the most demanding phase of flight must be less than 1.0. Aircraft manufacturers have even gone as far to say that fighter aircraft should have a roll mode time constant between 0.6 and 0.8 seconds [MIL-STD-1797B, 2006]. Based on this information, T_{roll} was set to 0.8 seconds. For the filter, Q_{roll}, once again the same order transfer function was chosen and is of the form

$$Q_{roll} = \frac{k_Q}{s + k_Q} \qquad (88)$$

Setting $k_Q = 1$ yields a low pass filter capable of damping out roll rate overshoots.

Finally, combining the desired dynamics and the roll filter into the roll DO, an analysis was performed using the non-linear Stevens and Lewis F-16 simulation. In the simulation, full deflection aileron step inputs were used to find the right gain (k_{roll}) necessary to meet the roll performance criteria for a fighter type aircraft. Taken from MIL-STD-1797B, Table 7 indicates the required time to achieve a stated bank angle change in a fighter-type aircraft that should result in Level 1 flying qualities.

Table 7. Roll Performance

Level	Speed Range*	Time to Achieve the Stated Bank Angle Change (seconds)				
		Category A			Category B	Category C
		$\phi_t = 30°$	$\phi_t = 50°$	$\phi_t = 90°$	$\phi_t = 90°$	$\phi_t = 30°$
1	$V_{o_{min}} \leq V < V_{o_{min}} + 20$ kts	1.1			2.0	1.1
	$V_{o_{min}} + 20$ kts $\leq V < 1.4V_{o_{min}}$	1.1			1.7	1.1
	$1.4V_{o_{min}} \leq V < 0.7V_{o_{max}}$			1.3	1.7	1.1
	$0.7V_{o_{max}} \leq V \leq V_{o_{max}}$		1.1		1.7	1.1

The values for $V_{o_{min}}$ and $V_{o_{max}}$ are dependent upon the maneuver being flown (air-to-air combat, ground attack, weapon delivery, air-to-air refueling, etc.). This research is primarily concerned with Category A phases of flight (flight phases that require rapid maneuvering, precision tracking, or precise flight-path control) [MIL-STD-1797B, 2006]. Therefore, the objective was to meet all the values specified under the Category A column in the design flight envelope $h \in [5000; 25000]$ feet and $M \in [0.4; 0.8]$. The results of the full deflection aileron step inputs produced a $k_{roll} = 10$.

Once again, now that all the values of the roll axis DO are known, a comparison was made at the four corners of the flight envelope between the open loop roll dynamics and the closed loop DO controlled roll dynamics. To do this, a unit step input was commanded to the aileron command input of a Stevens and Lewis non-linear F-16 model. The open loop results are illustrated in figure 37.
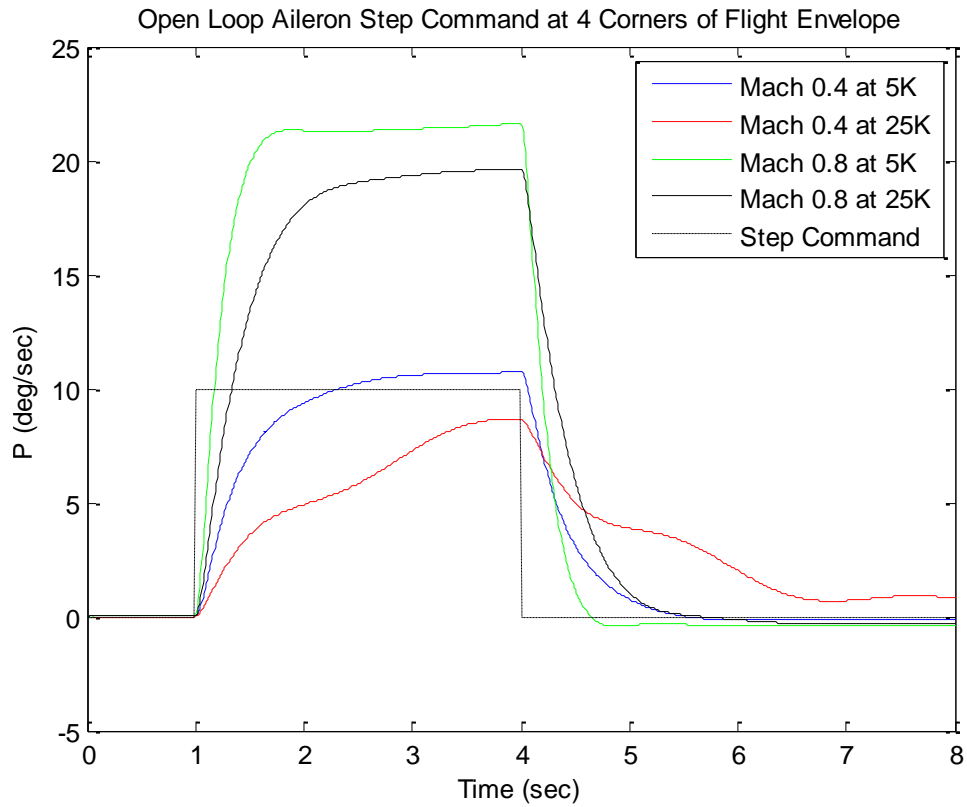
Figure 37. Open Loop Aileron Step Response

As expected, the dynamics at each corner of the flight envelope are significantly

different. However, wrapping the roll DO controller around the open dynamics produces

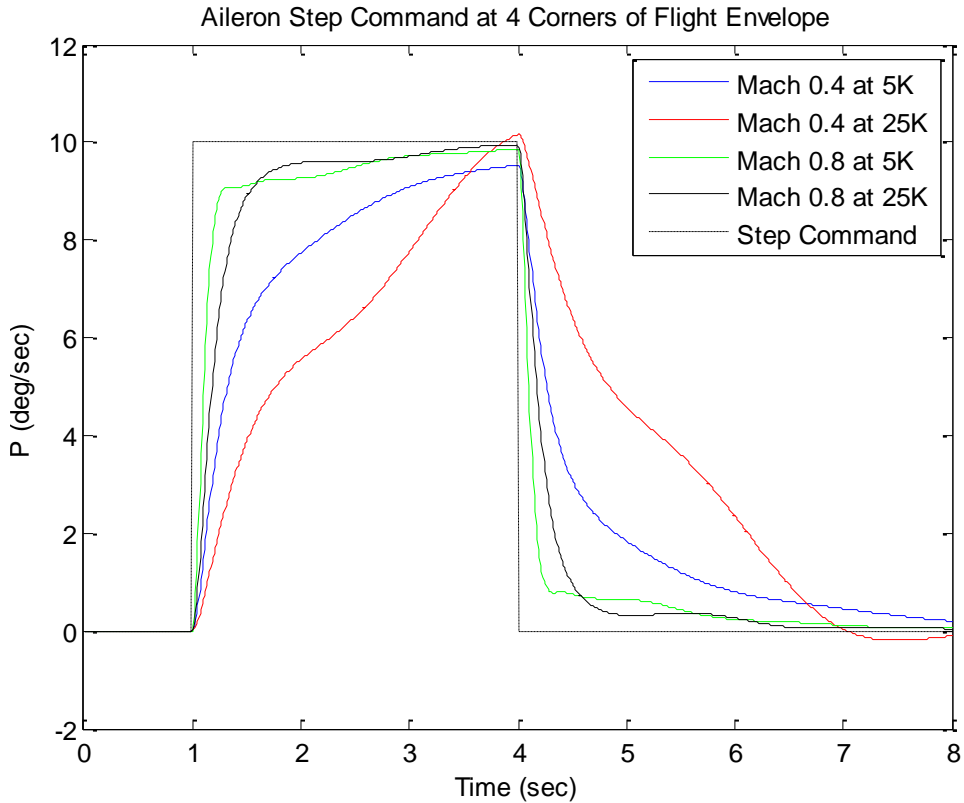the closed loop dynamics in Figure 38.

Figure 38. Disturbance Observer Aileron Step Response ($k_q = 1$)

A plot of the desired roll rate dynamics shown in Figure 39 matches reasonably well with the roll responses obtained from the roll axis DO step input. Roll-rate overshoot is almost non-existent making it easy for the pilot to set the desired bank angle when required for precision bank angle control. Secondly, in all cases, the input obtains close to the desired roll rate, it just takes the ones associated with a lower Mach number longer to get there. One reason is that roll rates must be slowed down to prevent roll overshoot in the conditions where there is insufficient damping or aileron control authority (slower airspeeds and/or higher altitudes). However, even though the responses are good, they are still not great.
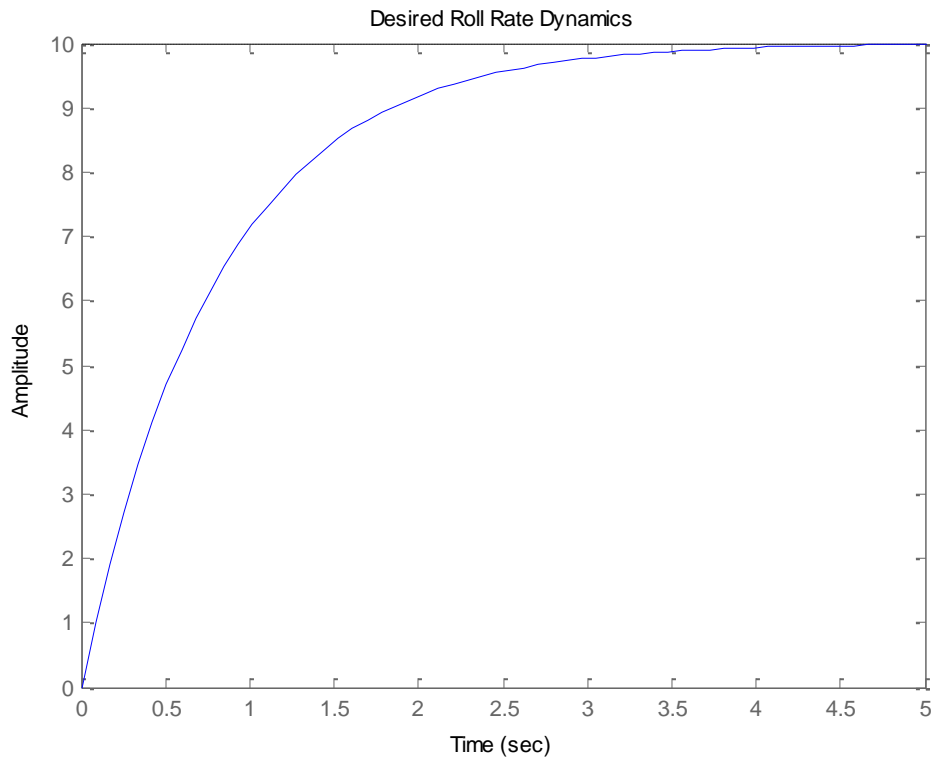
Figure 39. Desired Roll Rate Dynamics

Since a value of one was arbitrarily chosen for k_Q to produce a low pass filter, a second look at tuning the variable k_Q, was used in an attempt to produce better results. Figure 40 shows the step input results with $k_Q = 3$.
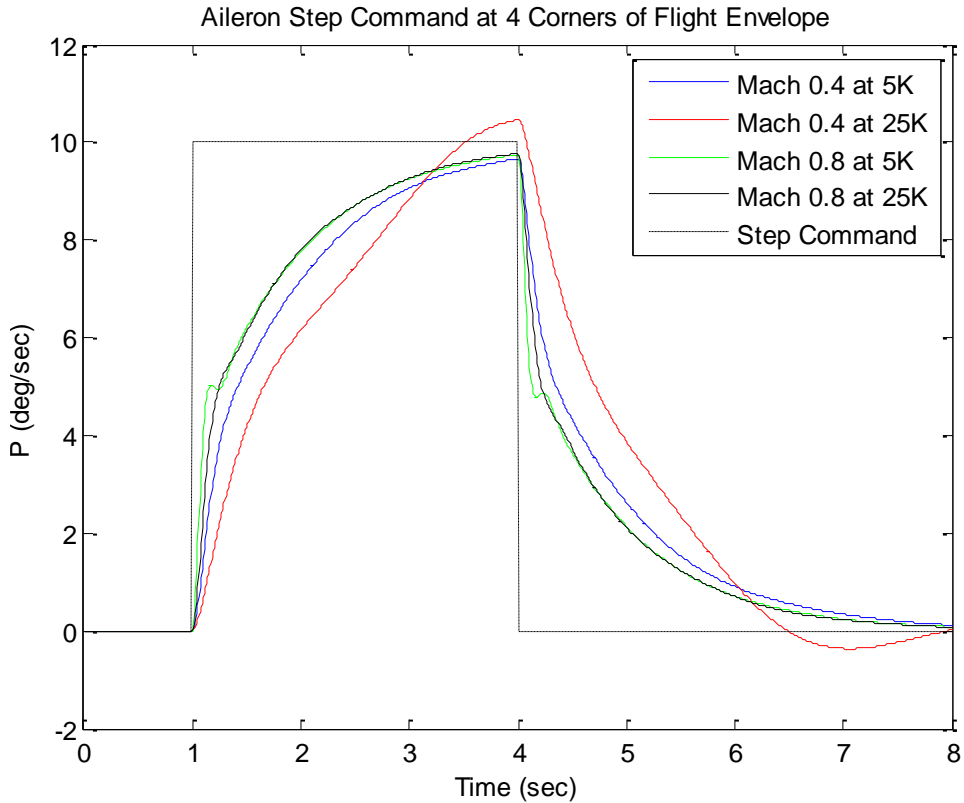
Figure 40. Disturbance Observer Aileron Step Response ($K_q = 3$)

In this regard, the roll DO appears to be working on par with the performance predicted by the pitch DO controller. To test this even further, the outputs of the nonlinear F-16 model were tied into the Aviation Visual Design Simulator (AVDS) which allowed a simulated F-16 to be flown around with a Sidewinder Precision 2 Joystick. Flying this pilot-in-the-loop simulation highlighted key information not initially apparent with the step input analysis. When $k_Q = 3$, the simulated F-16 appeared to continue rolling past the desired bank angle when control input was removed. However, when the filter with $k_Q = 1$ was used, the aircraft roll rate would stop soon after the control input was removed. Looking back at both step inputs it is now apparent that the roll off from the

step input is more gradual in the $k_Q = 3$ than in the $k_Q = 1$. Having flown in fighter aircraft and knowing how important it is to be able to set the desired bank angle, the roll filter with $k_Q = 1$ was used for implementation.

3.5.3 Yaw Axis Design.

As mentioned earlier, unlike the longitudinal axis, the lateral-directional axis does not easily separate into factors that define each mode [Stevens and Lewis, 2003]. In this regard, roll-yaw coupling exits. In an attempt to account for this, the command variable chosen must be able to produce yaw when the rudder pedals are pushed but also interact with the roll axis to maintain coordinated flight during aileron inputs. Several methods of feedback systems exist that allow for the interrelationship between the lateral and directional axes.

The first method is a beta (β) command feedback system. This method is probably the most logical in that when an aileron deflection is commanded, the coupled nature of the roll-yaw axis not only produces a roll but also some sideslip. By feeding a signal proportional to β, the sideslip induced by roll can be eliminated [Blakelock, 1991]. This method has both advantages and disadvantages. Sideslip is relatively easy to measure and generally more accurate than angle of attack, but it is sensitive to noise caused by airflow disturbances [Blakelock, 1991]. The likelihood of airflow disturbances require the sensitivity of the sideslip signal to be kept low so that the signal contains less noise. Keeping the sensitivity low prevents damping issues that could arise from feeding back a sensitive beta measurement.

The second method of feedback involves a $\beta - \dot{\beta}$ system. This method is currently used on the F-15 integrated flight/fire control system and works very well [Blakelock, 1991]. As stated in section 2.2.4, β can be measured from a wind vane or probe, while $\dot{\beta}$ cannot. Differentiating β to obtain $\dot{\beta}$ is usually not a good idea due to the noise amplification brought about by differentiation. Therefore, the only way to obtain $\dot{\beta}$ is to calculate it using the following relationship [Blakelock, 1991]

$$\dot{\beta} = p \sin(\alpha) - r \cos(\alpha) + g \frac{a_{lat} + \cos(\theta) \cos(\phi)}{V_{true}} \tag{89}$$

where g is the acceleration due to gravity and a_{lat} is the lateral acceleration. When attempting to design a standby controller that is capable of functioning following an air data system failure, V_{true} is an unknown measurement which creates a problem with this method of feedback.

The third method of feedback uses a combination of the stability axis yaw rate (r_s), a sideslip gain constant (K_β), β, and the term $\frac{g}{V_{true}} \cos(\theta) \sin(\phi)$ [Honeywell, 1996]. When combined together, the feedback variable becomes a measure of yaw rate in the form

$$Yaw_{CV} = r_s + K_\beta \beta - \frac{g}{V_{true}} \cos(\theta) \sin(\phi) \tag{90}$$

where the term $r_s - \frac{g}{V_{true}} \cos(\theta) \sin(\phi)$ provides zero-sideslip during turns. The term $K_\beta \beta$ also aids in sideslip prevention as well, by feeding back the sideslip angle, β. Typically, K_β can be defined as $\bar{q} / \bar{q}_{crossover}$ where $\bar{q}_{crossover}$ is the dynamic pressure ratio that correlates with sideslip and its transition from high adverse values at low speeds

to low proverse values at high speeds [Kisslinger and Wendl, 1971]. As mentioned previously, this method of feedback also involves true airspeed and becomes a problem when designing for an air data system failure.

The fourth and final method of feedback looked at is feeding back lateral acceleration. When in a coordinated turn, the resulting acceleration lies in a plane of symmetry and there is no lateral acceleration [Blakelock, 1991]. Thus, if a lateral accelerometer is used, and that signal is fed back through the control system to remove the lateral acceleration with rudder input, then a coordinated turn can be obtained. However, even though lateral accelerations are available when a Pitot static system fails, the ratio of acceleration to β is only 0.034 g/deg [Blakelock, 1991]. Because of this, the lateral accelerometer is not as effective.

After comparing all four methods of feedback, a β feedback system was chosen to provide the link between the lateral and directional axis. So now, both the roll and the yaw axis depend on measurements, α and β. Since α and β measurements are typically found in an air data system, α and β must either be estimated or assumed still available following an air data system failure.   Once again this highlights the fact that alpha and beta measurements will be used under the assumption that there is a method of accurately measuring or estimating their values.

Proceeding with the design of the yaw axis DO controller, a process similar to that described in section 2.3 will be used. A model of the controller is shown in figure 41 with β as the command variable (NCV)
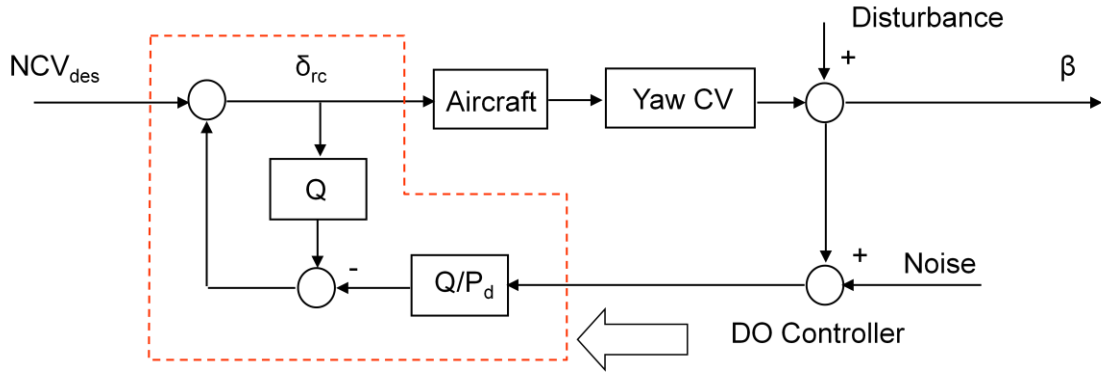
Figure 41. Yaw Axis Disturbance Observer Controller

where δ_{rc} is defined as the desired rudder command sent to the rudder actuator to produce the desired yaw angle. When considering the desired rudder dynamics, P_{d_yaw}, a one-degree-of-freedom dutch roll mode approximation was used. This approximation has errors since rudder displacement does cause some roll, but the major displacement is in the yaw axis [Blakelock, 1991]. Beginning with the three uncoupled, linearized lateral equations of motion and making several simplifying assumptions, Blakelock arrives at the one-degree-of-freedom dutch roll approximation given below:

$$\frac{\beta(s)}{\delta_r(s)} = \frac{-C_{n_{\delta r}}\frac{S\bar{q}b}{J_z}}{s^2 - \frac{b^2 S\bar{q}}{2uJ_z}C_{n_r}s + \frac{C_{n_\beta}S\bar{q}b}{J_z}} \tag{91}$$

where $C_{n_{\delta r}}$ is the change in yawing moment due to rudder, b is the aircraft span, S is the aircraft wing area, J_z is the moment of inertia about the z axis, C_{n_r} is the damping derivative associated with yaw, and C_{n_β} is the change in yawing moment due to sideslip. Since the dutch roll approximation transfer function is second order, it makes sense to

92

have the yaw desired dynamics, P_{d_yaw}, represented by a second order transfer function as well.

$$P_{d\_yaw} = \frac{\omega_y^2}{s^2 + 2\zeta_y \omega_y s + \omega_y^2}$$

(92)

Once again, referring back to MIL-STD-1797B, the recommended minimum natural frequency, ω_y, and the minimum damping ratio, ζ_y, associated with the dutch roll motion is 1.0 radians per second and 0.4 respectively. Based on data presented in MIL-STD-1797B, an $\omega_y = 3$ should produce Level 1 flying qualities. As far as ζ_y is concerned, pilots have found significant improvements in air-to-air and air-to-ground tracking with higher damping ratios [MIL-STD-1797B, 2006]. Therefore, a $\zeta_y = 0.7$ was selected. Below is a plot of the desired yaw dynamics that will be compared with the open and closed loop dynamics.
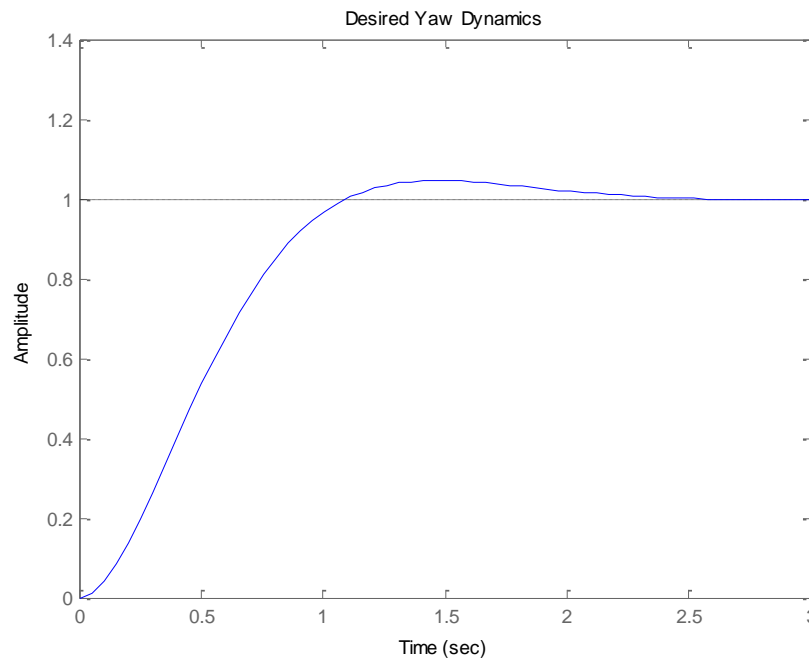
Figure 42. Desired Yaw Dynamics

However, before accomplishing this, a model similar to that created in the pitch

axis DO, was created to represent the directional motion of an aircraft. Using equation

91 as a starting point, the one-degree-of-freedom dutch roll dynamics formed the basis

for model development. Designing the model to encompass the design flight envelope

$h \in [5000; 25000]$ feet and $M \in [0.4; 0.8]$ required a simple adjustment by making $\bar{q}$ a

function of altitude and mach number. As a result, equation 91 becomes

$$\frac{\beta(s)}{\delta_r(s)}(h, M) = G(h, M) = \frac{-C_{n_{\delta r}} \dfrac{S\bar{q}(h, M)b}{J_z}}{s^2 - \dfrac{b^2 S\bar{q}(h, M)}{2uJ_z} C_{n_r} s + \dfrac{C_{n_\beta} S\bar{q}(h, M)b}{J_z}} \tag{93}$$

with everything else constant or nearly constant. Coupling actuator dynamics, G_a, with

$G(h,M)$ yielded a simplified model of the directional aircraft motion.

$$Aircraft = G(h, M) \cdot G_a \tag{94}$$

Once again, as was the case in the longitudinal dynamics model, there are obvious

modeling errors.

Attempting to account for these modeling errors, the directional aircraft model

was combined with a multiplicative uncertainty, $(1 + \Delta_m)$, to account for some of the

existing uncertainties in the aircraft model.

$$Aircraft = G(h, M) \cdot G_a \cdot (1 + \Delta_m) \tag{95}$$

Using the same multiplicative uncertainty presented in the pitch DO controller design

accounts for 20% modeling errors at low frequencies and 200% modeling errors at high

frequency. Finally, including the same performance weights, W_p, and command weights,

W_{cmd}, used earlier enabled the simplified directional aircraft model to account for

modeling uncertainties, penalize performance error, and place the control inputs in the desired frequency range. The finalized architecture of the directional aircraft model is shown in figure 43.
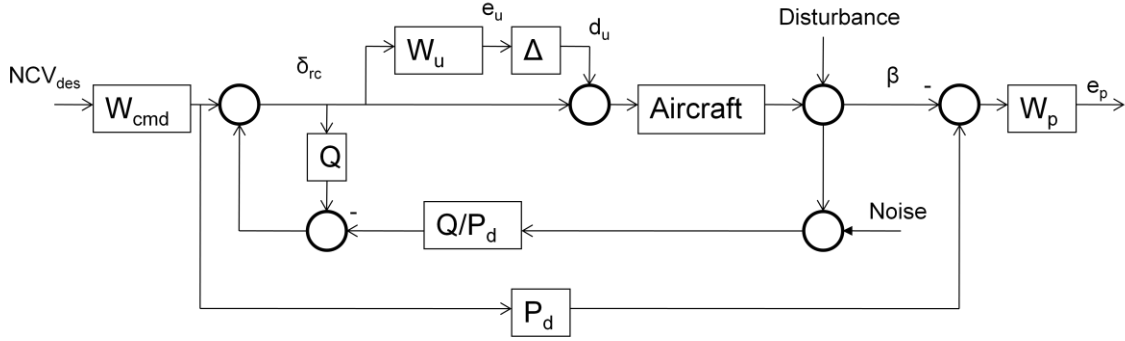
Figure 43. Yaw Axis Disturbance Observer Model and Controller

Finally, using the methods of H_∞ parameter space control design, the filter Q was designed to provide Robust Stability and Nominal Performance. Specifying Q_{yaw} as a second order transfer function of the form

$$Q_{yaw} = \frac{\omega_{Q_{yaw}}^2}{s^2 + 2\zeta_{Q_{yaw}}\omega_{Q_{yaw}}s + \omega_{Q_{yaw}}^2} \tag{96}$$

ensures causality, when calculating the design variables ζ_{Q_yaw} and ω_{Q_yaw}. Using the mapping conditions described in section 2.3.2, guaranteed Hurwitz Stability, Robust Stability and Nominal Performance.

Recall that Hurwitz Stability simply implies the poles of the characteristic equation are in the left hand plane. An analysis of this provided the initial design space for ζ_{Q_yaw} and ω_{Q_yaw} by plotting the values of ζ_{Q_yaw} and ω_{Q_yaw} that caused the poles

of the characteristic equation to lie on the imaginary axis. Below is a plot of the Hurwitz

Stability design space based on the four corners of the flight envelope.
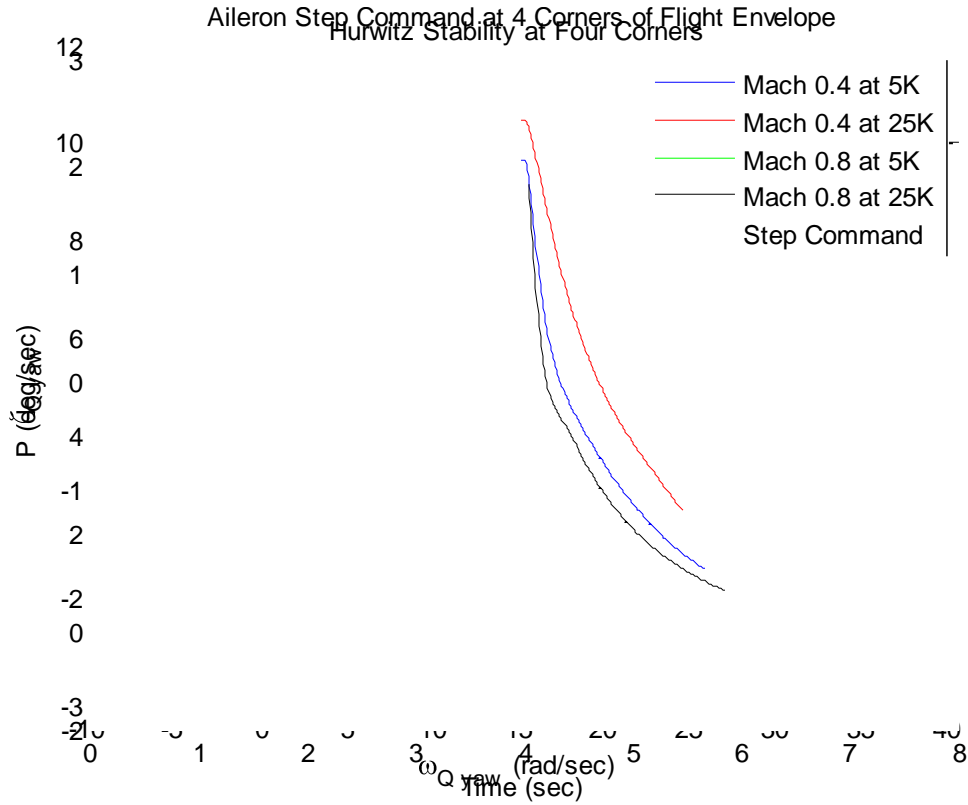
Figure 44. Hurwitz Stability at Four Corners of Flight Envelope

An *X* marks the design space where closed loop poles associated with the four corners of

the flight envelope are in the left hand plane.

Values of ζ_{Q_yaw} and ω_{Q_yaw} were determined to guarantee Robust stability and

Nominal Performance. By selecting values from within the design space provided by

Hurwitz Stability and plotting the criteria associated with Robust Stability and Nominal

Performance,

$$\left\|W_u \cdot T(h, M, \omega_Q, \zeta_Q)\right\|_\infty \leq 1 \qquad (Robust\ Stability) \qquad (97)$$

$$\left\|W_p \cdot E(h, M, \omega_Q, \zeta_Q) \cdot W_{cmd}\right\|_\infty \leq 1 \qquad (Nominal\ Performance)\ (98)$$

an iterative process was used until both mapping conditions were met. Figure 45 shows a plot of Robust Stability meeting the ≤ 1 constraint and Figure 46 shows a plot of Nominal Performance also meeting the ≤ 1 constraint.
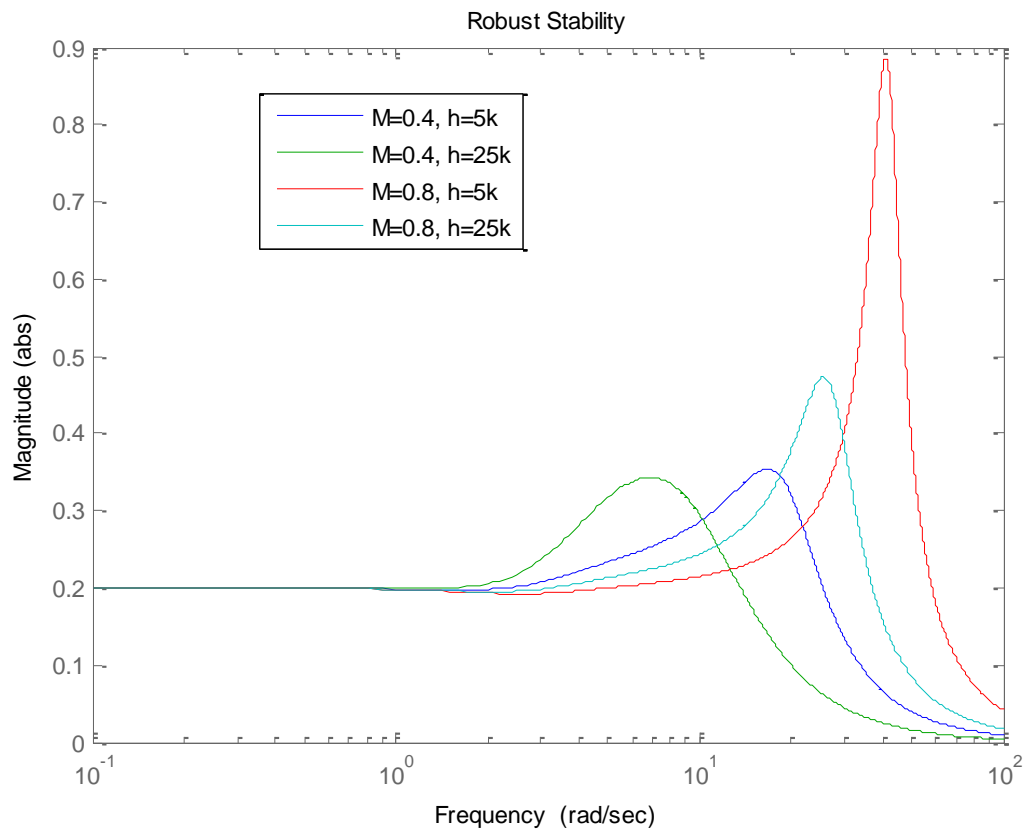
Figure 45. Robust Stability Plot
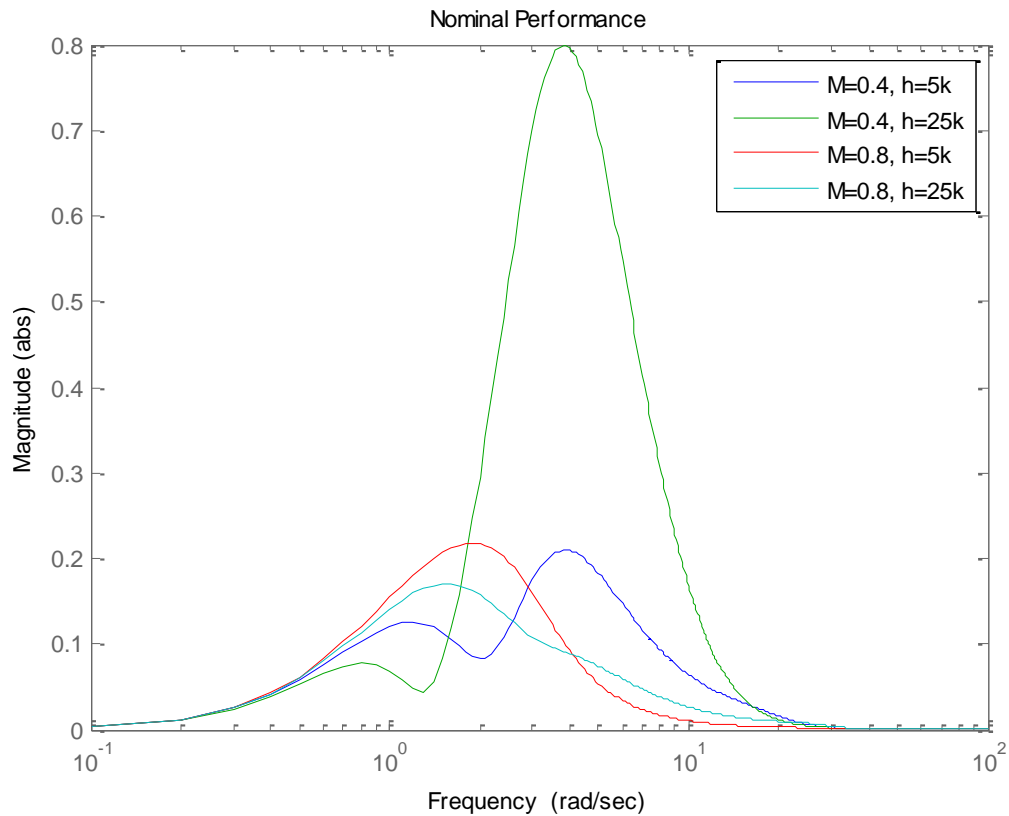
Figure 46. Nominal Performance Plot

As a result of this iterative process, values $\zeta_{Q\_yaw} = 0.9$ and $\omega_{Q\_yaw} = 150$ guaranteed

Robust Stability and Nominal Performance.

Now, with all the values of the yaw axis DO known, a comparison was made at

the four corners of the flight envelope between the open loop yaw dynamics and the

closed loop DO controlled yaw dynamics. A unit step input was commanded to the

rudder command input of a Stevens and Lewis non-linear F-16 model. The open loop

results are shown in Figure 47.
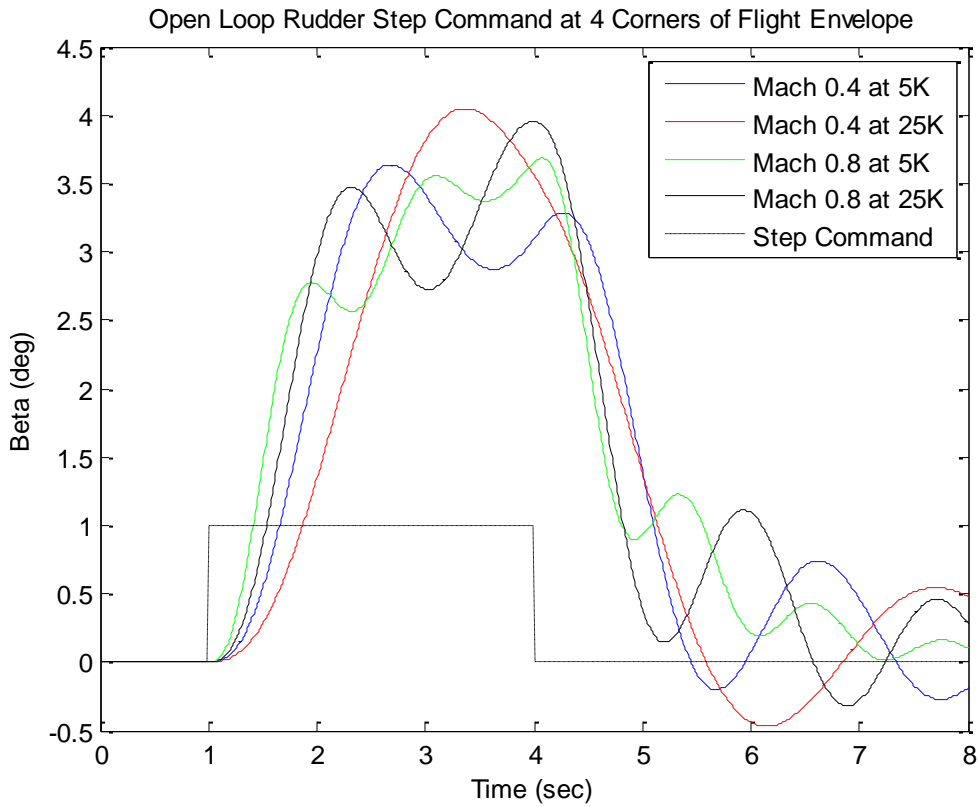
Figure 47. Open Loop Rudder Step Response

Again, as expected, the open loop dynamics were lightly damped and varied in response over the entire design flight envelope. Next, integrating the yaw DO controller with the nonlinear model produced the response illustrated in Figure 48.
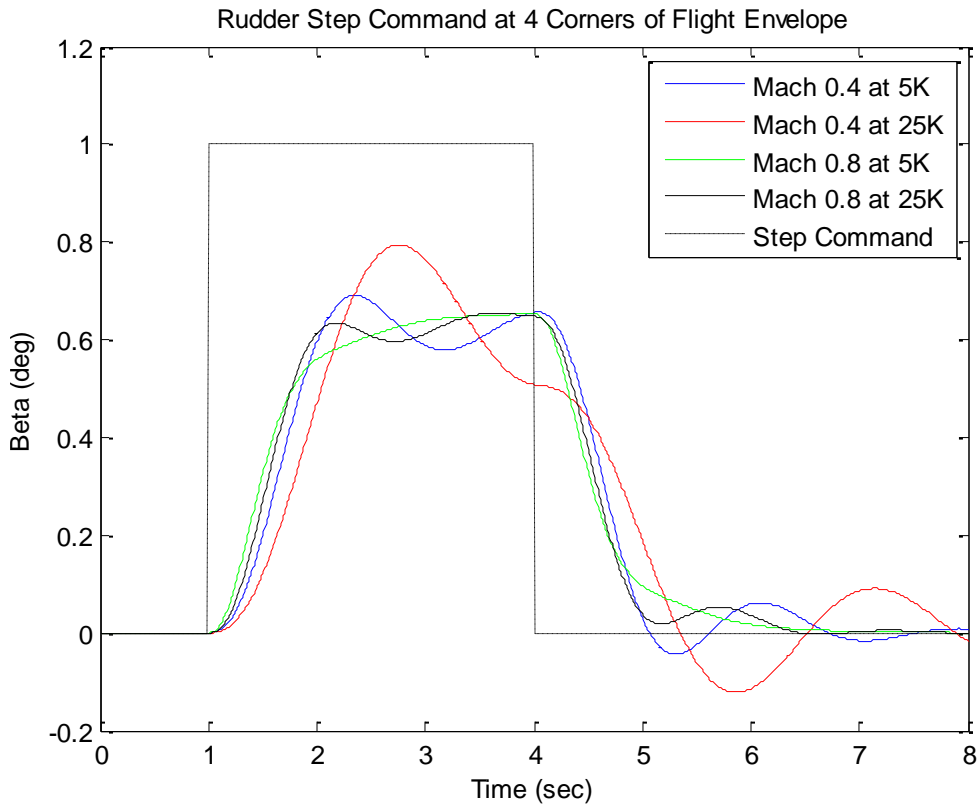
Figure 48. Disturbance Observer Rudder Step Response

Improvements were rather significant as large, lightly damped oscillations are now

smaller with improved damping. Secondly, the oscillations following the roll off of the

step input were not perfect but much improved.

3.6 Summary

The three alternative methods to standby-gain-scheduling were developed in this

chapter. Preliminary computer desktop simulation validated design theories of the DO

controller and led to the selection of the VEST 2 wind estimator. Results from the

Infinity Cube simulator testing of all three systems and the validation of the VEST 2

estimator with flight data are presented in the next chapter.

4.0 Results and Analysis

4.1 Chapter Overview

This chapter presents the results of the pilot-in-the-loop simulator testing conducted at the Air Force Research Laboratory/RBCD facility and the validation of the velocity estimator, VEST 2. During the pilot-in-the-loop simulator testing all three methods of standby-gain-scheduling (VEST 2 control, inertial control, and disturbance observer control) were compared. Cooper-Harper and Pilot-in-the-Loop Oscillation ratings as well as pilot comments and pilot performance were recorded to compare all three methods of standby-gain-scheduling. Section 4.3 discusses the validation of the velocity estimator algorithm, VEST 2. The validation was accomplished by post-processing simulator data from the block 40 F-16C simulator and actual flight data from a block 30 F-16D aircraft. The results obtained from the post-processing of the block 40 F-16C simulator data were used to tune the Kalman filter prior to post-processing actual aircraft data. Finally, the results from post-processing actual aircraft data were also used to determine the strengths and weaknesses of the VEST 2 algorithm during actual aircraft maneuvers.

4.2 Block 40 F-16C Simulator Results

This section describes the results of aircraft simulation testing conducted at the Air Force Research Laboratory AFRL/RBCD simulator building. A high-fidelity, six-degree-of-freedom, block 40 F-16C model with flight control system was used as the

simulated aircraft. Three controllers were integrated with this high-fidelity model: the baseline F-16 control system (F-16 controller); the baseline F-16 control system gain-scheduled by VEST 2 (VEST 2 controller); and the baseline F-16 control system gain-scheduled using inertial velocities (inertial controller). Unfortunately, problems arose with the integration of the DO controller in the block 40 F-16C simulator model and these issues were not resolved prior to testing. So, as a substitute, the Stevens and Lewis F-16 model was used in the Infinity Cube for this controller.

There were a few issues with the Stevens and Lewis model that arose during testing and must be kept in mind when analyzing the results. First, the Stevens and Lewis model did not have an alpha or g-limiter so one was added but it was not as good as the limiter in the high-fidelity model. Second, during the testing it was apparent that the throttles were scaled differently between the two models. Thirdly, there were no leading edge flaps in the Stevens and Lewis model which definitely affected performance at higher angles of attack. Finally, at higher angles of attack, the Stevens and Lewis model had a tendency to depart controlled flight and may have been a result of the marginal AOA limiter.

The models and controllers were installed on the Infinity Cube Simulator. This simulator had a 210 degree field of view created by four projection screens that were focused at infinity. The cockpit contained a heads up display, heads down display, throttle, and fly by wire side stick controller. Data collected from this test included desired and adequate performance metrics for landing and tracking tasks, Cooper-Harper (CH) ratings, Pilot-in-the-Loop Oscillation (PIO) ratings, and variables from the aircraft

104

equations of motion. All this information and pilot comments associated with each task were used to compare the performance of each standby-gain-scheduling controller.

There were two different types of tasks flown in the simulator. The first was a landing task that required the pilot to land a block 40 F-16C on a desired touchdown point with a desired AOA. The second task was an air-to-air tracking task where pilots attempted to follow a target aircraft around and maintain a desired position. The test matrix for the primary testing consisted of six landing and six tracking tasks.

Preparation for the primary testing took place over a period of three days where retired pilots of varying airframes with a wide range of experience were brought in to be part of a pilot study. This study served two purposes: to point out any issues with aircraft controllers, testing methods, performance criteria and task timing; the second purpose attempted to determine the required number of practice runs for each task prior to starting the primary testing. Throughout this process implementation issues were identified and the testing procedure was refined.

A result of the pilot study indicated the need for three practice landings and two practice tracking tasks prior to commencing the actual testing. The order of testing was varied so that half of the time landings were tested first and the other half of the time tracking tasks were tested first. The practice tasks were flown immediately before the type of task to help eliminate biased results based on unfamiliarity with the task. Finally, the disturbance observer (DO) controller was tested outside of its design envelope (0.4 to 0.8 Mach and 5,000 to 25,000 feet) for landing tasks. On average, typical approach and lading speeds are between 0.25 and 0.35 Mach in the altitude band of 1,000 to 2,000 ft. Being well outside of its design flight envelope, the performance of the DO controller

was marginal at best. Therefore, the decision was made to remove the DO standby controller from the lading task.

The primary testing took place over a period of three days and included 18 pilots with experience in a wide number of airframes. There were 10 fighter pilots, 6 tanker/airlift pilots, 1 bomber pilot, and 1 helicopter pilot. Experience levels were typically high with 1 pilot having completed Fighter Weapons School training. There were no Test Pilots and all pilots had little experience with applying Cooper-Harper and PIO ratings.

There were four controllers used for the tracking task: the nominal block 40 F-16C (F-16 controller); the block 40 F-16C with estimated dynamic pressure for gain-scheduling (VEST 2 controller); the block 40 F-16C with inertial dynamic pressure for gain-scheduling (inertial controller); and the DO controller (Stevens and Lewis F-16 model). As mentioned earlier, the landing task did not include the DO controller but included the other three controllers. Controllers for both the landing and tracking tasks were flown in a random order. For the landing task, each of the controllers used were flown twice. In the tracking task, each controller was flown at least once. In between each run, pilots were asked to give Cooper-Harper ratings and PIO ratings that described the controller just flown. They were also asked to provide any comments associated with their ratings.

4.2.1 Tracking Task.

Starting conditions for each tracking task consisted of two low altitude (M = 0.8, h =5,000 ft) initial conditions, two medium altitude (M = 0.8, h = 15,000 ft) initial

106

conditions and two high altitude (M = 0.8, h = 25,000 ft) initial conditions. During the

tracking task, target maneuvers were flown at a constant throttle setting, causing airspeed

to vary anywhere from M = 0.35 to M = 0.85. There were a total of six different flight

profiles flown with each profile containing a 2 g level turn, a 4 g level turn, a 6 g level

turn, a barrel roll, a pitchback and a sliceback. Each profile was flown in a slightly

different order to prevent test subjects from predicting target maneuvers. The

combination of both the maneuvers flown and the initial conditions allowed the tracking

task to cover the entire flight design envelope of the DO controller.

The objective of the tracking task was to chase the target through the different

maneuvers and stay within a specified cone behind the target. The desired cone was

within 30 degrees of the target's tail and between 2,000 and 3,000 feet. The adequate

cone was within 45 degrees of the targets tail and between 1,500 and 3,500 feet. Figure

49 is an example of the tracking task cone.
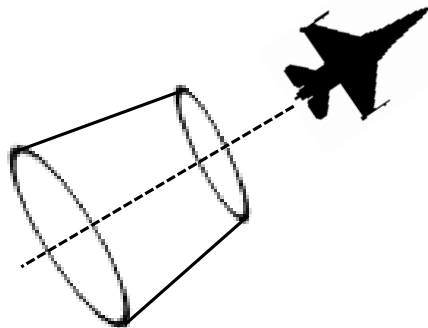
Figure 49. Tracking Task Cone

The heads-up display (HUD) was the primary means for pilots to determine where they

were in relation to the desired and adequate cones. In the HUD, the pilot had both a

digital readout and visual indication of range and a visual indication of their position

relative to the desired and adequate cone. Figure 50 is a snapshot of the HUD with the important information highlighted.
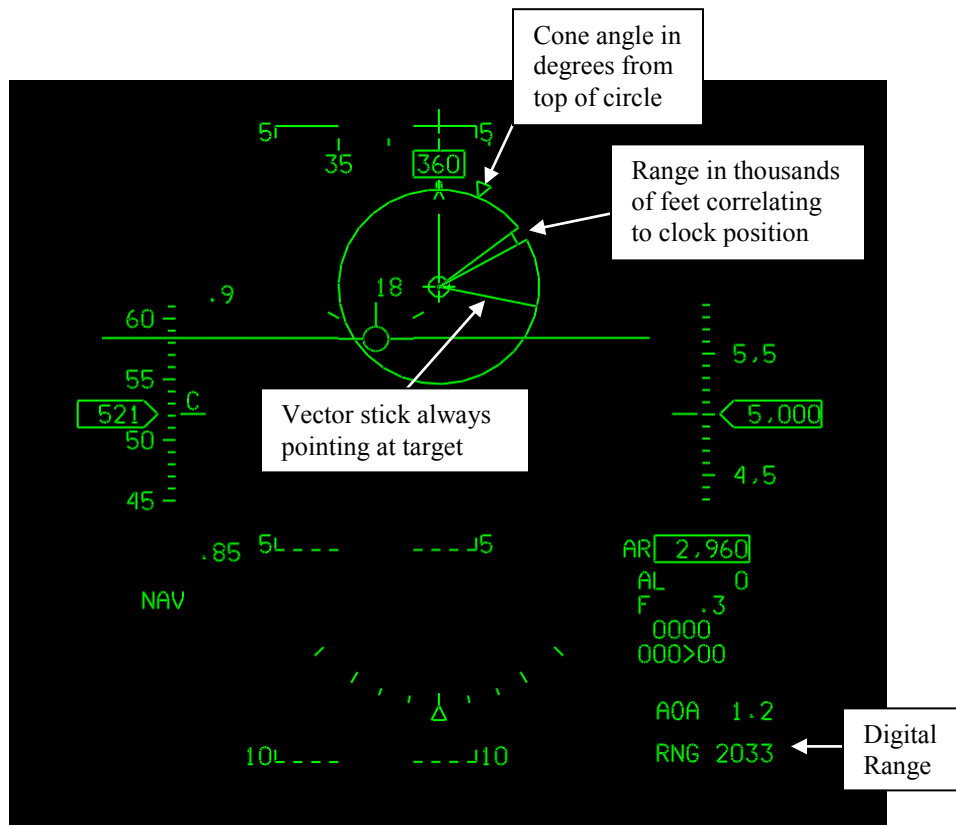
Figure 50. Tracking Task Heads-Up Display

All four controllers were flown a total of 27 times; nine times in each altitude block (low, medium, and high). For each run, the total time that the aircraft was in the desired and adequate cones was recorded to determine a measure of performance. The combined results of the tracking task performance are shown in Table 8.

Table 8. Tracking Task Performance

Tracking Performance	Standard F-16	F-16 with VEST 2 Gain-Scheduling	F-16 with Inertial Gain-Scheduling	F-16 with DO*
Desired Criteria Met	43%	48%	45%	37%
Adequate Criteria Met	78%	84%	81%	69%

*Stevens and Lewis Model

Similar performance was observed between the standard F-16 controller, the VEST 2 gain-scheduled controller, and the inertial gain-scheduled controller. There was a noticeable decrease in the level of performance obtained with The DO controller. Cooper-Harper ratings were assigned using Bailey's assessment process explained in section 2.5. The CH ratings shown in Figure 51 generally align with the results obtained from the desired and adequate performance criteria.
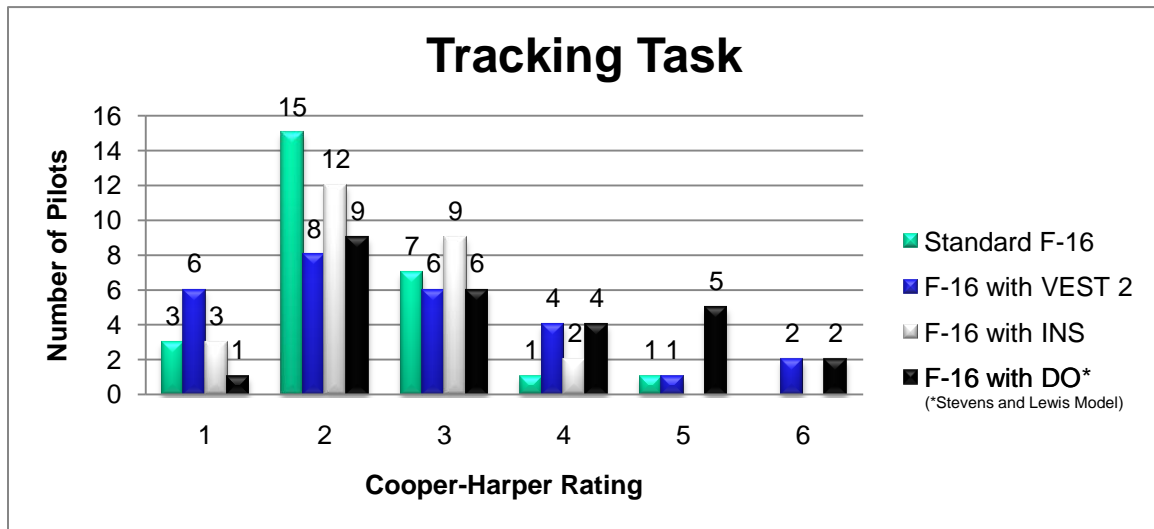
Figure 51. Tracking Task Cooper-Harper Ratings

Two CH ratings of 4 and two CH ratings of 6 for VEST 2 occurred on the first day of testing and were likely caused by an error in integration of the VEST 2 algorithm with the standard F-16 control laws. This issue may have shifted some of the CH ratings for VEST 2 to the right. This was corrected for the remainder of the testing.

In general, the Standard F-16, VEST 2, and the INS controllers had similar pilot comments that did not highlight any deficiencies. However, there was one pilot comment associated with the INS controller that was repeated several times and it was associated with control at high altitudes and slow airspeeds. The comments described a heavy stick and sluggish aircraft response associated with the high altitude flight. This might be explained by the combination of a strong wind at high altitudes and the aircraft traveling in the same direction as the wind. In this case, inertial velocities will causes the gain to be reduced because the aircraft thinks it is traveling faster through the air than it actually is. For the DO controller, pilot comments generally described a sensitive stick and annoying roll oscillations. These undesirable motions may have caused the overall decrease in performance. However, as stated earlier, the other major factor that cannot be ignored is the fact that the DO controller was implemented on the Stevens and Lewis F-16 model and not on the high-fidelity, six-degree-of-freedom, block 40 F-16C simulator model.

The PIO ratings illustrated in Figure 52 show that there were very little undesirable motions observed in three of the four controllers. The DO controller was the only controller that had undesirable motions. These undesirable motions were easily induced with some bounded roll PIOs that are likely associated with the sensitive stick.
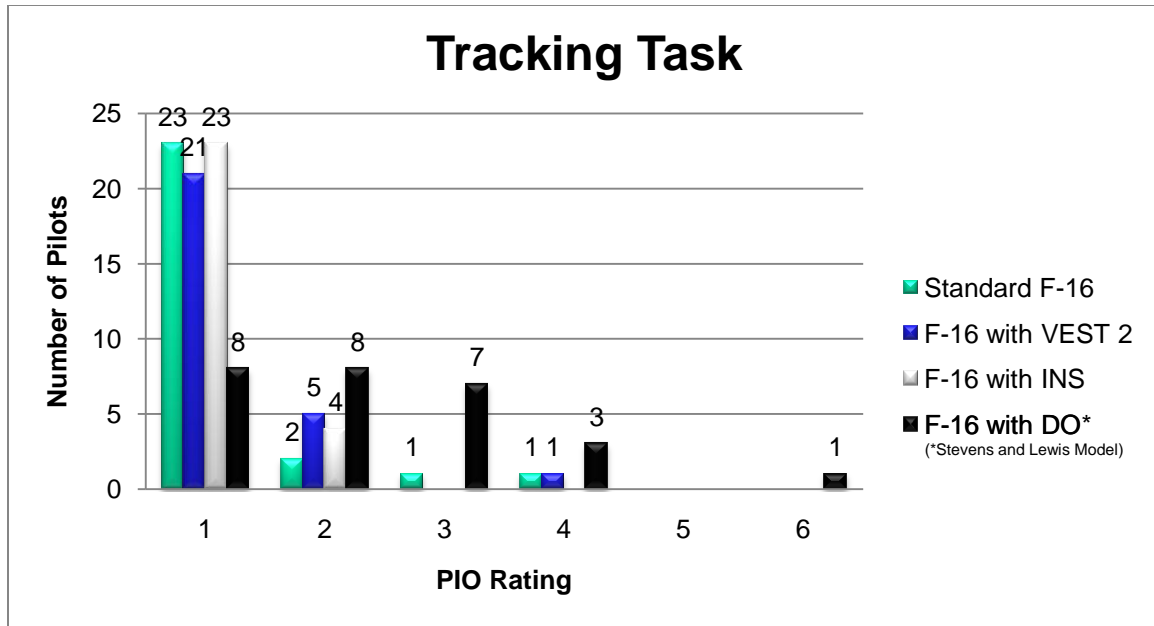
Figure 52. Tracking Task Pilot-in-the-Loop Oscillation Ratings

The PIO rating of 6 for the DO controller was given as a result of the aircraft departing controlled flight in an extremely nose high, slow speed flight attitude. The departure was attributed to the lower fidelity Stevens and Lewis model and not to the DO controller. Typically, a CH rating of 10 is associated with a departure from controlled flight but in this case, the pilot elected to give a CH rating of 6.

Results from the tracking task indicate that there is almost no difference between the Standard F-16, VEST 2, and the INS controllers when tracking a target up and away from the ground. This indicates that a VEST 2 gain-scheduled controller, and an inertial gain-scheduled controller would provide sufficient control to act as an alternative to standby-gain-scheduling at altitude. The DO controller was less effective at the tracking task but did show potential for further refinement and development; particularly improvements could be made in the roll axis.

4.2.2 Landing Task.

The six landing tasks were designed to force the test subjects to aim for and touch down at a specific point on the runway while simultaneously controlling aircraft speed and angle of attack (AOA). The desired touchdown point was marked by blocks that stuck up out of the runway and are shown in Figure 53.
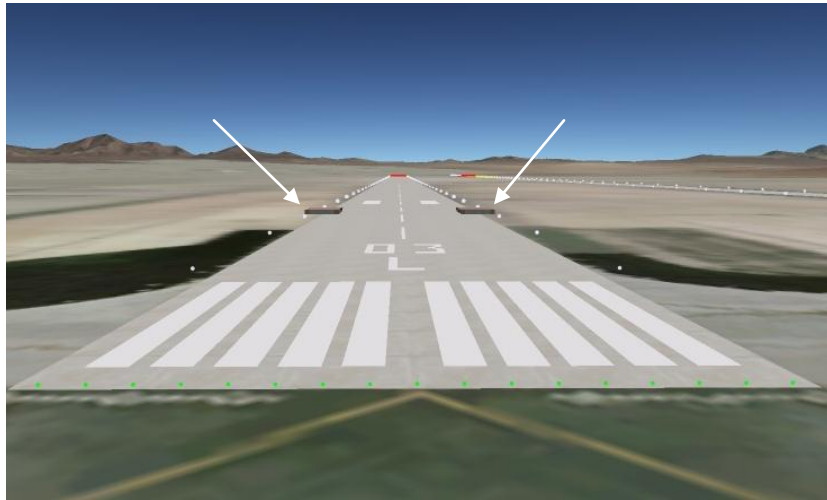
Figure 53. Desired Touchdown Point (Landing Task)

Initial approaches began at six nautical miles from the threshold, 1000 feet above the ground. There were two parallel landing runways allowing for the combination of both straight-in and side-step approaches. With the parallel runways, there were four different landing profiles that the pilots could fly:

1. Start on the left runway and land on the left runway.
2. Start on the left runway and land on the right runway.
3. Start on the right runway and land on the left runway.
4. Start on the right runway and land on the right runway.

Pilots were told 1.3 nautical miles from the desired touchdown point whether they were to sidestep to the other runway or land on the runway they were already lined up on. The sidestep was a deliberate attempt to drive the pilots gain up and also provide some lateral and directional maneuvering for evaluation.

The HUD was the primary means for pilots to determine their AOA at touchdown. In the HUD, the pilot had both a digital readout and visual indication of the AOA. Figure 54 is a snapshot of the HUD with the important information highlighted.
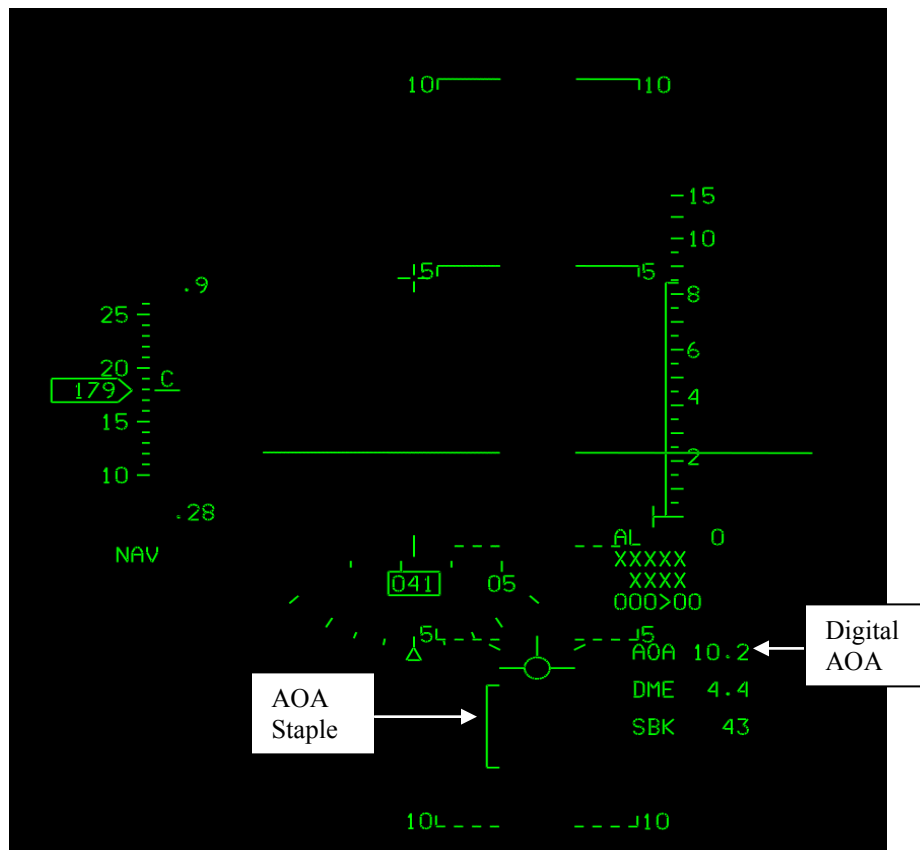
Figure 54. Landing Task Heads-Up Display

The objective of the landing task was to obtain desired performance by touching down within the blocks (750 ± 250 feet down the runway) and at 13±1 degrees of AOA. Adequate performance was obtained by touching down 750 ± 500 feet down the runway and at 13±2 degrees of AOA. If the desired touchdown point was obtained but it occurred with 15 degrees AOA then the overall performance for that landing was adequate.

Thirty-five landings were accomplished with each of the three controllers (standard F-16 controller, VEST 2 gain-scheduling controller, and inertial gain-scheduling controller). Recall that the DO controller was removed from this task since the task was well outside of the designed flight envelope. Table 9 below shows the performance results of the landing tasks.

Table 9. Landing Task Performance

Landing Performance	Standard F-16	F-16 with VEST 2 Gain-Scheduling	F-16 with Inertial Gain-Scheduling
Desired Criteria Met	18%	14%	4%
Adequate Criteria Met	32%	27%	32%

Similar desired performance was observed between the standard F-16 controller and the VEST 2 gain-scheduled controller. There was a noticeable decrease in the desired performance using the inertial gain-scheduled controller. This was largely attributed to the faster TAS that the pilots were flying on final and was caused by a head wind. In the

INS version, aircraft were actually traveling faster through the air than pilots thought when looking at airspeed in HUD (which was actually ground speed). As a result it was more difficult to land in the desired zone with the desired AOA. There were no trends relating to the sidestep maneuver nor were there any associated comments with maneuvers in the lateral or directional axis. The Cooper-Harper ratings associated with each controller are shown in Figure 55.
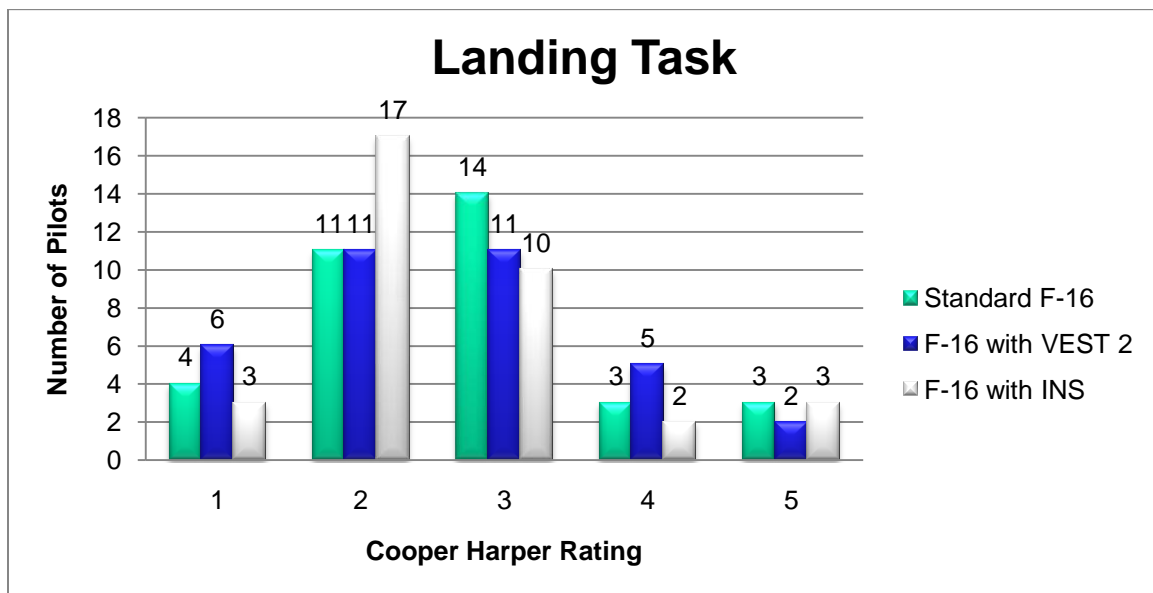
Figure 55. Landing Task Cooper-Harper Ratings

The only noticeable discrepancy is the large increase in CH ratings of 2 for the inertial gain-scheduled controller. By definition, a CH rating of 2 is associated with a desired performance and minimal pilot workload. However, as stated above, the inertial gain-scheduled controller had a much lower desired performance rating than the other two controllers. The reason for this spike in CH ratings of 2 is most likely due to two things. First, it was left up to the pilot to determine what level of performance was achieved on

each landing which introduces error into the CH rating system. Second, the faster TAS

that the pilots were flying on final caused by a head wind made the aircraft feel slightly

more responsive and the pilots liked this feel. Therefore, they were inclined to give a

higher CH rating not because they obtained desired performance but because the aircraft

felt more responsive flying at a slightly faster true airspeed. The PIO ratings for the

landing tasks are shown in Figure 56.
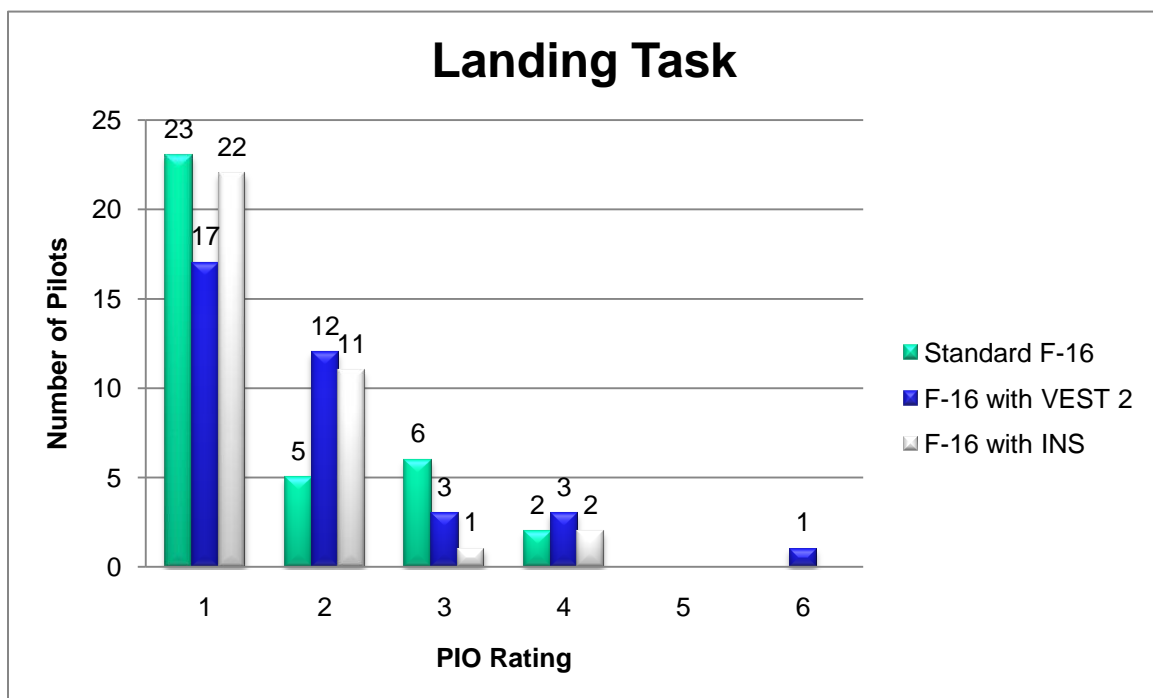
Figure 56. Landing Task Pilot-in-the-Loop Oscillation Ratings

The PIO ratings reviled that for the large majority of pilots, there were very little

undesirable motions during the lading phase. However there were some bounded pilot-

in-the-loop oscillations that did occur showing that each of the controllers are PIO prone.

The PIO rating of 6 for the VEST 2 controller occurred on the first day of testing when

there was an error in the integration of VEST 2 algorithm with the standard F-16 control

laws. This, coupled with pilot experience (helicopter pilot) is most likely why the VEST 2 controller received a PIO rating of 6.

Results from the landing task indicate that there is little difference between the Standard F-16 and the VEST 2 controller when landing. The desired performance of the inertial gain-scheduled controller most likely decreased as a result of the higher true airspeeds caused by the winds. In this test, where the maximum headwind was approximately 10 knots, the overall performance remained comparable to the other two controllers. The danger exists in this type of controller when there is a strong tailwind. If an aircraft with an inertial gain-scheduler is forced to land in a strong tailwind, it may stall before it touches down due to its slower true airspeed. This worst case scenario was not tested and needs further attention. Overall, based on the results obtained from the landing task, a VEST 2 gain-scheduled controller would provide sufficient control to act as an alternative to standby-gain-scheduling in the landing phase of flight.

4.3 Validation of Wind Estimator (VEST 2)

To validate the VEST 2 wind estimator, the data obtained from the desktop simulation were compared with the data obtained from both the F-16 simulator testing and actual aircraft flight data. For this comparison, the F-16 simulator data and the actual flight data were post-processed using the VEST 2 algorithm. Using the data from the F-16 simulator, the VEST 2 Kalman filter was tuned to obtain the best results. Then these results were compared to the results obtained from post-processing actual aircraft data. Finally, the results from the post-processing of the actual aircraft data were also used to

determine the strengths and weaknesses of the VEST 2 algorithm during actual aircraft maneuvers.

4.3.1 Post Processed Simulator Data.

For implementation with the block 40 F-16C control laws, the estimated TAS components from VEST 2 were used to calculate a compressible dynamic pressure. Compressible dynamic pressure is simply a calculation of dynamic pressure using calibrated airspeed (defined in section 2.2.2). This estimated compressible dynamic pressure was then used to drive the block 40 F-16 gain-schedule during both the tracking and the landing tasks.

The same wind profile described in section 3.3.4 was used in the simulation during the tracking task. The target maneuvers in the tracking task were all flown with the same wind profile in order to prevent the changes to the initial conditions associated with the simulator. Each run lasted between 2.5 and 3.5 minutes and started from the three different altitudes mentioned above. The processes for compiling all the runs were the same as used during the desktop simulation. An ensemble average was taken over the 27 runs using the shortest run time as the stopping point for all tracking runs. The results are listed in table 10 below and plots of each estimator are shown in Appendix A.

Table 10. Wind Estimator Tracking Task (Measured Alpha & Beta)

Measured Alpha and Beta	VEST	VEST TAS	VEST 2
Wind Speed Error Temporal Average (ft/sec)	-8.234	-20.27	-14.25
Wind Speed Error Standard Deviation (ft/sec)	±3.19	±7.591	±5.256
Wind Heading Error Temporal Average (deg)	-0.05425	-0.3006	0.1232
Wind Heading Error Standard Deviation (deg)	±6.879	±6.844	±6.861

Due to the length of each run being less than three minutes, there were some larger variations than those obtained through the 10 minute desktop simulations. Secondly, since the variability of the wind heading was set to ±10 degrees, the rate of change over the shorter period proved challenging for the wind estimators. Finally, one profile caused a rather large change in the estimated wind speed brought about by a large vertical maneuver. The correction to this maneuver and to the variability in wind heading conditions was slower than desired and suggested that each Kalman filter may need some additional tuning.

By post-processing the data obtained from each run, a study was done in order to improve the performance of the Kalman filter. The tuning involved changing the error covariance matrix, **P**, and the wind estimate uncertainty, **Q**. The final results of this tuning are displayed in Table 11 with plots displayed in appendix B.

Table 11. Wind Estimator Tracking Task with Tuning (Measured Alpha & Beta)

Measured Alpha and Beta with Tuning	VEST	VEST TAS	VEST 2
Wind Speed Error Temporal Average (ft/sec)	-3.559	-5.144	-4.352
Wind Speed Error Standard Deviation (ft/sec)	±1.775	±3.313	±2.368
Wind Heading Error Temporal Average (deg)	-0.4418	0.8155	-0.0774
Wind Heading Error Standard Deviation (deg)	±3.029	±3.878	±3.641

This tuning greatly improved the estimation by providing a more responsive filter. Knowing that a weakness associated with any form of the VEST Kalman filters is its requirement to have heading changes, a profile consisting of six minutes worth of maneuvering time, followed by a straight and level flight profile (long shot) lasting 10 minutes was tested. This was flown with the tuning included and the results are presented in the table below and in Appendix C.

Table 12. Wind Estimator Long Shot with Tuning (Measured Alpha & Beta)

Measured Alpha and Beta with Tuning	VEST	VEST TAS	VEST 2
Wind Speed Error Temporal Average (ft/sec)	-2.342	4.153	-0.9055
Wind Speed Error Standard Deviation (ft/sec)	±6.587	±6.945	±2.412
Wind Heading Error Temporal Average (deg)	-2.051	5.229	1.589
Wind Heading Error Standard Deviation (deg)	±5.558	±8.74	±4.32

By testing the filters in their weakest condition (straight and level flight), the results show that the tuning did not alter their performance. This eliminates the concern that the tuning adjustments may cause a filter to become divergent.

The final check for the tracking task was to see if the alpha and beta estimator would work any better on this set of data. Recalling that the best results were obtained using alpha estimate and setting beta equal to zero, an ensemble average was calculated by post-processing the data with the newly tuned values. The results in Table 13 were better than expected.

Table 13. Wind Estimator Tracking Task with Tuning (Est. Alpha, Beta=0)

Estimated Alpha (Beta=0) with Tuning	VEST	VEST TAS	VEST 2
Wind Speed Error Temporal Average (ft/sec)	12.46	10.66	11.56
Wind Speed Error Standard Deviation (ft/sec)	±5.63	±6.955	±6.194
Wind Heading Error Temporal Average (deg)	-0.192	-0.2641	4.708
Wind Heading Error Standard Deviation (deg)	±11.62	±13.17	±11.05

These results hint that a more accurate method of estimating alpha and beta could fulfill the requirement of completely removing the Pitot static system from VEST, VEST TAS, and VEST 2.

The landing task was flown as described is section 4.2.2 only using three controllers (recall the DO controller was eliminated from the landing task). Therefore, each pilot flew each controller twice. Once again, the ensemble average was computed

over 35 runs using the shortest run as the stopping point. Table 14 displays the results

and plots of each estimator are located in Appendix D.

Table 14. Wind Estimator Landing Task (Measured Alpha & Beta)

Measured Alpha and Beta	VEST	VEST TAS	VEST 2
Wind Speed Error Temporal Average (ft/sec)	1.658	--0.9731	0.3422
Wind Speed Error Standard Deviation (ft/sec)	±1.165	±0.9102	±0.1441
Wind Heading Error Temporal Average (deg)	-0.007153	0.6174	0.3123
Wind Heading Error Standard Deviation (deg)	±0.01136	±0.3016	±0.1479

Once again, the results were also post processed with the already established tuning to

see what affect it had on the landings. Table 15 shows the landing tasks with tuning and

the plots can be found in Appendix E.

Table 15. Wind Estimator Landing Task with Tuning (Measured Alpha and Beta)

Measured Alpha and Beta with Tuning	VEST	VEST TAS	VEST 2
Wind Speed Error Temporal Average (ft/sec)	1.295	-0.9024	0.1962
Wind Speed Error Standard Deviation (ft/sec)	±0.885	±0.6988	±0.1165
Wind Heading Error Temporal Average (deg)	0.001077	0.05273	0.02582
Wind Heading Error Standard Deviation (deg)	±0.05949	±0.1743	±0.09209

Comparing both the landing tasks, it is evident that the tuning improved the estimator's

performance as well.

Results from both the tracking tasks and landing tasks indicate that the wind estimator is more than capable of producing a reliable wind estimate which in turn leads to a reliable true airspeed needed for gain-scheduling. Using the tracking task as a measure of performance, VEST 2's average wind speed error was -2.6 ± 1.4 knots with a heading error of 0.1 ± 3.6 degrees. Realizing that accurate measurements of alpha and beta will likely not be available following an air data system failure, VEST 2 also achieved good results with an estimated alpha and a beta equal to zero. In this case the average wind speed error was 6.8 ± 3.7 knots with a heading error of 4.7 ± 11.1 degrees. Therefore, the estimated wind speed from the VEST 2 algorithm makes a viable substitute for determining true airspeed used in traditional gain-scheduling.

4.3.2 Post Processed Flight Data.

Finally, VEST 2 was selected for further analysis using actual aircraft data from a block 30 F-16D. The flight data was post processed using the airspeed estimator algorithm. The benefit of post-processing actual aircraft data is that all the measurements required to make the wind estimator algorithm work contain actual measurement noise. One of the limitations to the simulator testing conducted above was that all the feedback variables were clean (i.e. there was no noise associated with each signal). Using actual aircraft data recorded from a data acquisition system provides raw data that can be used to realistically test the wind estimators.

The data used for post-processing were taken from three different sorties. To ensure that all the data were used, data from two of the longer sorties were broken up into four sets so that the total runtime for each data set was over 28 minutes. Then, using a

123

very similar analysis process to the one previously described, an ensemble average (average of each data point associated with a specific time) of the five blocks of data was taken. From this ensemble average, the temporal average and standard deviations were calculated.

The three sorties flown were part of the Test Pilot School Performance Phase curriculum. The first sortie was an Aerodynamic Modeling data sortie that included the following maneuvers: a military power climb from 10,000 feet pressure altitude (PA) to 40,000 feet PA; dynamic maneuvers that included roller coasters, wind-up turns, and split-s; cruise data points (straight and level unaccelerated flight); and a maximum range descent (idle and 218 KCAS) from 25,000 feet to 10,000 feet. See appendix F, Figures (90-93) for the comparisons of wind speed and heading estimations. The second sortie was a Turn Performance data sortie that included the following maneuvers: stabilized turns at various airspeeds and load factors using military power; stabilized turns at various airspeeds and load factors using maximum power; a maximum power level acceleration at 35,000 feet PA; and a penetration descent (idle, 300 KCAS and speed brake) from 40,000 feet PA to 10,000 feet PA. See appendix F, Figures (94-97) for the comparisons of wind speed and heading estimations. The third sortie flown was a Level Acceleration data sortie that included the following maneuvers: military power and maximum power level accelerations; a maximum range descent (idle and 218 KCAS) from 40,000 feet to 10,000 feet PA; and a penetration descent (idle, 300 KCAS and speed brake) from 40,000 feet to 10,000 feet PA. See appendix F, Figures (98-101) for the comparisons of wind speed and heading estimations.

There was no balloon data available to get wind truth data for any of these sorties. The next best truth source for wind speed would have been an actual recording of the calculated winds from the block 30 F-16D air data system. Unfortunately, the data acquisition systems are not setup to record F-16 wind calculations. As a result, the data acquisition measurements of true airspeed (TAS), inertial navigation system (INS) speeds and a few other measurements were used to calculate the truth data for the winds. Since the data coming from the data acquisition system is somewhat noisy, the calculated truth data was also noisy. To correct this, an F-16 wind filter similar to the one in the aircraft was built to filter the raw data and provide a more stable measure of truth data. An example of the filtered wind data is illustrated in Appendix G.

Figures 57 and 58 show the ensemble average wind speed and heading error from the VEST 2 wind estimator using measured values of alpha and beta.
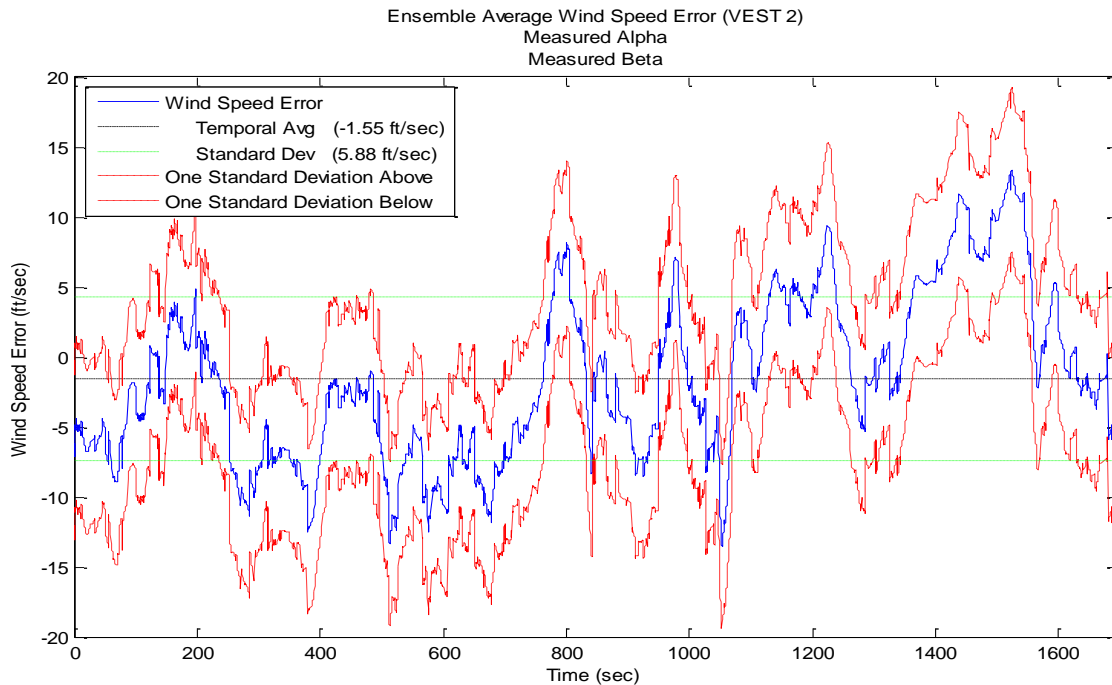
Figure 57. VEST 2 Wind Speed Error with Flight Data (Meas. Alpha & Beta)
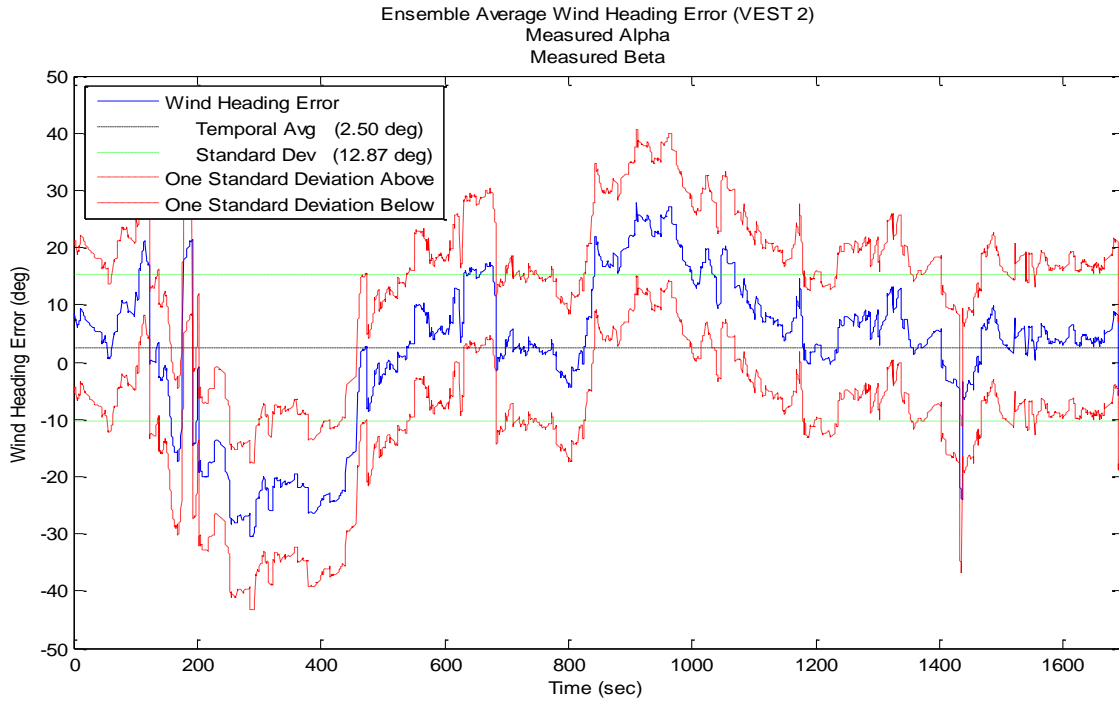
Figure 58. VEST 2 Wind HDG Error with Flight Data (Meas. Alpha & Beta)

A comparison between the VEST 2 results from the desktop simulation, simulator tracking task, and the VEST 2 results from flight data is shown in Table 16.

Table 16. VEST 2 Performance Comparison (Measured Alpha and Beta)

Measured Alpha and Beta	**VEST 2 Flight Data**	**VEST 2 Simulator Data**	**VEST 2 Desktop Simulation**
Wind Speed Error Temporal Average (ft/sec)	-1.55	-4.352	1.742
Wind Speed Error Standard Deviation (ft/sec)	±5.88	±2.368	±5.462
Wind Heading Error Temporal Average (deg)	2.50	-0.0774	0.4313
Wind Heading Error Standard Deviation (deg)	±12.87	±3.641	±2.857

When subjected to noisy aircraft data, the performance of the VEST 2 wind estimator is on par with the results obtained in both the simulator testing and the desktop simulation. The largest change was associated with the standard deviations and was somewhat expected based on the noisy measurements coming from the aircraft.

Taking this analysis one step farther, figures 59 and 60 show the wind speed and heading error from the VEST 2 wind estimator using an estimated alpha and setting beta equal to zero.
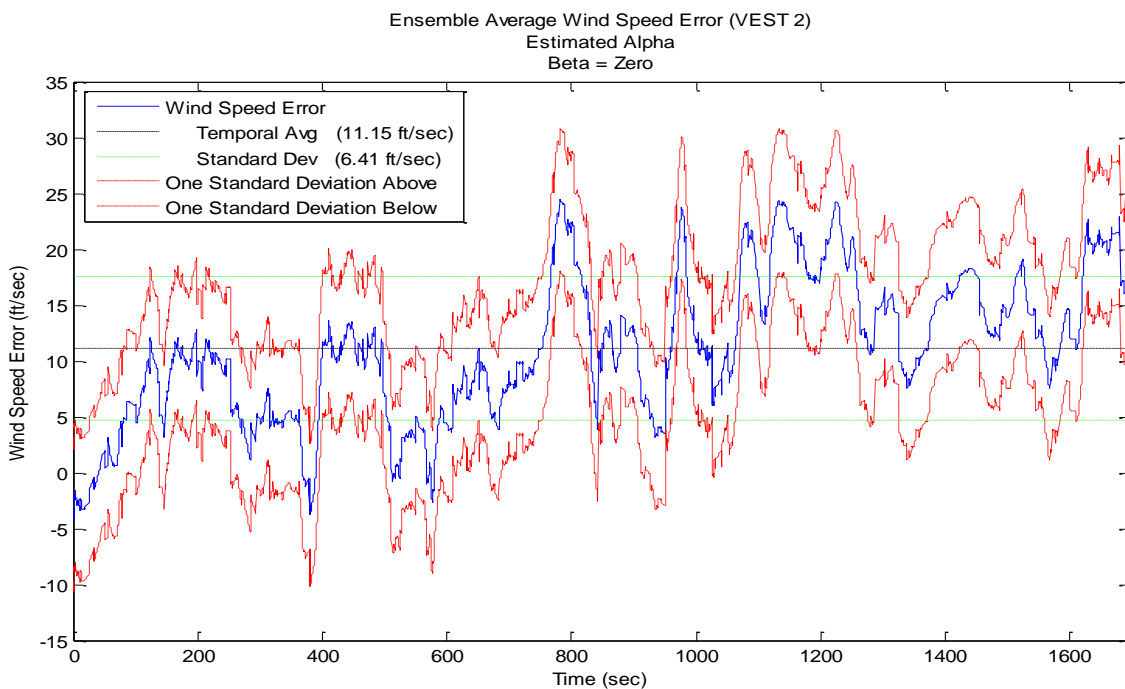
Figure 59. VEST 2 Wind Speed Error with Flight Data (Est. Alpha, Beta = 0)

Ensemble Average Wind Heading Error (VEST 2)
Estimated Alpha
Beta = Zero
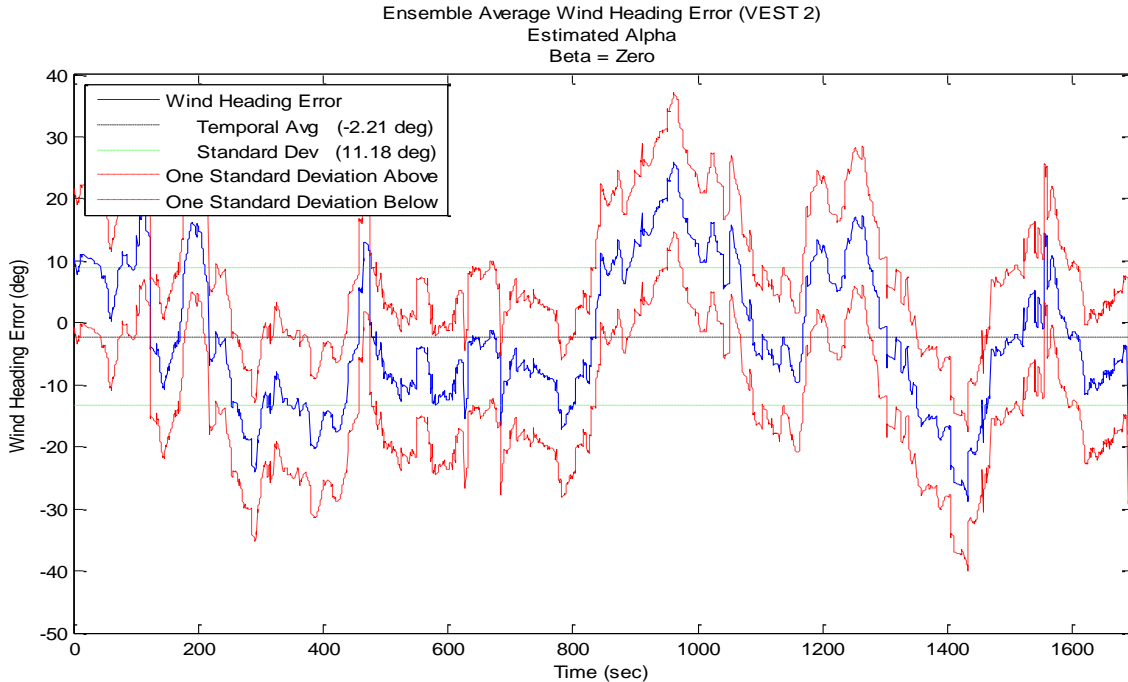
Figure 60. VEST 2 Wind HDG Error with Flight Data (Est. Alpha, Beta = 0)

Once again, a comparison between the VEST 2 results from the desktop simulation, simulator tracking task, and the VEST 2 results from flight data is shown in Table 17.

Table 17. VEST 2 Performance Comparison (Estimated Alpha, Beta = 0)

Estimated Alpha (Beta = 0)	VEST 2 Flight Data	VEST 2 Simulator Data	VEST 2 Desktop Simulation*
Wind Speed Error Temporal Average (ft/sec)	11.15	11.56	18.15
Wind Speed Error Standard Deviation (ft/sec)	±6.41	±6.194	±14.2162
Wind Heading Error Temporal Average (deg)	-2.21	4.708	23.581
Wind Heading Error Standard Deviation (deg)	±11.18	±11.05	±48.2201

*Desktop Simulation results were obtained prior to tuning the Kalman filter.

Results from the VEST 2 wind estimator using estimated alpha and setting beta equal to zero matched very closely with the previous results obtained in the simulator tracking task. The desktop simulation results were actually worse but this is likely caused by these results being obtained prior to the Kalman filter tuning. Using this estimator with the flight data resulted in an average wind speed error of 6.6 ± 3.8 knots with a heading error of -2.2 ± 11.2 degrees. Post-processing actual aircraft data and using estimated values of alpha with beta equal to zero realistically demonstrated the capability of the VEST 2 wind estimator to estimate wind velocities following an air data system failure. Therefore, the estimated wind speed from the VEST 2 algorithm makes a viable substitute for determining true airspeed used in traditional gain-scheduling.

4.3.3 VEST 2 Performance During Aircraft Maneuvers.

The results from post-processing actual aircraft data were used to identify the strengths and weaknesses of the VEST 2 algorithm. Aircraft maneuvers were isolated to determine how VEST 2 was affected. Recall from section 3.3.3 that the VEST 2 algorithm consisted of both the VEST and VEST TAS estimations. When a breakdown in the VEST 2 algorithm occurred, a deeper analysis was conducted to determine if the cause was rooted in VEST, VEST TAS or caused by some other issue. Plots of aircraft maneuvers and the velocity estimations for the Aerodynamic Modeling, Turn Performance, and Level Acceleration sorties can be found in Appendices H, I and J respectively. It is important to note that the plots of the individual maneuvers are subsets of the post processed data from the entire flight. This means that some of the wind estimations were not starting out with zero error at the beginning of each maneuver or set

129

of maneuvers. At times, this made it difficult to determine if and when the estimator's performance was affected by a maneuver. The performance of the VEST 2 estimator was broken down by flight since the wind conditions were different for each of the data flights and are discussed in the following order: 1) Aerodynamic Modeling Sortie; 2) Turn Performance Sortie; 3) Level Acceleration Sortie.

4.3.3.1 Aerodynamic Modeling Sortie.

The Aerodynamic Modeling Sortie was flown on 4 October 2008. The magnitude of the winds ranged from 17 knots at the surface to 130 knots at 40,000 feet pressure altitude (PA). The wind direction varied anywhere from 040 to 120 depending on aircraft location and altitude.

The first maneuver flown was a bleed rate climb from 10,000 to 40,000 feet PA. The VEST 2 wind estimator's estimation of wind speed continued to increase as the actual winds leveled off between 35,000 and 40,000 feet. Here, VEST 2 continued to predict an increase in the wind speed correlating to the increasing altitude. This was caused by the VEST component of the wind estimator and can be seen when comparing Figures 111 and 112 of Appendix H. Recall that the VEST portion of the VEST 2 algorithm used a model of the linear lapse rate of winds with respect to an aircraft's change in altitude to estimate the perturbation initial conditions. Because the altitude continued to increase, the estimates of wind speed were driven up by the perturbation initial conditions model. However, once the aircraft leveled off and began to turn, the wind speed estimate quickly converged with the actual wind speed.

The second set of maneuvers flown was a combination of roller coasters, windup turns, and split-s manuevers. The VEST 2 algorithm effectively estimated both wind speed and heading for the majority of the maneuvering. There were slight deviations in heading during the windup turn and split-s maneuvers. This is likely due to the logic placed on the residuals (explained in Section 3.3.4) that was associated with higher flight path angle maneuvering. Recall that the purpose of this residual logic was to maintain responsiveness while simultaneously preventing large fluctuations caused by rapid onset, high-g maneuvers at high flight path angles. Based on the results shown in Figures 115 and 117 of Appendix H, the logic might have restricted the ability of the estimator to respond to the changing conditions in these maneuvers. Nonetheless, as soon as these relatively short duration maneuvers were completed, the VEST 2 estimator quickly converged back to the actual wind speed and heading.

The third type of maneuver flown was a two-step climb from 20,000 to 32,000 feet PA. This maneuver showed how the VEST 2 algorithm was dependent on the changes in aircraft heading to provide a responsive estimate. As seen in figure 118 of Appendix H, the filter responded slowly to changes in wind conditions during a constant heading climb. However, when the climb was broken up by a 50 degree heading change, the VEST 2 estimator quickly converged on the actual wind conditions. This result highlighted the known limitation that the VEST 2 estimator required heading changes to provide the most accurate estimate.

The fourth maneuver flown was a set of three minute cruise points broken up by a change in heading. From Figures 120 and 121, the estimator provided a fairly constant estimate that updated only when the heading change occurs. This once again highlighted

131

the limitation that the VEST 2 algorithm required heading change to provide the best estimate.

The final maneuver flown on the Aerodynamic Modeling Sortie was a maximum range, constant airspeed, constant heading descent. Figures 122 and 123 illustrate that the estimated heading wandered towards the end of the descent. Breaking the VEST 2 algorithm down into its components, VEST (Figure 124) and VEST TAS (Figure 125), it was evident that the VEST TAS estimator provided a much better estimate for this constant airspeed, constant heading descent. Holding a constant airspeed during the descent took advantage of the perturbation initial conditions model in the VEST TAS estimator. Recall that this model used the change in ground speed components to estimate the change in TAS components. Therefore, since calibrated airspeed and aircraft headings were held constant during the descent, the VEST TAS algorithm was able to use the changes in ground speed to estimate the wind conditions more effectively.

4.3.3.2 Turn Performance Sortie.

The Turn Performance Sortie was flown on 3 October 2008. The magnitude of the winds ranged from 30 knots at the surface to 100 knots at 40,000 feet pressure altitude (PA). The wind direction varied anywhere from 040 to 140 depending on aircraft location and altitude.

The first maneuver flown was a set of maximum power level turns at 20,000 feet PA. Figure 126 in Appendix I shows that the VEST 2 algorithm effectively estimated both wind magnitude and heading for the majority of the maneuvering. At times the estimations appeared to lag the actual wind conditions but when the VEST 2 algorithm

132

was broken down into its components, VEST and VEST TAS, there were no apparent explanations. It is likely that the slight lag in the estimation was caused by values chosen for the error covariance matrix and the wind estimate uncertainty matrix associated with the filter tuning process.

The second maneuver flown was a maximum power level acceleration at 35,000 feet PA. Figure 130 in Appendix I shows that the wind speed estimate differed slightly from the actual wind speed. Once again, breaking the VEST 2 algorithm down into its components, VEST (Figure 132) and VEST TAS (Figure 133), it is evident that the VEST TAS estimator provided a slightly better estimate for this constant heading, changing airspeed level acceleration. It is also interesting to point out that the aircraft transitions through Mach one around the 700 second mark. During this transition, it appears that the raw wind measurements are influenced by the transonic region where as VEST 2 (including both VEST and VEST TAS) is not.

The third maneuver flown was a constant airspeed, constant heading, penetration descent from 40,000 to 10,000 feet PA. Looking at figures 134 and 135, it was apparent that both the estimated wind speed and heading fail to respond to the changing wind conditions.   Breaking the VEST 2 algorithm down into its components, VEST (Figure 136) and VEST TAS (Figure 137) further highlights this issue. Investigating further, Figures 138 and 139 show the VEST and VEST TAS estimators without the residual logic incorporated in the algorithm. These results showed that the residual logic (designed to limit the sensitivity to high-g, rapid onset maneuvers at high flight path angles) actually hindered the responsiveness of the VEST TAS algorithm in stabilized

133

flight. In fact, without the residual logic, the VEST TAS portion provided an excellent estimation of the actual wind conditions.

The final set of maneuvers flown on the Turn Performance Sortie was the execution of the recovery and landing (Figures 139-144 in Appendix I). Maneuvers flown during the recovery and landing phase of flight are usually limited to the following: small climbs and descents; low g maneuvering; gradual airspeed changes; configuration changes; and landing. Very similar to the analysis just described, the VEST TAS with no residual logic provided the best estimation of the wind components in stabilized or gentile maneuvering flight. This once again highlighted the fact that the residual logic actually hinderd the responsiveness of the VEST TAS algorithm in stabilized or gentile maneuvering flight.

4.3.3.3 Level Acceleration Sortie.

The Level Acceleration Sortie was flown on 29 September 2008. The magnitude of the winds ranged from 5 knots at the surface to 50 knots at 40,000 feet pressure altitude (PA). The wind direction varied anywhere from 260 thru north to 160 depending on aircraft location and altitude.

The first maneuvers flown were military power level accelerations at 15,000; 25,000; and 35,000 feet PA. Figures 146 and 147 in Appendix J demonstrated the ability of the VEST 2 algorithm to accurately estimate the wind magnitude and direction. The level acceleration at 35,000 feet PA was difficult to assess since the wind estimations were not starting out with zero error at the beginning of the maneuver. However, based

on a comparison of Figures 150-153, the VEST TAS portion of the algorithm appears to provide the most accurate estimate for this maneuver.

The second maneuver was a constant heading, constant speed, maximum range descent. Figures 154-157 in Appendix J show that the VEST 2 estimator was slow to respond to the changing wind heading conditions. Recall that the same maneuver was flown in the Aerodynamic Modeling Sortie where the results showed that the VEST TAS estimator provided the best estimate for this constant airspeed, constant heading descent. However, during this maneuver, there was no apparent difference between the VEST TAS estimate and the VEST estimate.

The third series of maneuvers flown were the maximum power level accelerations at 10, 20, 30 and 40 thousand feet PA. Once again these maneuvers highlighted the limitation that the VEST 2 algorithm requires heading change to provide the best estimate. In this case, there was one heading change of approximately 200 degrees in-between the second and third Level Acceleration. The change in heading enabled the estimator to provide an accurate update but as soon as the heading was stabilized, the VEST 2 estimator once again failed to respond to the changing wind conditions. Figures 158-163 look at all the possible combinations of the VEST 2 estimator and reemphasize the fact that the VEST 2 algorithm requires heading change to provide the most accurate estimate.

The final maneuver flown on the Level Acceleration Sortie was a penetration descent similar to the one flown on the Turn Performance Sortie. During this maneuver there were two turns that occurred during the descent that allowed the estimator to provide relatively accurate estimates of the wind components. Figures 164 and 165 in

Appendix J illustrate these results. Additionally, looking at the VEST estimator results in Figure 166, it is clear that the linear lapse rate of winds with respect to an aircraft's change in altitude has a significant impact on the VEST algorithm's ability to correctly estimate wind speed. In this case, these results lead to a larger error simply because the magnitude of the winds only changed 45 knots over 30,000 feet of altitude change.

4.4 Summary

This chapter presented the results from the F-16 simulator testing and post-processing of aircraft flight data. It also validated the VEST 2 wind estimator and highlighted some of its strengths and weaknesses. The simulator testing involved the comparison of three alternatives to standby-gain-scheduling during landing and tracking tasks. Results from the tracking task indicated that there was almost no difference between the Standard F-16, VEST 2, and the INS controllers when tracking a target up and away from the ground. This indicated that a VEST 2 gain-scheduled controller and an inertial gain-scheduled controller would provide sufficient control to act as an alternative to standby-gain-scheduling at altitude. The DO controller was less effective at the tracking task but did show potential for further refinement and development. The results obtained from the landing task showed that a VEST 2 gain-scheduled controller would provide sufficient control to act as an alternative to standby-gain-scheduling in the landing phase of flight. Results from both the tracking tasks and landing tasks indicate that the wind estimator (VEST 2) is capable of producing a reliable wind estimate which in turn leads to a reliable true airspeed needed for gain-scheduling.

Preliminary results from the desktop simulation of VEST 2 in Section 3.3.4 indicated that accurate estimates would only be possible using actual measured quantities of alpha and beta. However, by post-processing data obtained from a high-fidelity, six-degree-of-freedom, block 40 F-16C simulator, reasonable results were obtained using an estimated alpha and setting beta equal to zero. Actual aircraft data recorded from a data acquisition system provided raw data that realistically tested and validated the simulator results obtained from the VEST 2 wind estimator. Using this estimator with the flight data resulted in an average wind speed error of 6.6 ± 3.8 knots with a heading error of -2.2 ± 11.2 degrees. These results showed that the estimated wind speed from the VEST 2 algorithm could make a viable substitute for determining the true airspeed used in traditional gain-scheduling.

The validation of the VEST 2 wind estimator was accomplished by comparing the estimate obtained from the desktop simulation data, high-fidelity F-16 simulator data, and actual aircraft flight data with truth wind data. The results from this comparison validated the VEST 2 wind estimator and showed that it is possible to produce good wind estimates without the use of an air data system.

Finally, the results from the post-processing of the actual aircraft data were also used to determine the strengths and weaknesses of the VEST 2 algorithm during actual aircraft maneuvers. The strength of the VEST 2 algorithm was its ability to provide accurate wind estimates during maneuvering flight. The strength of the VEST 2 wind estimator was also its biggest weakness in that the estimator became somewhat unresponsive under the constant heading flight condition. This was not entirely true as the VEST TAS portion of the VEST 2 wind estimator showed an ability to continue to

137

provide a good wind estimates despite the constant heading condition. It was also determined that the residual logic, implemented with the intent to maintain responsiveness while simultaneously preventing large estimation errors, limited the ability of the estimator to respond during aggressive maneuvers. The residual logic also had an unintended limitation by limiting the responsiveness of the estimator in constant heading flight. Another unexpected strength of the VEST 2 estimator was its ability to provide accurate estimates of winds during transonic flight, something that cannot be said for a normal Pitot static system. Finally, when the VEST 2 estimator was broken down into its components, the VEST TAS component tended to perform better than the VEST component during aircraft maneuvers. The limitation of the VEST estimator was its model of the linear lapse rate of wind speed that caused its estimates to increase or decrease faster than the actual wind speed during altitude changes.

5.0 Discussion

5.1 Overview

The objective of this research was to determine if alternative methods of standby-gain-scheduling could provide robust control despite the absence of an air data system. Three different methods of standby-gain-scheduling were developed and compared. The first alternative method built upon an algorithm which used inertial data to estimate the aircraft's true velocity [McLaren, 2008]. This estimated true velocity was used to drive the gains in an F-16 controller. The second method simply used inertial velocities to drive the gains in an F-16 controller. The final method used a disturbance observer controller which controlled aircraft dynamics without the use of gain-scheduling. In the event of an air data system failure, any of the alternative methods to standby-gain-scheduling researched would eliminate the pilot's requirement to make switch actuations to correctly schedule the standby-gains in a large flight envelope. Secondly, aircraft performance may prove to be more effective than the traditional standby-gain settings allowing the pilot to continue with a combat mission as opposed to selecting the standby-gain, flying a particular airspeed and returning to base. Possible future research areas include improved airspeed estimate filtering, alternative methods to estimating alpha and beta, continued refinement and development of the disturbance observer controller, and actual flight testing of each standby controller.

5.2 Conclusions of Research

The purpose of each alternative to standby-gain-scheduling was to eliminate mandatory switch actuations by the pilot, provide aircraft performance equal to the baseline method of control and reduced dependency on the air data system. This work compared alternative methods of standby-gain-scheduling following an air data system failure through desktop simulation, simulator testing, and by post-processing aircraft data. The simulator testing involved the comparison of three alternatives to standby-gain-scheduling during landing and tracking tasks. Results from the tracking task indicated that there was almost no difference between the Standard F-16, VEST 2, and the INS controllers when tracking a target up and away from the ground. This indicated that a VEST 2 gain-scheduled controller and an inertial gain-scheduled controller would provide sufficient control to act as an alternative to traditional gain-scheduled control at altitude. The DO controller was less effective at the tracking task but did show potential for further refinement and development, particularly in the lateral and directional axis. The results obtained from the landing task showed that a VEST 2 gain-scheduled controller could provide sufficient control to act as an alternative to standby-gain-scheduling in the landing phase of flight. Results from both the tracking tasks and landing tasks indicate that the wind estimator (VEST 2) is capable of producing a reliable wind estimate which in turn leads to a reliable true airspeed needed for gain-scheduling.

Preliminary results from the desktop simulation testing of the wind estimator, VEST 2, indicated that accurate estimates would only be possible using actual measured quantities of alpha and beta. However, by post-processing data obtained from a high-

fidelity, six-degree-of-freedom, block 40 F-16C simulator, reasonable results were obtained using an estimated alpha and setting beta equal to zero. Actual aircraft data recorded from a data acquisition system provided raw data that realistically tested and validated the simulator results obtained from the VEST 2 wind estimator. Using this estimator with the flight data resulted in an average wind speed error of 6.6 ± 3.8 knots with a heading error of -2.2 ± 11.2 degrees. These results were enough to conclude that the estimated wind speed from the VEST 2 algorithm could make a viable substitute for determining the true airspeed used in traditional gain-scheduling.

Finally, the strength of the VEST 2 algorithm during actual aircraft maneuvers was its ability to provide accurate wind estimates during maneuvering flight. The strength of the VEST 2 wind estimator was also its biggest weakness in that the estimator became somewhat unresponsive under the constant heading flight conditions. However, the VEST TAS portion of the VEST 2 wind estimator showed some ability to continue to provide a good wind estimates despite the constant heading condition. Another unexpected strength of the VEST 2 estimator was its ability to provide accurate estimates of winds during transonic flight, something that cannot be said for a normal Pitot static system. Finally, the limitation of the VEST estimator, a sub-component of VEST 2, was its model of the linear lapse rate of wind speed that caused its estimates to increase or decrease faster than the actual wind speed during altitude changes. This affected the wind speed estimates of VEST 2, often increasing the estimated wind speed error.

5.3 Significance of Research

Currently, the Air Force has advanced fighter aircraft that require a pilot to make switch actuations to correctly schedule flight control system standby-gains in the event of air data system failures. This takes time away from other pertinent tasks to manually position the standby-gains via the landing gear handle, air-to-air refueling door switch or some other means. Additionally, the standby-gain settings are suboptimal for an advanced fighter flight envelope and are primarily designed to allow for the safe recovery and landing of an aircraft. Suboptimal settings can lead to decreased aircraft handling qualities and increased pilot work load throughout a majority of the normal flight envelope.

Each of the alternative methods to standby-gain-scheduling discussed in this paper could be implemented in a modern day fighter. The wind estimator, VEST 2, and the inertial velocity gain-scheduler would be ready for implementation onto an aircraft today. The disturbance observer would require additional research and development in order to make it airworthy. However, in the event of an air data system failure, any of the alternative methods to standby-gain-scheduling researched would eliminate the pilot's requirement to make switch actuations to correctly schedule the standby-gains in a large flight envelope. Secondly, the aircraft performance may prove to be more effective than the traditional standby-gain settings allowing the pilot to continue with a combat mission as opposed to selecting the standby-gain, flying a particular airspeed and returning to base. Finally, this research may someday contribute to the removal of Pitot tubes in an attempt to reduce the radar cross section of an aerial vehicle.

5.4 Recommendations for Future Research

Future research should focus on improving airspeed estimates, continued refinement and development of the disturbance observer controller, and actual flight testing of each standby controller.

The average estimated wind error and standard deviation from the VEST 2 algorithm could be improved through Kalman filter tuning and a more in depth study of its weaknesses. Investigating the wind estimator's performance during individual aircraft maneuvers would highlight potential weaknesses in the estimator and likely lead to improved wind estimates.

Continued refinement of the disturbance observer (DO) controller is necessary to prepare this method of control for flight test. More emphasis should be placed on the lateral and directional axis to improve aircraft control. Additionally, atmospheric disturbances and noise should be added to the disturbance observer simulation to test the robustness of the DO controller. In its current state, the DO controller is still dependent on accurate measurements of alpha and beta. Future research could also look at developing a DO controller that either uses estimates of alpha and beta or completely removes the DO controller's dependence on alpha and beta. Additionally, a separate research area that would have a direct impact on this research would involve developing a more accurate estimate of alpha and beta derived from aircraft sensors still available following an air data system failure.

Finally, all three systems need to be flight tested to validate their performance. The United States Air Force Test Pilot School's Variable Stability In-Flight Simulator

Test Aircraft (VISTA) would be the perfect platform for testing any of these alternative methods to standby-gain-scheduling. The flight envelope on board the variable stability system of the VISTA is representative of a large, fighter-type flight envelope and would provide adequate room to conduct maneuvers that would effectively test each standby controller.

5.5 Summary

The research objective of this thesis was met by comparing alternative methods of standby-gain-scheduling following an air data system failure and validating the velocity estimator (VEST 2) algorithm with simulation and flight test data. Three alternatives to the traditional standby-gain-scheduling were developed and compared in a block 40 F-16C simulator. The results of this research clearly show the potential for effective aircraft control with minimal performance degradation following an air data system failure. The VEST 2 controller and the inertial velocity controller showed almost no performance degradation or increased pilot workload when compared to the nominal block 40 F-16C controller. Even though the DO controller resulted in decreased aircraft performance and increased in pilot workload, it still managed to obtain at least adequate performance with a tolerable workload throughout the designed flight envelope (0.4 – 0.8 Mach and 5,000 – 25,000 ft). This result demonstrated the potential for using a DO controller for large flight envelope control without the need for gain-scheduling.

Future research should focus on improving airspeed estimates, continued refinement and development of the disturbance observer controller, and actual flight testing of each standby controller.

Bibliography

Ackermann, J., P. Blue, T. Bunte, L. Guvenc, D. Kaesbauer, M. Kordt, M. Muhler, D. Odenthal. *Robust Control: The Parameter Space Approach, Second Edition.* London: Springer, 2002.

Bailey, R.E. *The Application of Pilot Rating and Evaluation Data for Fly-by-wire flight control system design.* AIAA-90-2826, AIAA Atmospheric Flight Mechanic Conference, Portland OR, August 1990.

Blakelock, John H., Automatic Control of *Aircraft and Missiles, Second Edition.* New York: John Wiley & Sons, Incorporated, 1991.

Blue, P., D. Odenthal, M Muhler. *Designing Robust Large Envelope Flight Controllers for High-Performance Aircraft.* AIAA 2002-4450, Guidance, Navigation, and Control Conference and Exhibit, Monterey CA, August 2002.

Brandt, S., R. Stiles, J. Bertin, R. Whitford. *Introduction to Aeronautics: A Design Perspective.* Reston VA: American Institute of Aeronautics and Astronautics, Incorporated, 2004.

Brogan, William L. *Modern Control Theory, Third Edition*. New Jersey: Prentice Hall, 1991.

Cooper, G. E. and Harper, R.P, Jr. *The Use of Pilot Rating in the Evaluation of Aircraft Handling Qualitie.* NASA TN D-5153, 1989.

Department of Defense. *Flying Qualities of Piloted Aircraft*. MIL-STD-1797B. Wright-Patterson AFB, 15 February 2006.

Erb, Russell E. Class textbook, PF 701B, Pitot Statics Textbook. United States Air Force Test Pilot School, Edwards AFB CA, 1 March 2005.

Gray, Doug. "Using GPS to Accurately Establish True Airspeed," unpublished paper available at http://ww.ntps.edu/HTML/Downloads.htm , June 1998.

Hodgkinson, John. *Aircraft Handling Qualities.* Reston VA: American Institute of Aeronautics and Astronautics, Incorporated, 1999.

Honeywell Technology Center. *Application of Multivariable Control Theory to Aircraft Control Laws, Final Report: Multivariable Control Design Guidelines.* WL-TR-96-3099, May 1996.

Kayton, Myron and Walter R. Fried. *Avionics Navigation Systems, Second Edition*. New York: John Wiley & Sons, Incorporated, 1997.

Kisslinger, Robert L. and Michael J. Wendl. *Survivable Flight Control System Interim Report: Studies, Analyses, and Approach.* AFFDL-TR-71-20, May 1971.

Leggett, David B. Class Lecture, MECH 629, Aircraft Handling Qualities and Performance. School of Aeronautical Engineering, Air Force Institute of Technology, Wright-Patterson AFB OH, Summer Quarter 2007.

Liebst, Bradley S. Class handout, MECH 629, Aircraft Handling Qualities and Performance. School of Aeronautical Engineering, Air Force Institute of Technology, Wright-Patterson AFB OH, Summer Quarter 2007.

Liebst, Bradley S. Class handout, MECH 628, Aircraft Control. School of Aeronautical Engineering, Air Force Institute of Technology, Wright-Patterson AFB OH, Spring Quarter 2007.

Maybeck, Peter S. Notes for Volume 1 of Stochastic Models, Estimation and Control. Air Force Institute of Technology, Wright-Patterson AFB OH, Published in 1982.

McLaren, Scott A. *Velocity Estimate Following Air Data System Failure*. MS thesis, AFIT/GAE/ENY/08-M21. School of Aeronautical Engineering, Air Force Institute of Technology, Wright-Patterson AFB OH, February 2008.

Nelson, Robert C. *Flight Stability and Automatic Control, Second Edition*. Boston: McGraw-Hill, Incorporated, 1998.

Rasmussen Simulation Technologies, *AVDS (Aviation Visual Design Simulator) User's Manual*, February 2006.

Stevens, Brian L. and Frank L. Lewis. *Aircraft Control and Simulation, Second Edition*. New Jersey: John Wiley & Sons, Incorporated, 2003.

Wylie, C.R., Jr. *Advanced Engineering Mathematics, Third Edition*. New York: McGraw-Hill Book Company, 1960.

Appendix A. Tracking Task Wind Estimator Plots
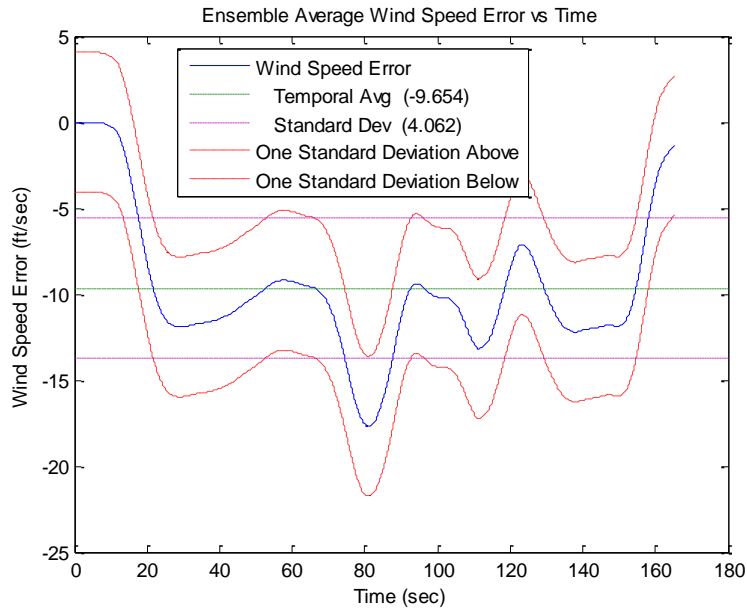
Figure 61. VEST Wind Speed Error (Meas. Alpha & Beta)
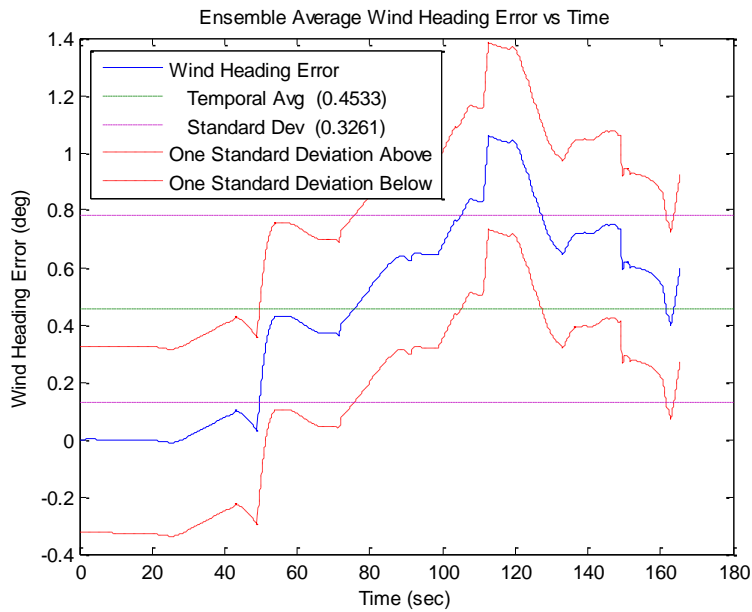
Figure 62. VEST Wind HDG Error (Meas. Alpha & Beta)
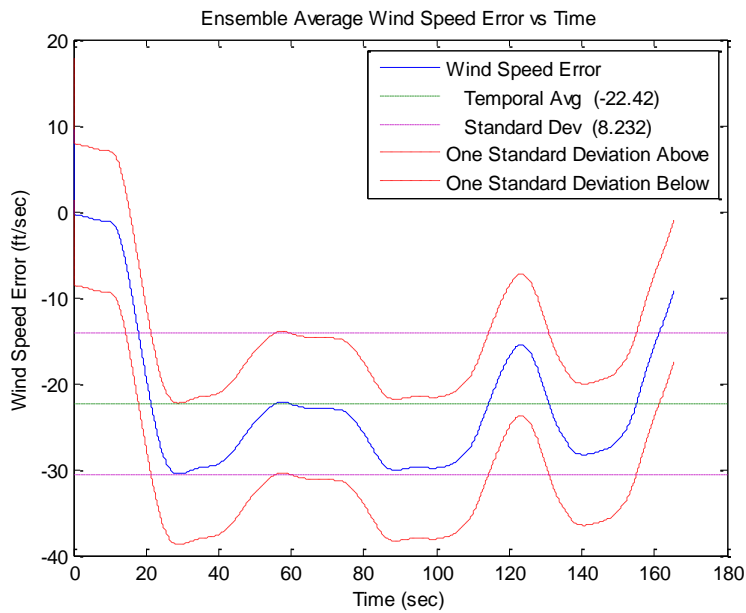
Figure 63. VEST TAS Wind Speed Error (Meas. Alpha & Beta)
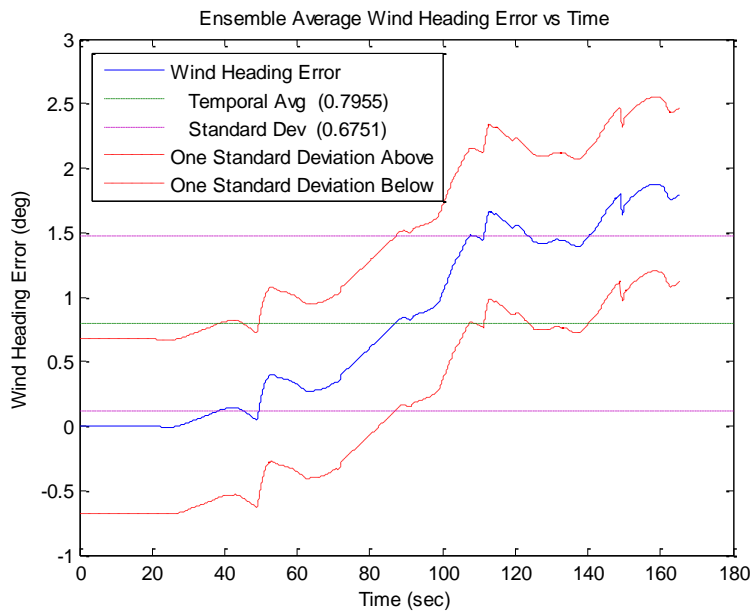
Figure 64. VEST TAS Wind HDG Error (Meas. Alpha & Beta)

148
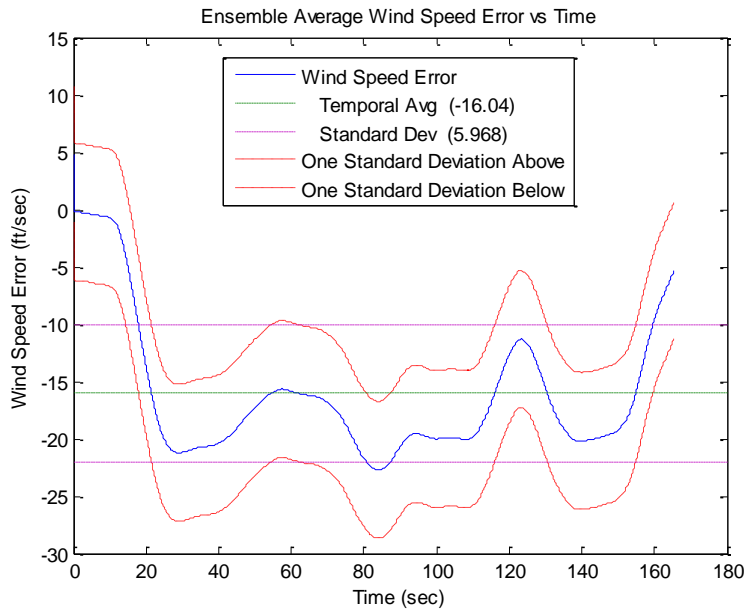
Figure 65. VEST 2 Wind Speed Error (Meas. Alpha & Beta)
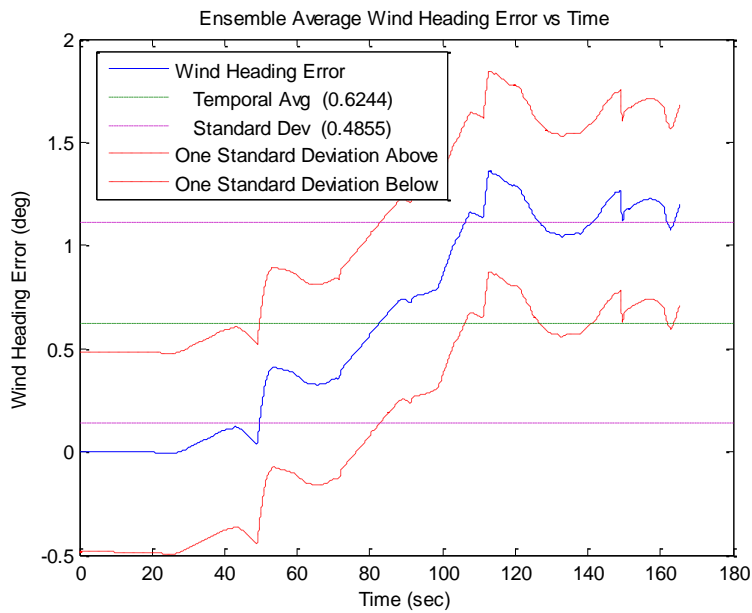
Figure 66. VEST 2 Wind HDG Error (Meas. Alpha & Beta)

149
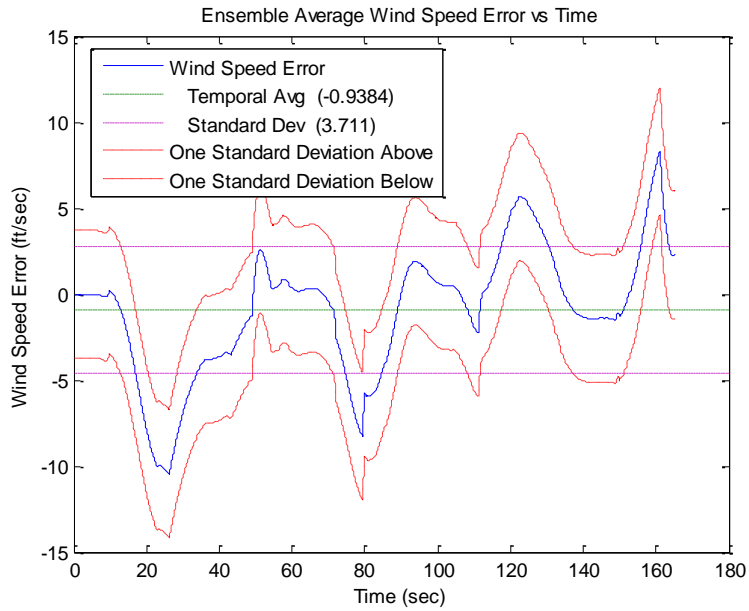
Figure 67. VEST Wind Speed Error with Tuning (Meas. Alpha & Beta)
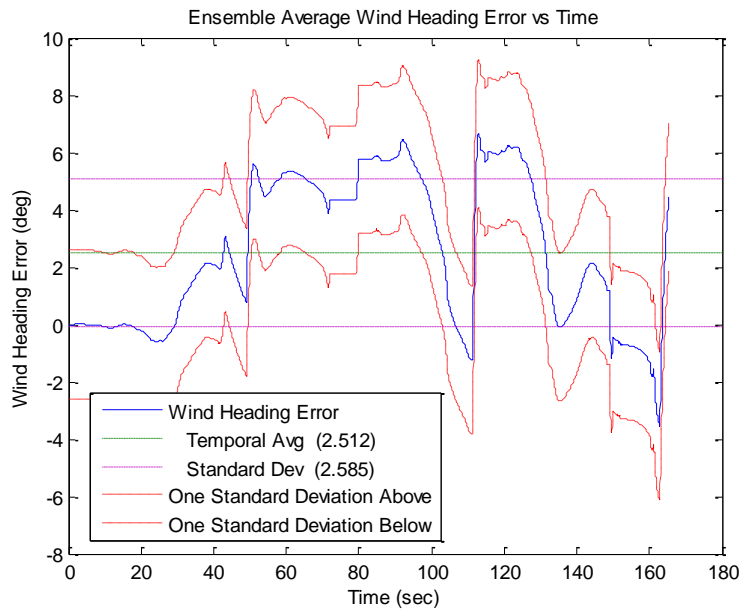
Figure 68. VEST Wind HDG Error with Tuning (Meas. Alpha & Beta)
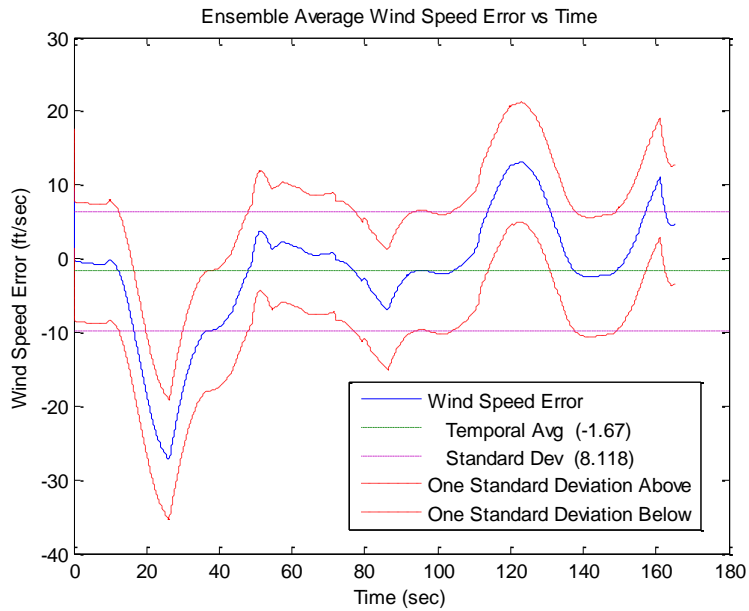
Figure 69. VEST TAS Wind Speed Error with Tuning (Meas. Alpha & Beta)
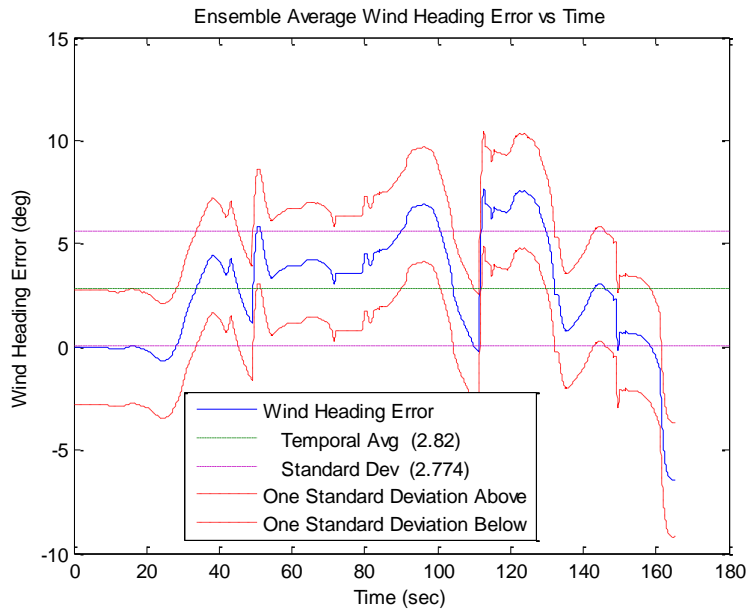
Figure 70. VEST TAS Wind HDG Error with Tuning (Meas. Alpha & Beta)

152
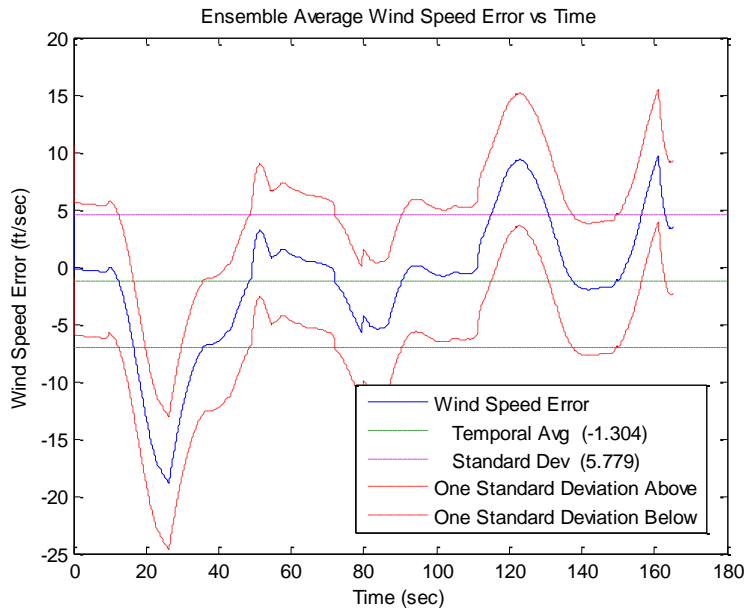
Figure 71. VEST 2 Wind Speed Error with Tuning (Meas. Alpha & Beta)
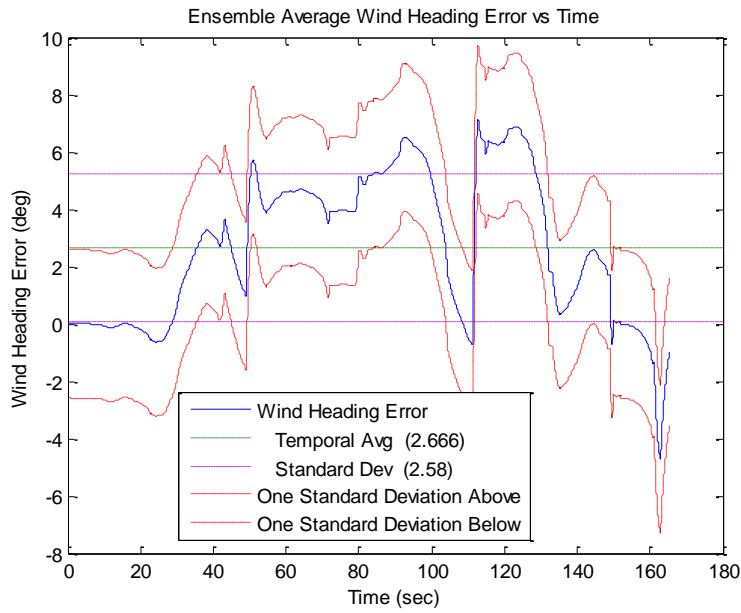
Figure 72. VEST 2 Wind HDG Error with Tuning (Meas. Alpha & Beta)

153

Appendix C. Longshot Task Wind Estimator Plots with Tuning
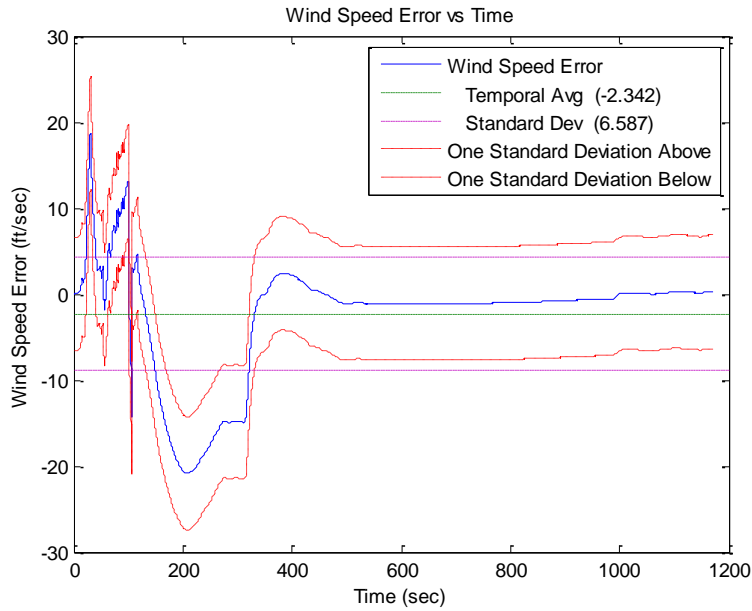
Figure 73. VEST Wind Speed Error with Tuning (Meas. Alpha & Beta)
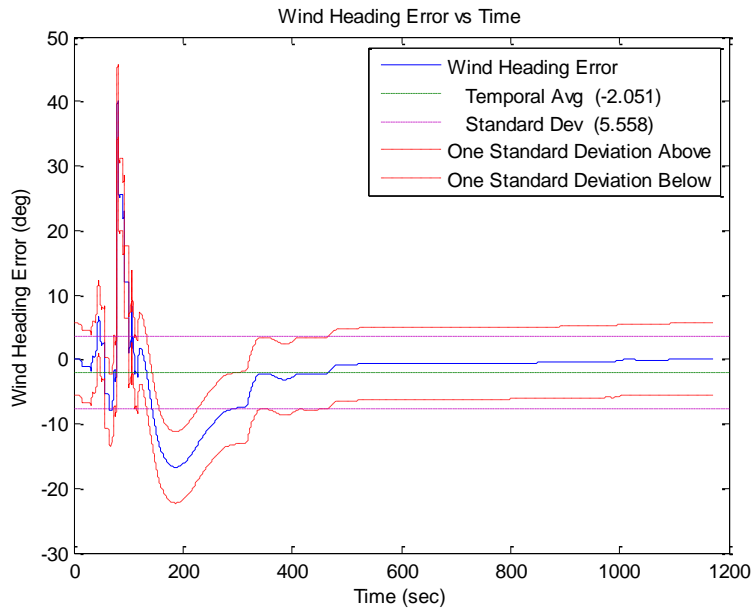
Figure 74. VEST Wind HDG Error with Tuning (Meas. Alpha & Beta)
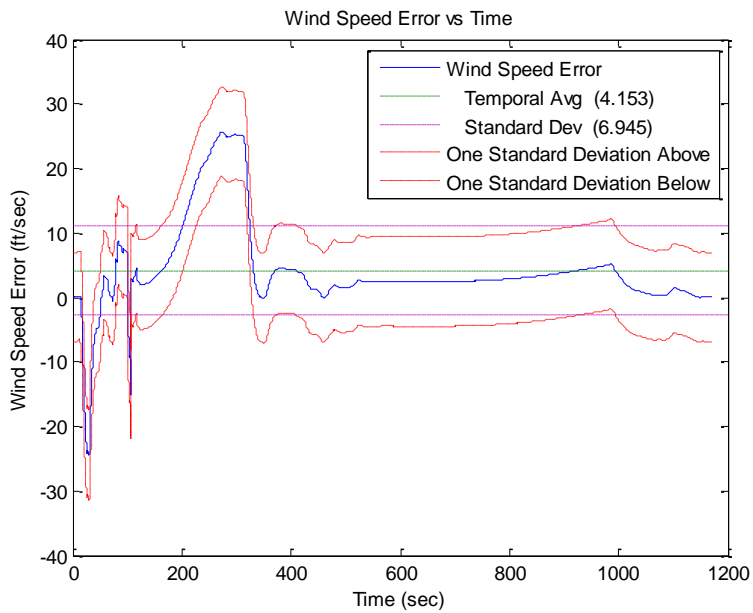
Figure 75. VEST TAS Wind Speed Error with Tuning (Meas. Alpha & Beta)
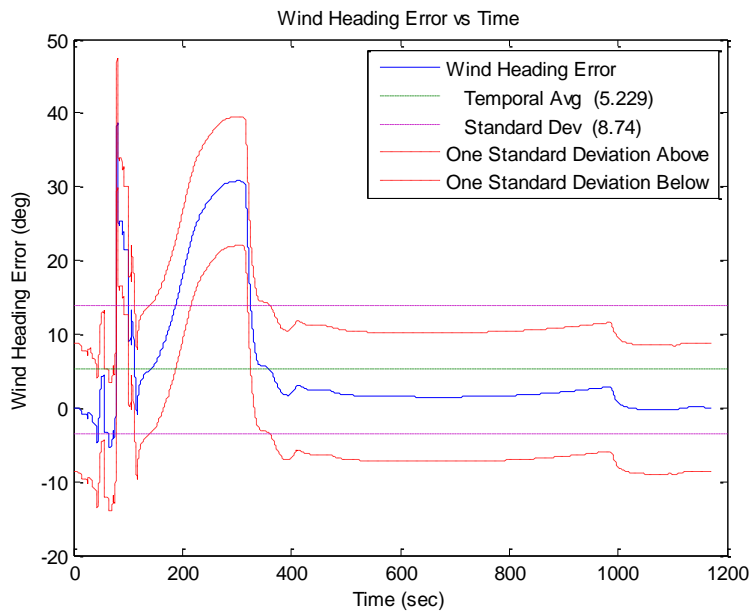
Figure 76. VEST TAS Wind HDG Error with Tuning (Meas. Alpha & Beta)
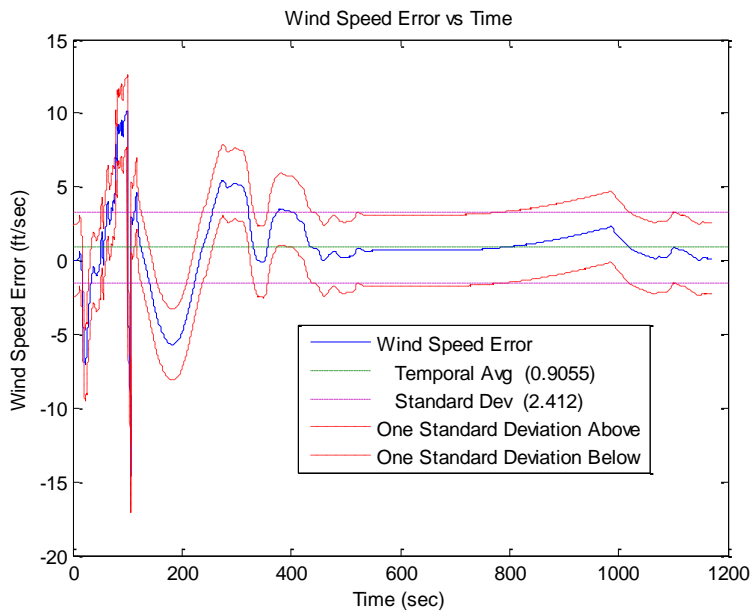
Figure 77. VEST 2 Wind Speed Error with Tuning (Meas. Alpha & Beta)
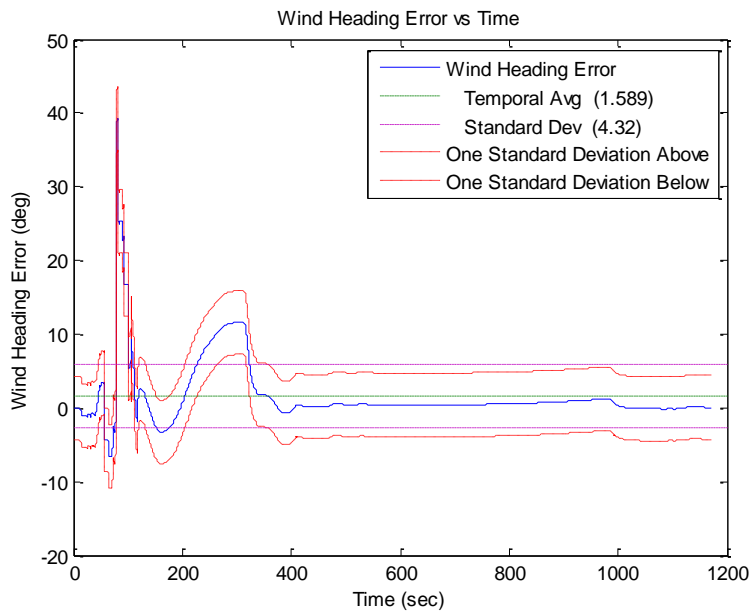
Figure 78. VEST 2 Wind HDG Error with Tuning (Meas. Alpha & Beta)
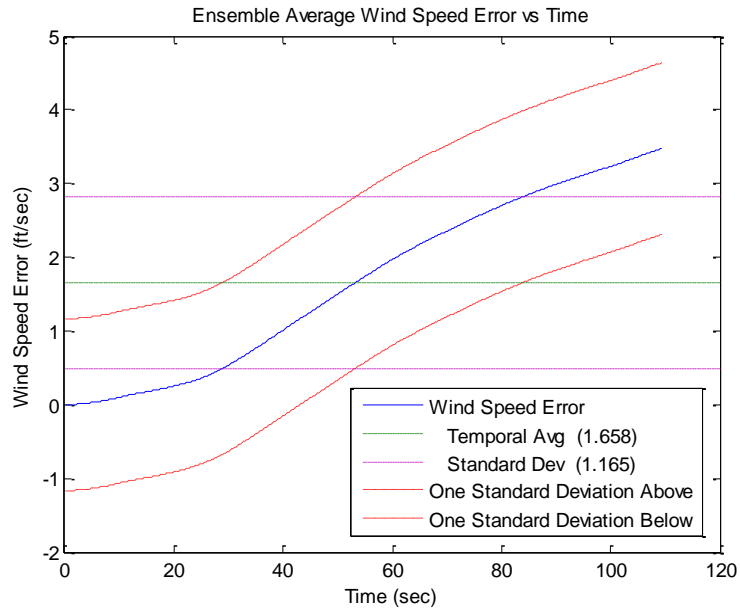
Figure 79. VEST Wind Speed Error (Meas. Alpha & Beta)
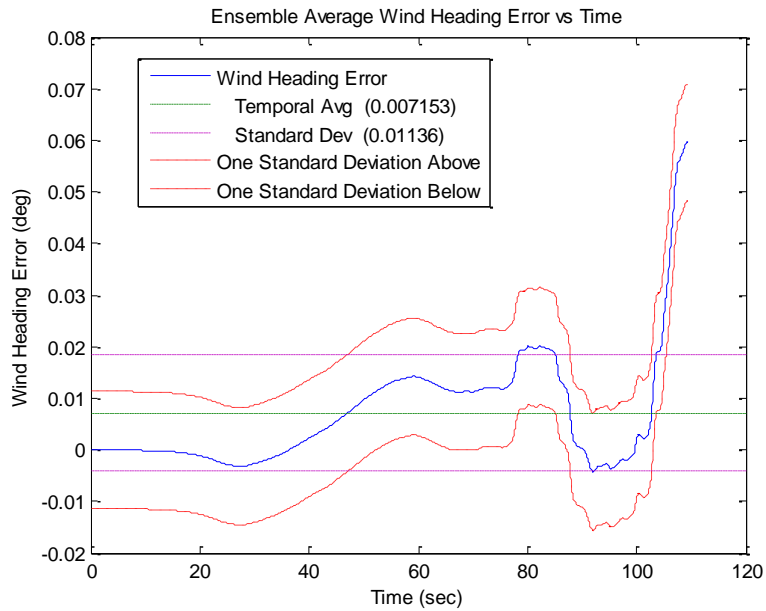
Figure 80. VEST Wind HDG Error (Meas. Alpha & Beta)

159
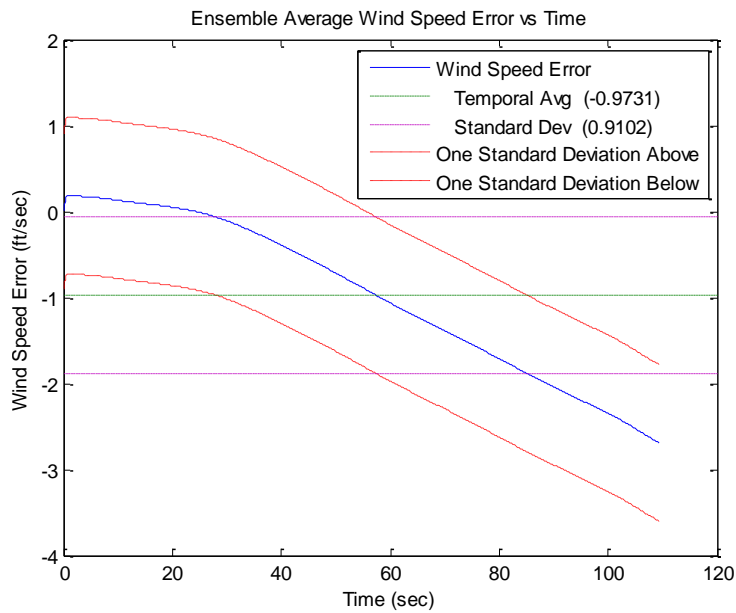
Figure 81. VEST TAS Wind Speed Error (Meas. Alpha & Beta)
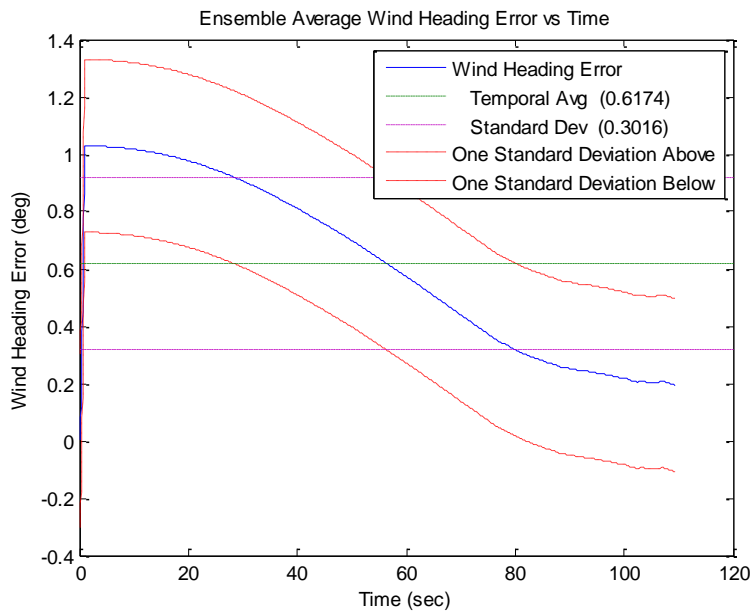
Figure 82. VEST TAS Wind HDG Error (Meas. Alpha & Beta)

160
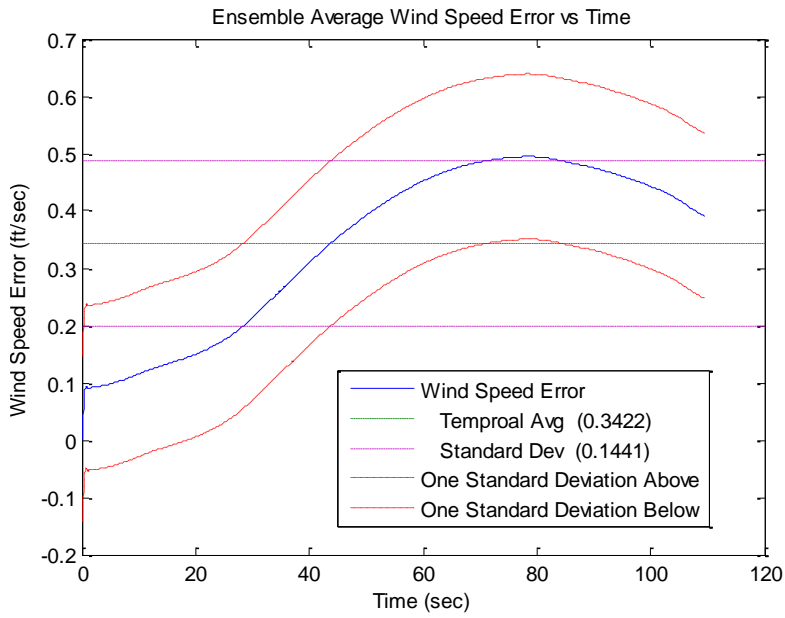
Figure 83. VEST 2 Wind Speed Error (Meas. Alpha & Beta)
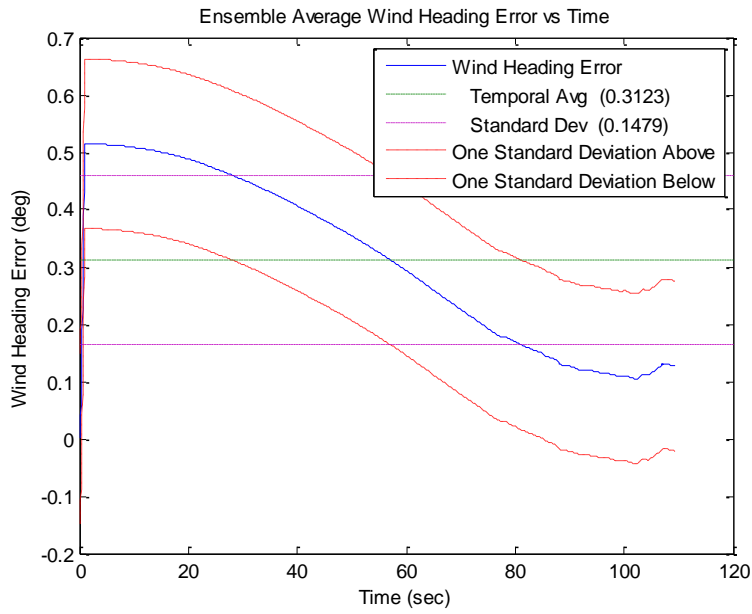
Figure 84. VEST 2 Wind HDG Error (Meas. Alpha & Beta)

161

Appendix E. Landing Task Wind Estimator Plots with Tuning
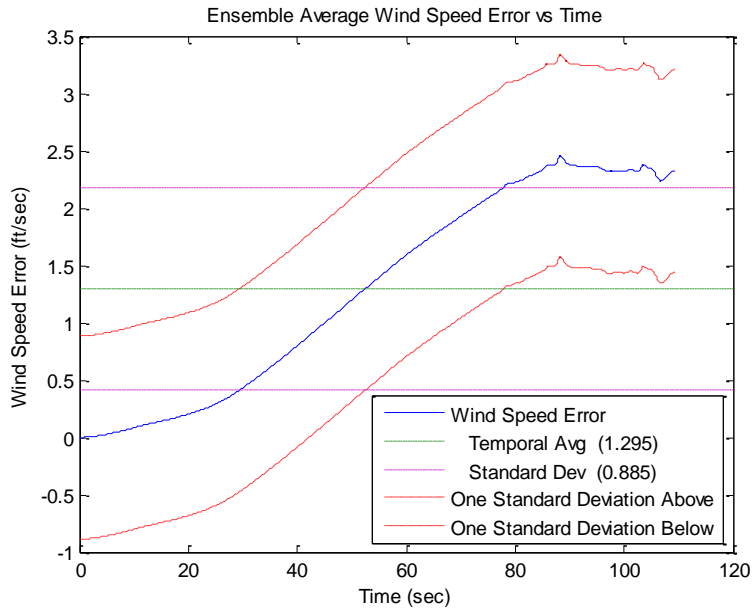
Figure 85. VEST Wind Speed Error with Tuning (Meas. Alpha & Beta)
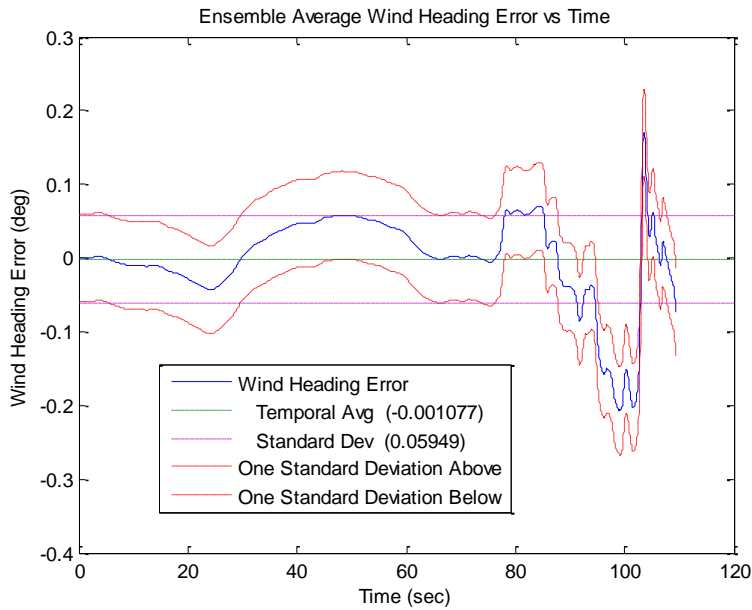
Figure 86. VEST Wind HDG Error with Tuning (Meas. Alpha & Beta)

163
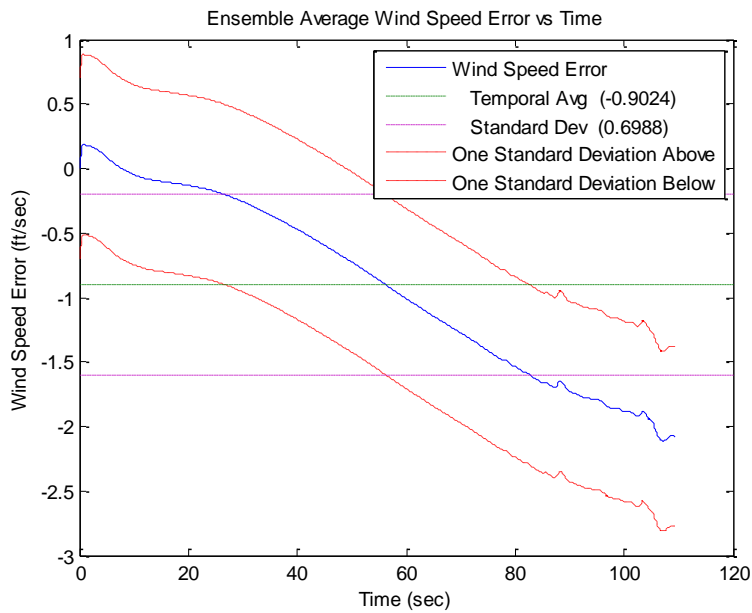
Figure 87. VEST TAS Wind Speed Error with Tuning (Meas. Alpha & Beta)
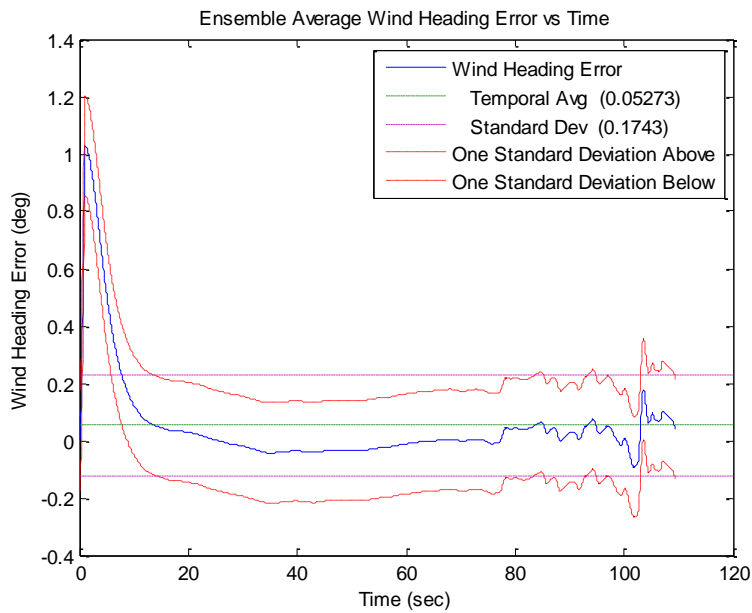
Figure 88. VEST TAS Wind HDG Error with Tuning (Meas. Alpha & Beta)

164
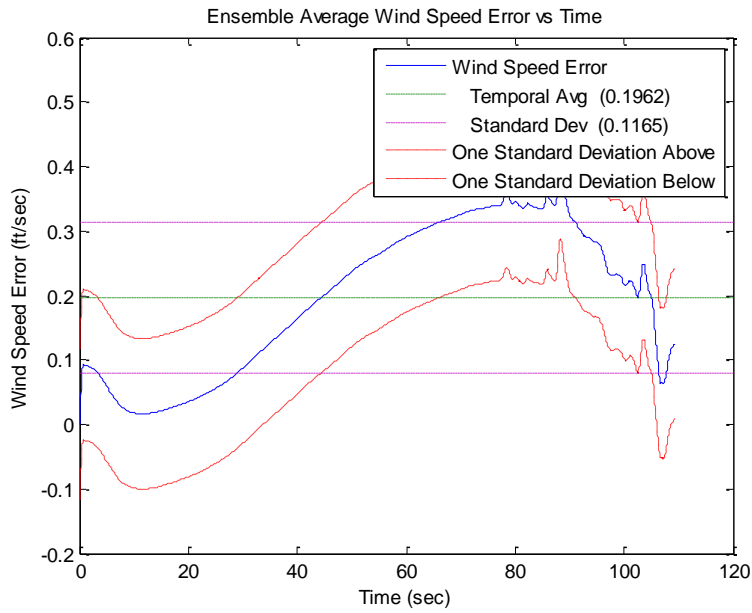
Figure 89. VEST 2 Wind Speed Error with Tuning (Meas. Alpha & Beta)
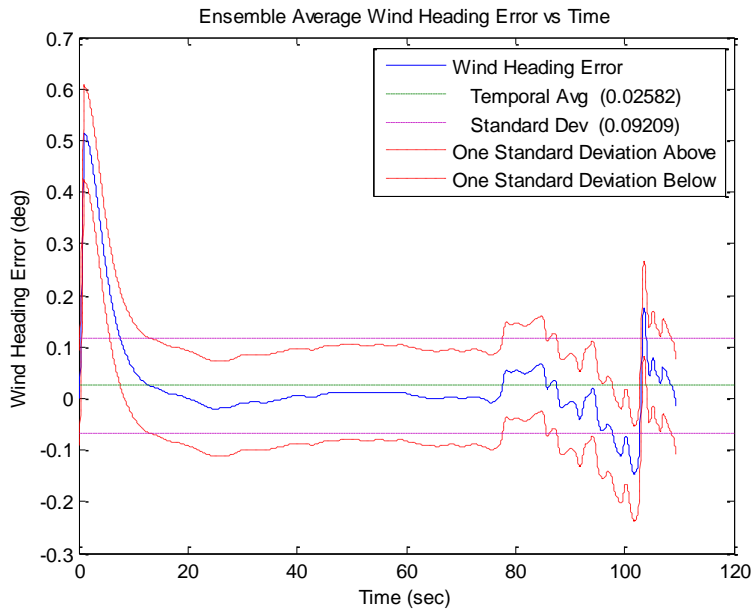
Figure 90. VEST 2 Wind HDG Error with Tuning (Meas. Alpha & Beta)

165

Appendix F. Aircraft Flight Data Post-Processing Plots

VEST 2 Wind Speed Comparison (Aerodynamic Modeling Sortie)
Measured Alpha
Measured Beta
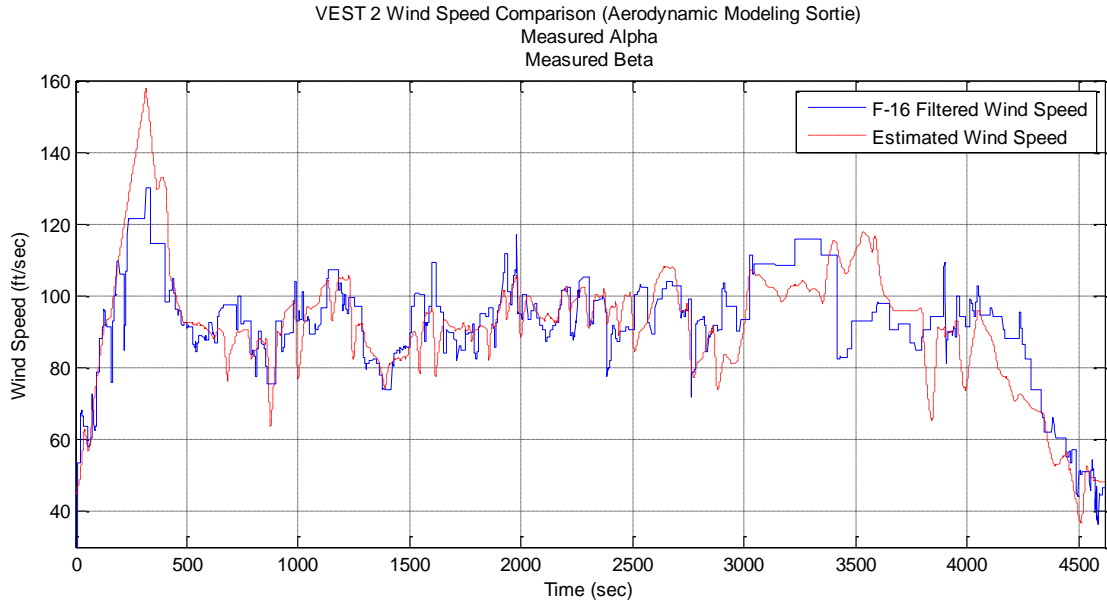
Figure 91. Aerodynamic Modeling VEST 2 Wind Speed (Meas. Alpha & Beta)

VEST 2 Wind Heading Comparison (Aerodynamic Modeling Sortie)
Measured Alpha
Measured Beta
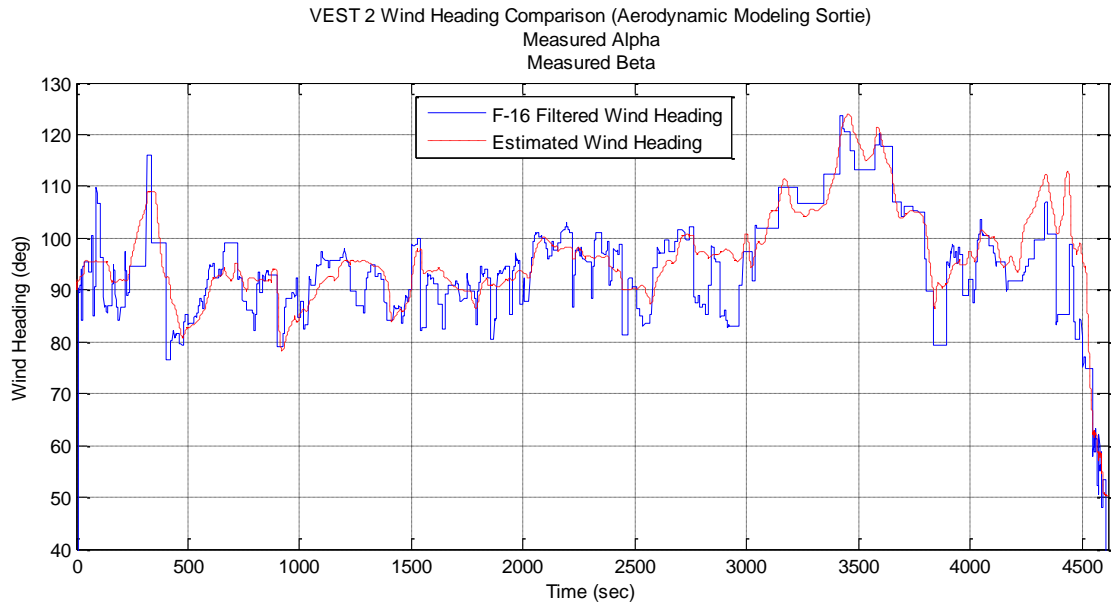
Figure 92. Aerodynamic Modeling VEST 2 Wind HDG (Meas. Alpha & Beta)

167
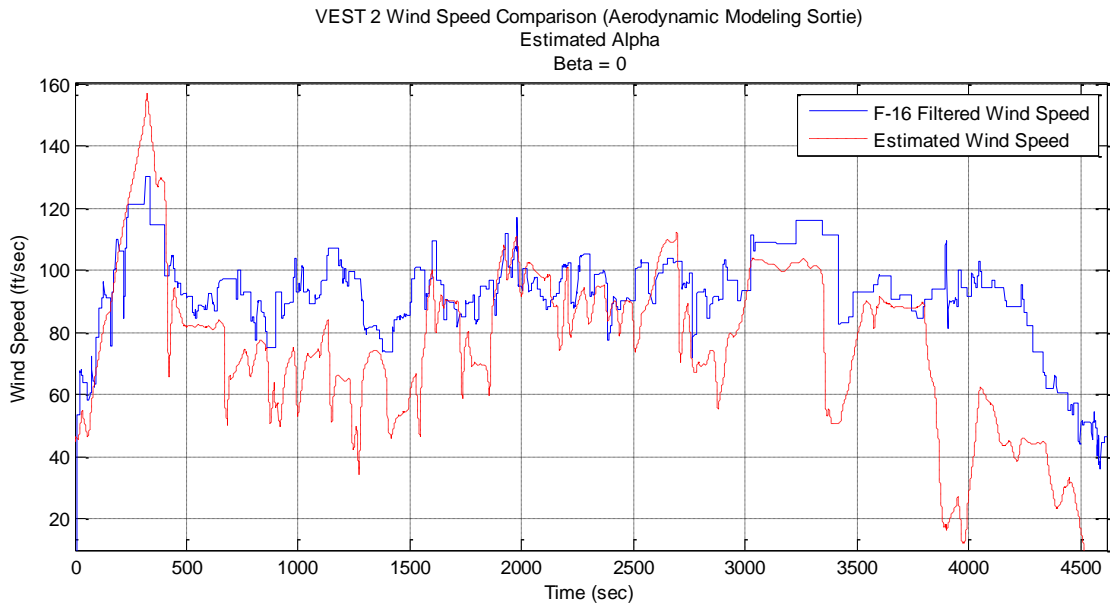
Figure 93. Aerodynamic Modeling VEST 2 Wind Speed (Est. Alpha, Beta=0)
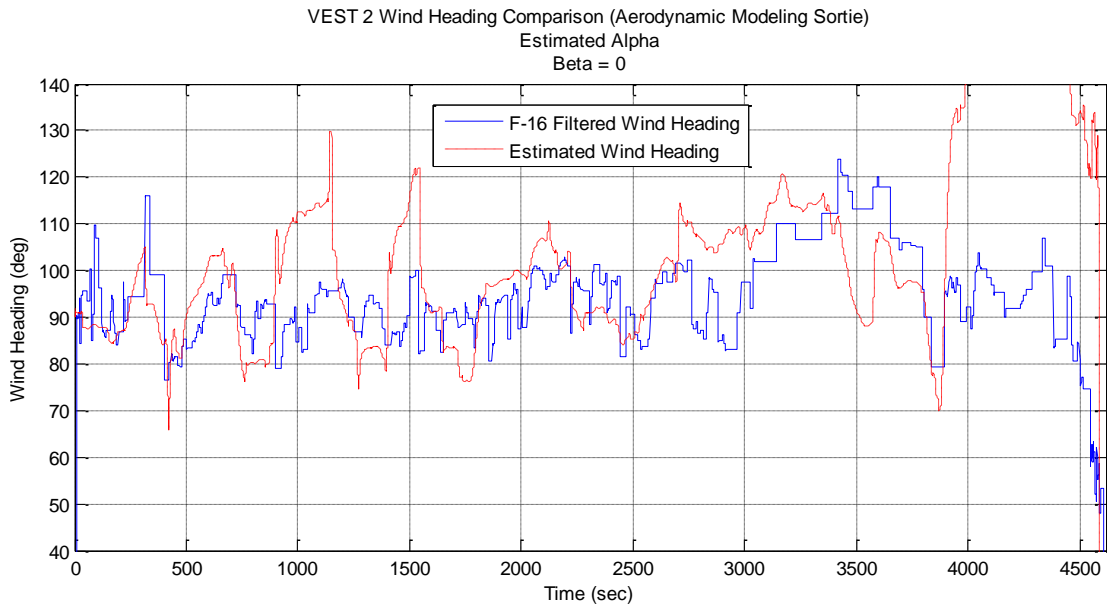
Figure 94. Aerodynamic Modeling VEST 2 Wind HDG (Est. Alpha, Beta=0)
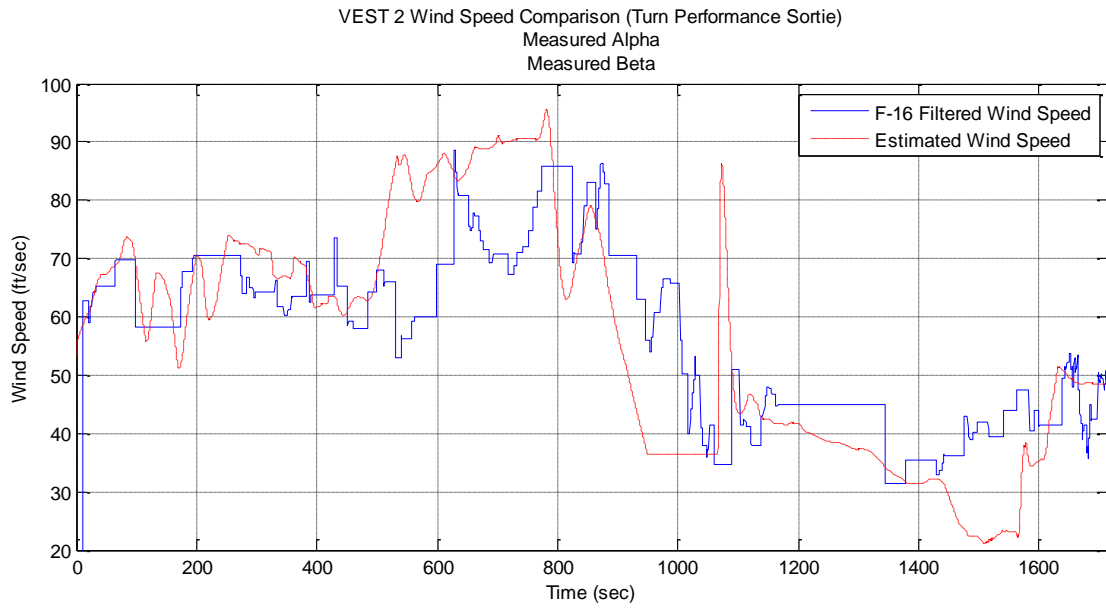
Figure 95. Turn Performance VEST 2 Wind Speed (Meas. Alpha & Beta)
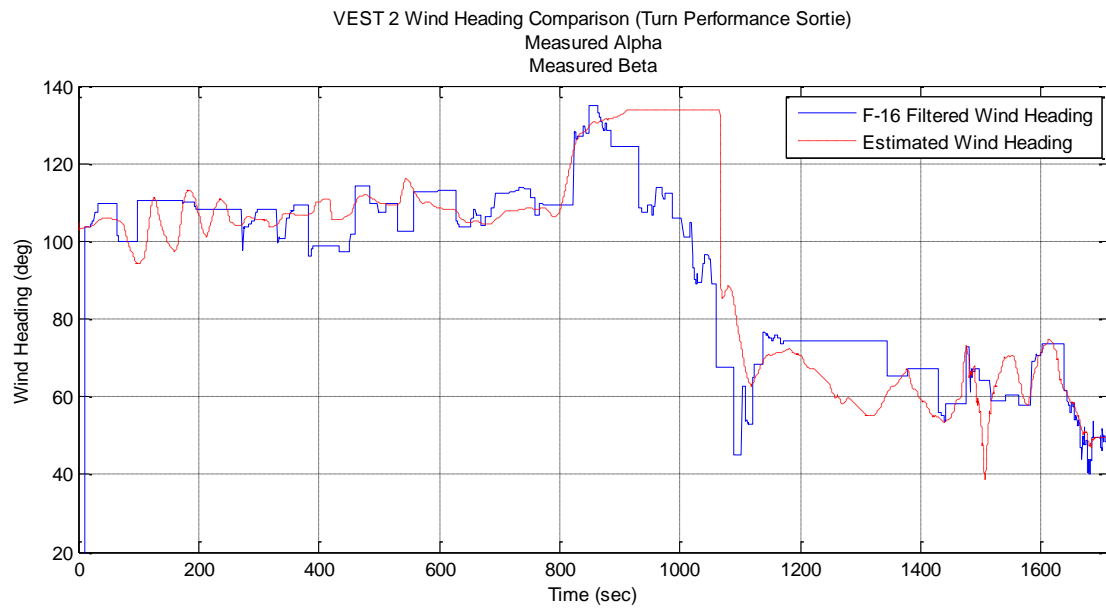
Figure 96. Turn Performance VEST 2 Wind HDG (Meas. Alpha & Beta)

169
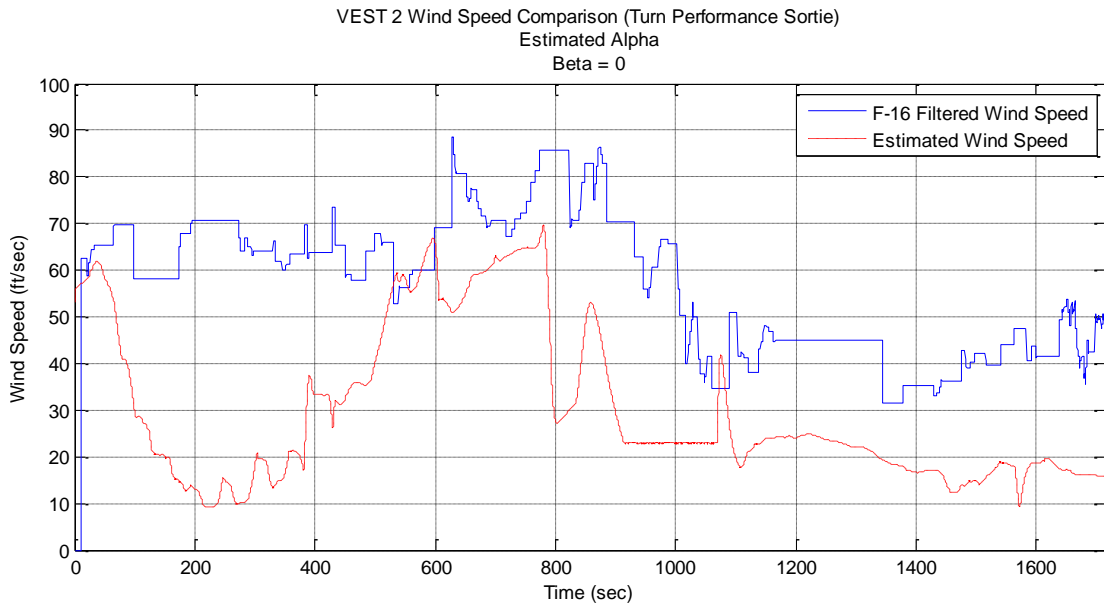
Figure 97. Turn Performance VEST 2 Wind Speed (Est. Alpha, Beta=0)
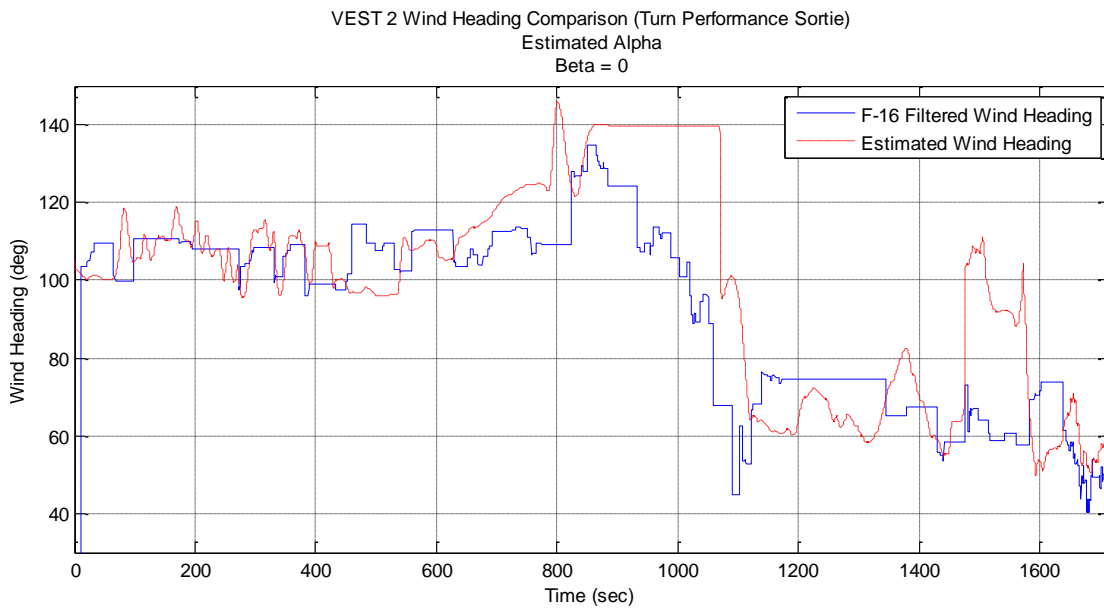
Figure 98. Turn Performance VEST 2 Wind HDG (Est. Alpha, Beta=0)

170
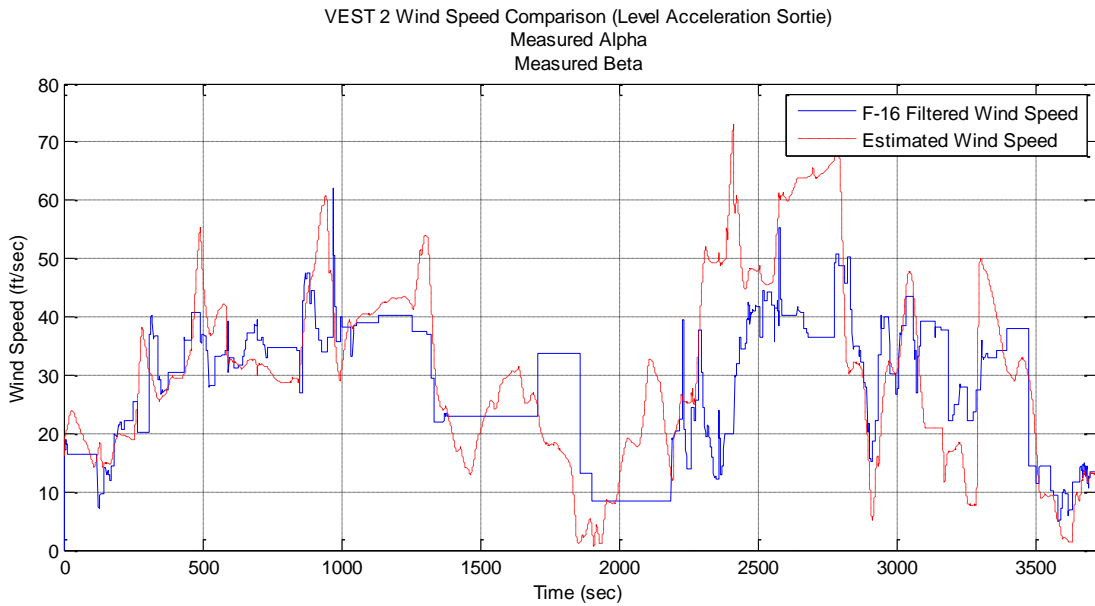
Figure 99. Level Acceleration VEST 2 Wind Speed (Meas. Alpha & Beta)
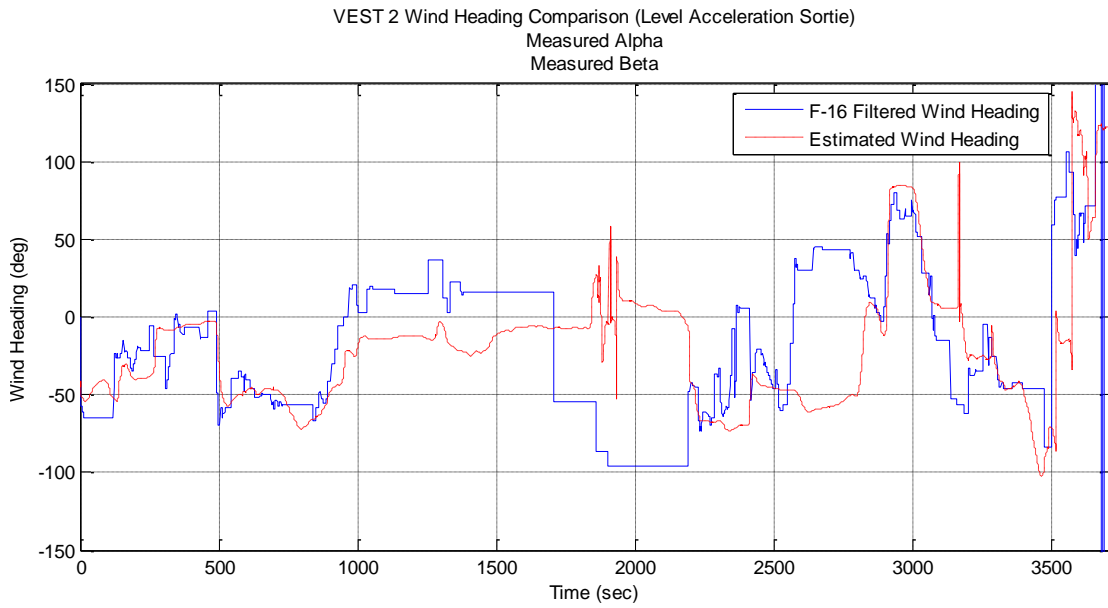
Figure 100. Level Acceleration VEST 2 Wind HDG (Meas. Alpha & Beta)

171
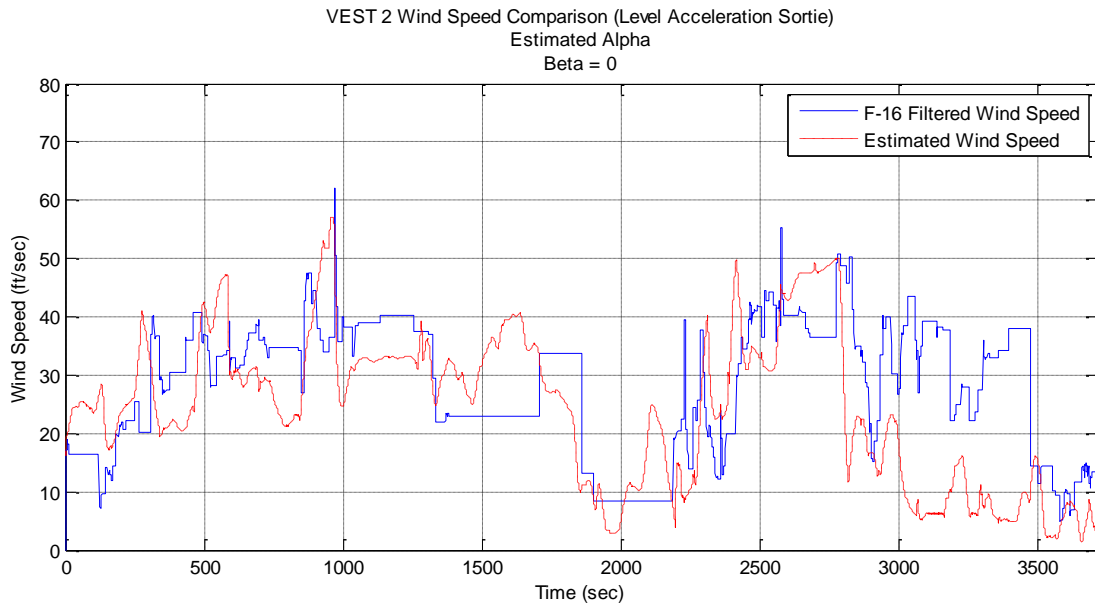
Figure 101. Level Acceleration VEST 2 Wind Speed (Est. Alpha, Beta= 0)
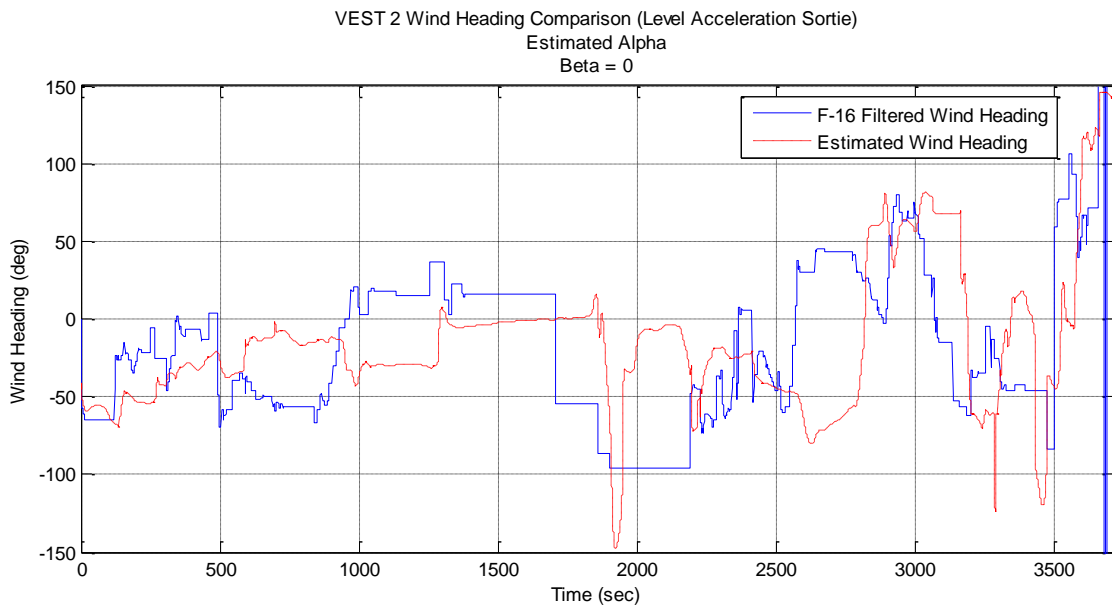
Figure 102. Level Acceleration VEST 2 Wind HDG (Est. Alpha, Beta=0)

172

Appendix G. Aircraft Wind Truth Data Comparison
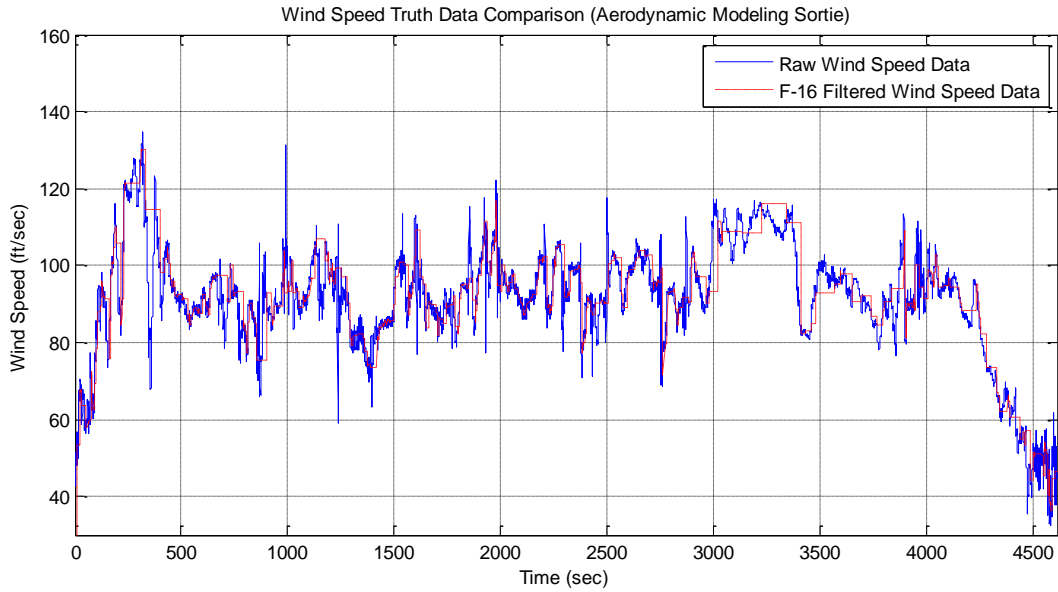
Figure 103. Aerodynamic Modeling Wind Speed Truth Data
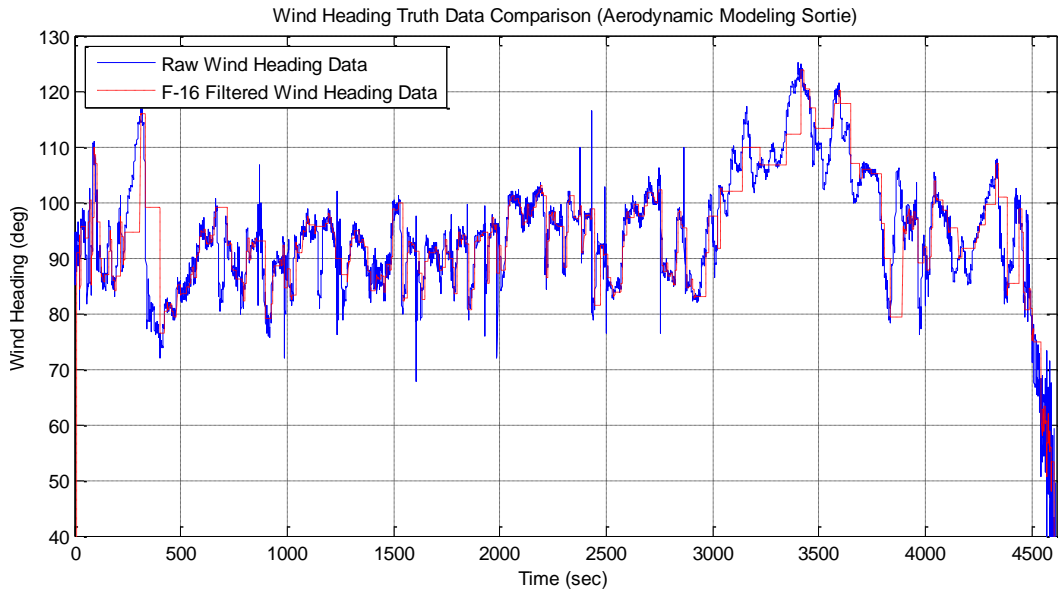
Figure 104. Aerodynamic Modeling Wind HDG Truth Data
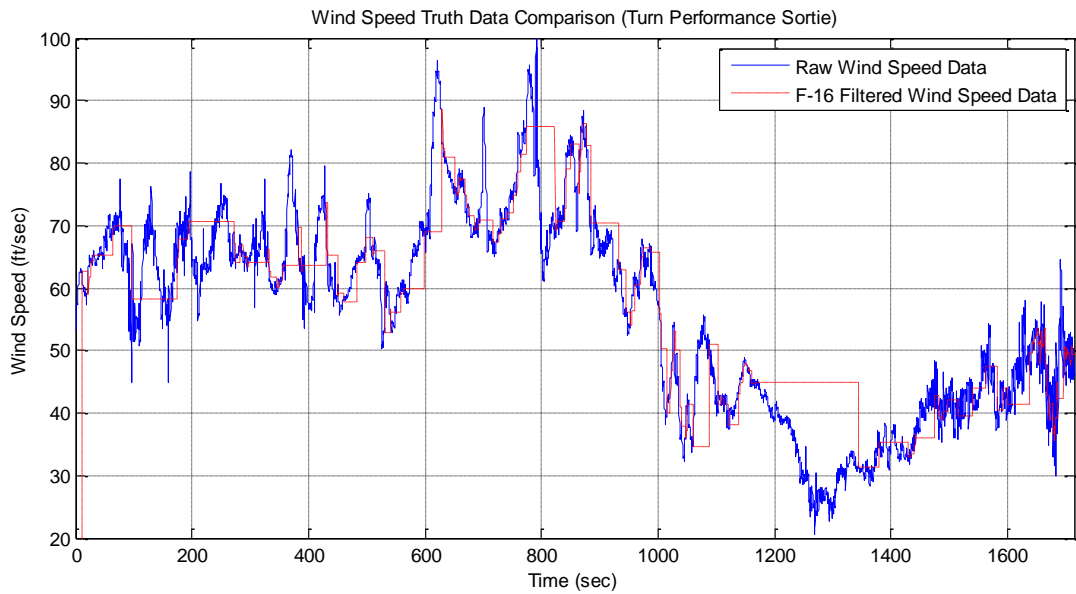
Figure 105. Turn Performance Wind Speed Truth Data
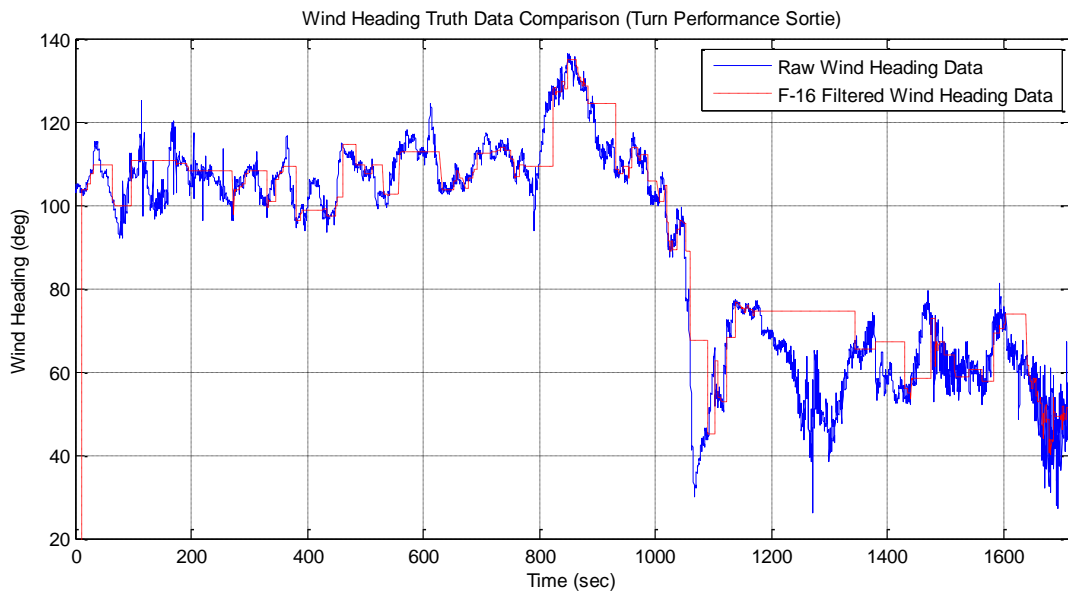
Figure 106. Turn Performance Wind HDG Truth Data

174
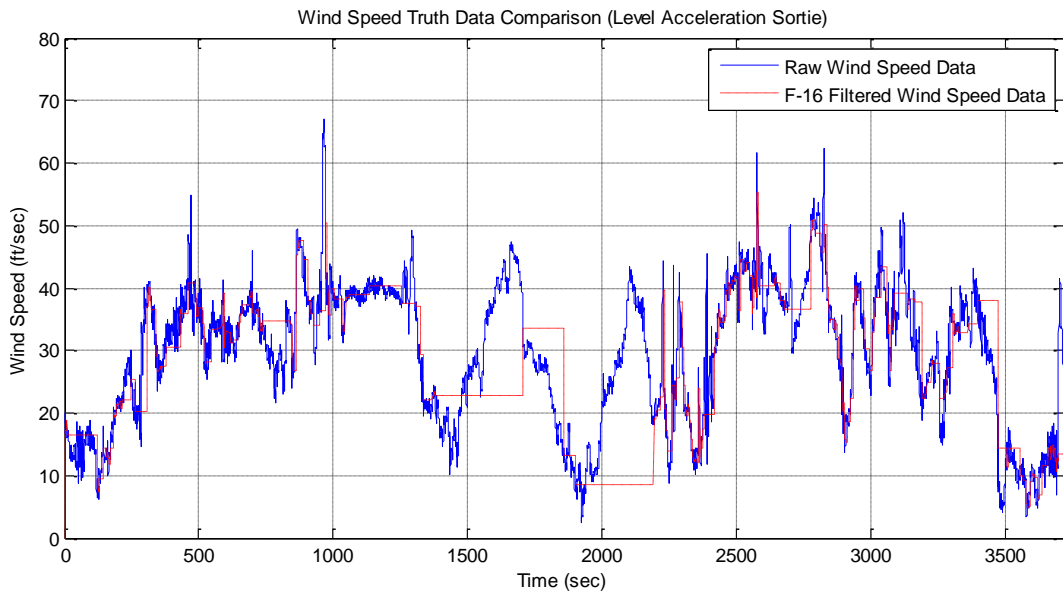
Figure 107. Level Acceleration Wind Speed Truth Data
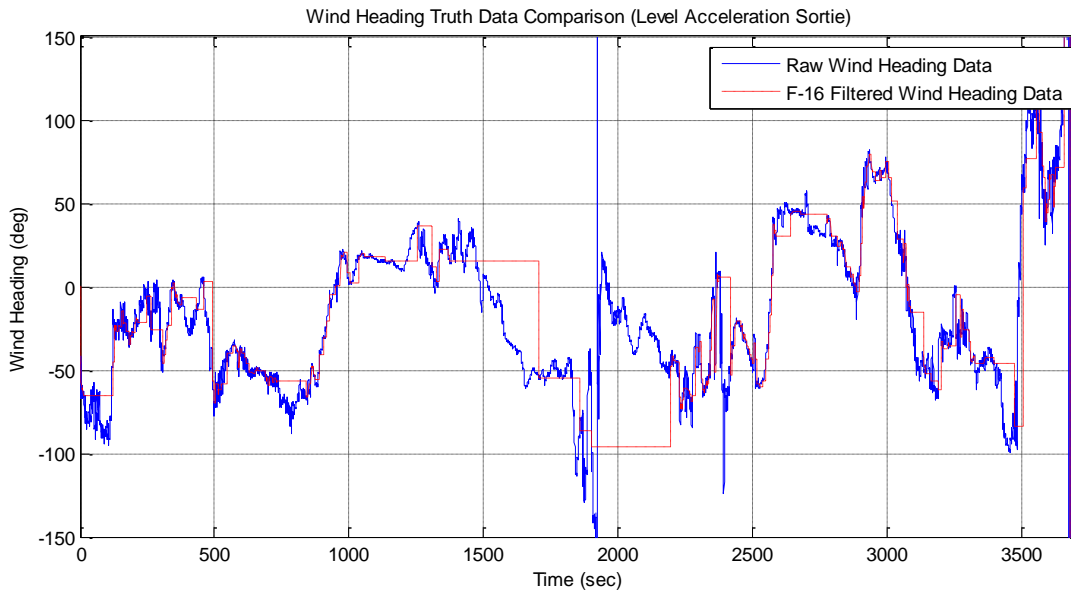
Figure 108. Level Acceleration Wind HDG Truth Data

175

Aerodynamic Modeling Sortie
(Bleed Rate Climb)
VEST 2
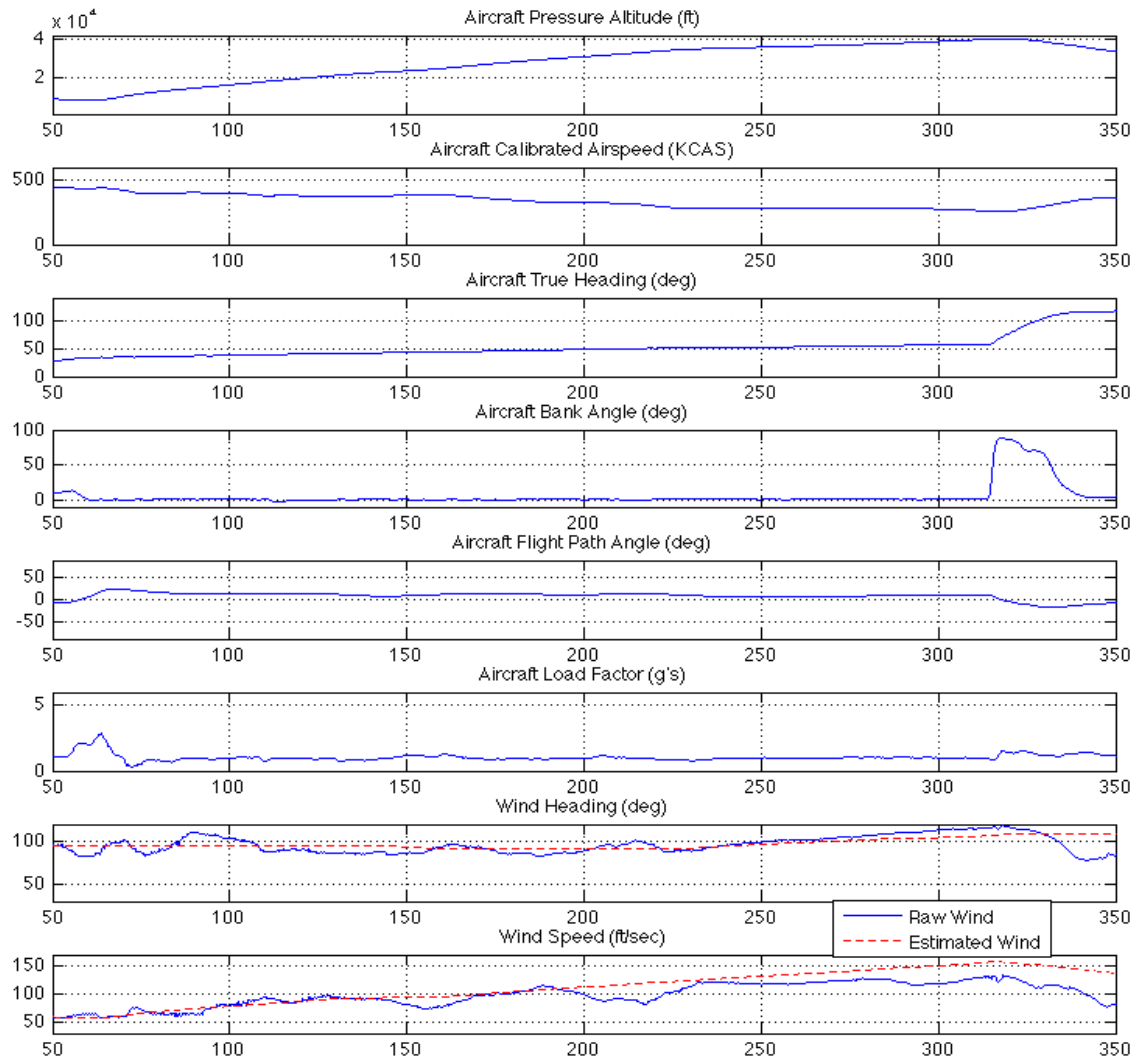
Figure 109. Bleed Rate Climb (VEST 2)

Aerodynamic Modeling Sortie
(Bleed Rate Climb)
VEST 2
F-16 Filtered Winds
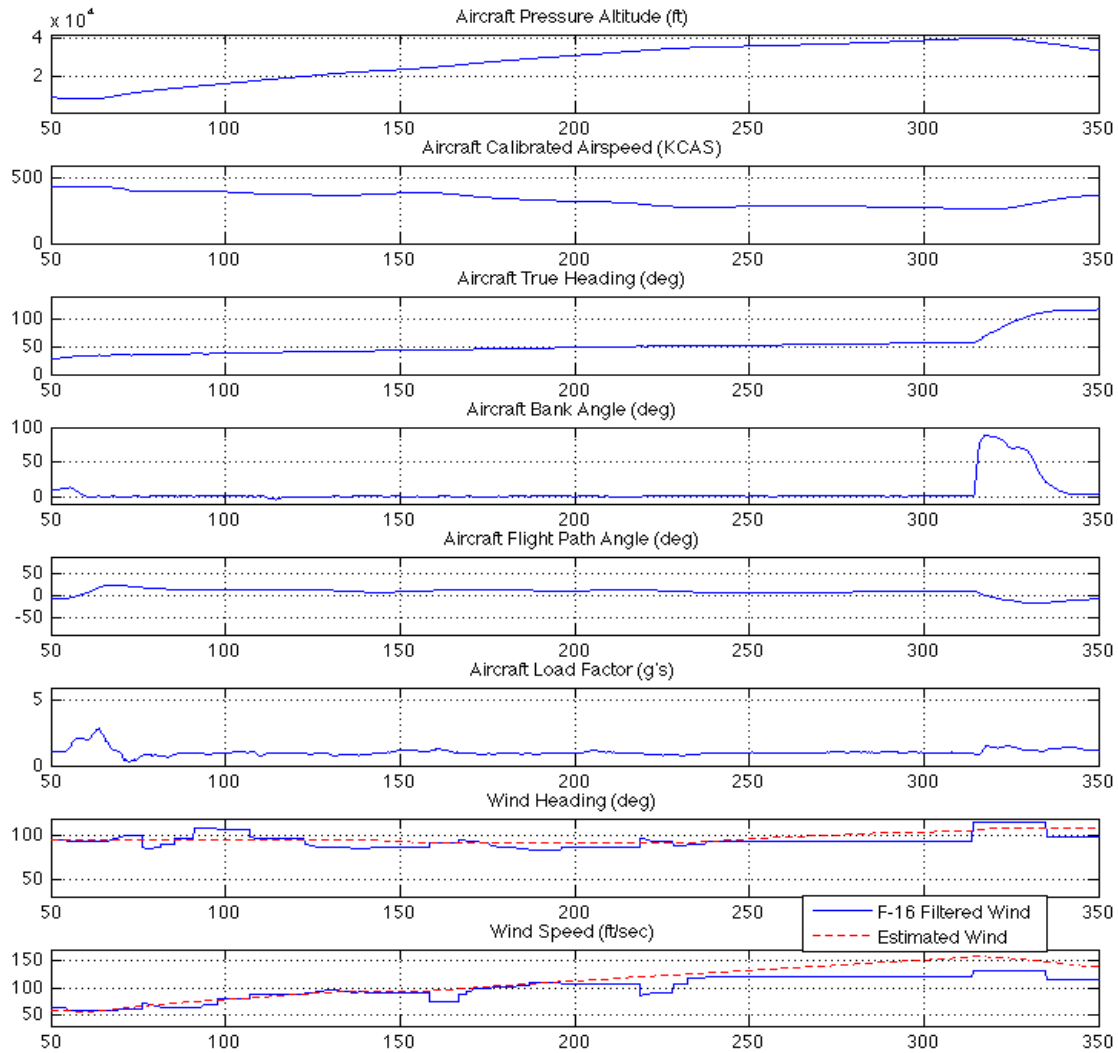
Figure 110. Bleed Rate Climb (VEST 2)

Aerodynamic Modeling Sortie
(Bleed Rate Climb)
VEST
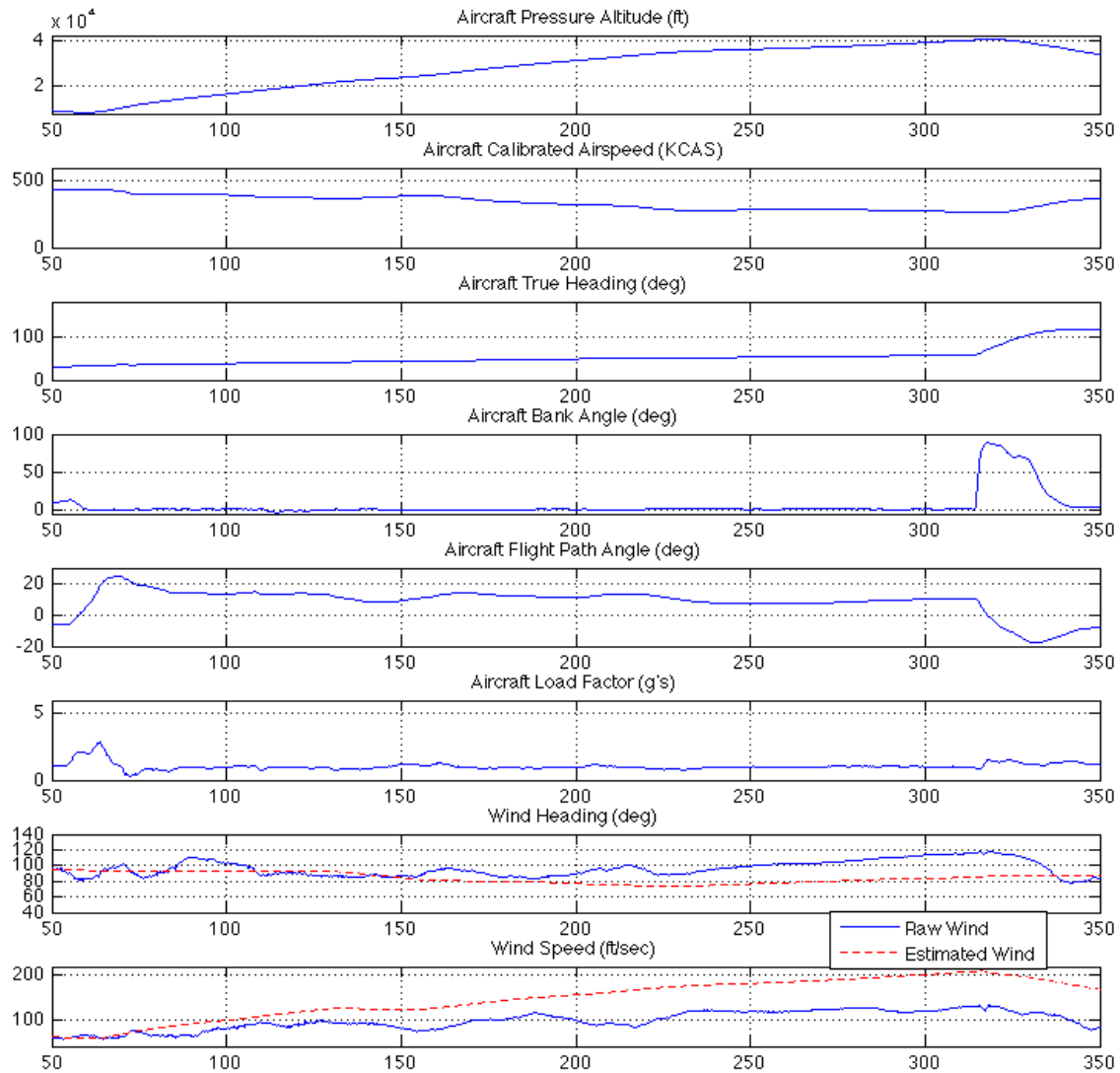
Figure 111. Bleed Rate Climb (VEST)

Aerodynamic Modeling Sortie
(Bleed Rate Climb)
VEST TAS
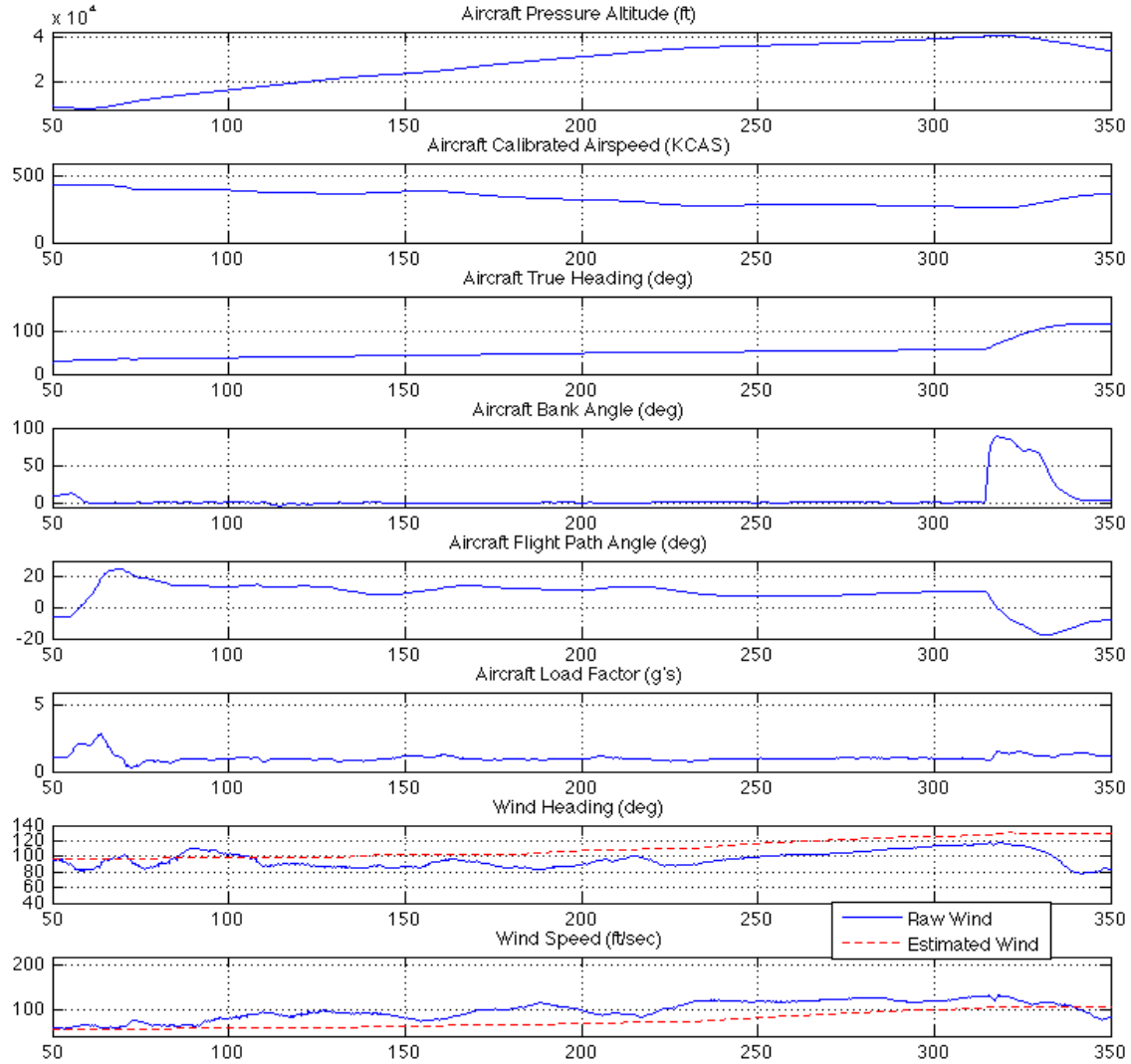
Figure 112. Bleed Rate Climb (VEST TAS)

Aerodynamic Modeling Sortie
(Multiple Roller Coasters, Windup Turns, Split-S's)
VEST 2
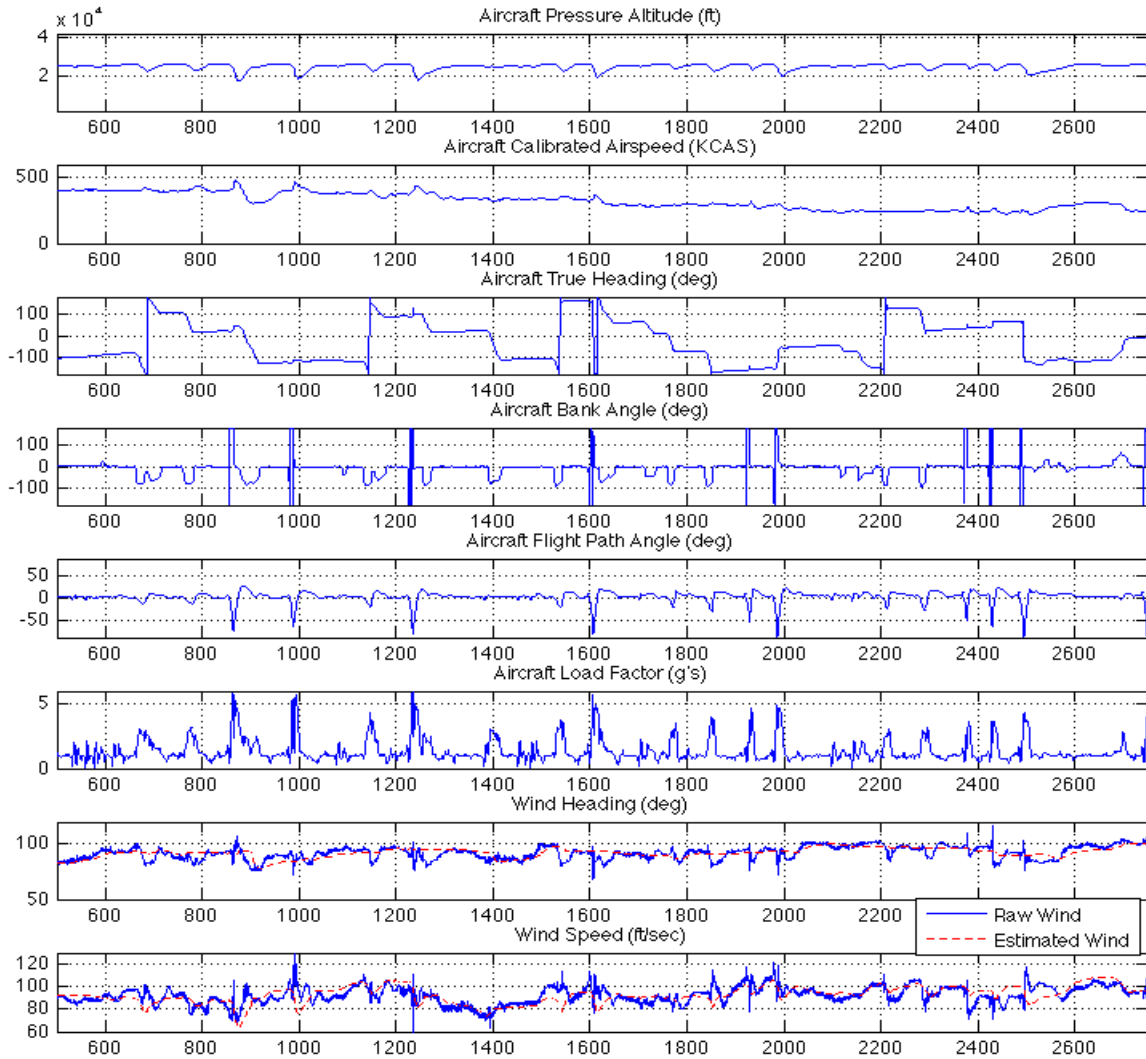
Figure 113. Roller Coasters, Windup Turns, and Split-S (VEST 2)

Aerodynamic Modeling Sortie
(Multiple Roller Coasters, Windup Turns, Split-S's)
VEST 2
F-16 Filtered Winds
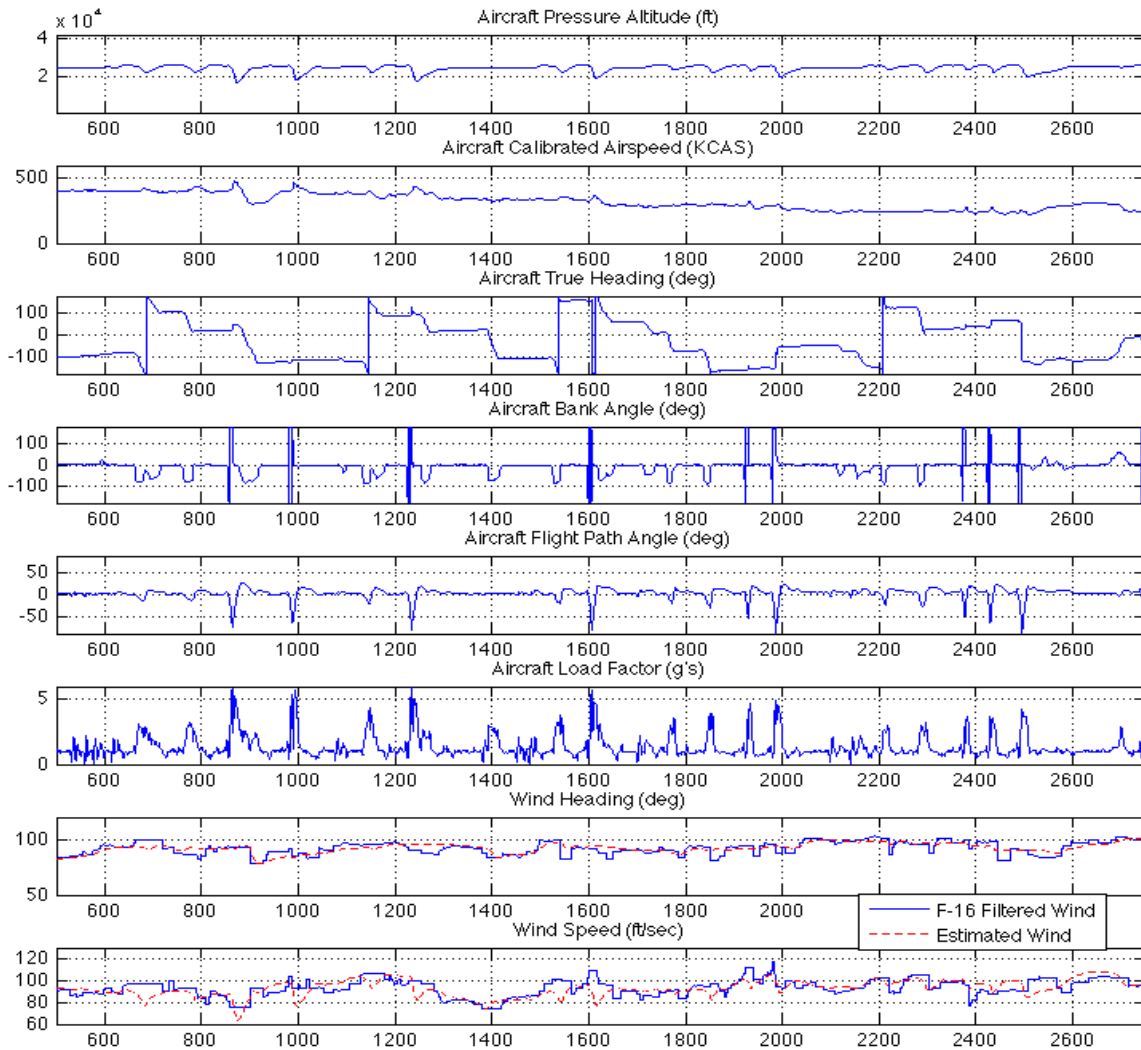
Figure 114. Roller Coasters, Windup Turns, and Split-S (VEST 2)

Aerodynamic Modeling Sortie
(Single Roller Coaster, Single Windup Turn, Single Split-S)
VEST 2
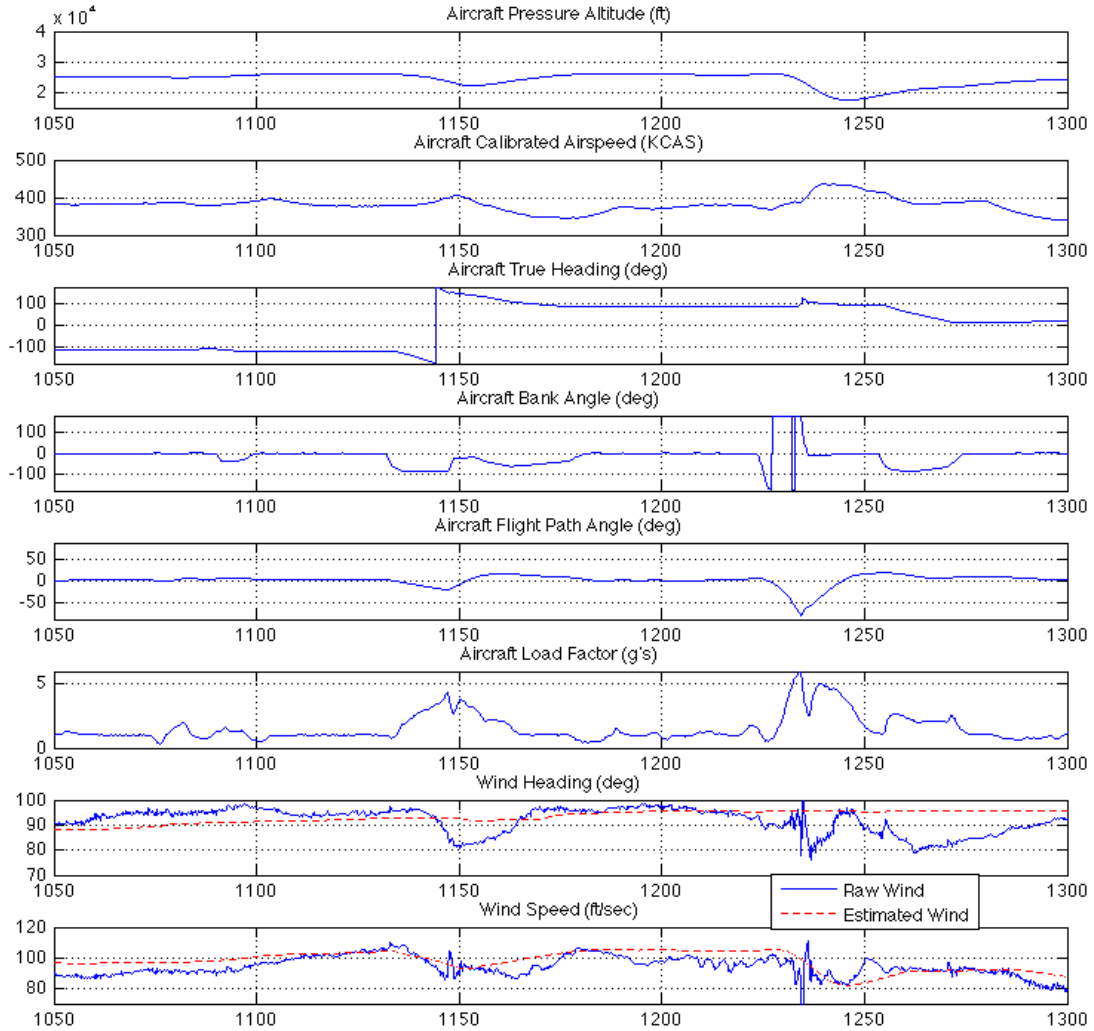
Figure 115. Roller Coaster, Windup Turn, and Split-S (VEST 2)

Aerodynamic Modeling Sortie
(Single Roller Coaster, Single Windup Turn, Single Split-S)
VEST 2
F-16 Filtered Winds
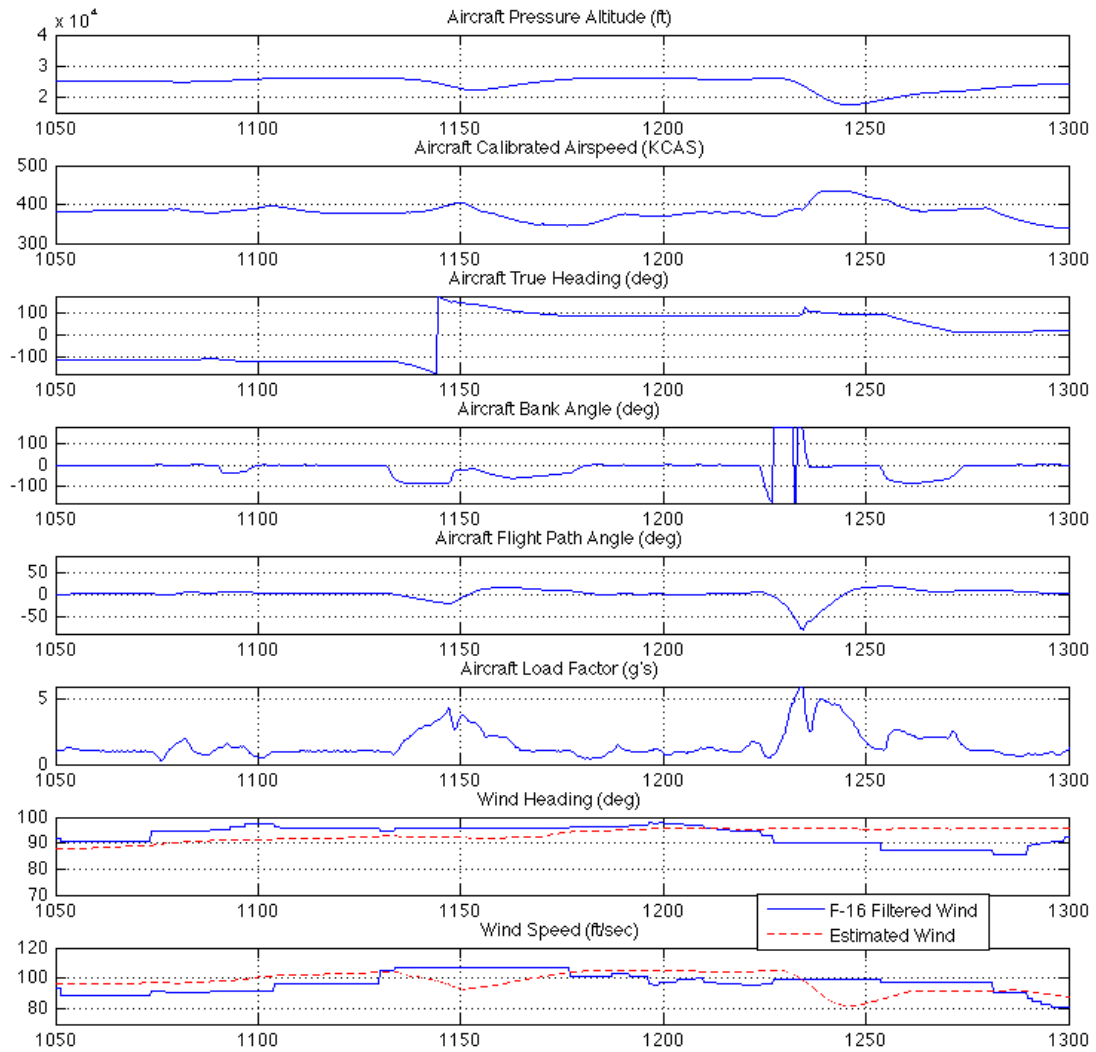
Figure 116. Roller Coaster, Windup Turn, and Split-S (VEST 2)

Aerodynamic Modeling Sortie
(Single Roller Coaster, Single Windup Turn, Single Split-S)
VEST 2 (No Residual Logic)
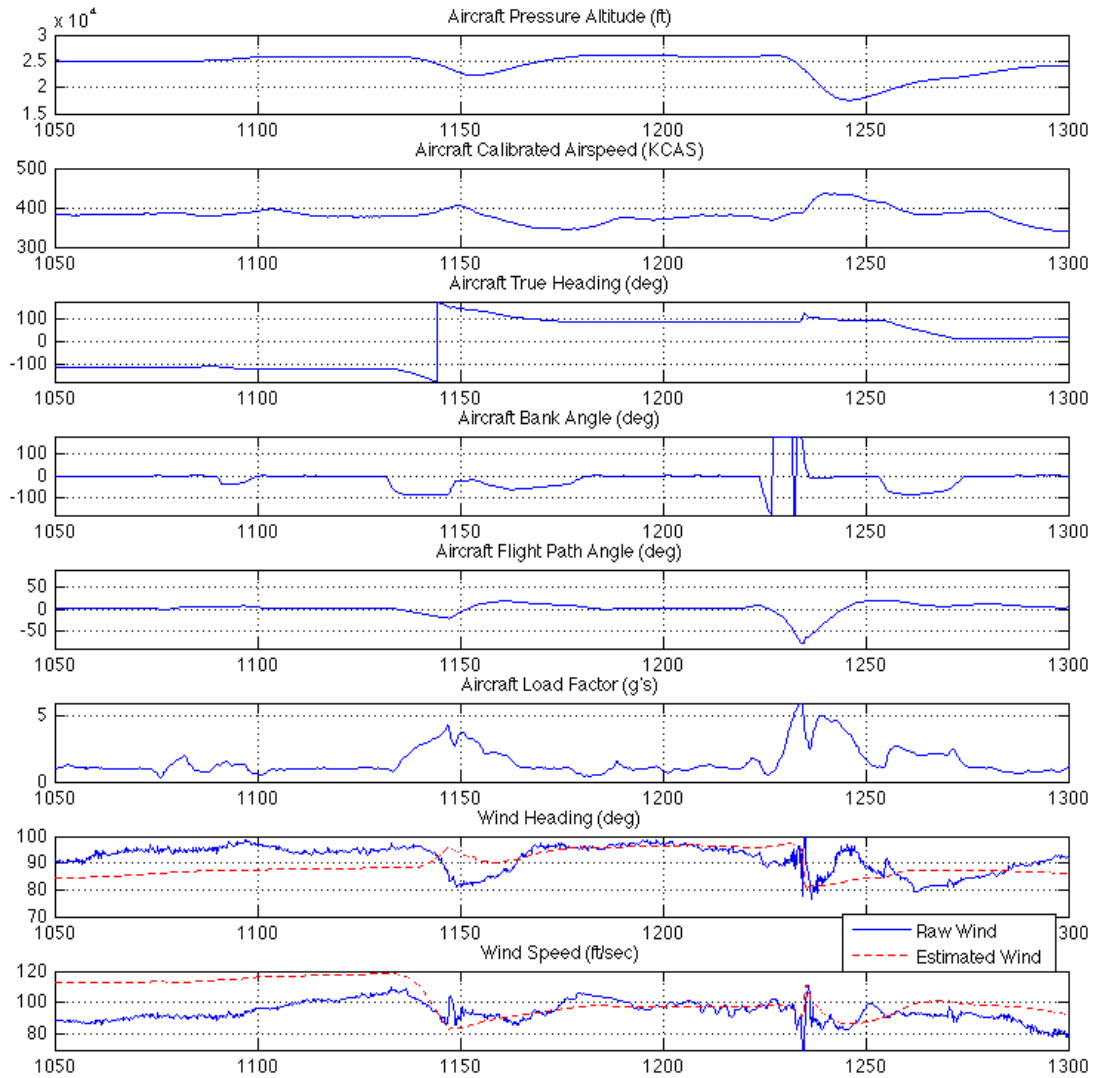
Figure 117. Roller Coaster, Windup Turn, Split-S (VEST 2 - No Residual Logic)

Aerodynamic Modeling Sortie
(Climb)
VEST 2
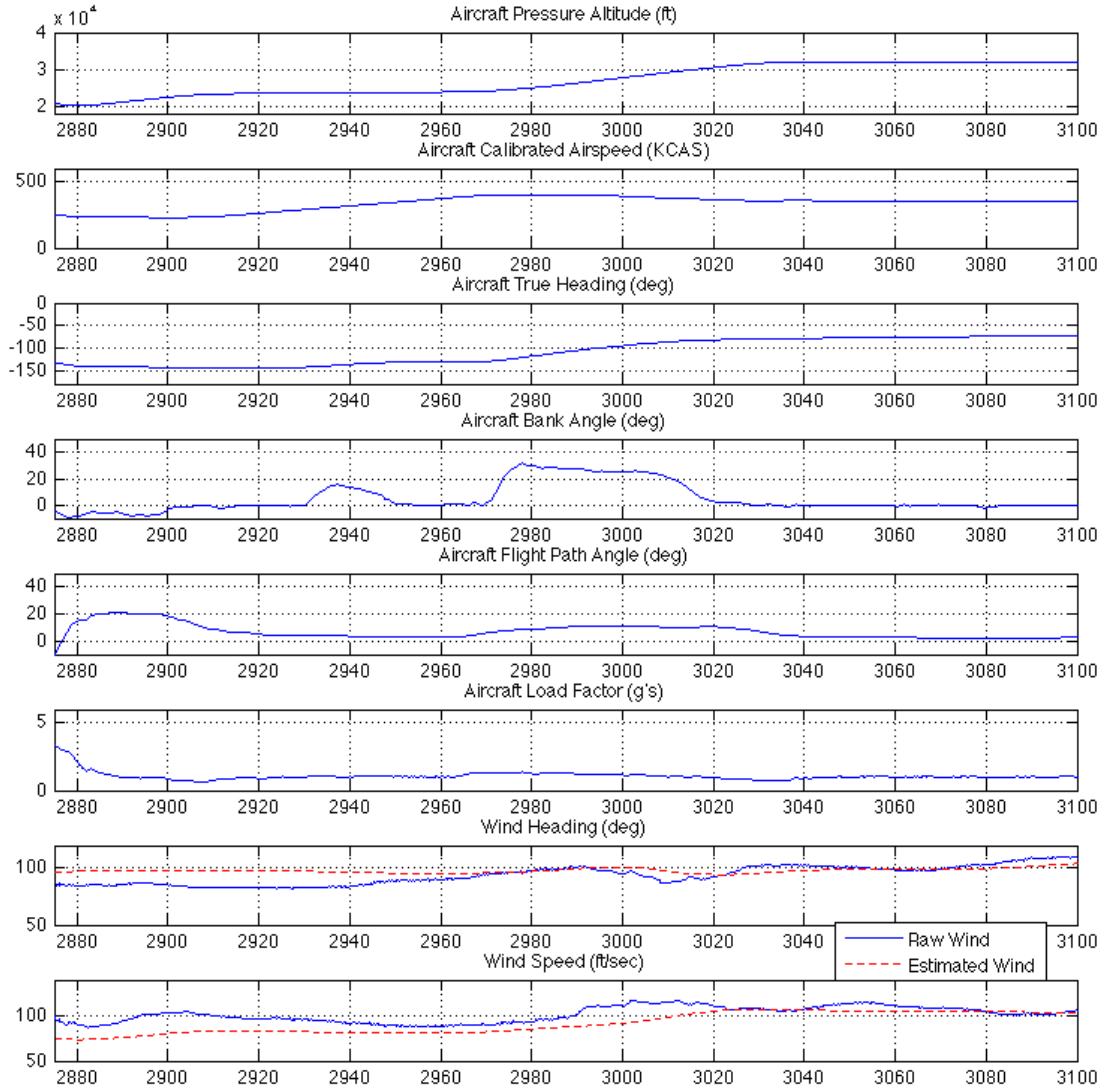
Figure 118. Climb (VEST 2)

Aerodynamic Modeling Sortie
(Climb)
VEST 2
F-16 Filtered Winds
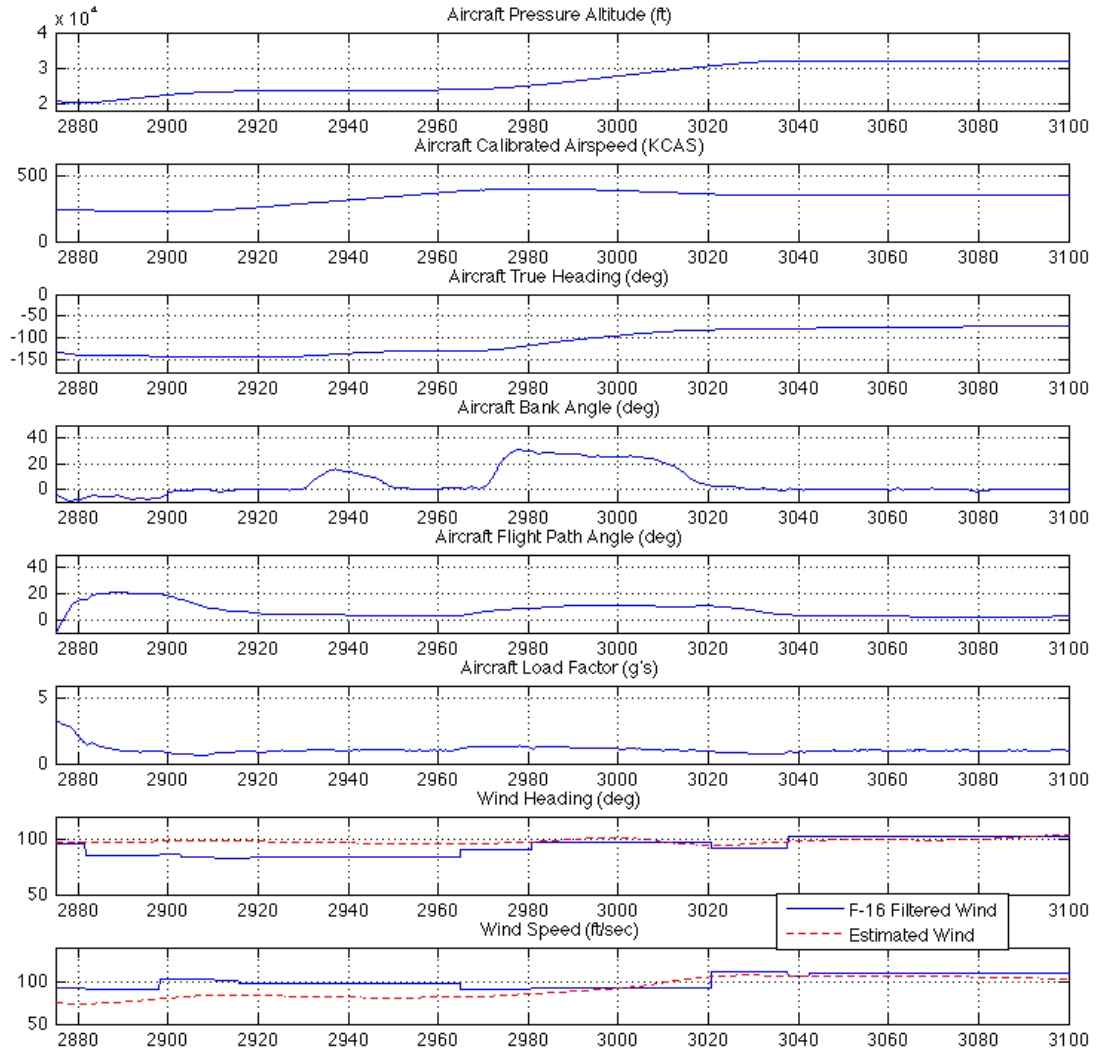
Figure 119. Climb (VEST 2)

Aerodynamic Modeling Sortie
(Cruise Points)
VEST 2
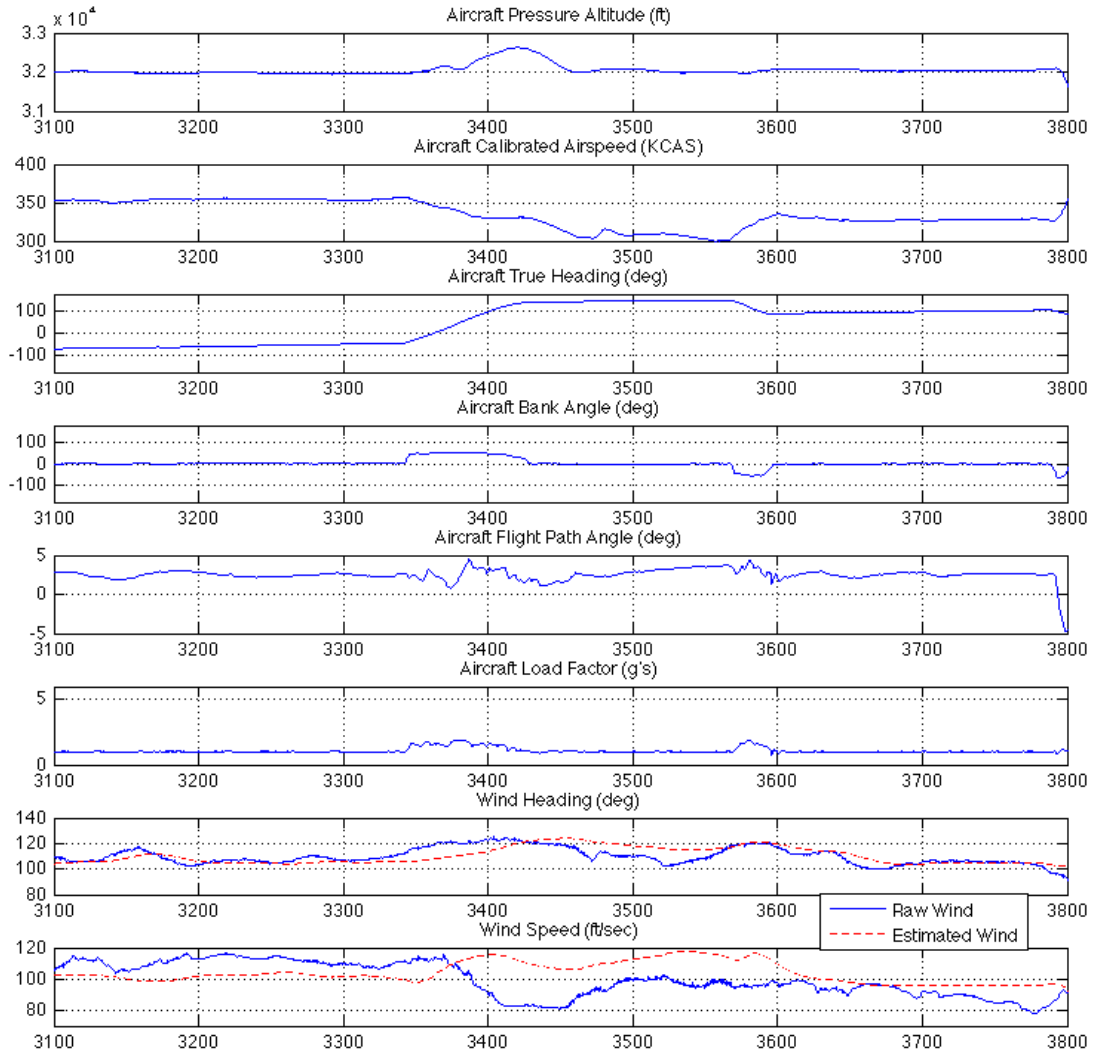
Figure 120. Cruise Points (VEST 2)

Aerodynamic Modeling Sortie
(Cruise Points)
VEST 2
F-16 Filtered Winds
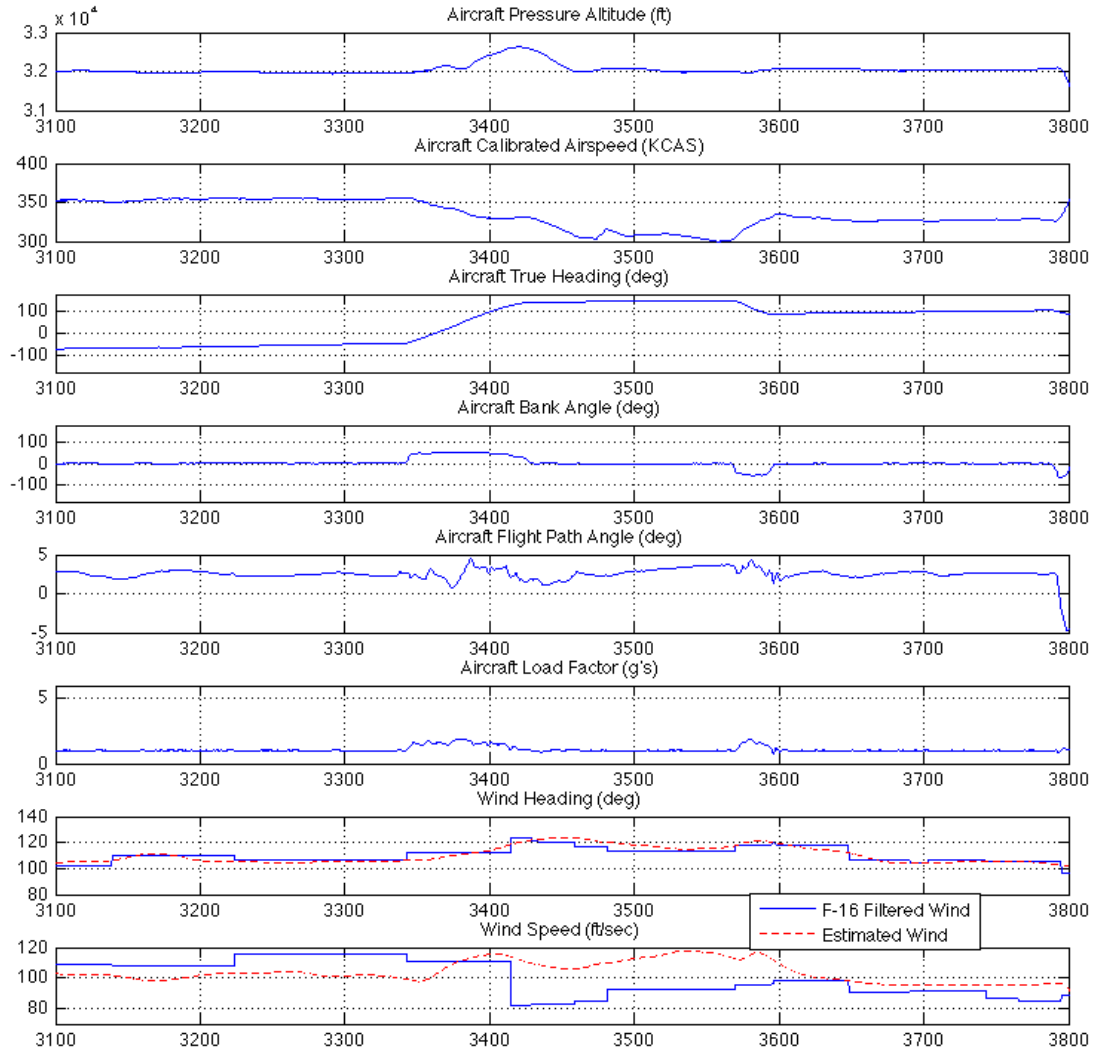
Figure 121. Cruise Points (VEST 2)

Aerodynamic Modeling Sortie
(Maximum Range Descent)
VEST 2
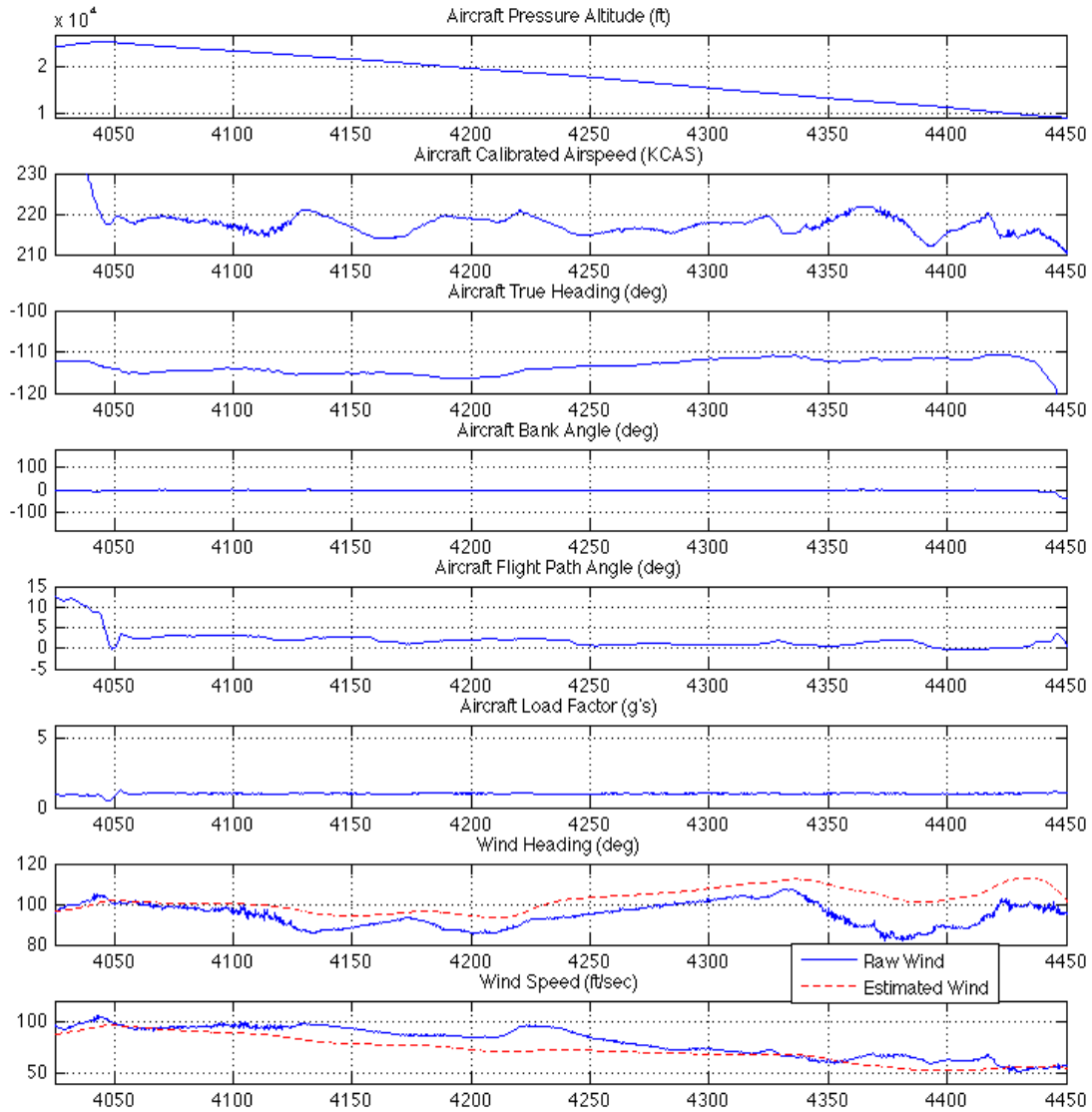
Figure 122. Maximum Range Descent (VEST 2)

Aerodynamic Modeling Sortie
(Maximum Range Descent)
VEST 2
F-16 Filtered Winds
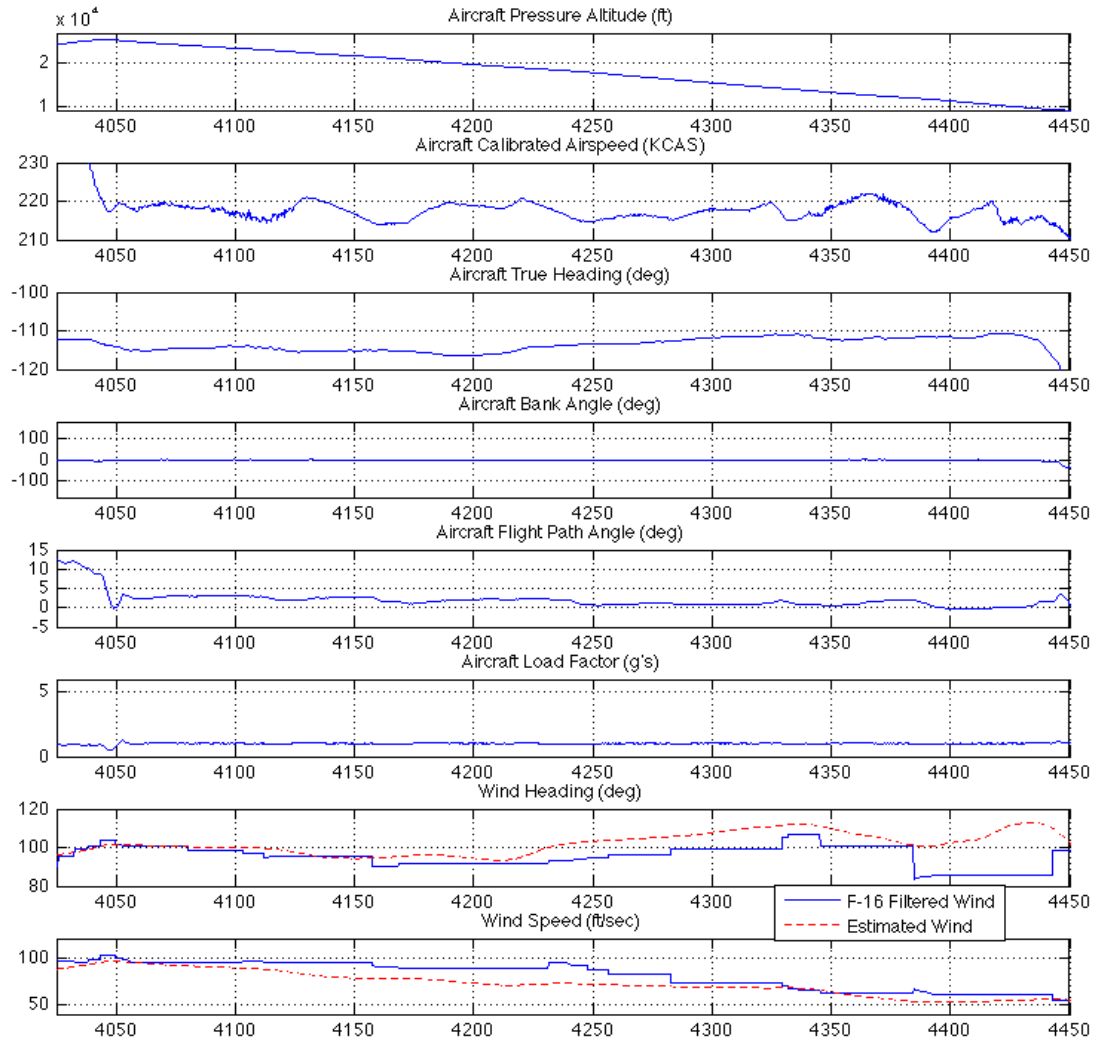
Figure 123. Maximum Range Descent (VEST 2)

Aerodynamic Modeling Sortie
(Maximum Range Descent)
VEST
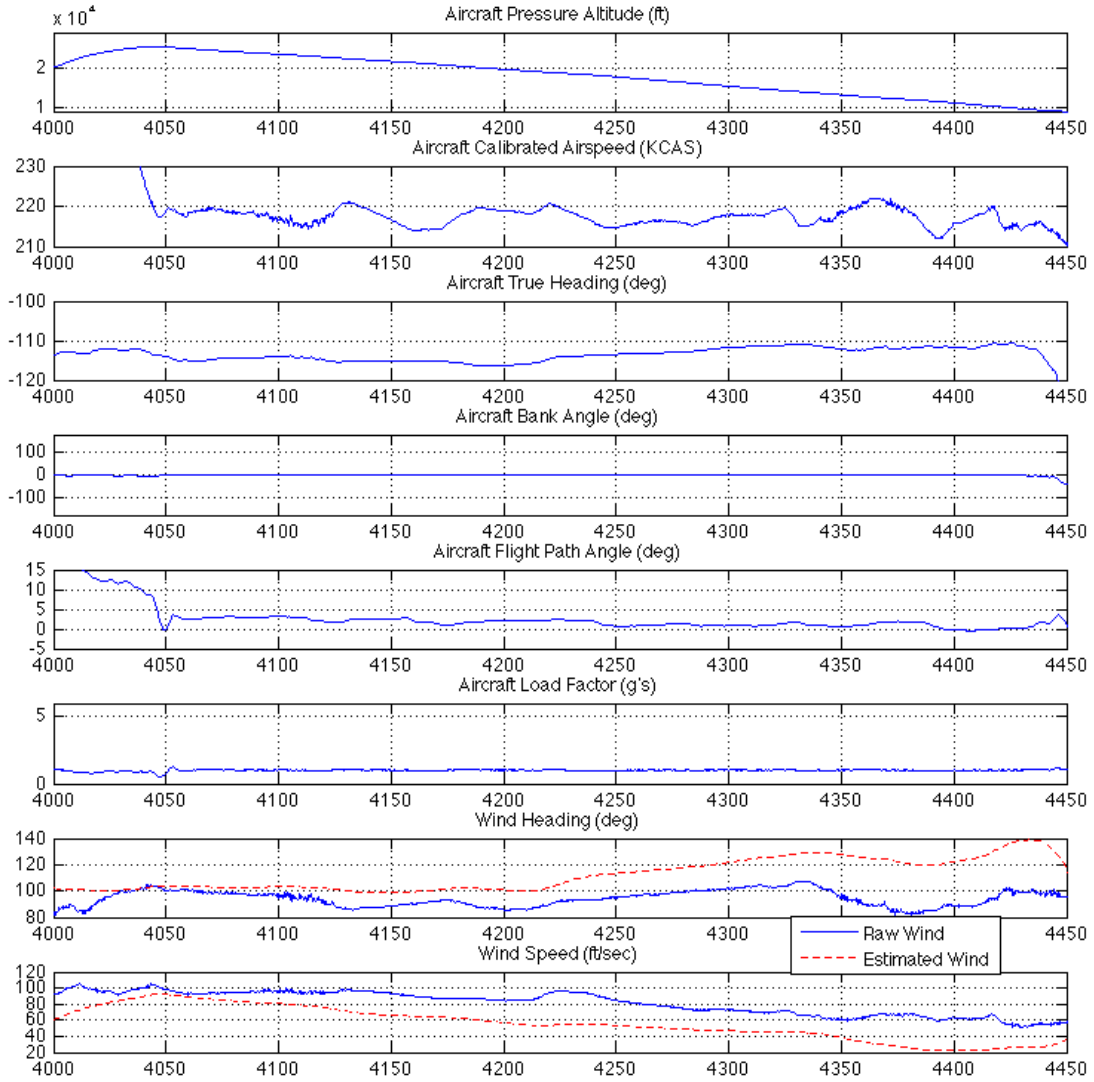
Figure 124. Maximum Range Descent (VEST)

Aerodynamic Modeling Sortie
(Maximum Range Descent)
VEST TAS
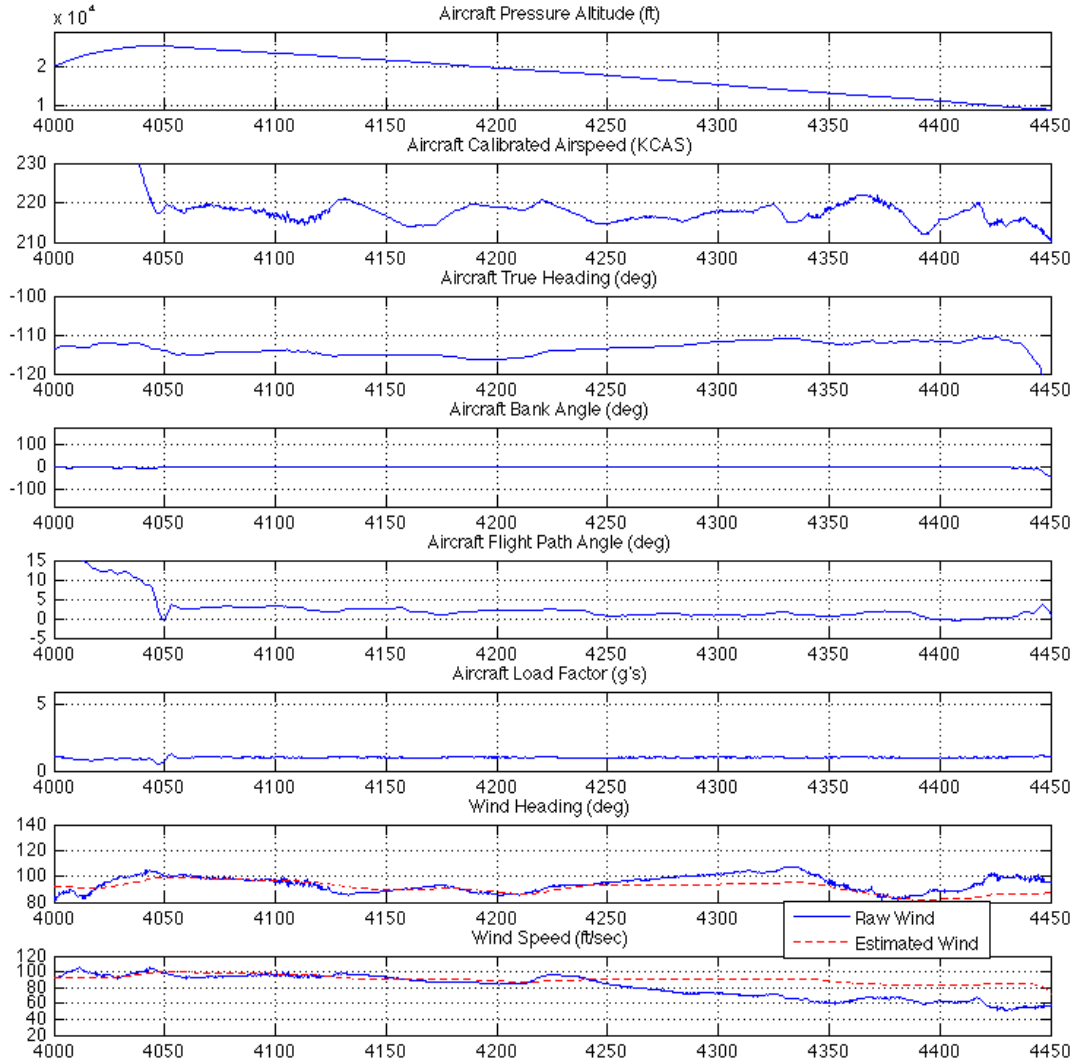
Figure 125. Maximum Range Descent (VEST TAS)

Appendix I. Turn Performance Sortie Maneuver Plots

Turn Performance Sortie
(Maximum Power Level Turns)
VEST 2
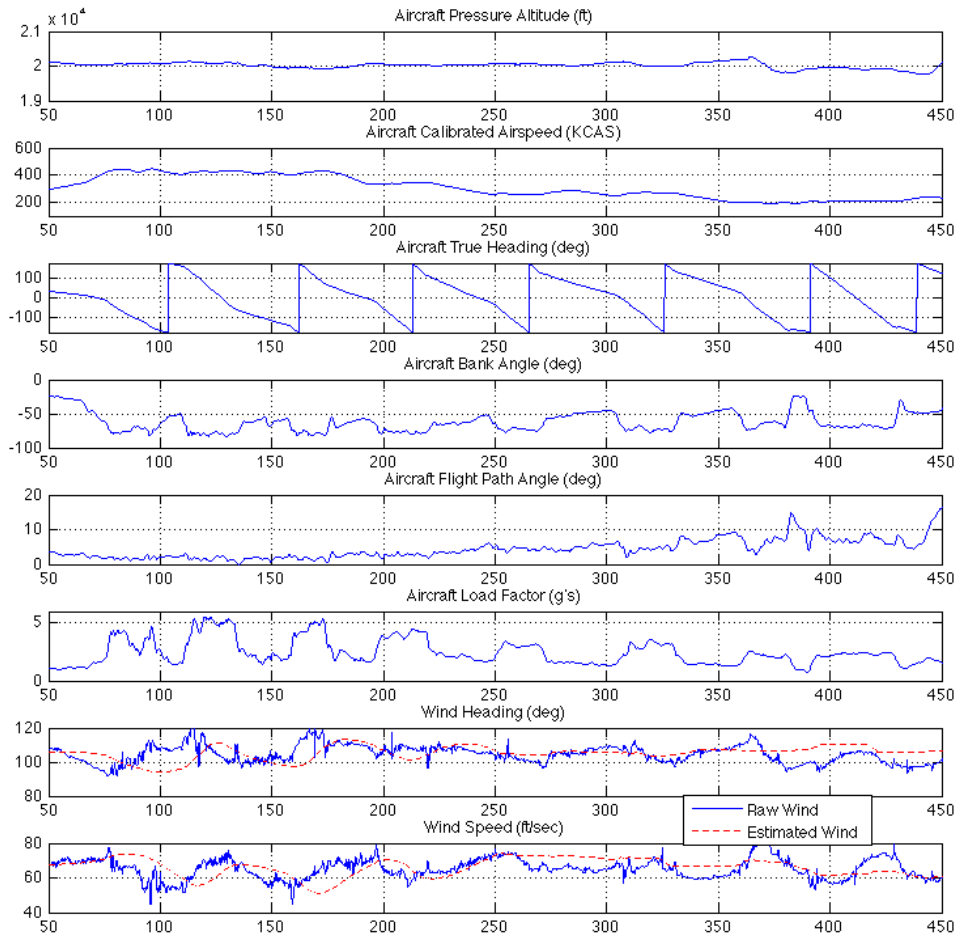
Figure 126. Maximum Power Level Turns (VEST 2)

Turn Performance Sortie
(Maximum Power Level Turns)
VEST 2
F-16 Filtered Winds
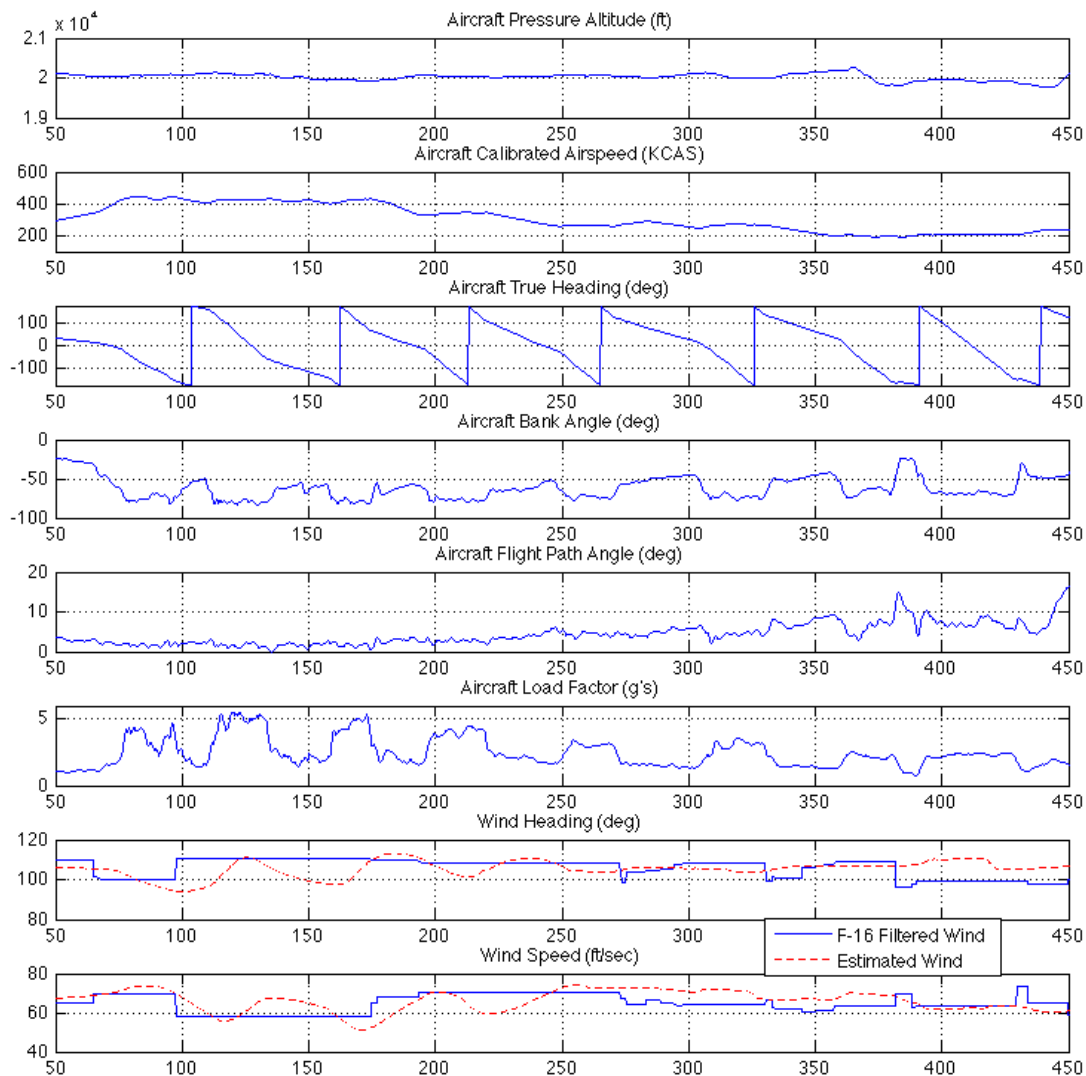
Figure 127. Maximum Power Level Turns (VEST 2)

Turn Performance Sortie
(Maximum Power Level Turns)
VEST
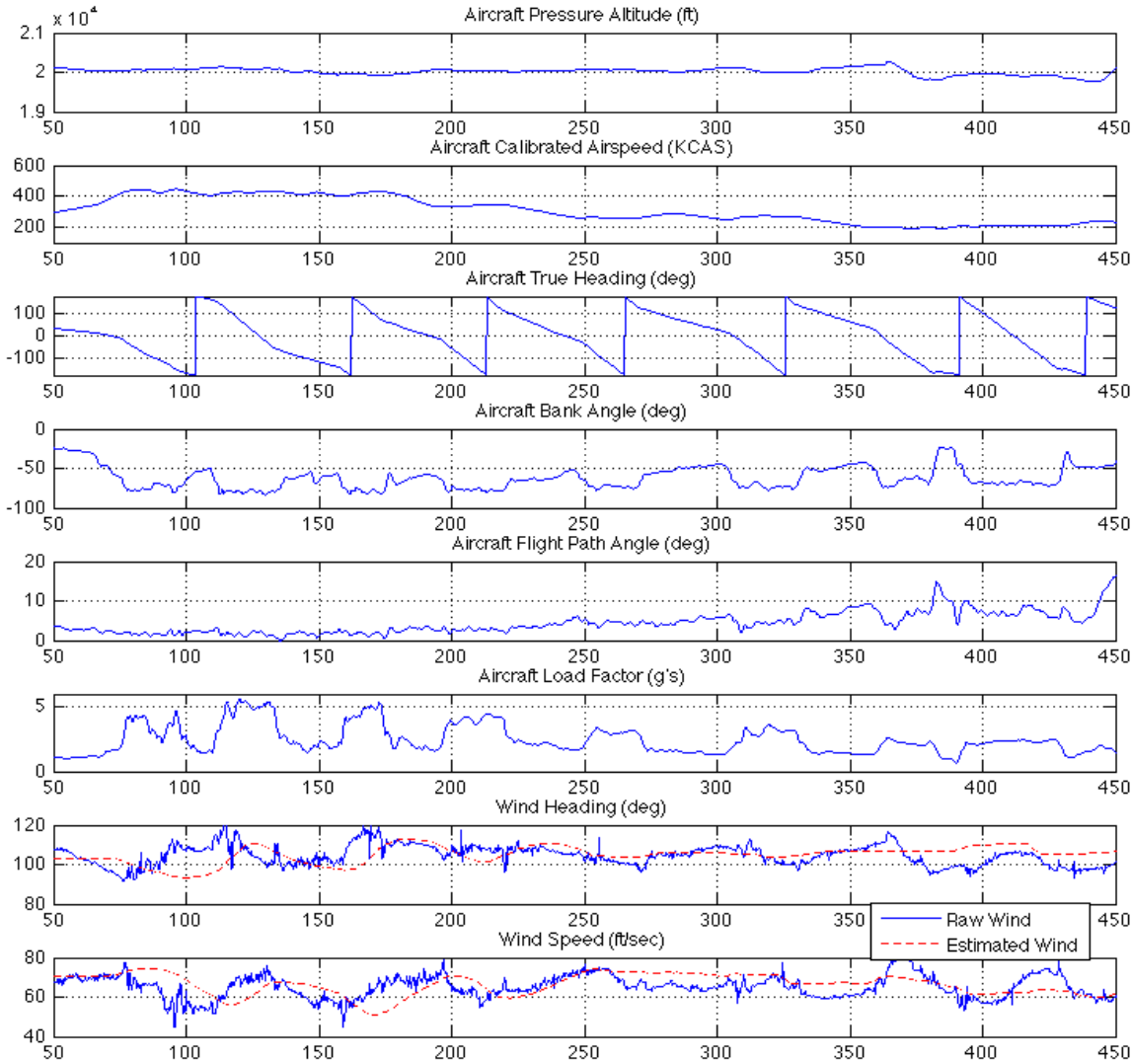
Figure 128. Maximum Power Level Turns (VEST)

Turn Performance Sortie
(Maximum Power Level Turns)
VEST TAS
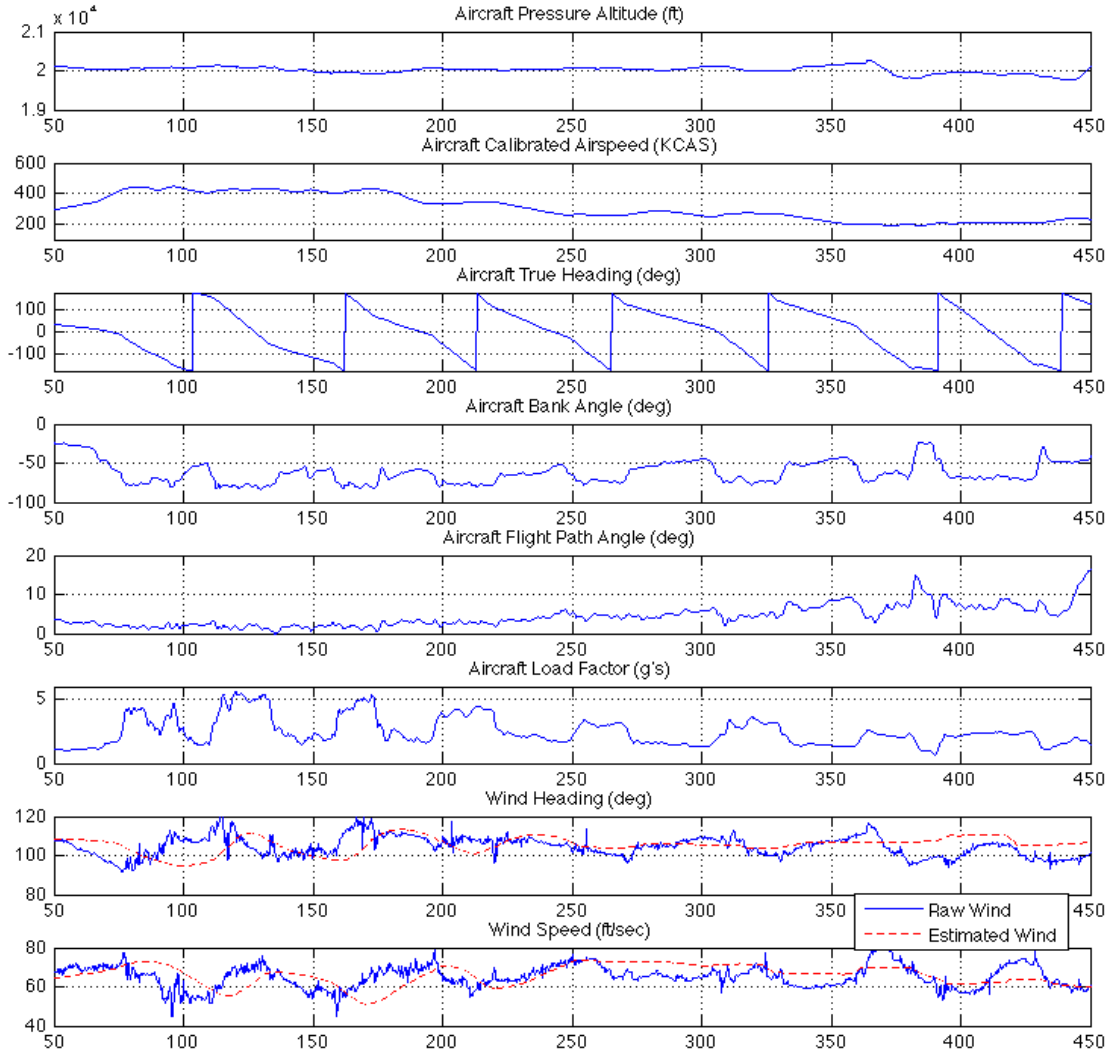
Figure 129. Maximum Power Level Turns (VEST TAS)

Turn Performance Sortie
(Maximum Power Level Acceleration)
VEST 2
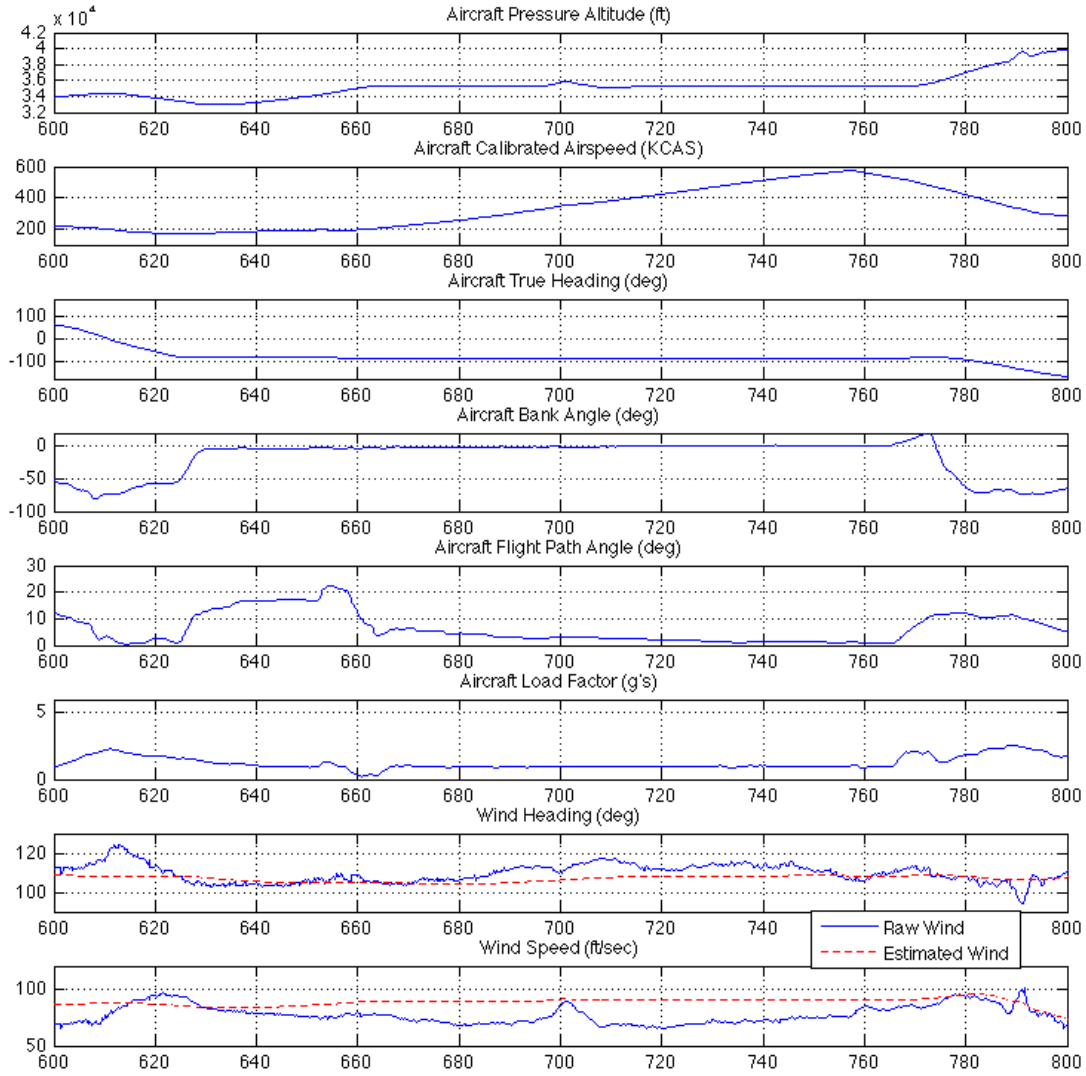
Figure 130. Maximum Power Level Acceleration (VEST 2)

Turn Performance Sortie
(Maximum Power Level Acceleration)
VEST 2
F-16 Filtered Winds
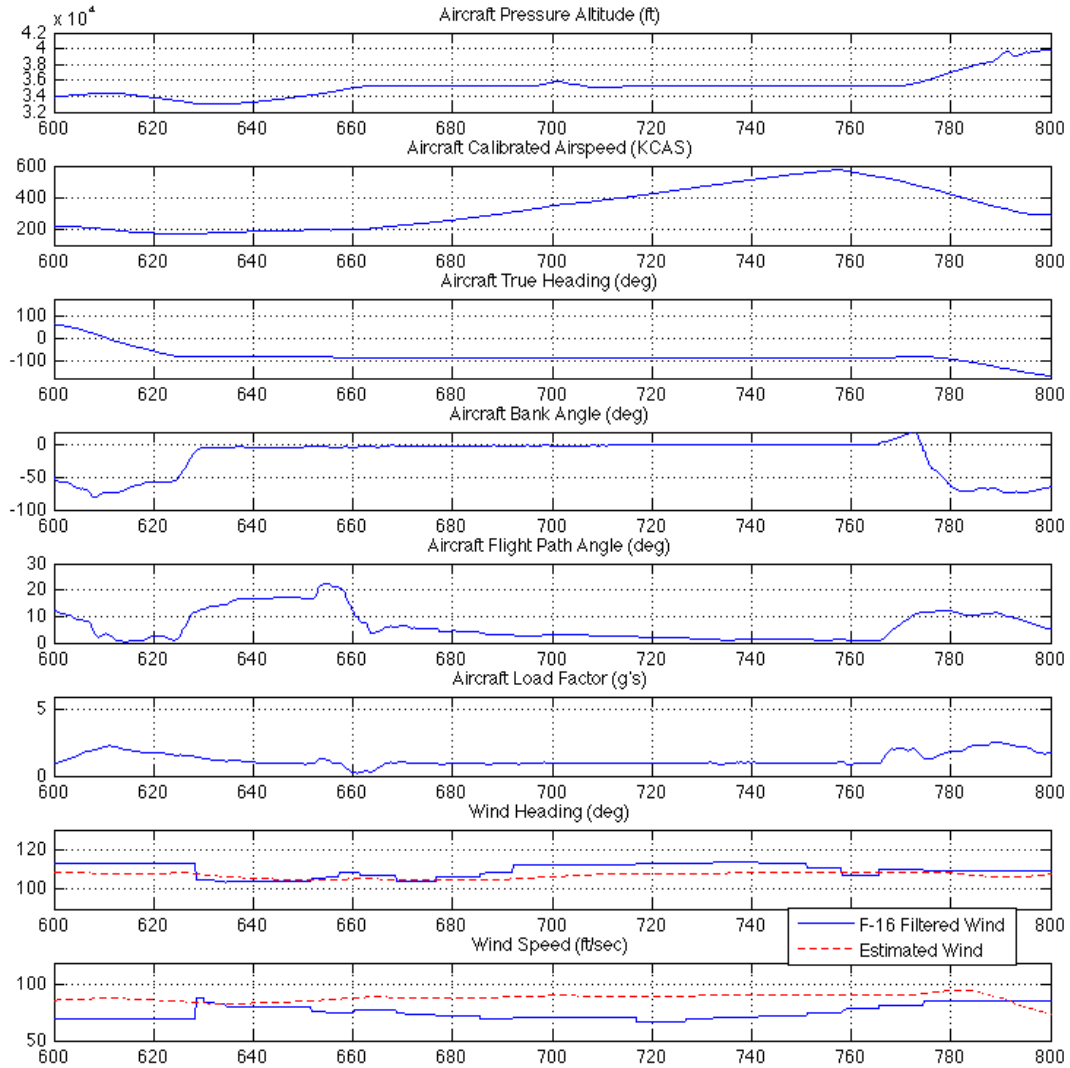
Figure 131. Maximum Power Level Acceleration (VEST 2)

Turn Performance Sortie
(Maximum Power Level Acceleration)
VEST
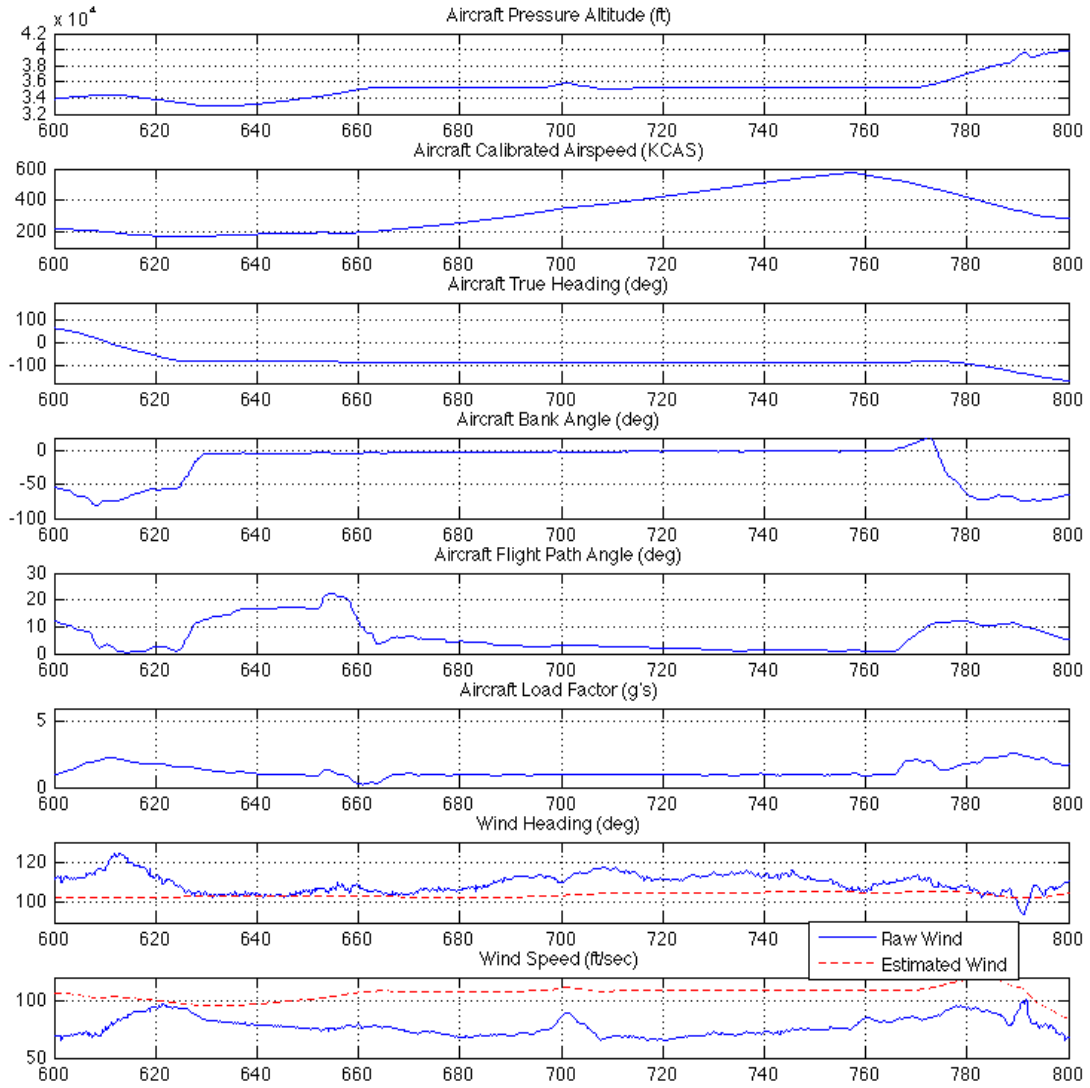
Figure 132. Maximum Power Level Acceleration (VEST)

Turn Performance Sortie
(Maximum Power Level Acceleration)
VEST TAS
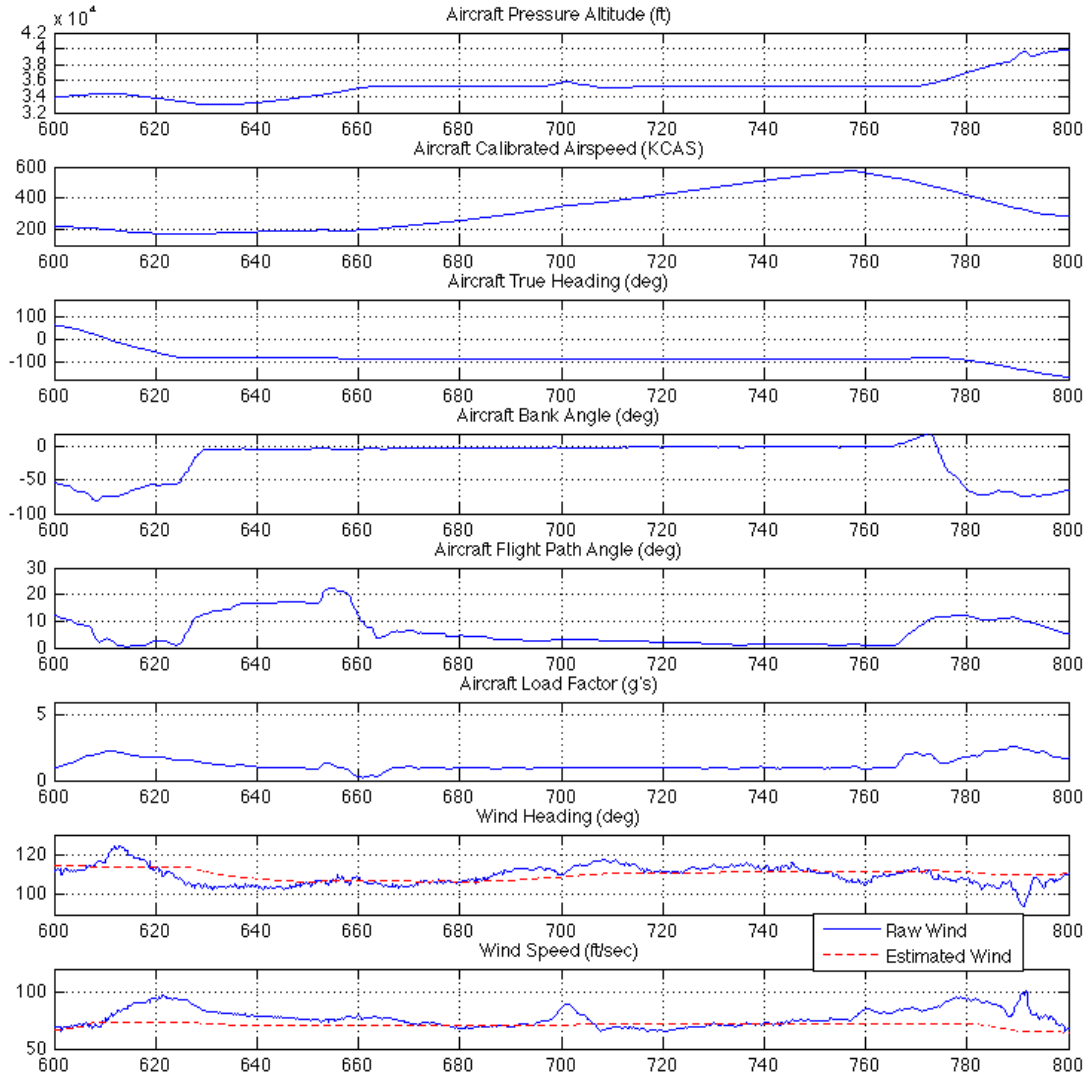
Figure 133. Maximum Power Level Acceleration (VEST TAS)

Turn Performance Sortie
(Penetration Descent)
VEST 2
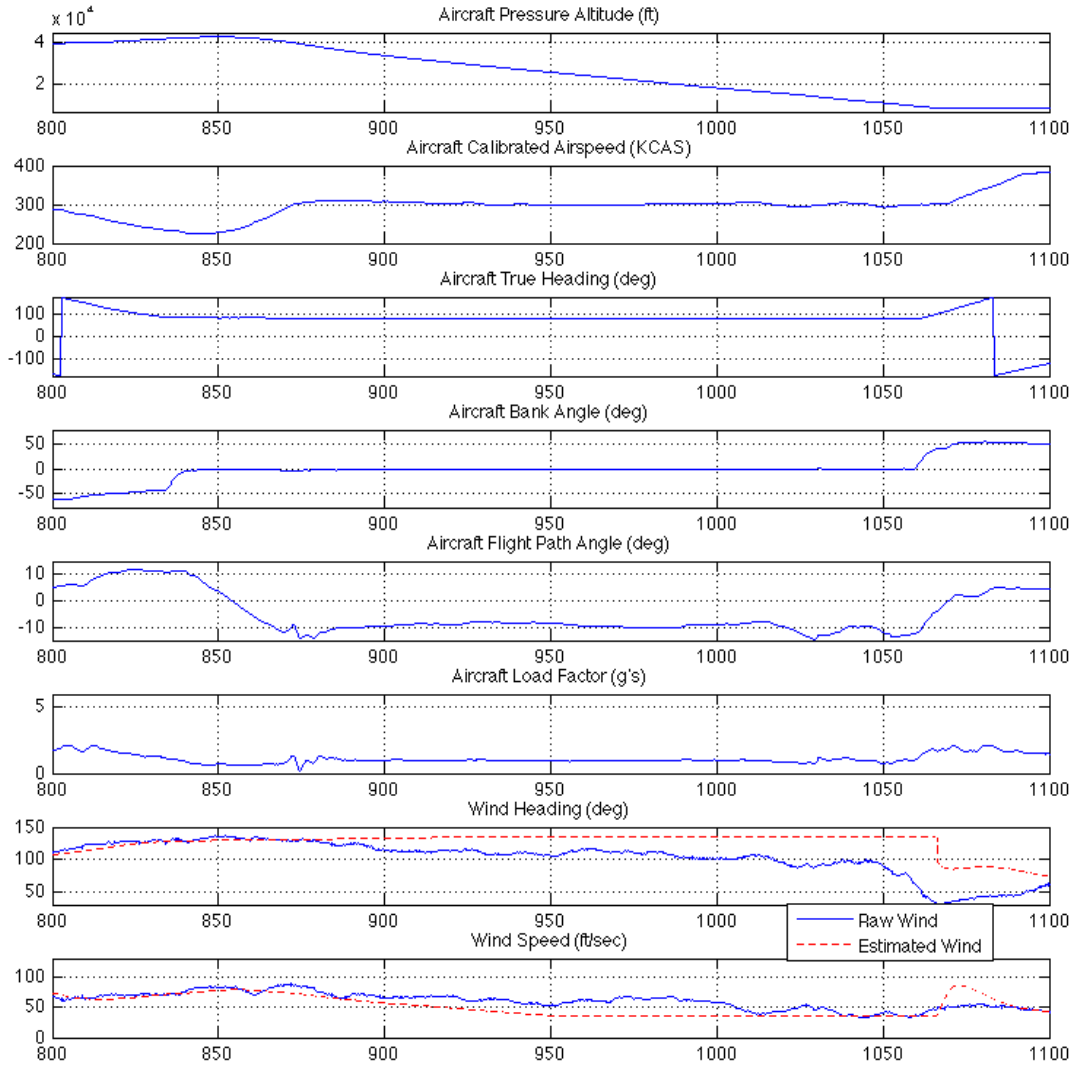
Figure 134. Penetration Descent (VEST 2)

Turn Performance Sortie
(Penetration Descent)
VEST 2
F-16 Filtered Winds
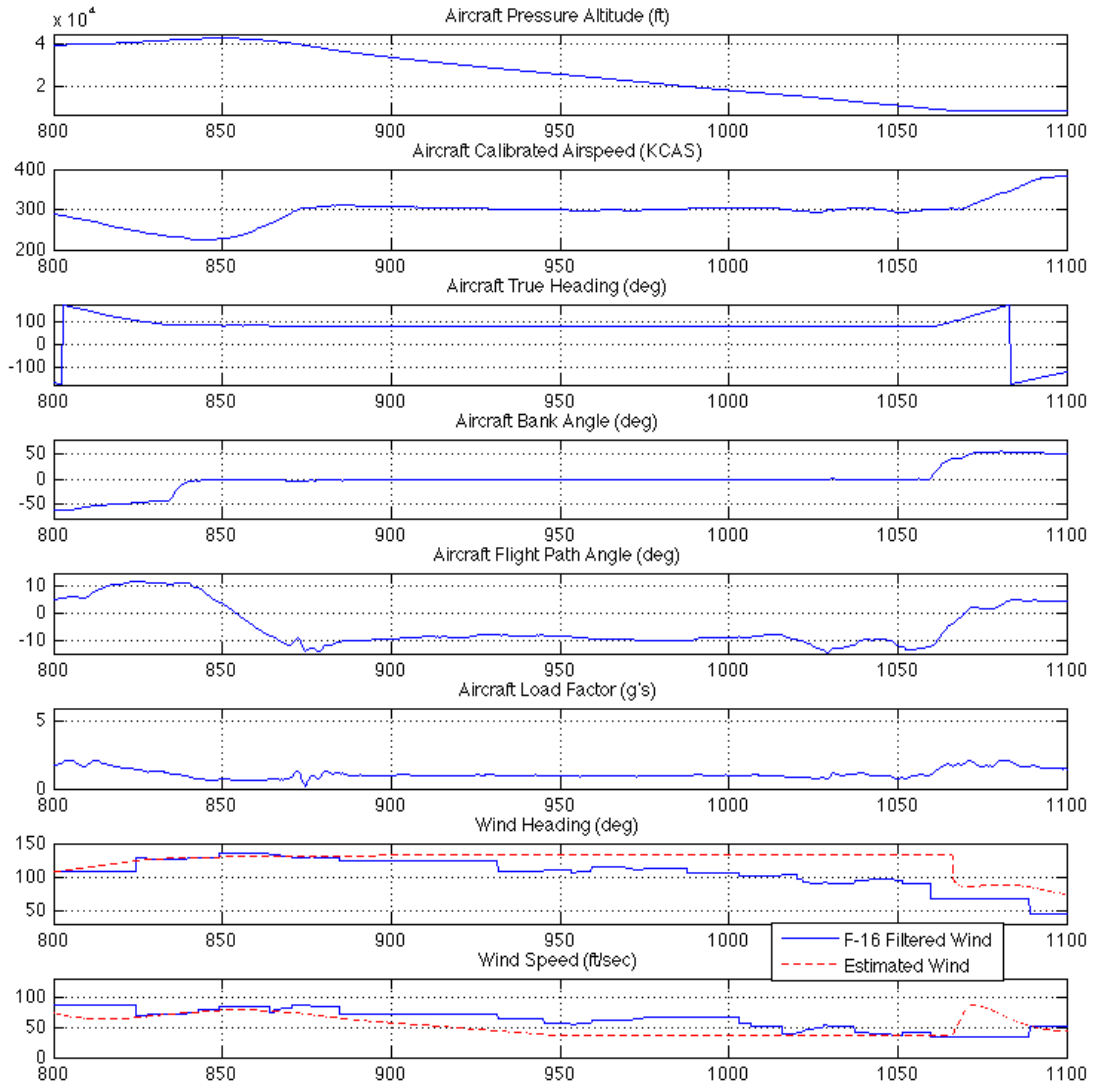
Figure 135. Penetration Descent (VEST 2)

Turn Performance Sortie
(Penetration Descent)
VEST
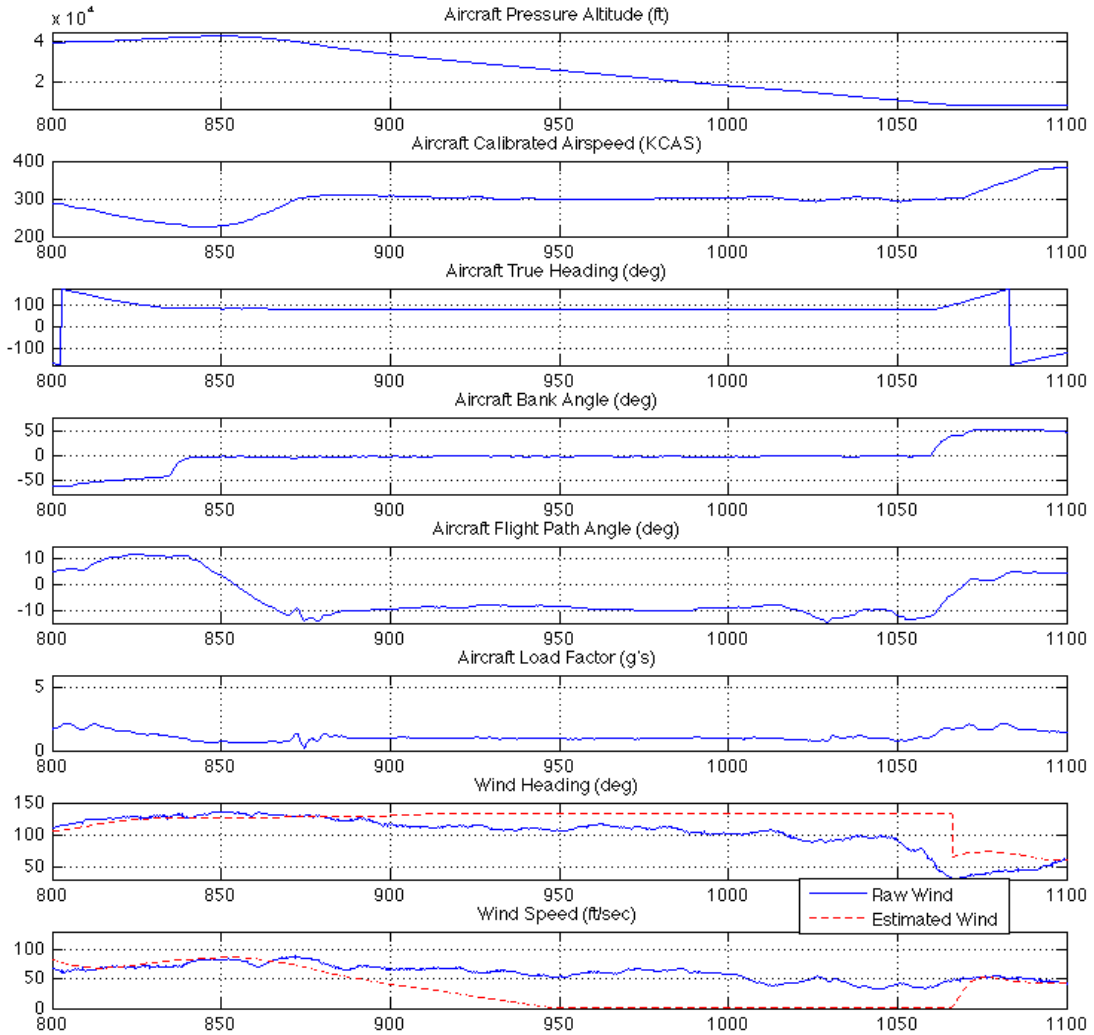
Figure 136. Penetration Descent (VEST)

Turn Performance Sortie
(Penetration Descent)
VEST TAS
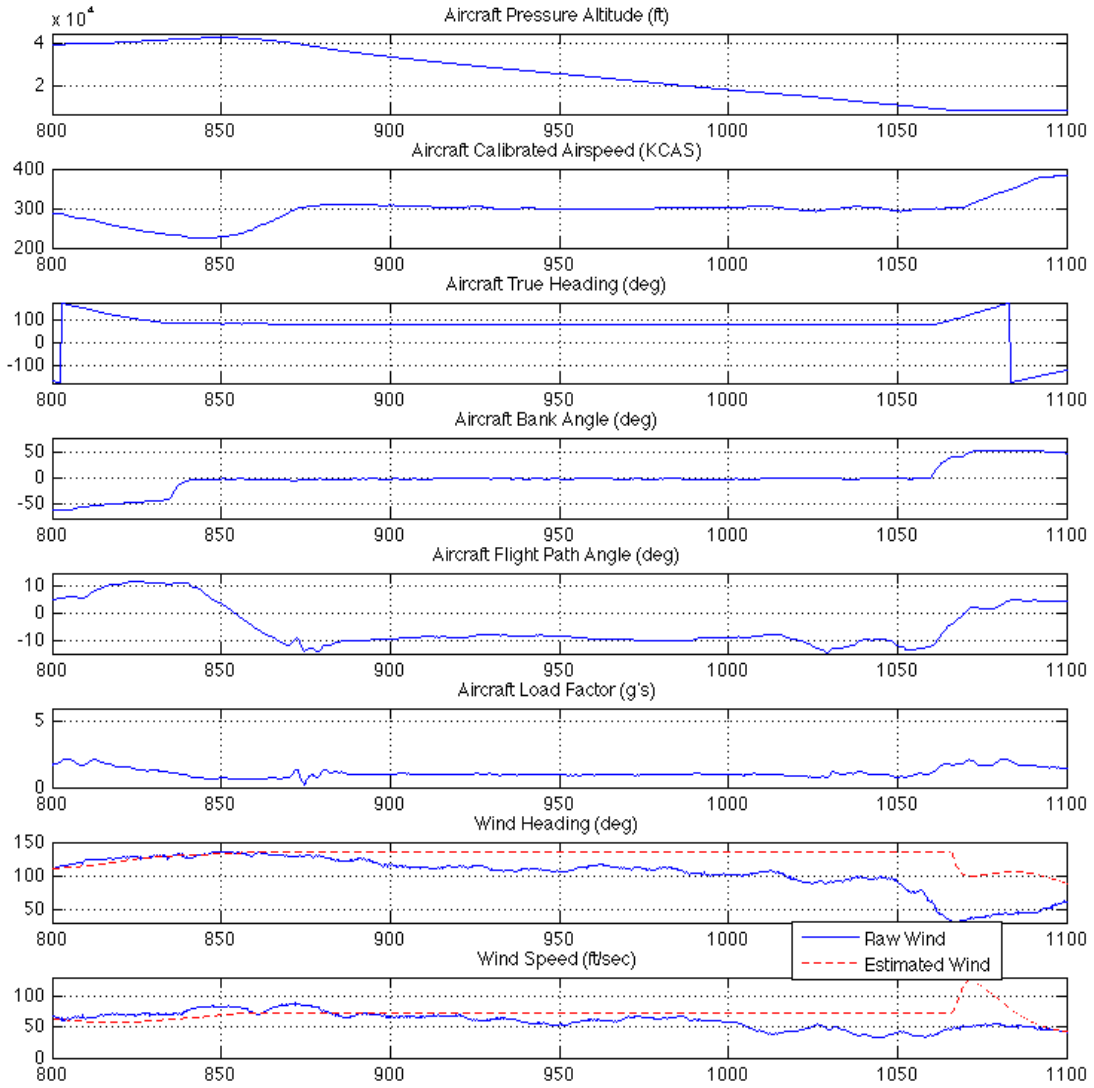
Figure 137. Penetration Descent (VEST TAS)

Turn Performance Sortie
(Penetration Descent)
VEST (No Residual Logic)
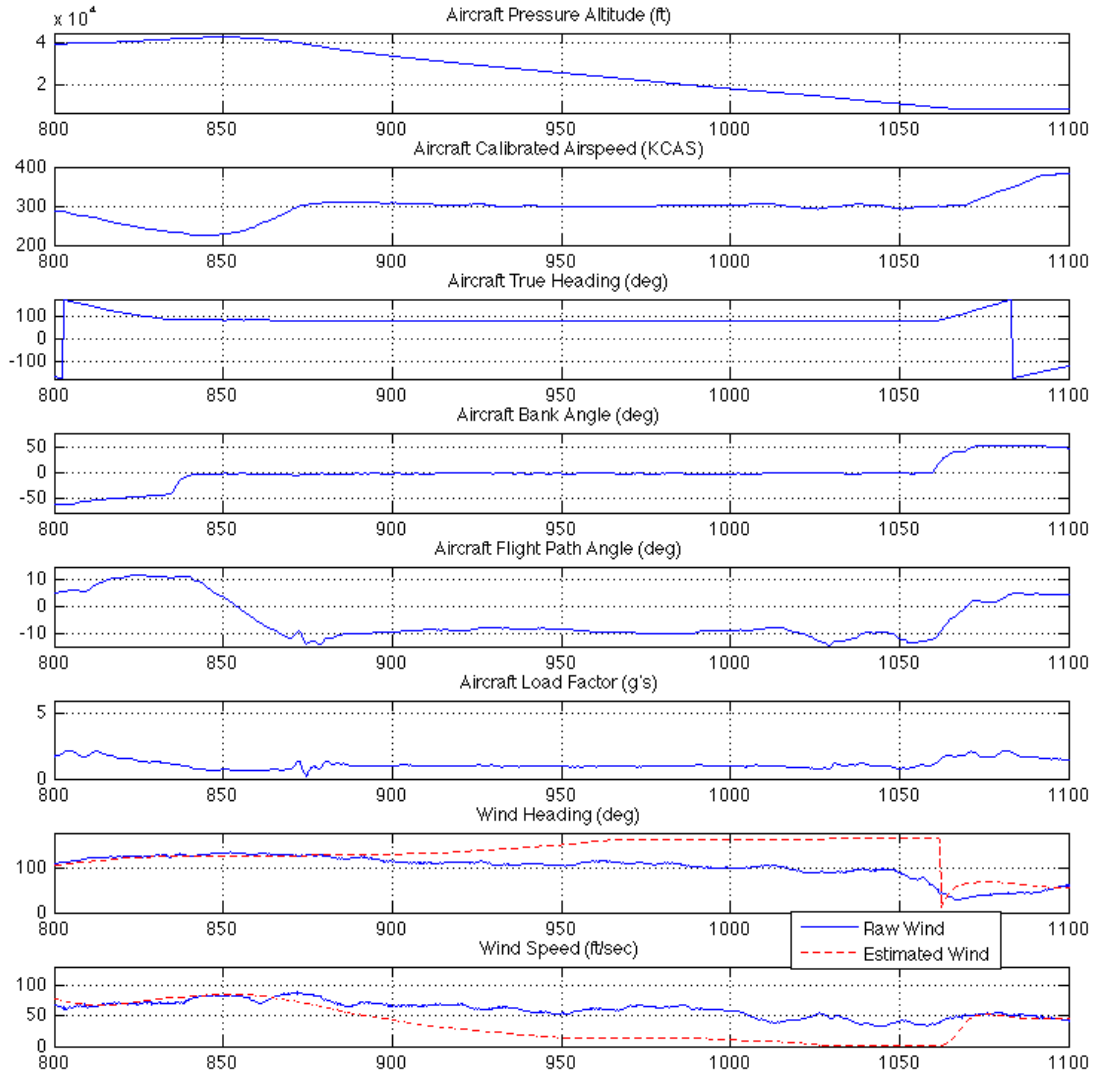
Figure 138. Penetration Descent (VEST - No Residual Logic)

Turn Performance Sortie
(Penetration Descent)
VEST TAS (No Residual Logic)
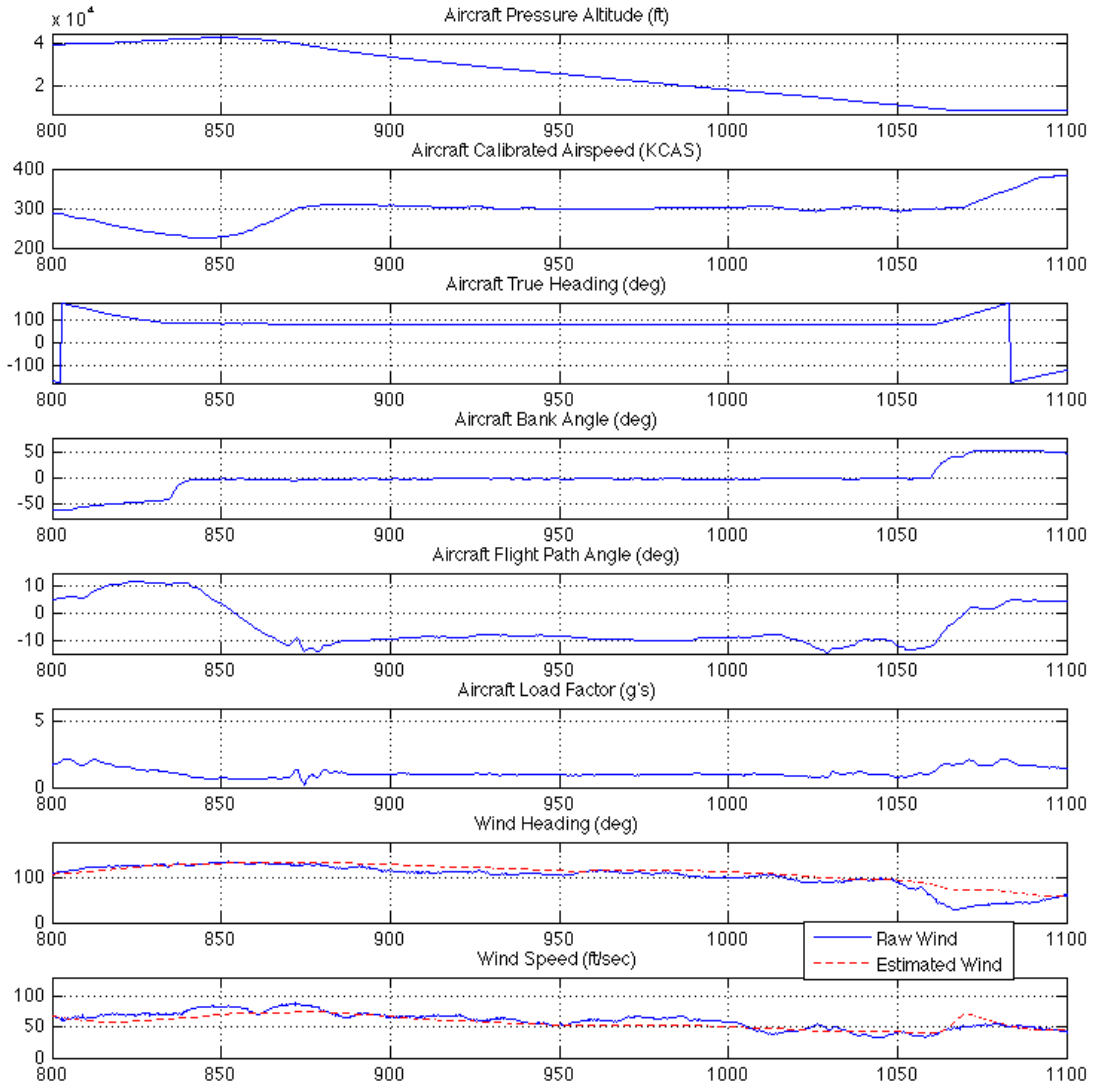
Figure 139. Penetration Descent (VEST TAS - No Residual Logic)

Turn Performance Sortie
(Recovery and Landing)
VEST 2
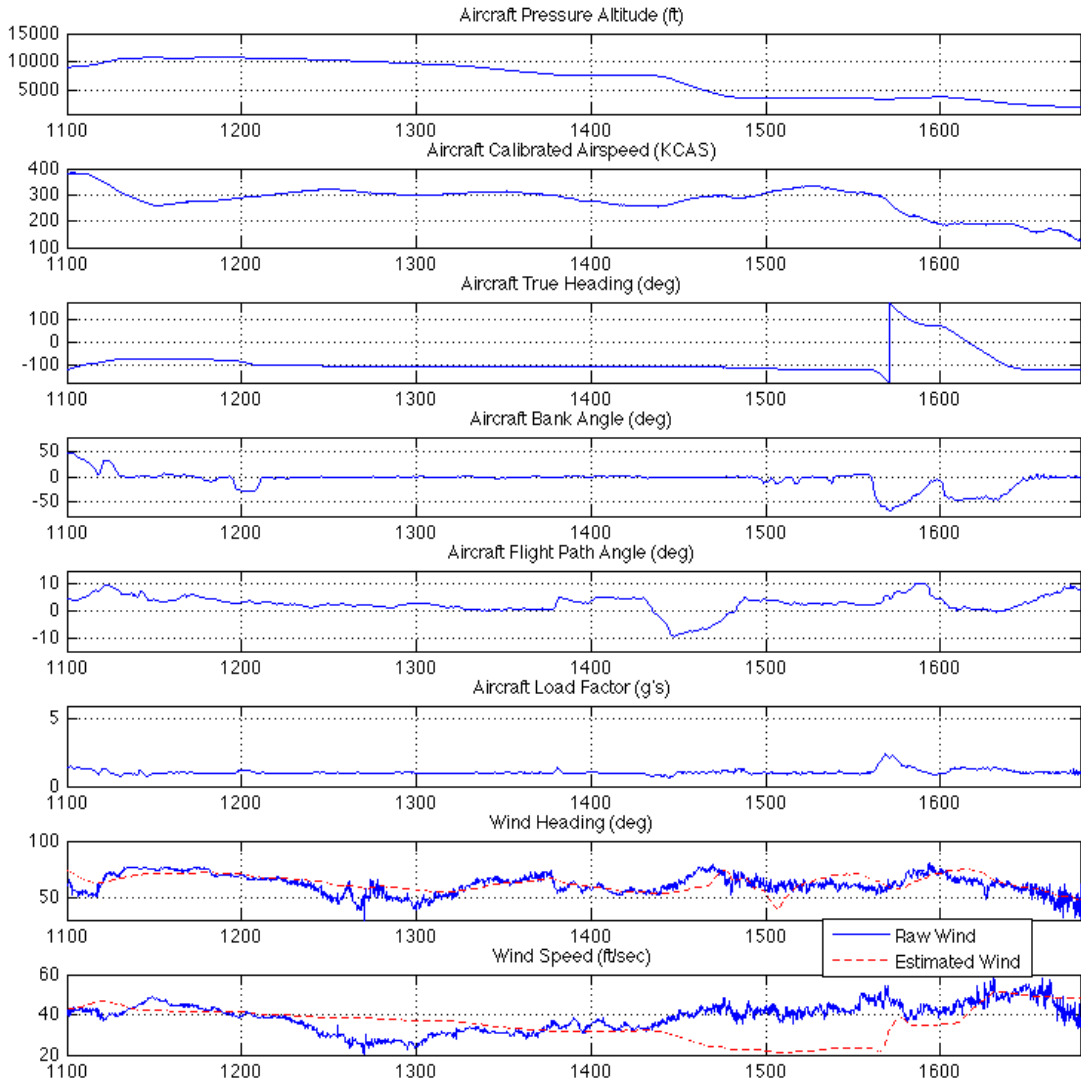
Figure 140. Recovery and Landing (VEST 2)

Turn Performance Sortie
(Recovery and Landing)
VEST 2
F-16 Filtered Winds
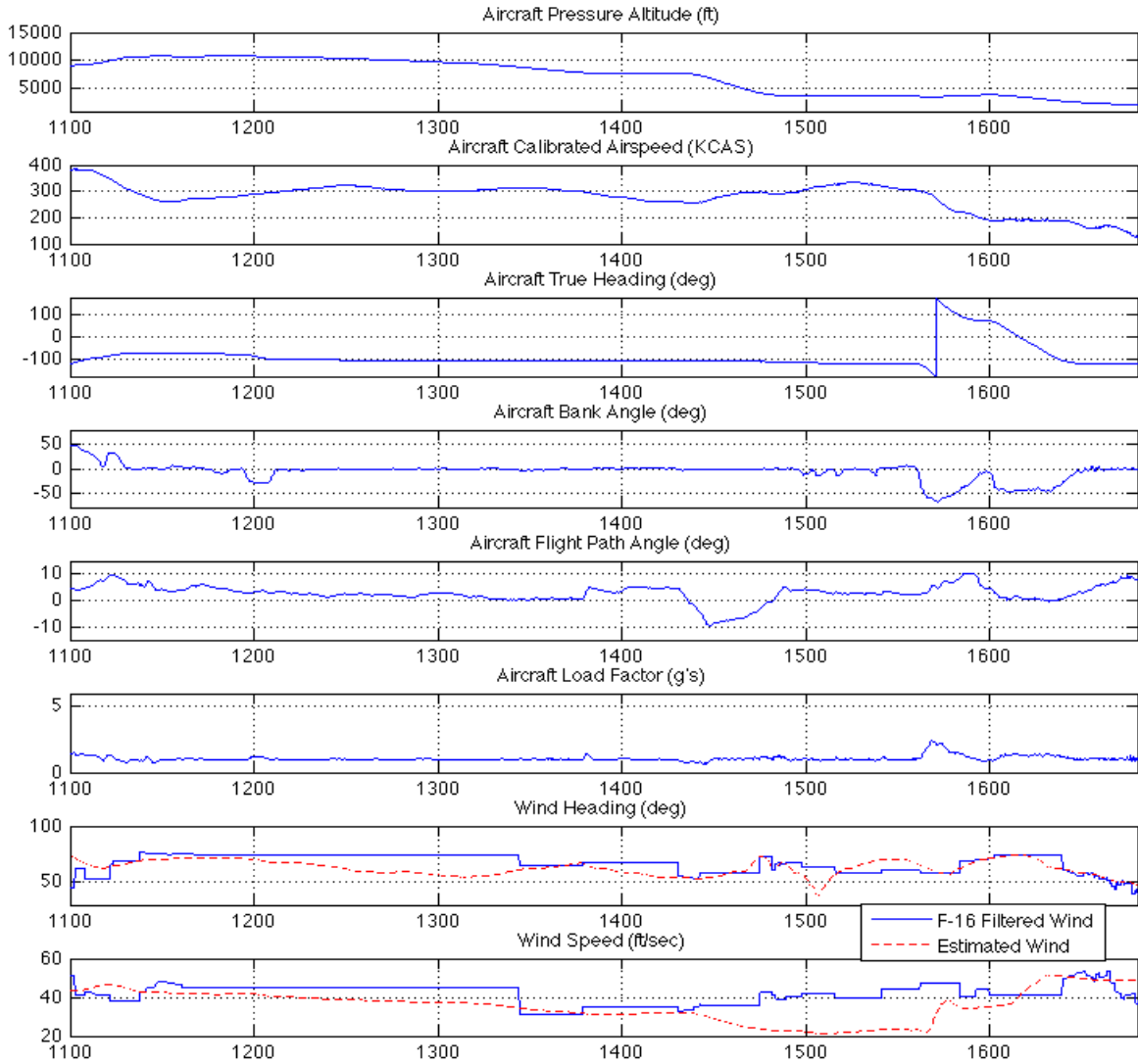
Figure 141. Recovery and Landing (VEST 2)

Turn Performance Sortie
(Recovery and Landing)
VEST
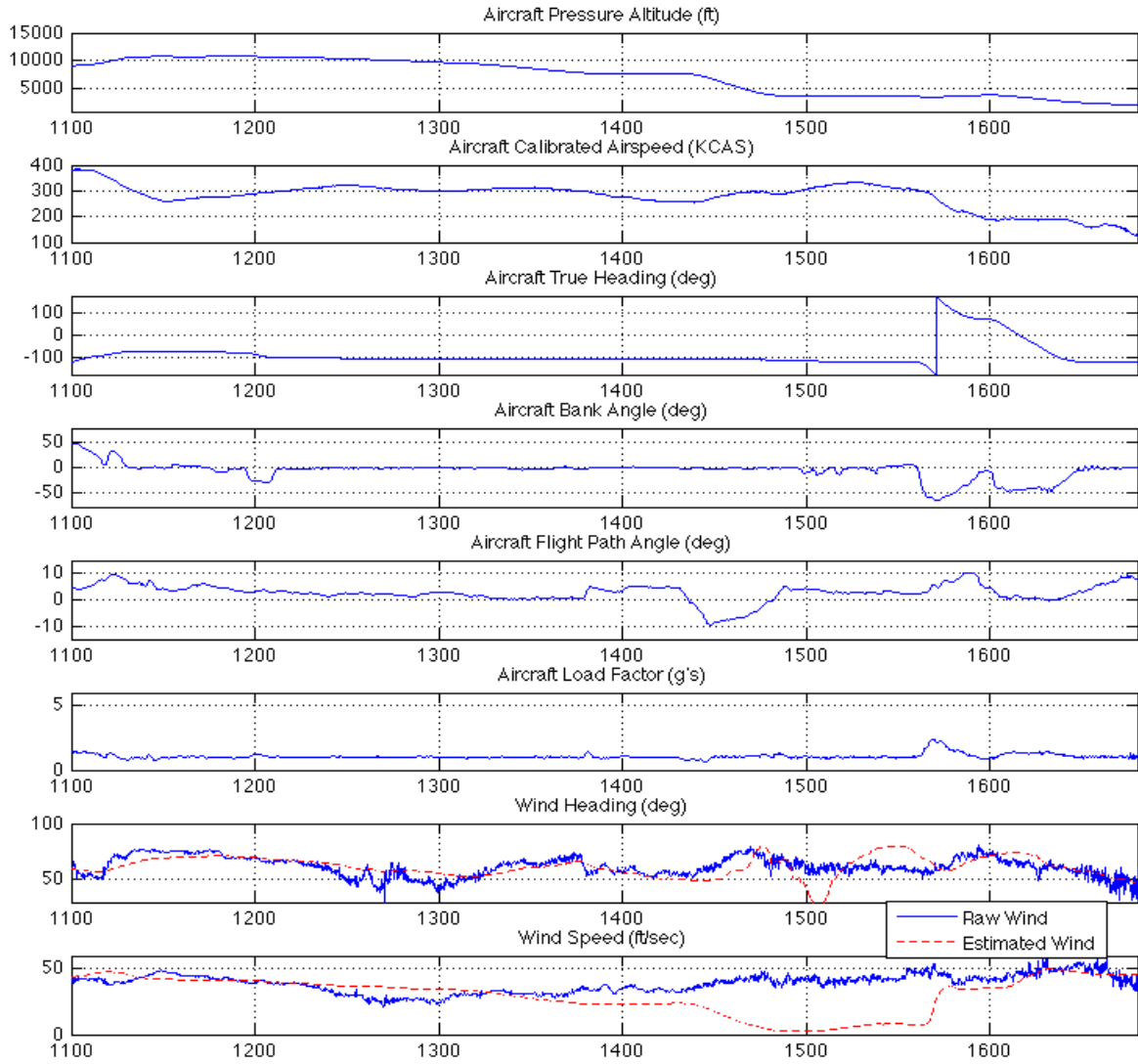
Figure 142. Recovery and Landing (VEST)

Turn Performance Sortie
(Recovery and Landing)
VEST TAS
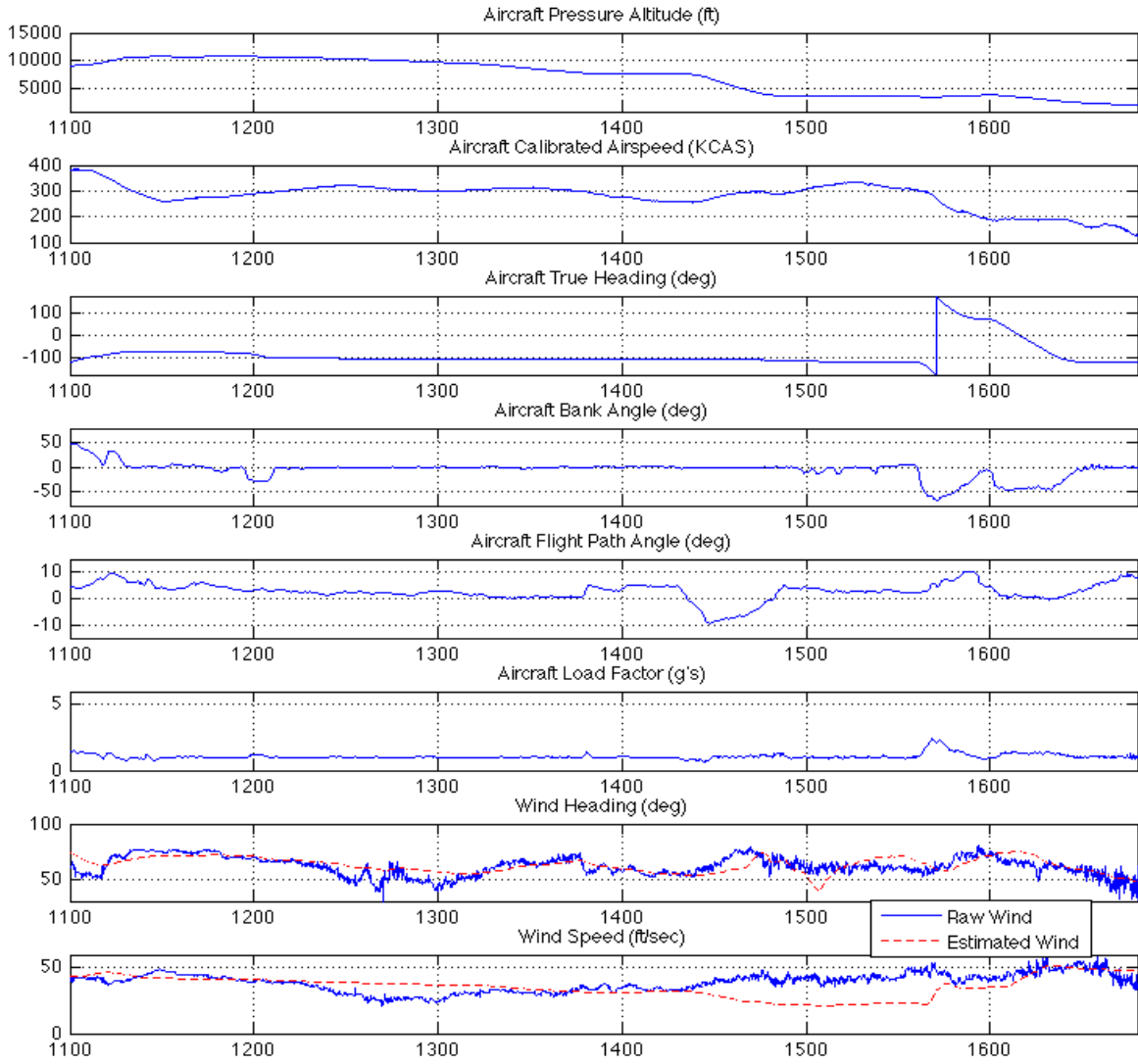
Figure 143. Recovery and Landing (VEST TAS)

Turn Performance Sortie
(Recovery and Landing)
VEST (No Residual Logic)
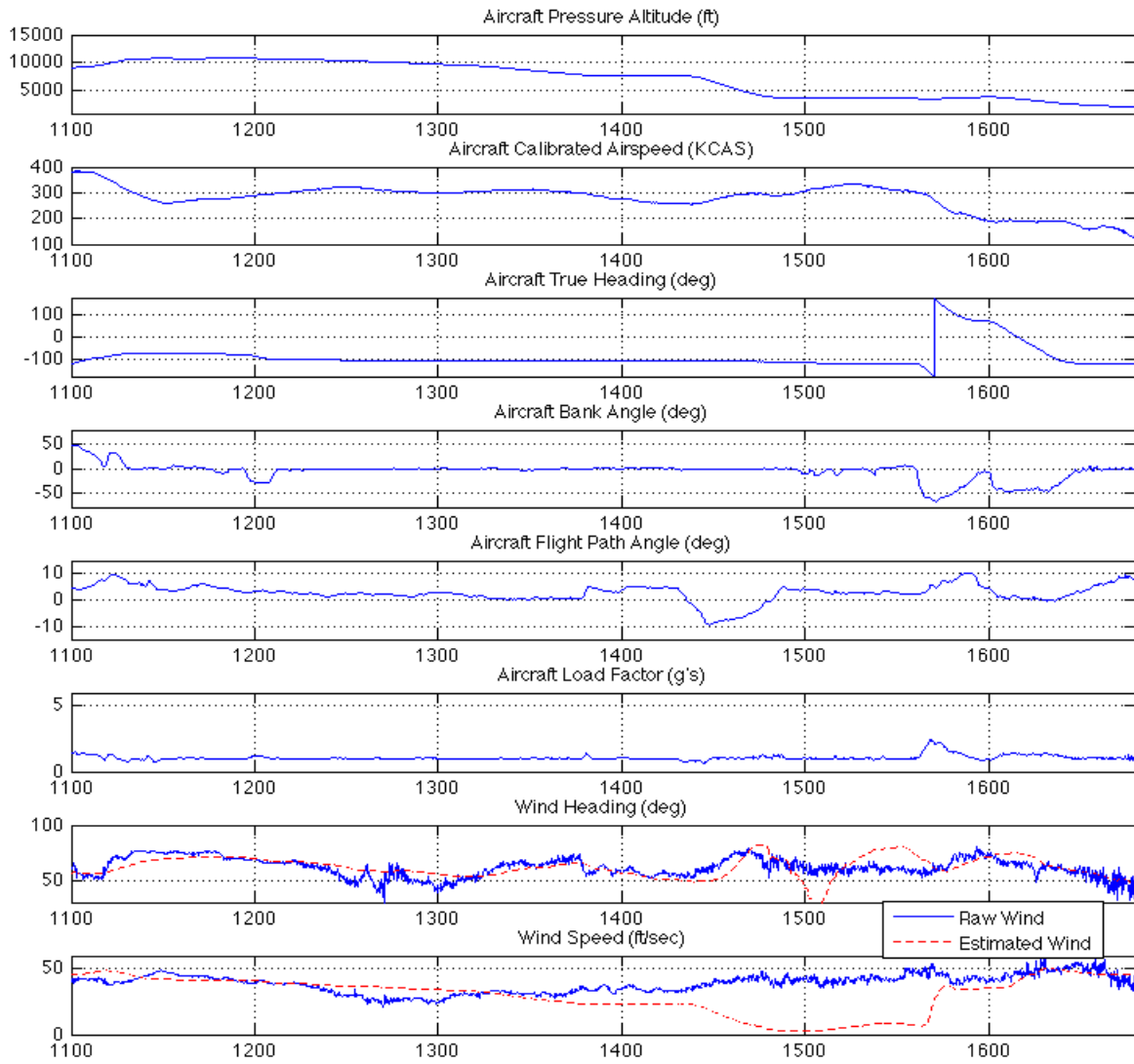
Figure 144. Recovery and Landing (VEST - No Residual Logic)

Turn Performance Sortie
(Recovery and Landing)
VEST TAS (No Residual Logic)
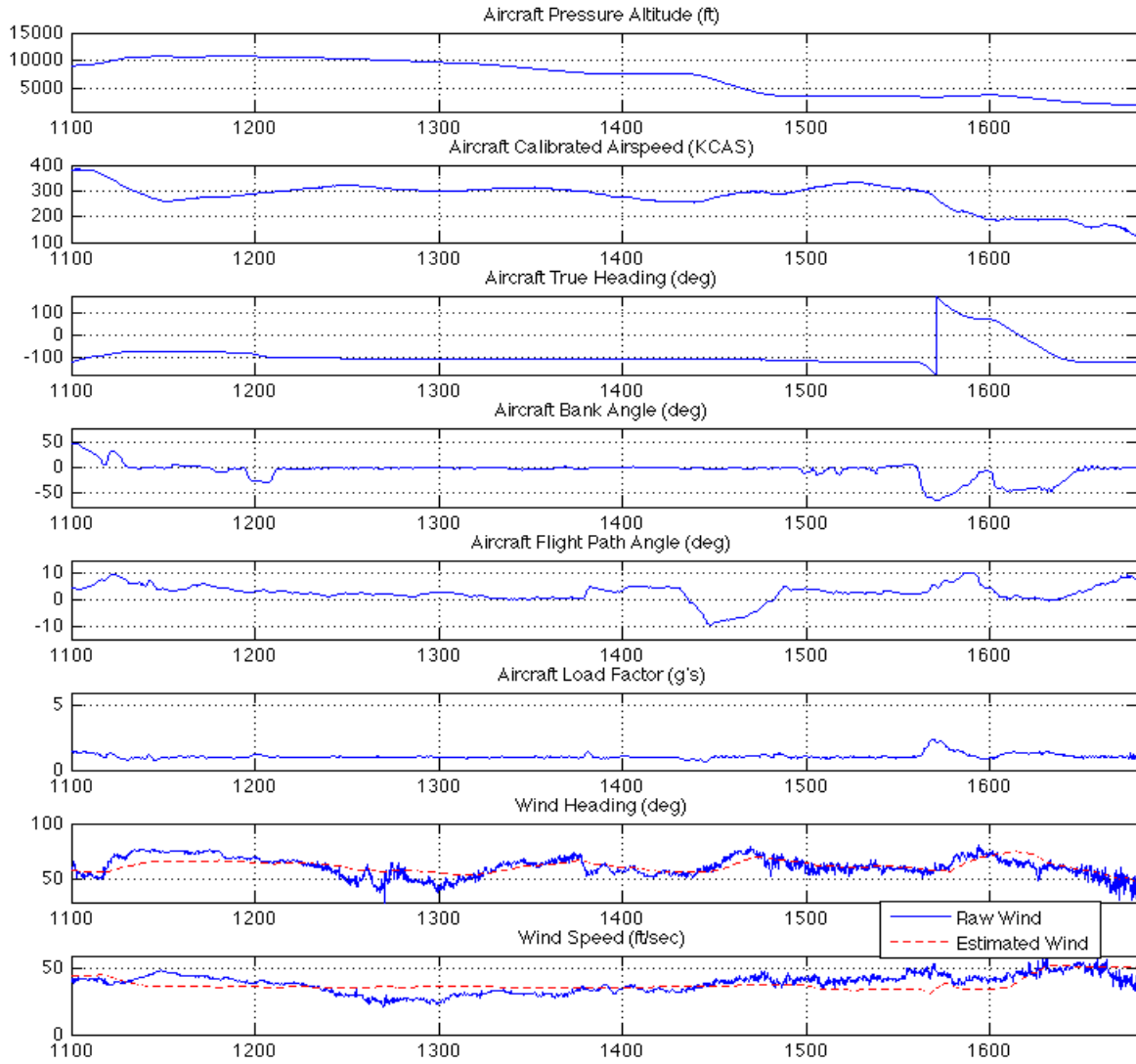
Figure 145. Recovery and Landing (VEST TAS - No Residual Logic)

214

Level Acceleration Sortie
(Military Power, 15K and 25K)
VEST 2
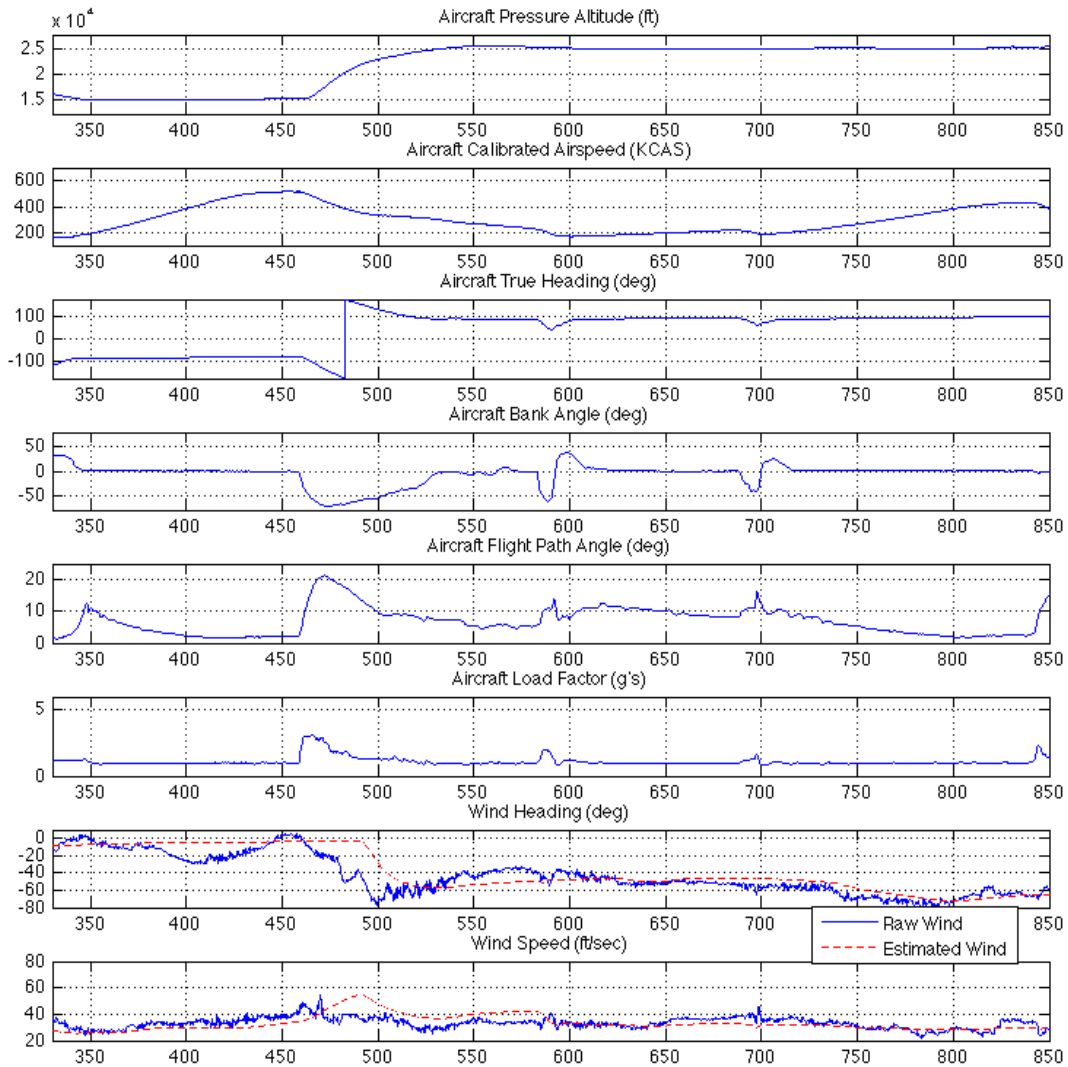
Figure 146. 15K and 20K Level Acceleration (VEST 2)

Level Acceleration Sortie
(Military Power, 15K and 25K)
VEST 2
F-16 Filtered Winds
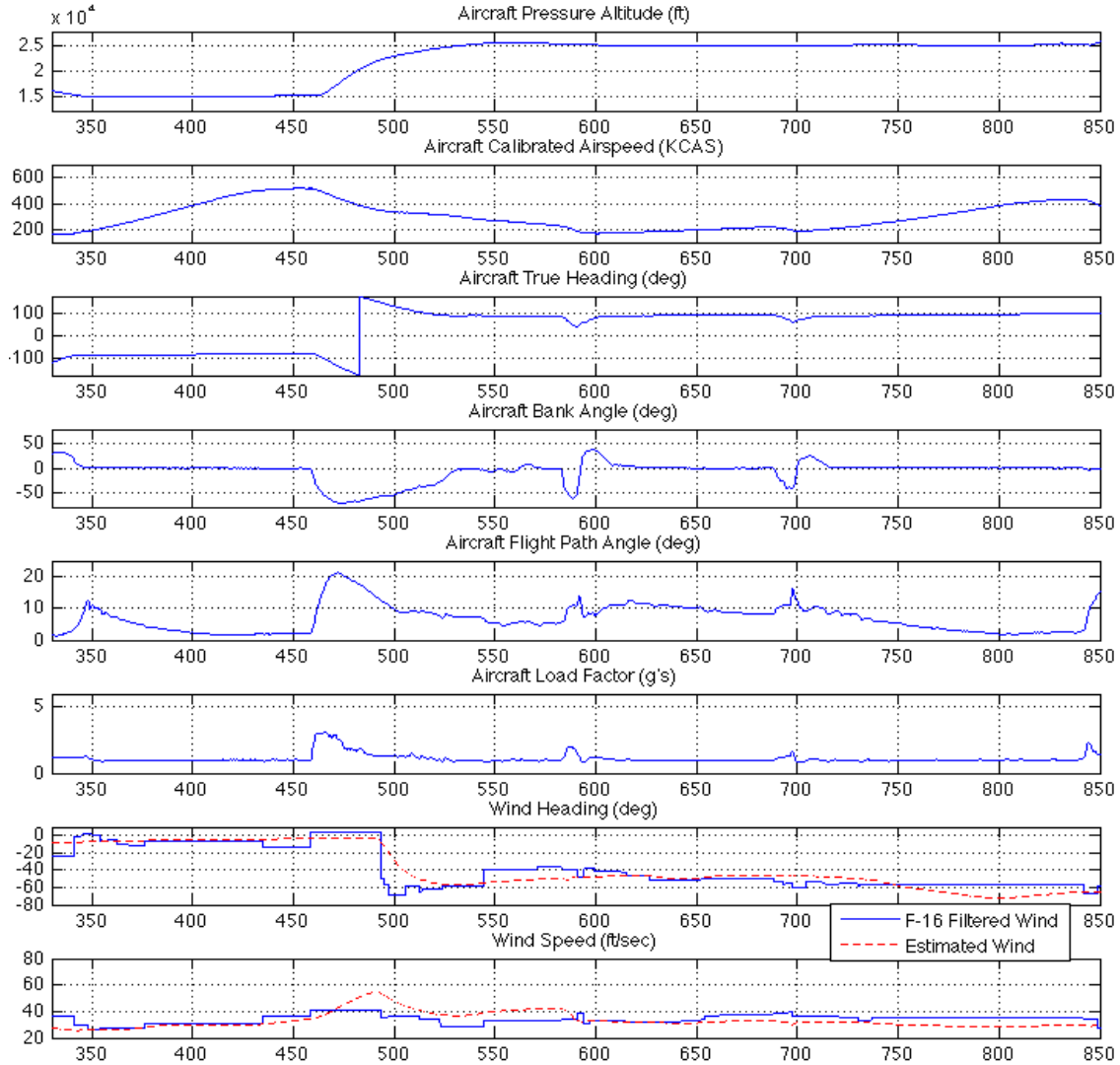
Figure 147. 15K and 20K Level Acceleration (VEST 2)

Level Acceleration Sortie
(Military Power, 15K and 25K)
VEST
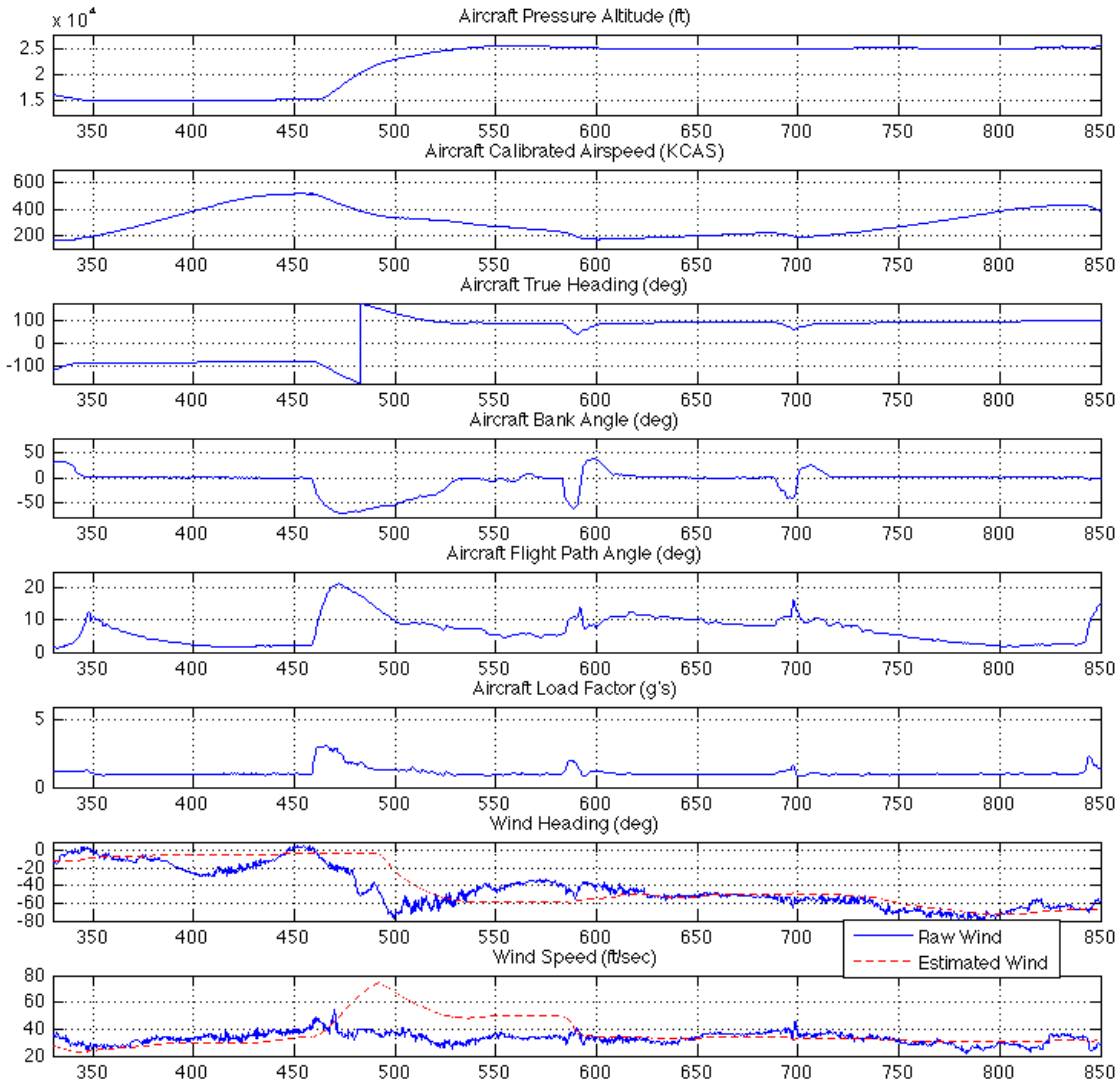
Figure 148. 15K and 20K Level Acceleration (VEST)

Level Acceleration Sortie
(Military Power, 15K and 25K)
VEST TAS
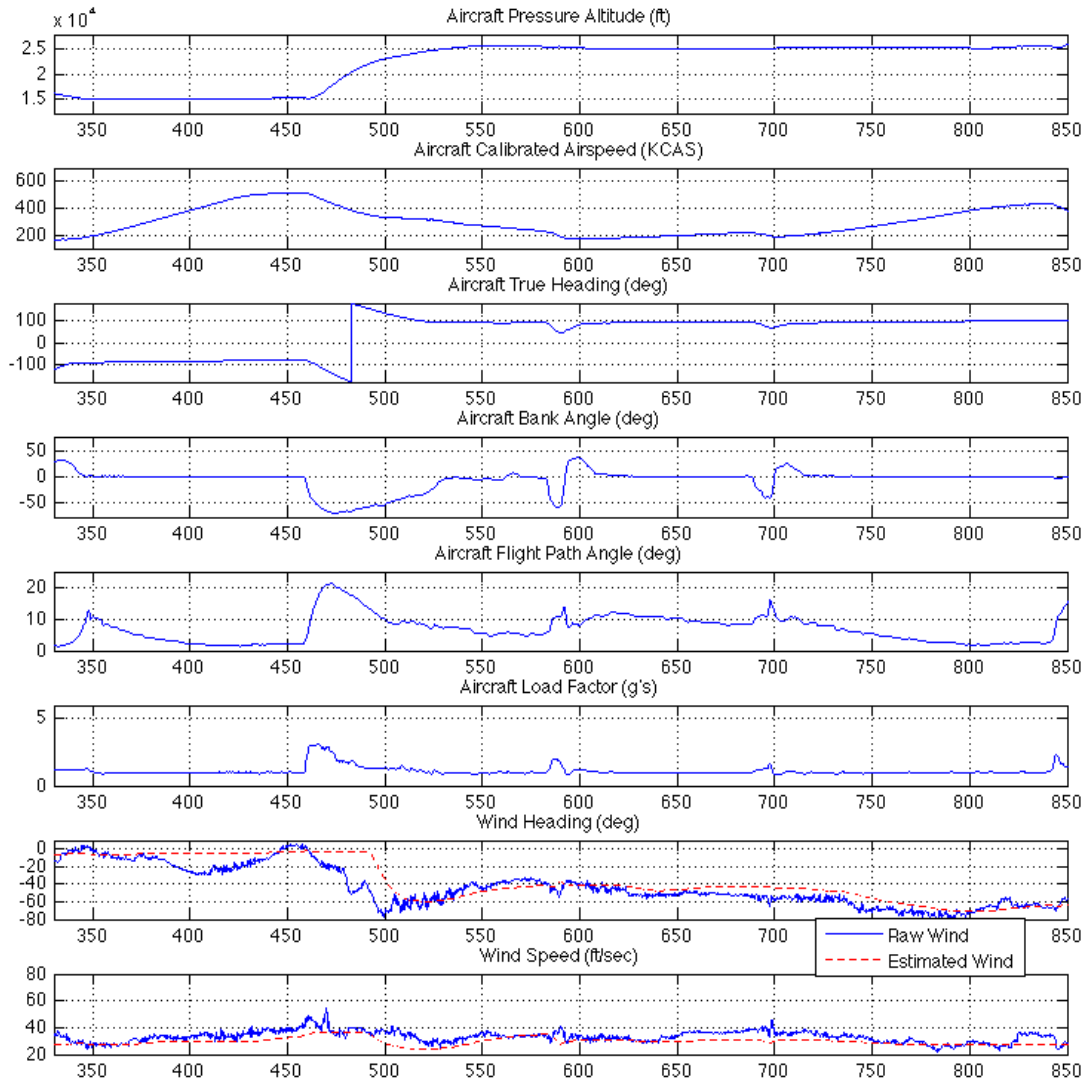
Figure 149. 15K and 20K Level Acceleration (VEST TAS)

Level Acceleration Sortie
(Military Power, 35K)
VEST 2
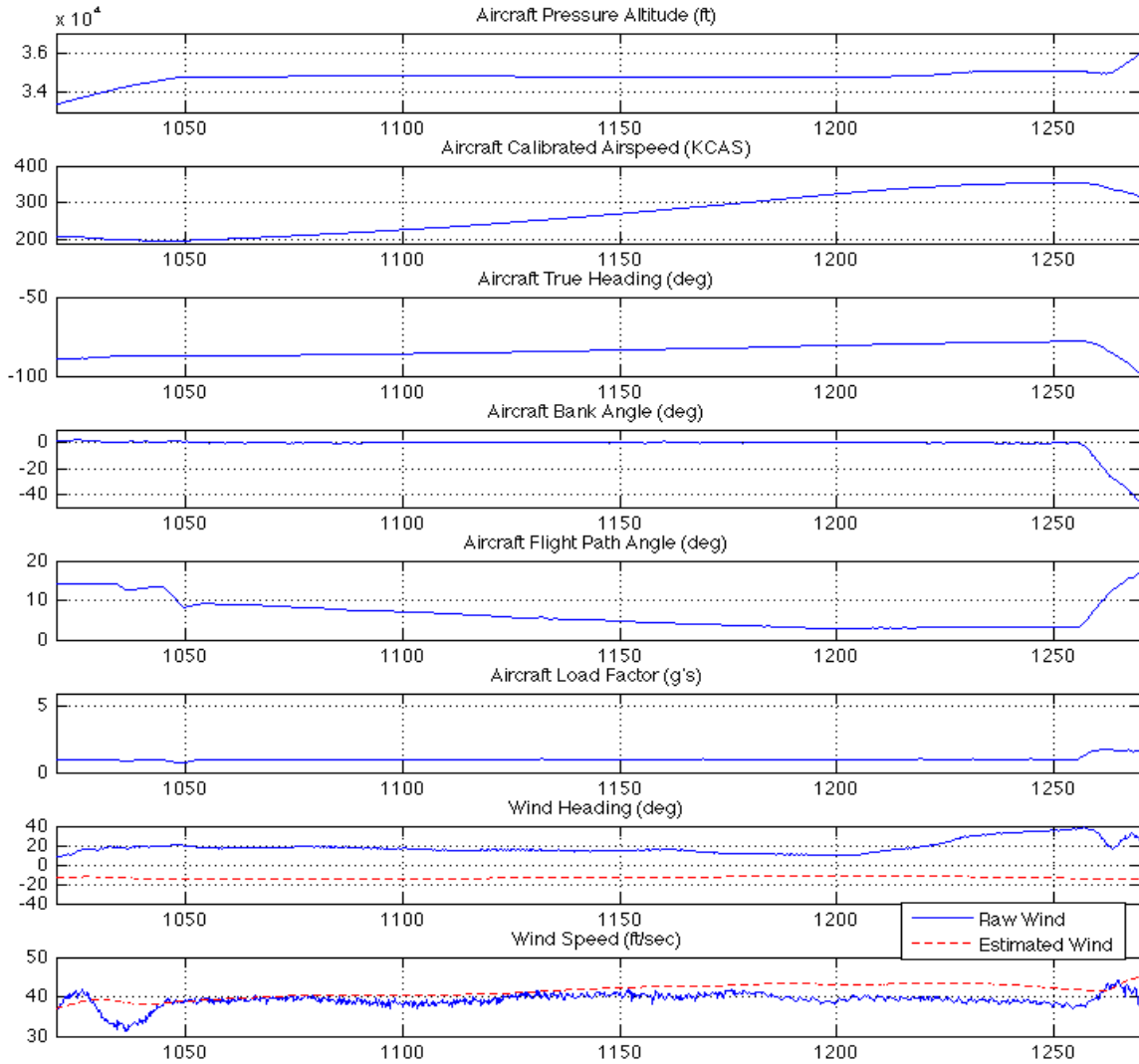
Figure 150. 35K Level Acceleration (VEST 2)

Level Acceleration Sortie
(Military Power, 35K)
VEST 2
F-16 Filtered Winds
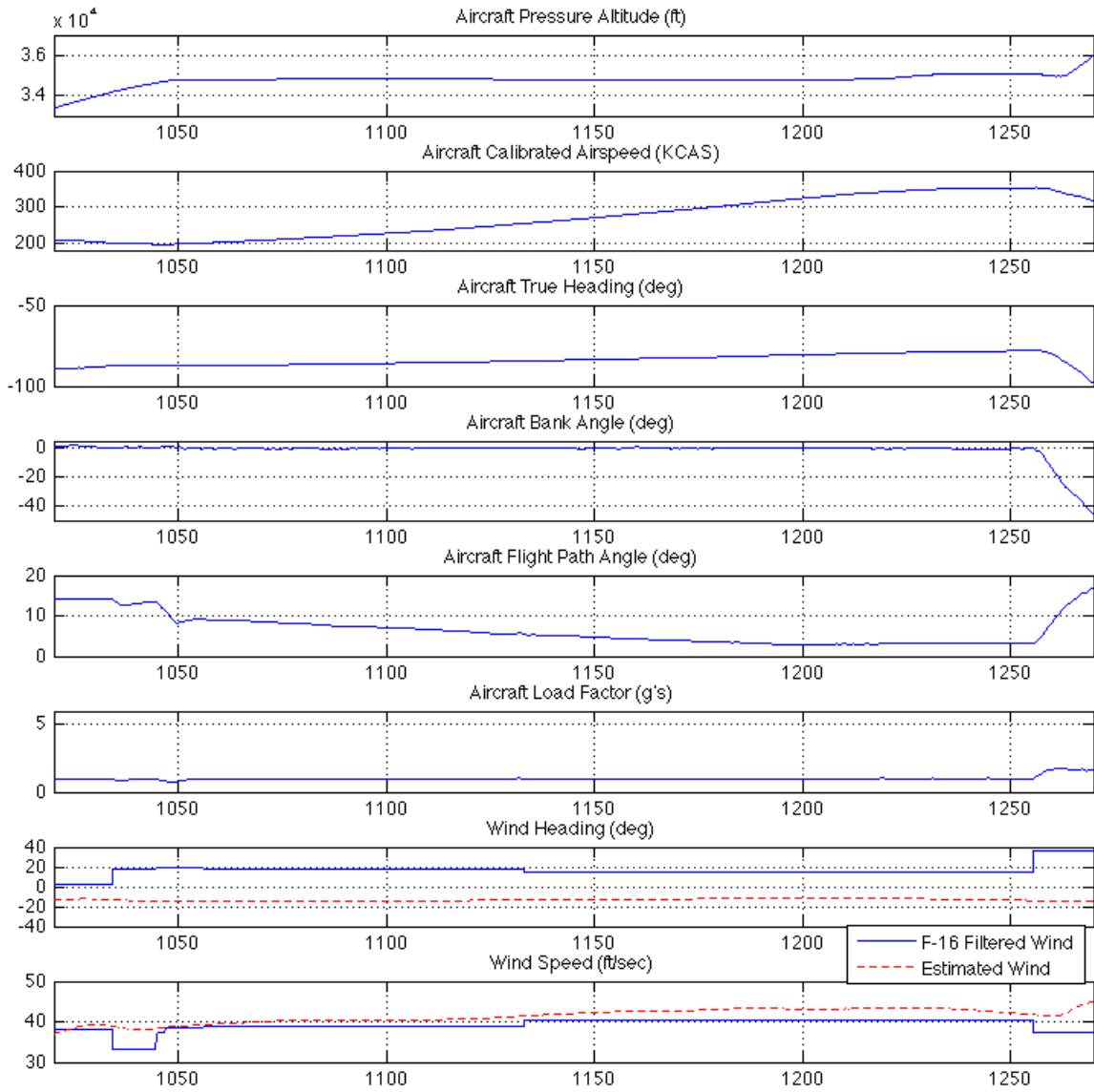
Figure 151. 35K Level Acceleration (VEST 2)

Level Acceleration Sortie
(Military Power, 35K)
VEST
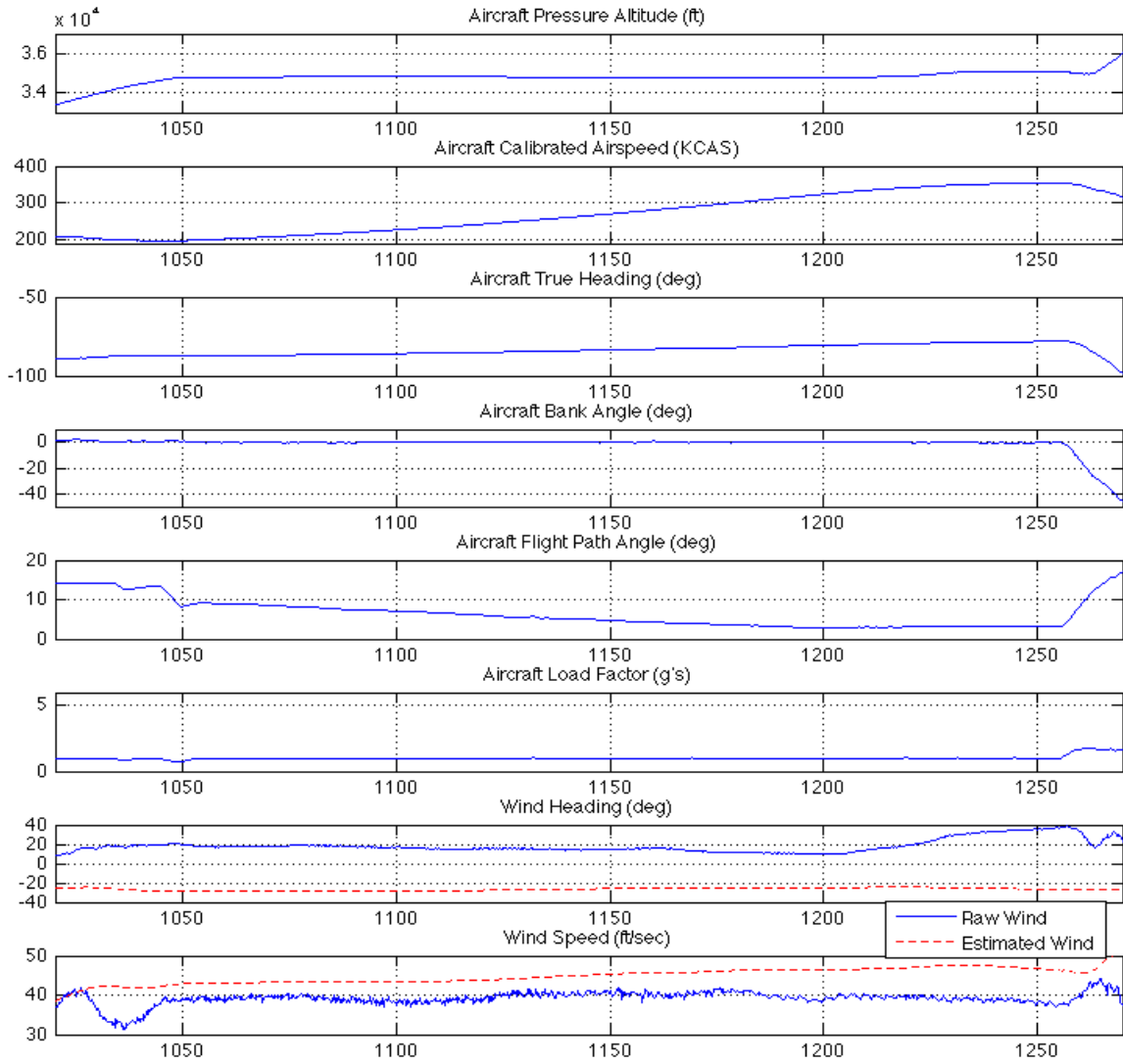
Figure 152. 35K Level Acceleration (VEST)

Level Acceleration Sortie
(Military Power, 35K)
VEST TAS
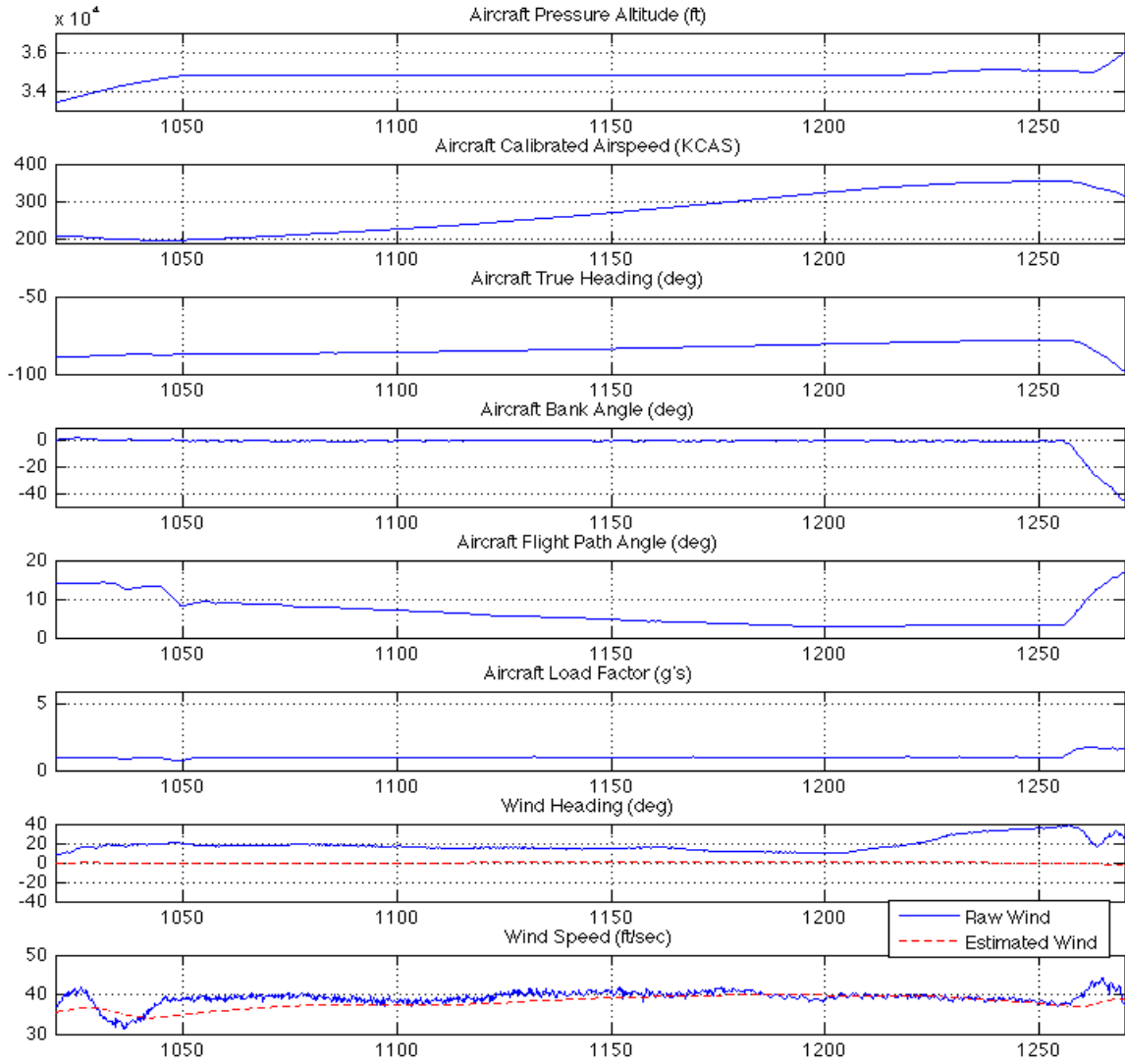
Figure 153. 35K Level Acceleration (VEST TAS)

Level Acceleration Sortie
(Maximum Range Descent)
VEST 2
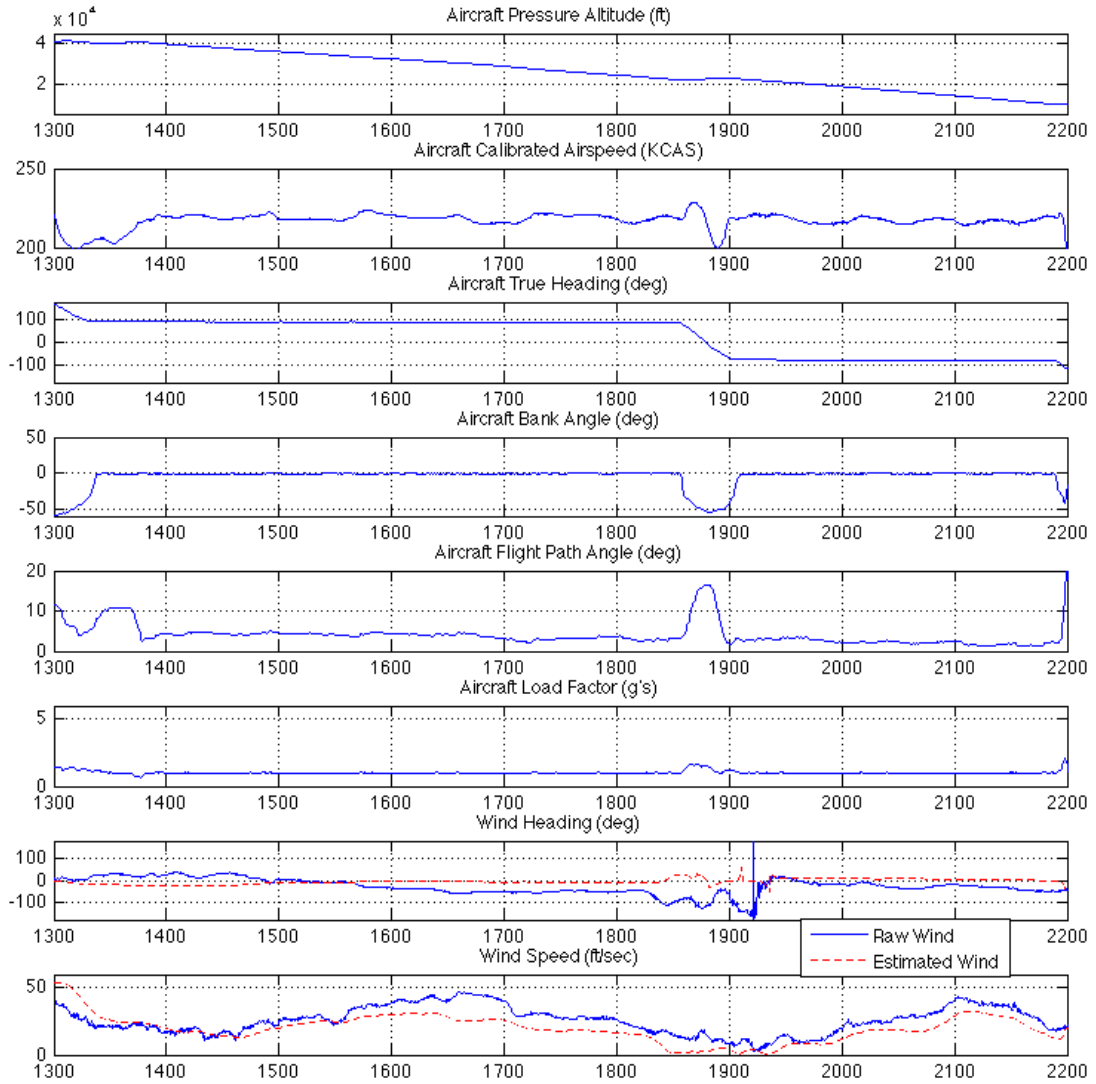
Figure 154. Maximum Range Descent (VEST 2)

Level Acceleration Sortie
(Maximum Range Descent)
VEST 2
F-16 Filtered Winds
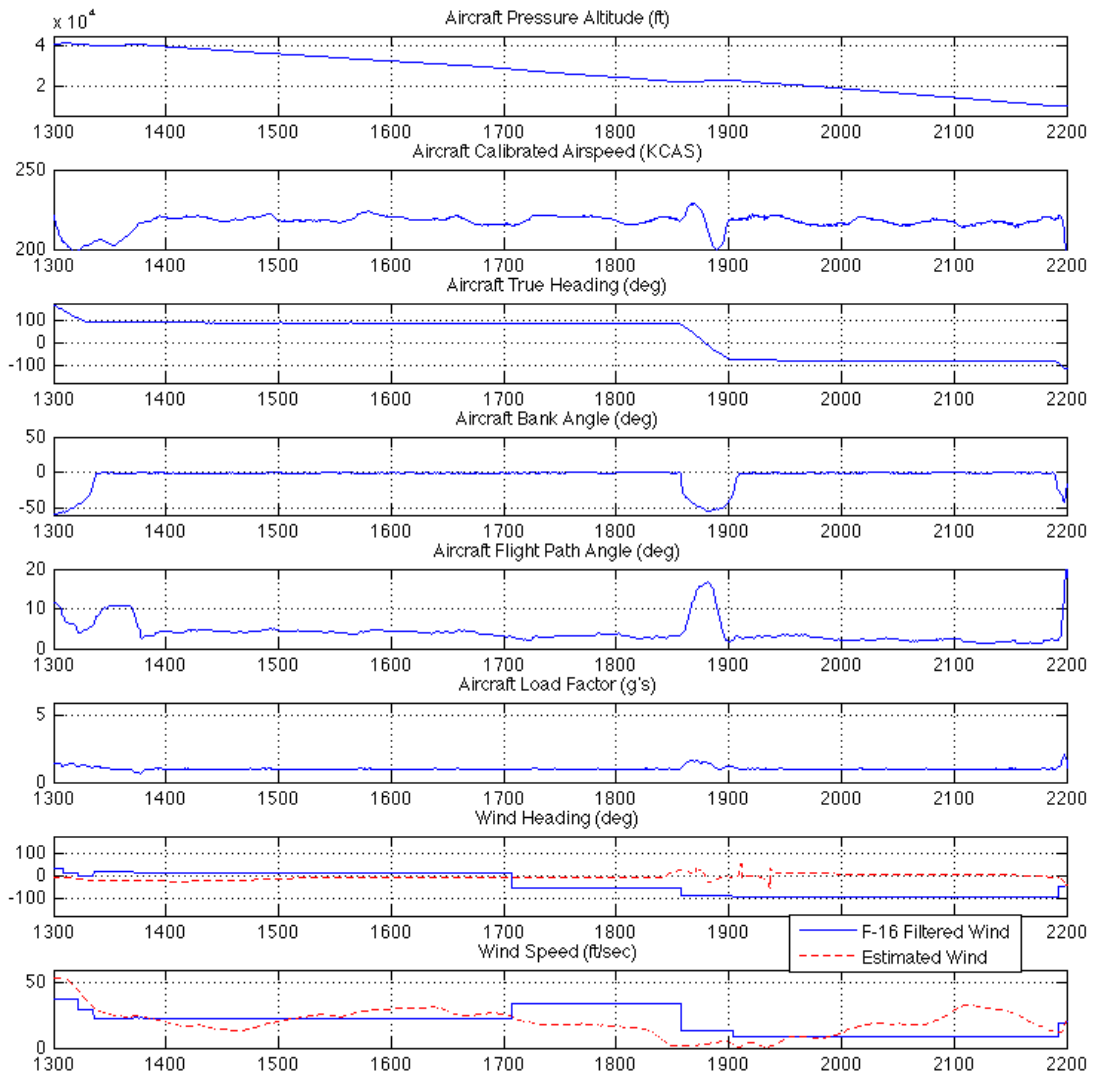
Figure 155. Maximum Range Descent (VEST 2)

Level Acceleration Sortie
(Maximum Range Descent)
VEST
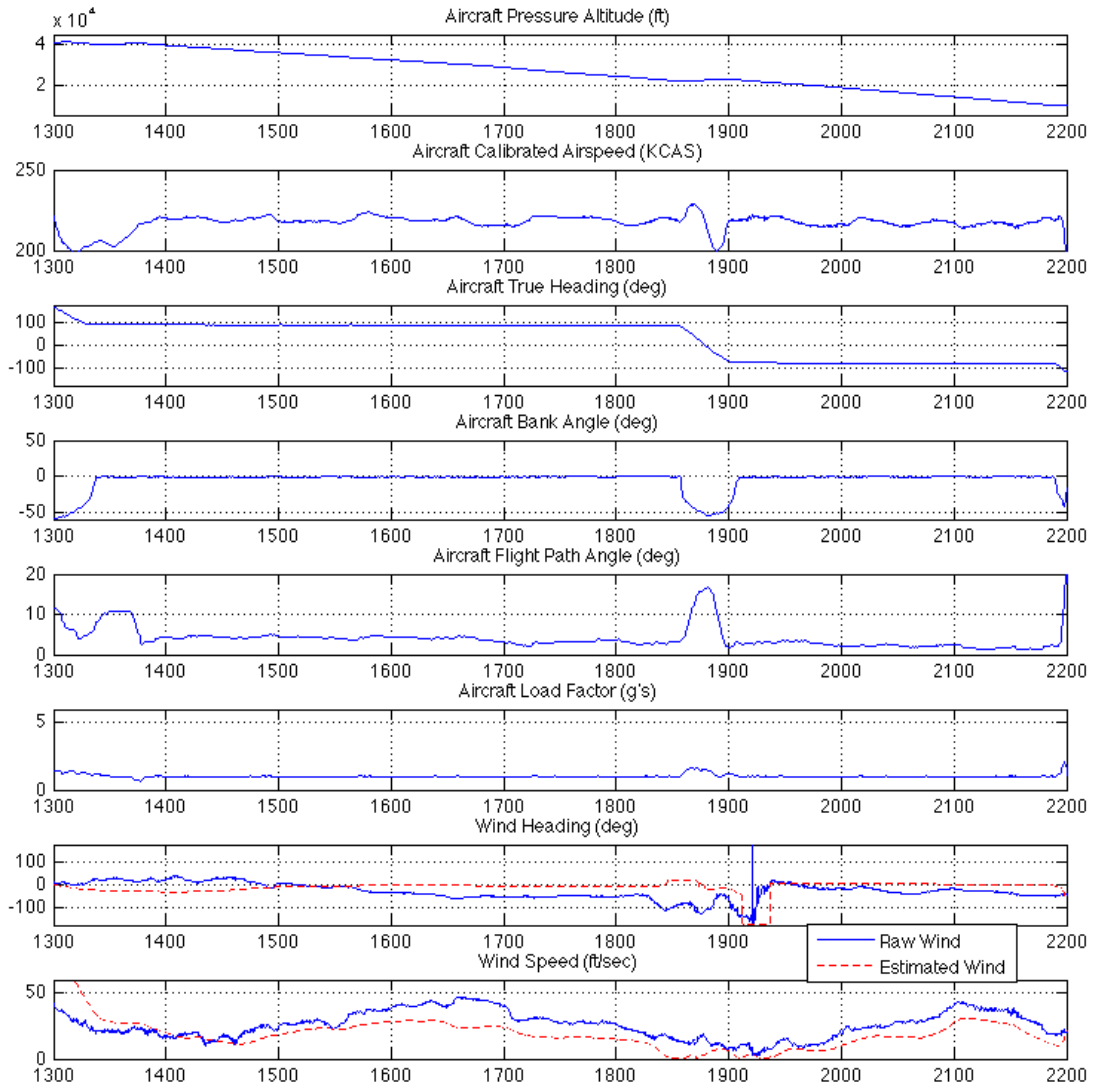
Figure 156. Maximum Range Descent (VEST)

Level Acceleration Sortie
(Maximum Range Descent)
VEST TAS
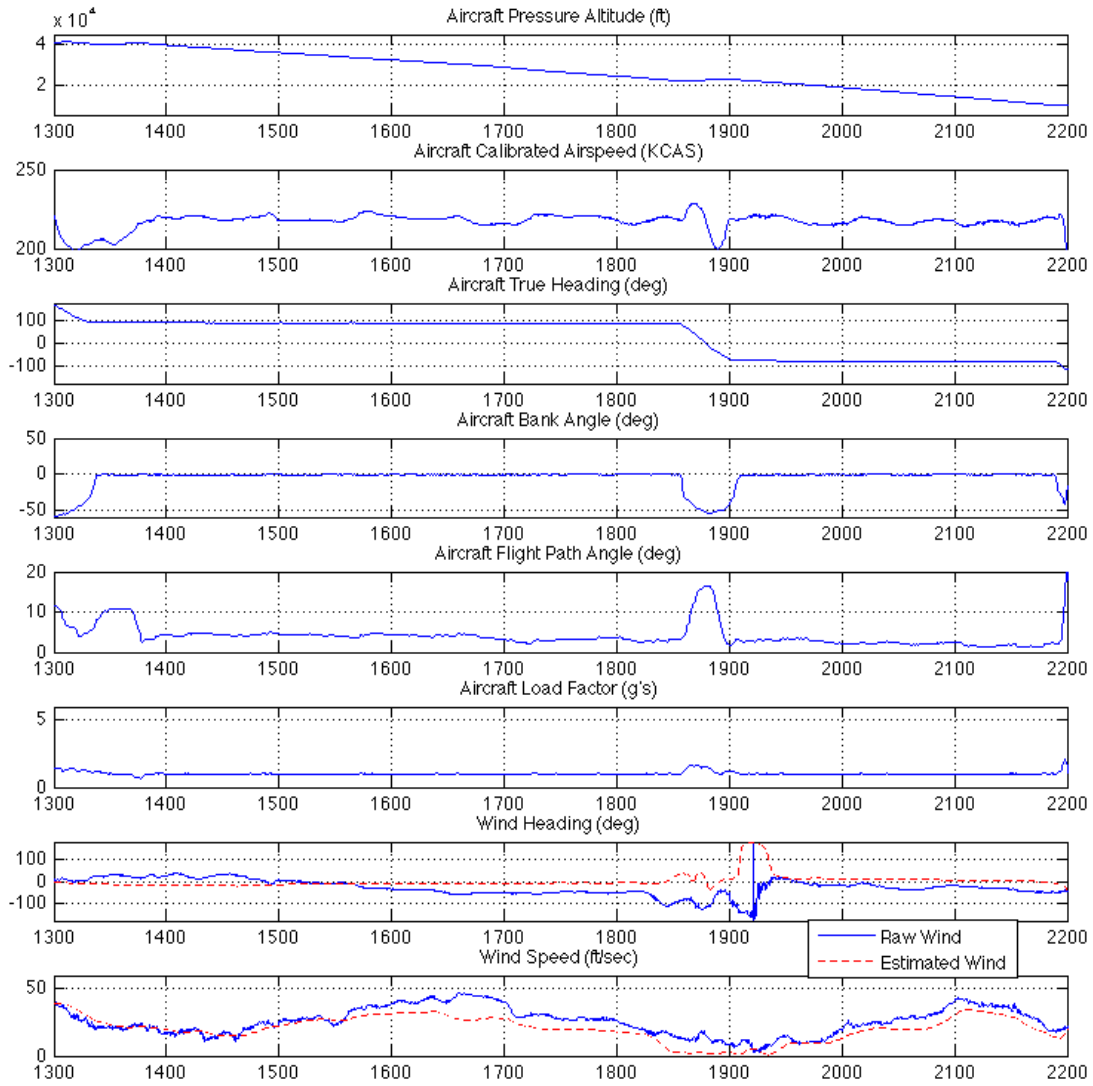
Figure 157. Maximum Range Descent (VEST TAS)

Level Acceleration Sortie
(Maximum Power, 10K, 20K, 30K, and 40K)
VEST 2
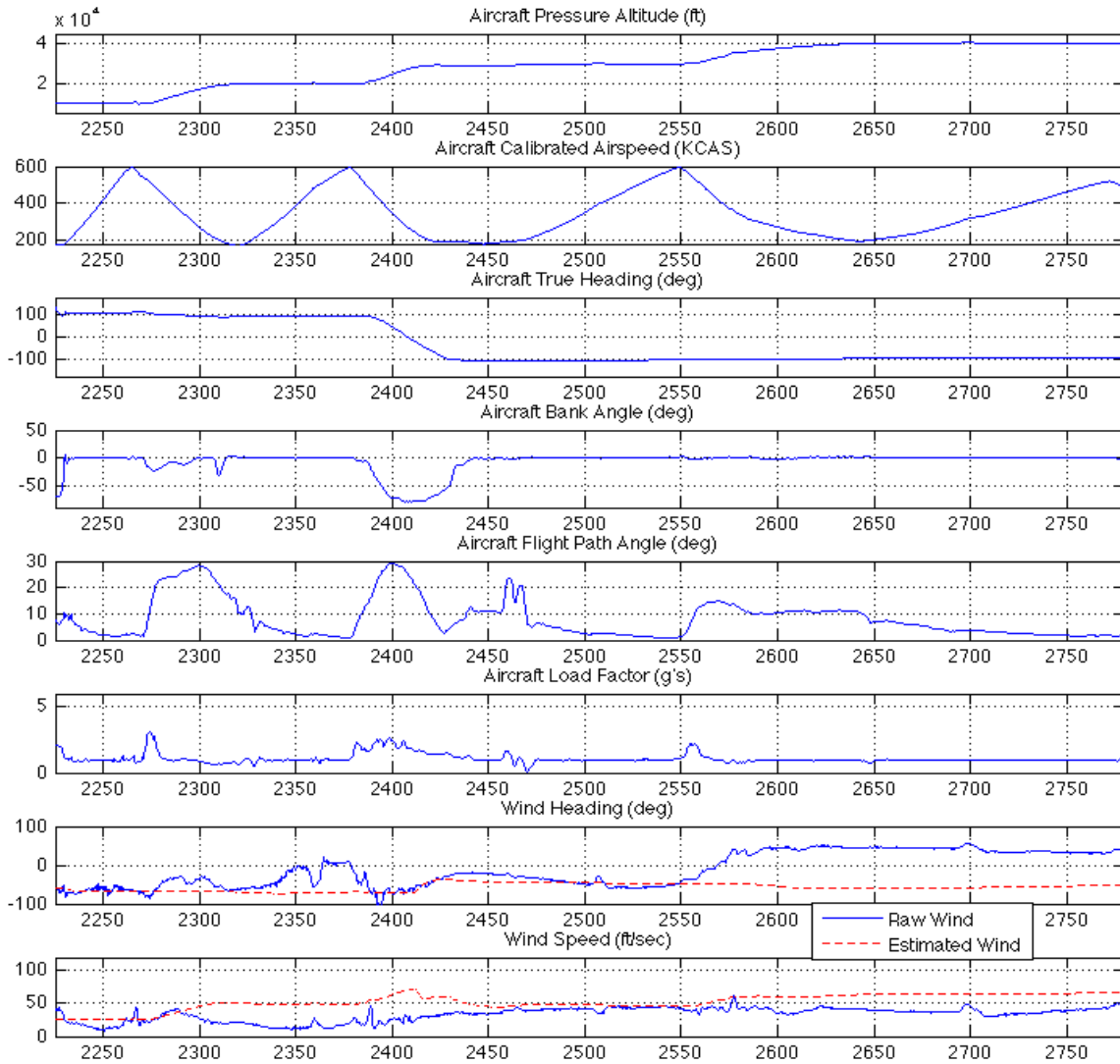
Figure 158. 10K, 20K, 30K and 40K Level Acceleration (VEST 2)

Level Acceleration Sortie
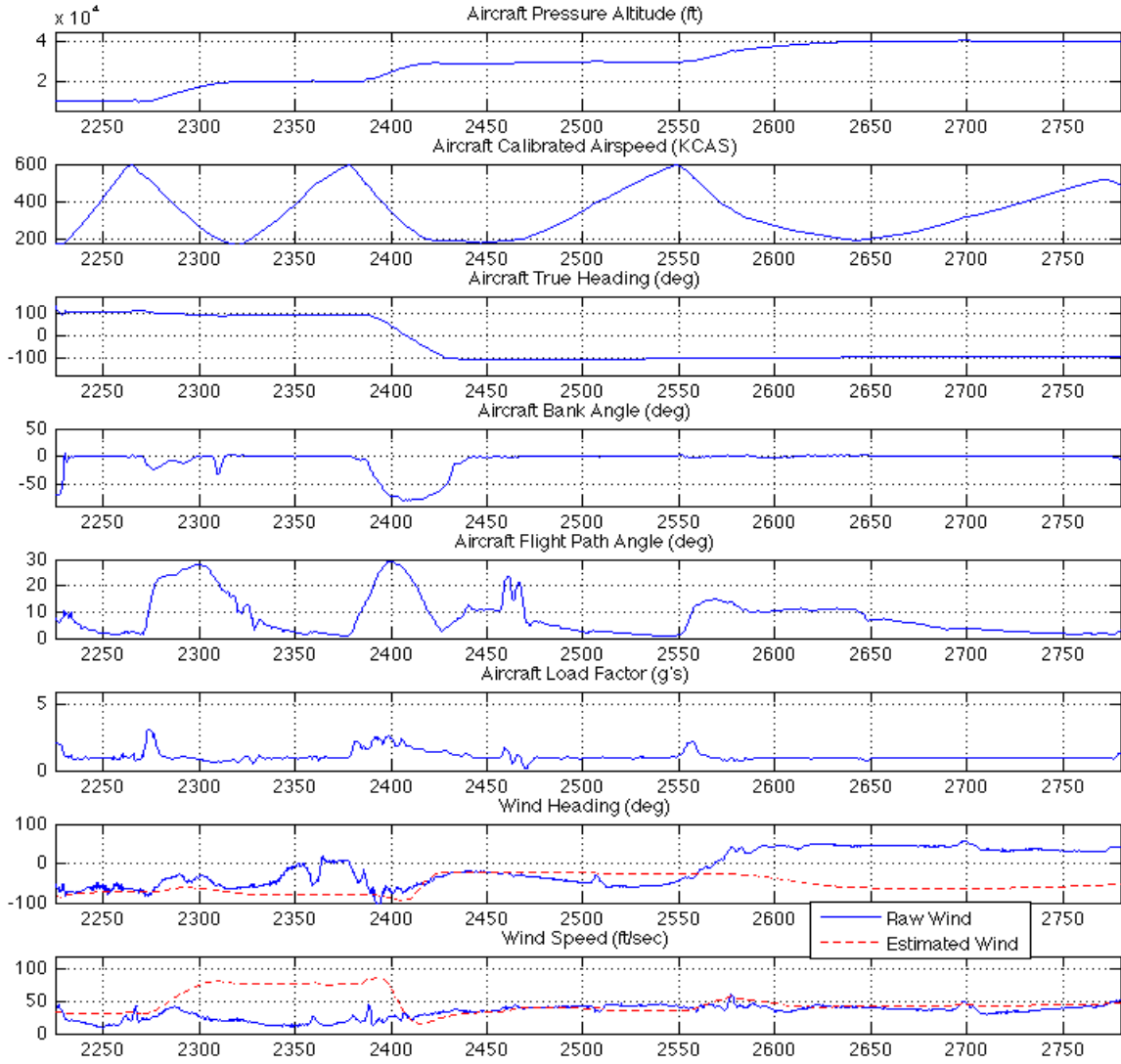(Maximum Power, 10K, 20K, 30K, and 40K)
VEST 2
F-16 Filtered Winds
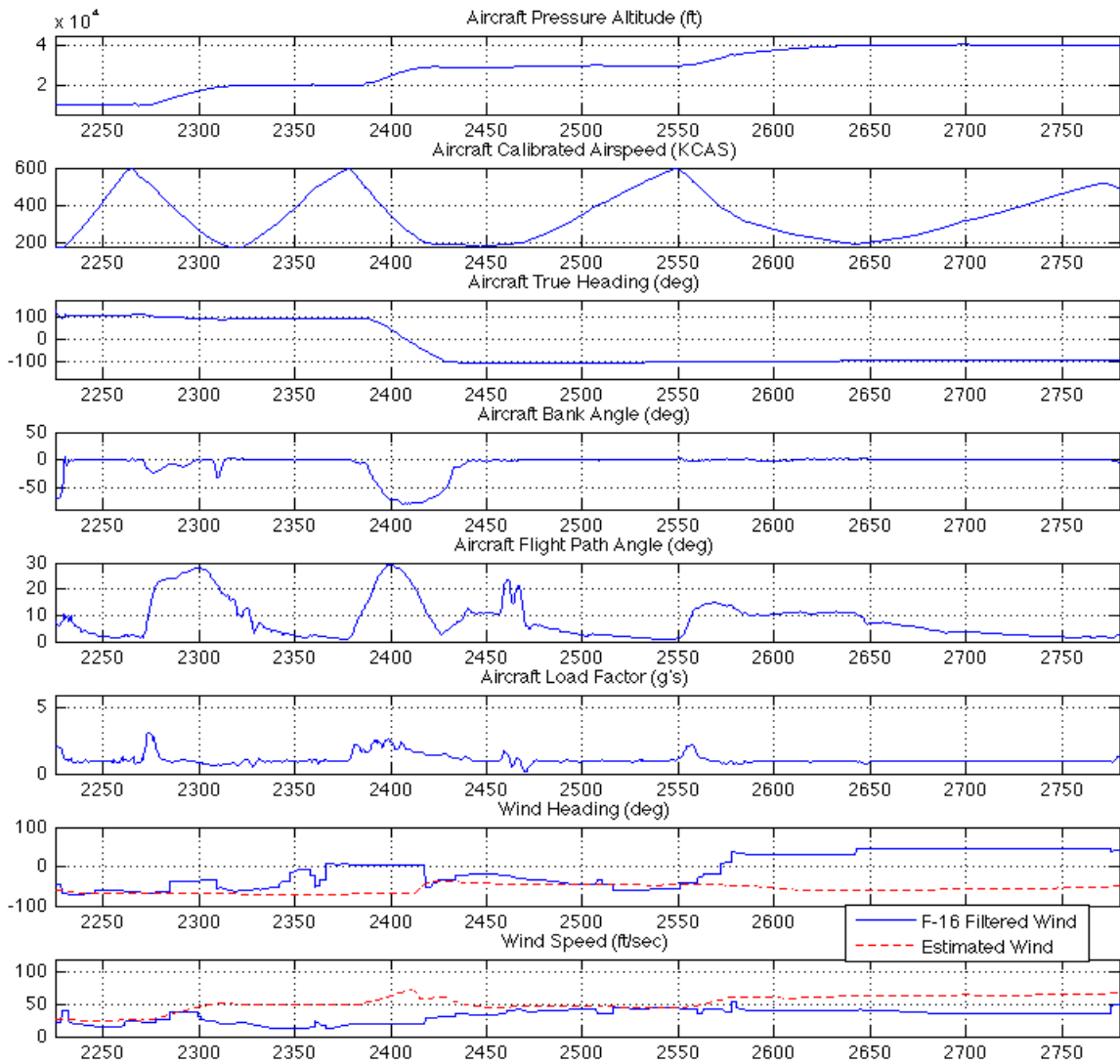
Figure 159. 10K, 20K, 30K and 40K Level Acceleration (VEST 2)

Level Acceleration Sortie
(Maximum Power, 10K, 20K, 30K, and 40K)
VEST
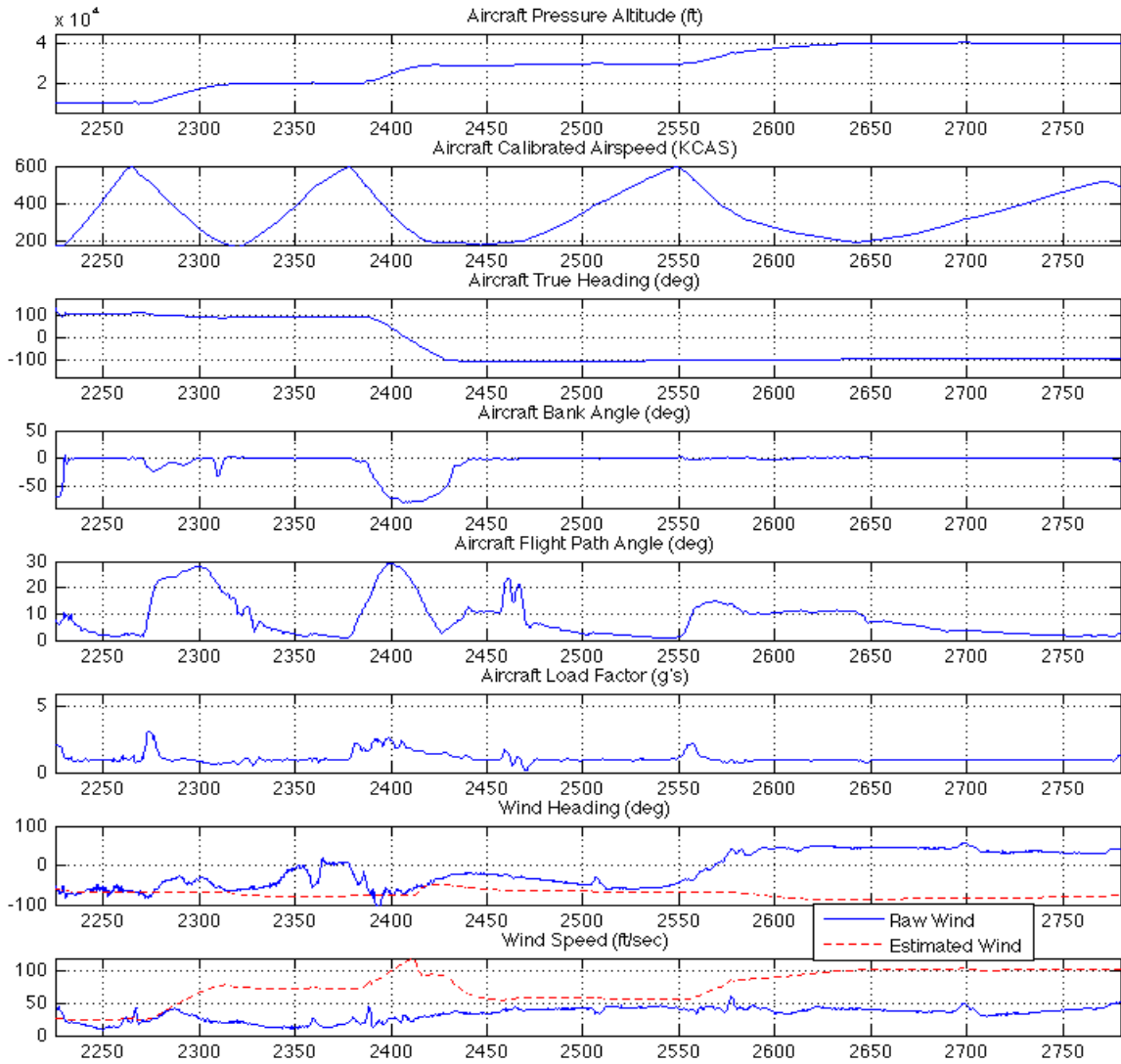
Figure 160. 10K, 20K, 30K and 40K Level Acceleration (VEST)

Level Acceleration Sortie
(Maximum Power, 10K, 20K, 30K, and 40K)
VEST TAS
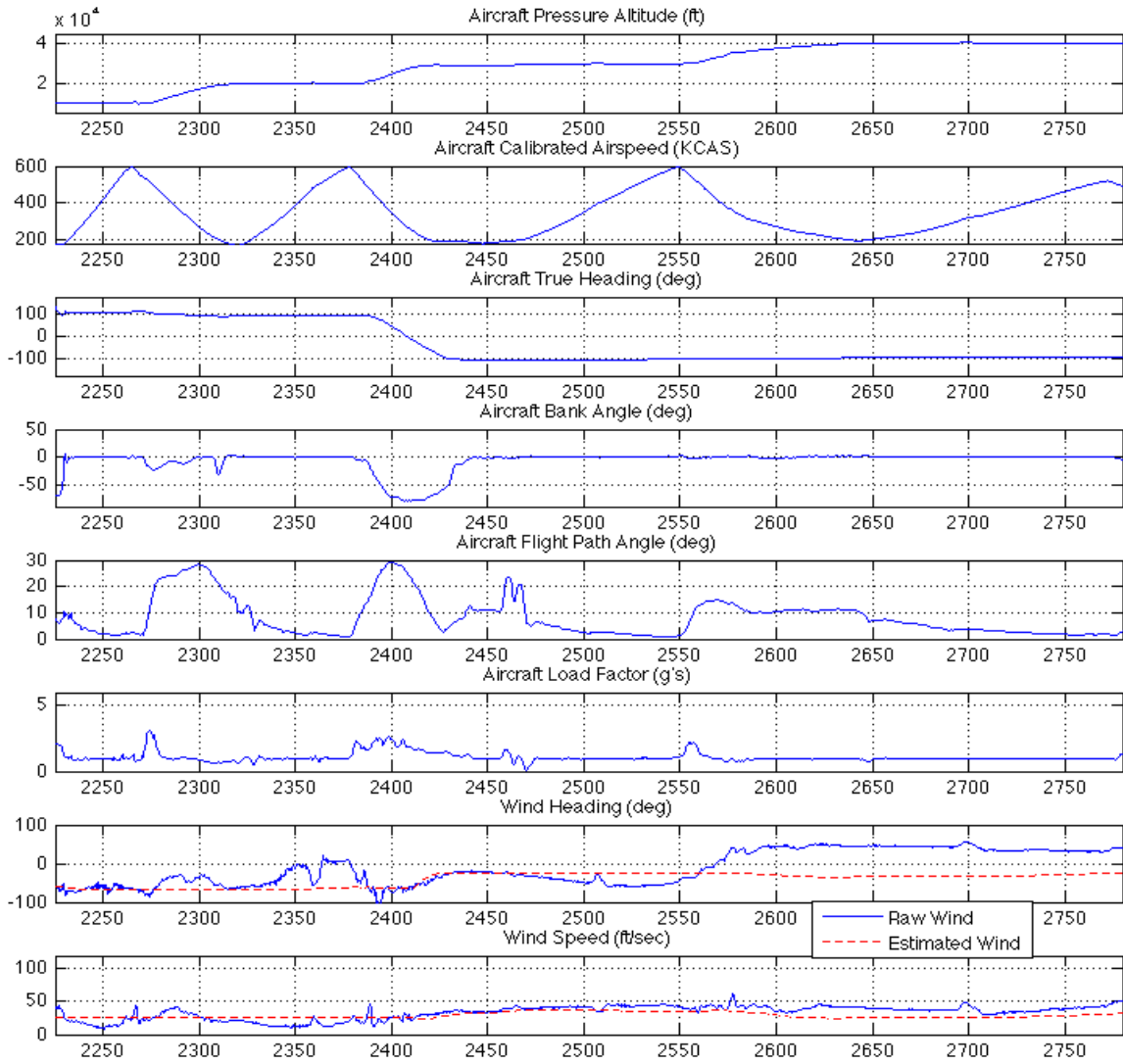
Figure 161. 10K, 20K, 30K and 40K Level Acceleration (VEST TAS)

Level Acceleration Sortie
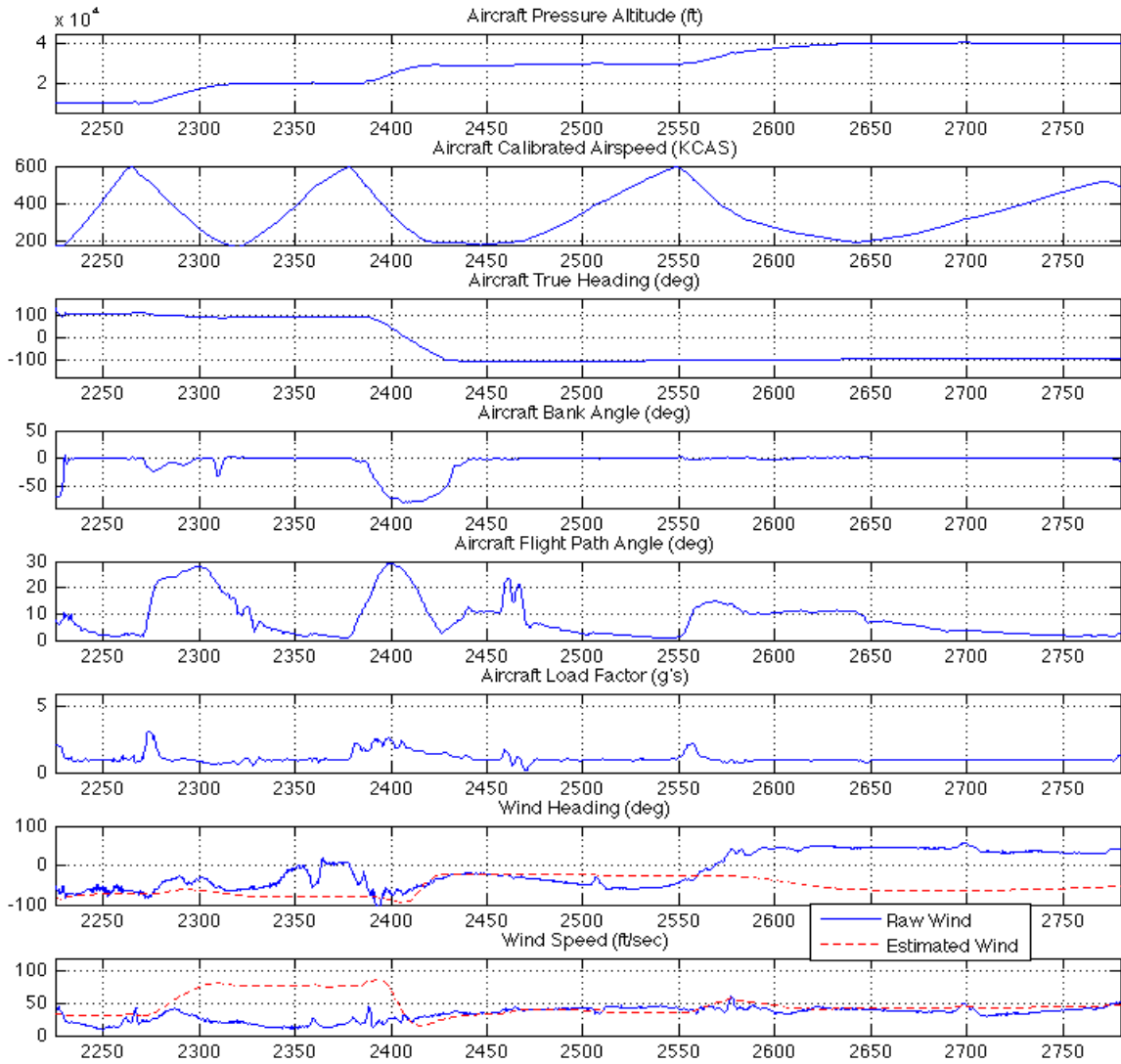(Maximum Power, 10K, 20K, 30K, and 40K)
VEST (No Residual Logic)

Figure 162. 10K, 20K, 30K and 40K Lvl Acc. (VEST - No Residual Logic)
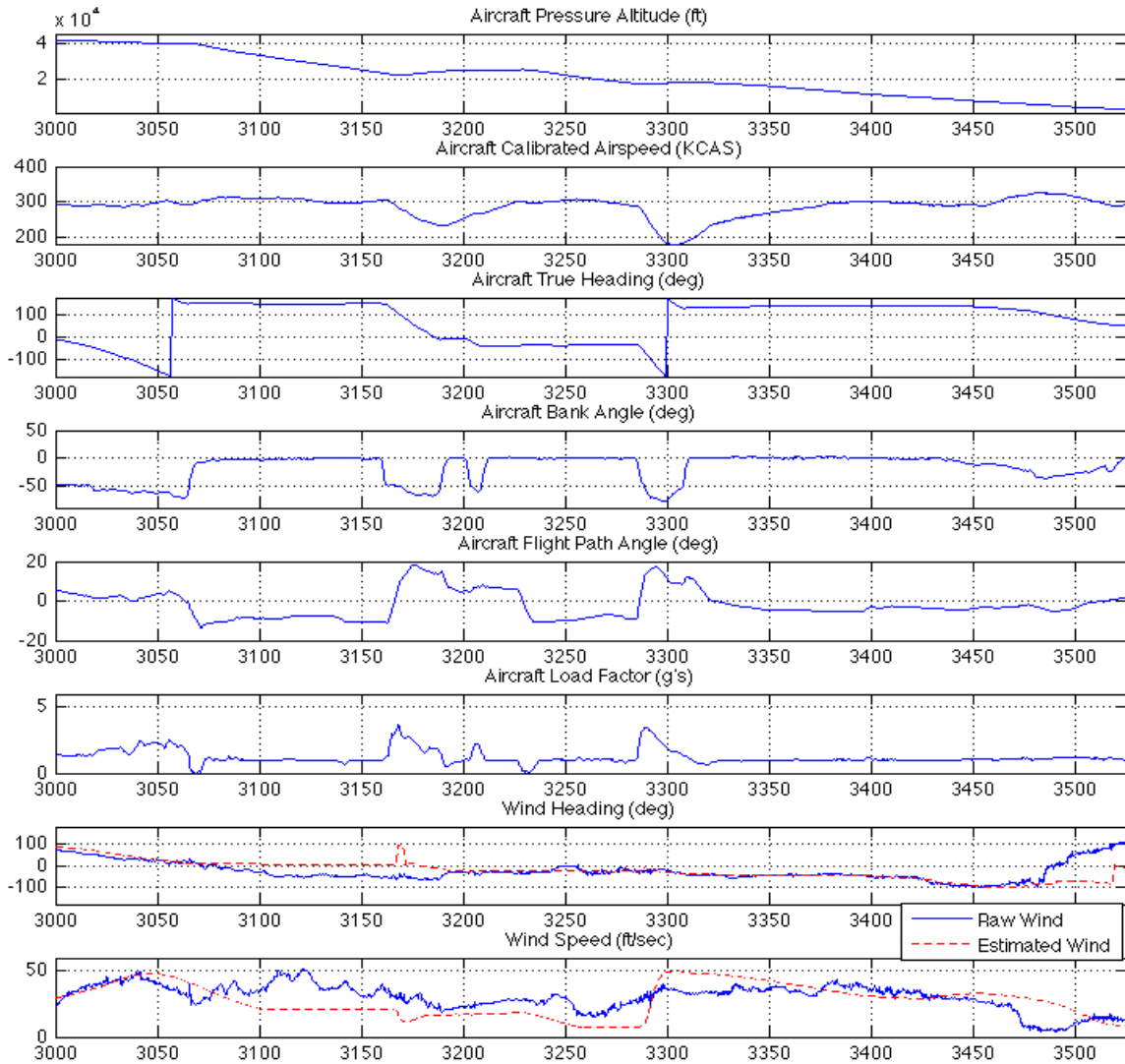
231

Level Acceleration Sortie
(Maximum Power, 10K, 20K, 30K, and 40K)
VEST TAS (No Residual Logic)

Figure 163. 10K, 20K, 30K and 40K Lvl Acc. (VEST TAS - No Residual Logic)

Level Acceleration Sortie
(Penetration Descent)
VEST 2

Figure 164. Penetration Descent (VEST 2)

Level Acceleration Sortie
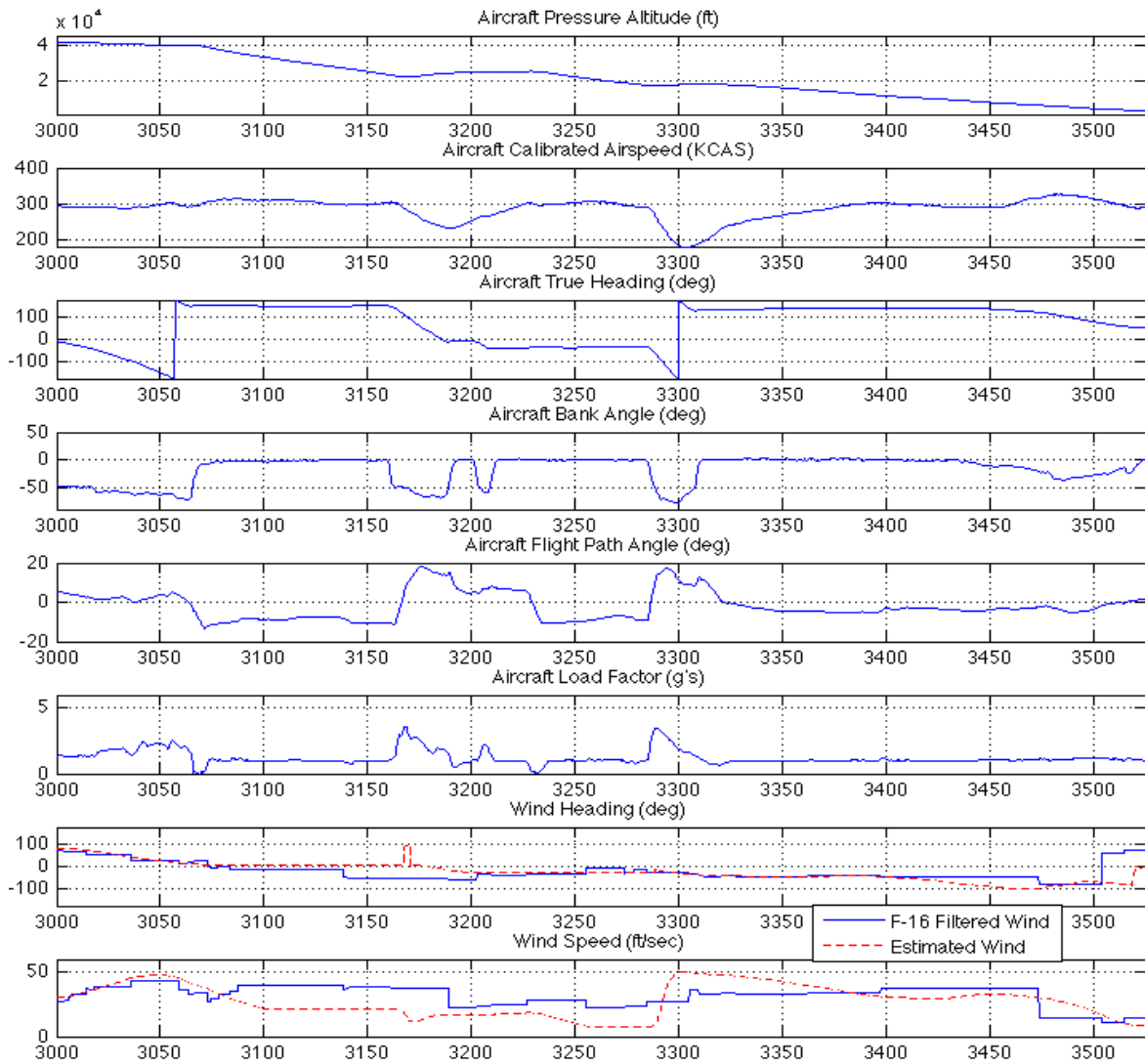(Penetration Descent)
VEST 2
F-16 Filtered Winds

Figure 165. Penetration Descent (VEST 2)

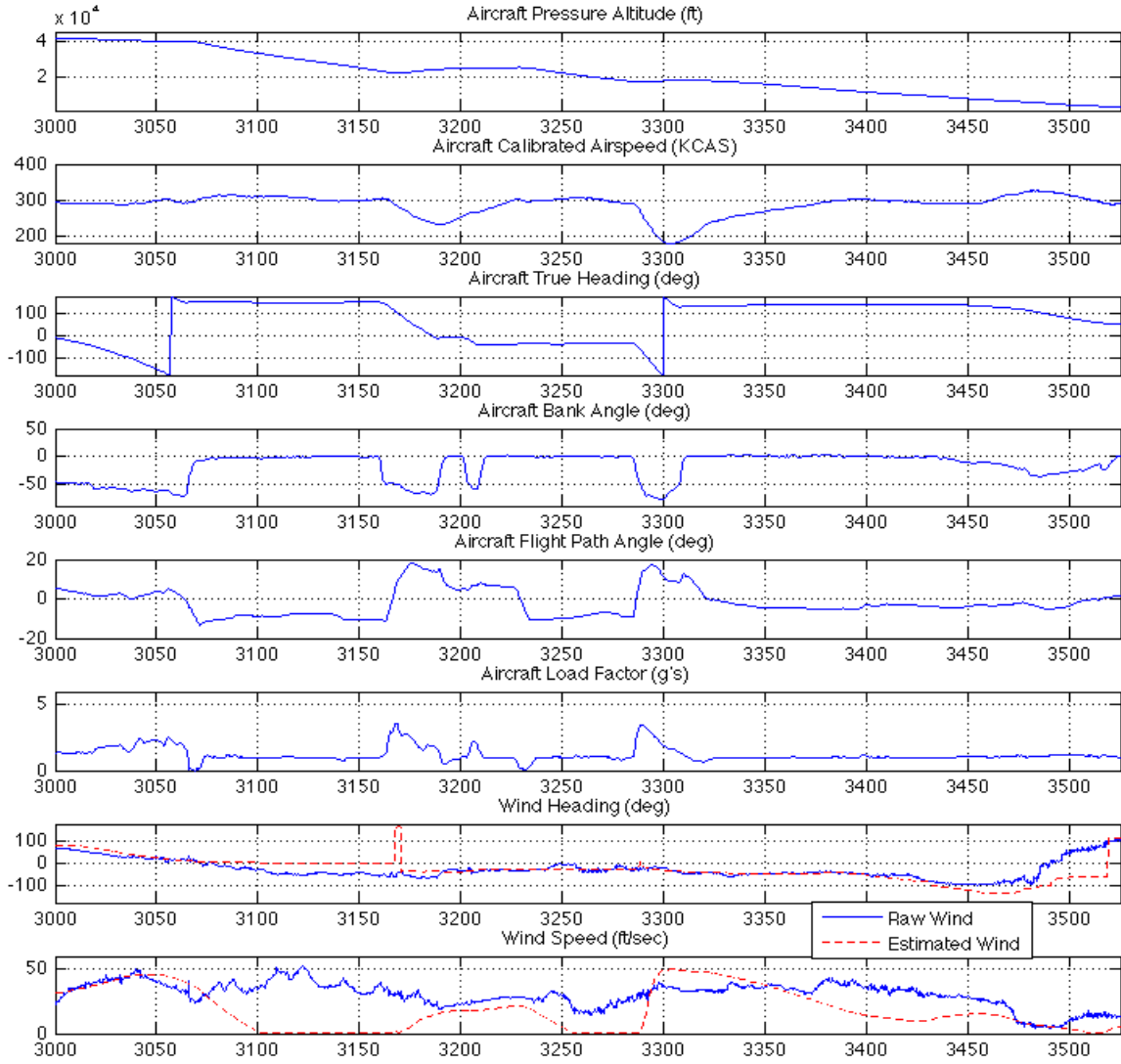Level Acceleration Sortie
(Penetration Descent)
VEST

Figure 166. Penetration Descent (VEST)

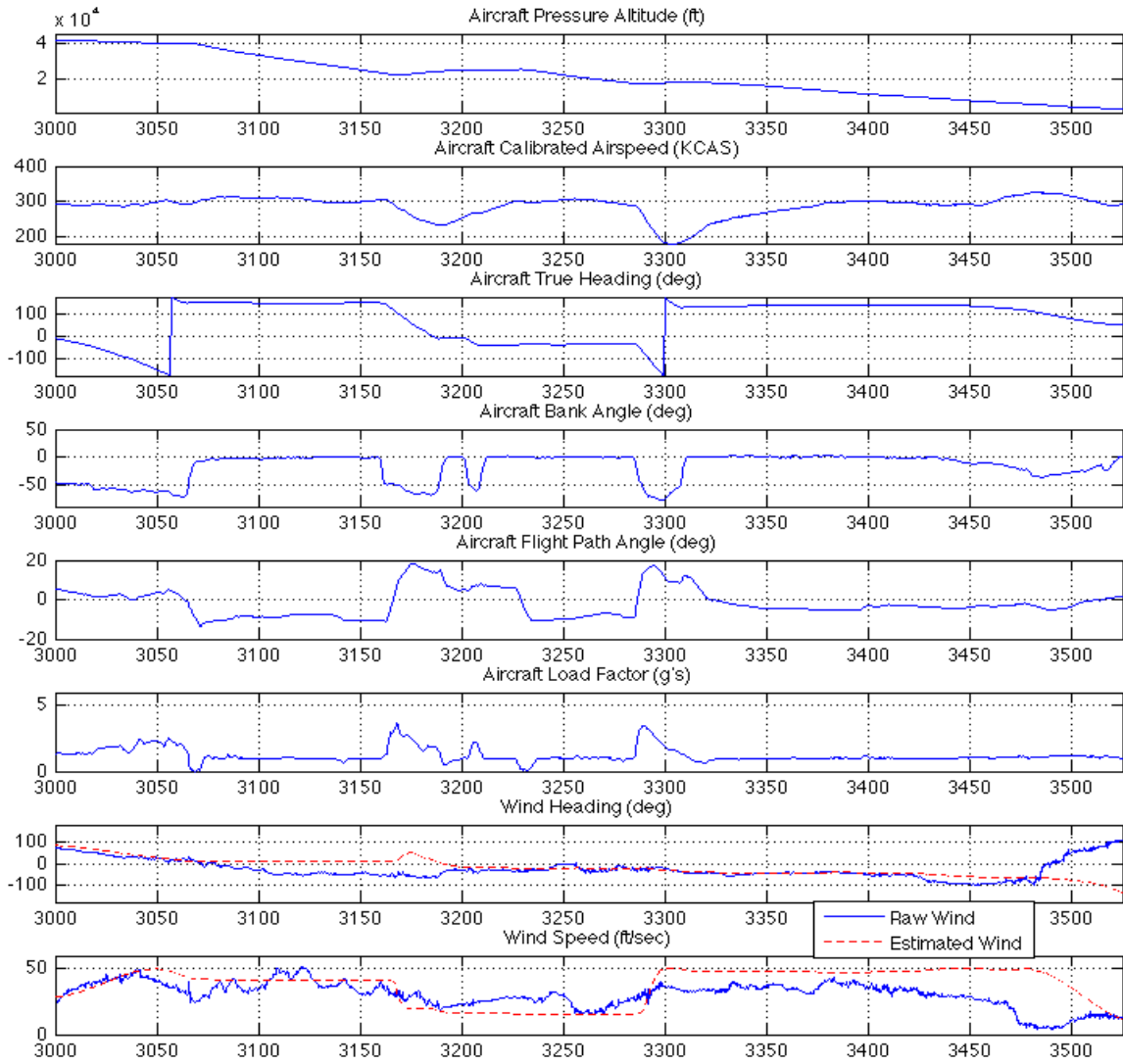Level Acceleration Sortie
(Penetration Descent)
VEST TAS

Figure 167. Penetration Descent (VEST TAS)

1. REPORT DATE (DD-MM-YYYY) September 2009	2. REPORT TYPE Master's Thesis	3. DATES COVERED (From – To) Jan 2007 – Sept 2009

4. TITLE AND SUBTITLE

Alternative Methods to Standby Gain Scheduling Following Air Data System Failure

5a. CONTRACT NUMBER

5b. GRANT NUMBER

5c. PROGRAM ELEMENT NUMBER

6. AUTHOR(S)

Coldsnow, Matthew W., Major, USAF

5d. PROJECT NUMBER

5e. TASK NUMBER

5f. WORK UNIT NUMBER

7. PERFORMING ORGANIZATION NAMES(S) AND ADDRESS(S)
Air Force Institute of Technology
Graduate School of Engineering and Management (AFIT/EN)
2950 Hobson Way
WPAFB OH 45433-7765

8. PERFORMING ORGANIZATION REPORT NUMBER

AFIT/GAE/ENY/09-S02

9. SPONSORING/MONITORING AGENCY NAME(S) AND ADDRESS(ES)

intentionally left blank

10. SPONSOR/MONITOR'S ACRONYM(S)

11. SPONSOR/MONITOR'S REPORT NUMBER(S)

12. DISTRIBUTION/AVAILABILITY STATEMENT

APPROVED FOR PUBLIC RELEASE; DISTRIBUTION UNLIMITED.

13. SUPPLEMENTARY NOTES

14. ABSTRACT
The United States Air Force has advanced fighter aircraft that lose the ability to operate in a large portion of their operating flight envelope when an air data system failure is experienced. These aircraft are reverted to a fixed set of standby-gains that limit their maneuverability, degrade handling qualities, and increase susceptibility to departure. The purpose of this research was to determine if three alternative methods of standby-gain-scheduling could provide robust control with minimal performance degradation despite the lack of air data. To accomplish this, three methods of standby-gain-scheduling were developed, integrated, and tested in the Infinity Cube simulator at the Air Force Research Laboratory/RBCD building. The first method improved upon an algorithm which used inertial data to estimate an aircraft's true velocity used to drive the gains in an F-16 controller. This algorithm was validated by post-processing high-fidelity simulator data and actual flight data. The second method simply used inertial velocities to drive the gains in an F-16 controller. The final method used a disturbance observer controller which controlled aircraft dynamics without the use of gain-scheduling. The results showed the potential for effective aircraft control with minimal performance degradation following an air data system failure. Potential benefits to this research include eliminating the need to make switch actuations to correctly schedule the standby-gains; improving aircraft performance when flying with standby-gains; allowing the pilot to continue with a combat mission instead of returning to base with an air data system failure; and helping contribute to the removal of Pitot tubes in an attempt to eliminate a failure mode and to reduce the radar cross section of an aerial vehicle.

15. SUBJECT TERMS
Standby Gain Scheduling, Velocity Estimator, Disturbance Observer, Air Data System Failure.

16. SECURITY CLASSIFICATION OF:			17. LIMITATION OF ABSTRACT	18. NUMBER OF PAGES	19a. NAME OF RESPONSIBLE PERSON Paul A. Blue, Lt Col, USAF
a. REPORT	b. ABSTRACT	c. THIS PAGE			19b. TELEPHONE NUMBER (Include area code) paul.blue@stratcom.mil
U	U	U	UU	248	